



UNIVERSITÀ DEGLI STUDI DI MILANO

Ph.D. PROGRAMME in CHEMISTRY

XXXVI cycle

Department of Food, Environmental and Nutritional Sciences

NATURE-INSPIRED COMPOUNDS AS MULTI-TARGET DIRECTED LIGANDS

CHIM/06

Ph.D. candidate: CECILIA PINNA

R12850

Tutor: Prof. ANDREA PINTO

Ph.D. dean: Prof. DANIELE PASSARELLA

A.A. 2023/2024

To Camilla and Jacopo,

The best siblings

I could ever dream of.

Index

Abbreviations	0
1. Chapter 1: Introduction	1
1.1. The global burden of microbial infections	2
1.2. Natural phytoalexins: an arsenal against bacterial and fungal pathogens	5
1.2.1. Myxochelins.....	6
1.2.2. Stilbenoids	10
1.2.3. Strobilurins	21
1.2.4. Phenolic acids and phenylamides	28
1.3. Bibliography	32
Chapter 2: Aim of the research project	49
2.1. Bibliography	52
Chapter 3: Study of natural siderophores as potential antifungal agents targeting ferroptosis	53
3. Synthesis of natural siderophores and their analogues as antifungal agents targeting ferroptosis.....	55
3.1 Introduction	55
3.2 Results and discussion.....	57
3.4. Materials and Methods.....	65
3.5. Bibliography.....	87
Chapter 4: Biocatalyzed synthesis of phenolamides and evaluation of their antimicrobial activity.....	91
Published article:	93
4.1 Introduction	94
4.2 Results and discussion.....	95
4.3 Conclusions	98
4.4 Materials and Methods.....	99
4.5 Bibliography.....	105
Chapter 5: In-depth investigation of natural stilbenoids' mode of action.....	109

General introduction	111
5.1. Design and synthesis of stilbenoid-bearing affinity probes for target proteins identification in bacterial pathogens.	112
Abstract.....	112
5.1.1. Introduction	112
5.1.2. Results and discussion.....	115
5.1.3 Conclusions	124
5.1.4 Materials and Methods.....	125
5.2 Immunomodulating activity of stilbenoids on bacteria-induced immune response.....	145
Published article:	145
Abstract.....	145
5.2.1. Introduction	146
5.2.2. Results.....	147
5.2.3. Discussion.....	156
5.2.4. Materials and Methods.....	159
5.2.5. Conclusions	164
5.2.6. Experimental procedures for stilbenoids synthesis	164
5.3. Bibliography	171
Chapter 6: Design and Synthesis of Multi-Target Hybrid Compounds	179
General introduction	181
6.1. Evaluation of stilbenoids antifungal activity against rice blast pathogen <i>Pyricularia oryzae</i> and combination of stilbenoid skeleton with quinone outside inhibitors (QoI) β -methoxyacrylic pharmacophore for the development of novel hybrid fungicides for crop protection.	183
Published article:	183
Abstract.....	183
6.1.1. Introduction	184
6.1.2. Results and Discussion.....	187
6.1.3 Materials and methods	192

6.2. Design and synthesis of multi-target hybrid compounds: combination of QoI β -methoxyacrylate pharmacophore and succinate dehydrogenase inhibitors (SDHI) structural features.	207
6.2.1. Introduction	207
6.2.2. Results and Discussion	208
6.2.3. Materials and methods	211
6.2.4. Bibliography.....	219
Chapter 7: Target-based virtual screening for the identification of novel scaffolds for the treatment of <i>Pyricularia oryzae</i> infections.	225
Published article:	227
Abstract.....	227
7.1. Introduction	228
7.2. Results	229
7.3. Discussion.....	238
7.4. Materials and Methods.....	240
7.5. Bibliography.....	252

Abbreviations

Å	Ångström
Ac ₂ O	acetic anhydride
ACN	acetonitrile
Af-BPP	Affinity-based protein profiling
AIBN	2,2-azobisisobutyronitrile
BBr ₃	boron tribromide
BCl ₃	boron trichloride
Bi(OTf) ₃	bismuth(III) trifluoromethanesulfonate
Boc	<i>tert</i> -butyloxycarbonyl
C ₄ H	cinnamate-4-hydroxylase
CBr ₄	carbon tetrabromide
CCl ₄	carbon tetrachloride
CD ₃ OD	deuteromethanol
CDCl ₃	deuteriochloroform
CH ₃ I	methyl iodide
CHCl ₃	chloroform
CHS	chalcone synthase
CHX	cyclohexane
Cs ₂ CO ₃	caesium carbonate
CuSO ₄ ·5H ₂ O	copper(II) sulfate pentahydrate
DCM	dichloromethane
DDQ	2,3-dichloro-5,6-dicyano-1,4-benzoquinone
DIPEA	<i>N,N</i> -diisopropylethylamine
DMAP	4-dimethylaminopyridine
DMF	<i>N,N</i> -dimethylformamide
DMHS	3,4'-dimethoxy-5-hydroxystilbene
DMP	Dess-Martin periodinane
DMSO	dimethyl sulfoxide
DPPA	diphenylphosphorylazide
dppp	1,3-Bis(diphenylphosphino)propane
EDC·HCl	<i>N</i> -(3-dimethylaminopropyl)- <i>N'</i> -ethylcarbodiimide hydrochloride
eq	equivalent
Et ₂ O	diethylether
EtOAc	ethyl acetate
EtOH	ethanol
FRAC	Fungicide Resistance Action Committee
Hex	hexane
HIO ₄	periodic acid

HoBt	1-hydroxybenzotriazole
HRP	horseradish peroxidase
IC ₅₀	half maximal inhibitory concentration
K ₂ CO ₃	potassium carbonate
KF	potassium fluoride
KOH	potassium hydroxide
LDA	lithium diisopropylamide
LDL	low-density lipoprotein
LiAlH ₄	lithium aluminium hydride
LiOH·H ₂ O	lithium hydroxide monohydrate
m.p.	melting point
MBC	minimal bactericidal concentration
MeOH	methanol
MIC	minimal inhibitory concentration
min	minute
MsAcT	acyl transferase from <i>Mycobacterium smegmatis</i>
NaBH ₄	sodium borohydride
NaH	sodium hydride
NaIO ₄	sodium periodate
NaN ₃	sodium azide
NaOH	sodium hydroxide
NBS	<i>N</i> -bromosuccinimide
<i>n</i> -BuLi	butyllithium
NF-κB	nuclear factor kappa B
NH ₂ NH ₂ ·H ₂ O	hydrazine monohydrate
NIS	<i>N</i> -iodosuccinimide
P(Cy) ₃ ·HBF ₄	tricyclohexylphosphine tetrafluoroborate
P(OEt) ₃	triethylphosphite
PAL	phenylalanine ammonia lyase
PBS	phosphate-buffered saline
Pd(dppf)Cl ₂	[1,1'-Bis(diphenylphosphino)ferrocene]dichloropalladium(II)
Pd(OAc) ₂	palladium acetate
Pd(PPh ₃) ₄	tetrakis(triphenylphosphine)palladium
PdCl ₂ (PPh ₃) ₂	bis(triphenylphosphine)palladium (II) dichloride
PPh ₃	triphenylphosphine
<i>p</i> -TsOH	<i>para</i> -toluensulfonic acid
rt	room temperature
SIBX	Stabilized 2-iodobenzoic acid
STS	stilbene synthase
TBAF	tetrabutylammonium fluoride
TBAI	tetrabutylammonium iodide
TBDMSCl	<i>tert</i> -butyl-dimethylsilyl chloride
<i>t</i> -BuOH	<i>tert</i> -butyl alcohol

TEA	triethylamine
TEM	transmission electron microscopy
TFA	trifluoroacetic acid
THF	tetrahydrofuran
TNF α	tumor necrosis factor α
WHO	World Health Organization

1. Chapter 1: Introduction

1.1. The global burden of microbial infections

Microbial infections represent nowadays a serious concern in different fields, including, above all, public health and the agrifood sector. Despite the considerable advances made in the last century in the treatment of microbial infections, several bacterial and fungal pathogens are still responsible for a high number of hospitalization and deaths, as well as for huge crop losses worldwide. Indeed, microbial infections are not limited to illnesses and symptoms (e.g., pneumonia, severe skin illnesses, nausea, vomiting, abdominal cramping, diarrhea, hypotension) in humans, but they include plant diseases targeting the most important cultures (e.g., cereals), hindering the food supply chain also in post-harvest phases (handling, packaging and storage). Moreover, the intensive use or overuse of antimicrobial agents has led to the spread of resistance phenomena, which is making the negative impact of bacterial and fungal pathogens even more dramatic. According to the European Centre for Disease Prevention and Control 33,000 people are dying every year in Europe because of antibiotic-resistant bacteria, being Italy in second place with 19 deaths per 100,000 inhabitants every year. A recent study published on Lancet in 2022 claimed that in 2019 gram positive and gram negative bacteria, both susceptible and resistant to pharmacological treatments, caused the death of 13.7 million people. Five leading pathogens —*Staphylococcus aureus*, *Escherichia coli*, *Streptococcus pneumoniae*, *Klebsiella pneumoniae*, and *Pseudomonas aeruginosa*—were found to be responsible for 54.9% of the infection-related deaths considered in the study (7.7 million). These bacteria were associated with 13.6% of all deaths globally and with 56.2% of all sepsis deaths in 2019. *S. aureus* alone has been associated with more than 1 million deaths [1]. These bacterial species, also including *Enterococcus faecalis*, had already emerged to be the major cause of hospital and community-acquired infections [2]. In 2019 drug-resistant bacterial infections were reported to contribute to approximately 5 million deaths, globally. This number is expected to increase up to 10 million by 2050 if no action is taken to combat antibiotic resistant bacteria [3]. In 2017 the WHO published the first list of antibiotic-resistant "priority pathogens" – a catalogue of 12 families of bacteria that pose the greatest threat to human health. *P. aeruginosa*, together with various *Enterobacteriaceae* (including *Klebsiella*, *E. coli*, *Serratia*, and *Proteus*) belong to the first risk category, marked as "critical". This class includes multi-drug resistant bacteria, that have become non-susceptible to several antibiotics (e.g. carbapenems and third generation

cephalosporins) and that pose a particular threat in hospitals and nursing homes. The second class in the list, marked as “high risk”, includes increasingly drug-resistant bacteria, as methicillin-resistant *S. aureus*. Moreover, there are some pathogenic microorganisms responsible for the contamination of food and drinks whose ingestion can lead to foodborne illnesses. Together with *Listeria monocytogenes*, *Salmonella enterica* and *Bacillus cereus*, *S. aureus* represents one of the most dangerous food pathogens, constituting an additional threat to public health [4].

On the other hand, there are several fungal pathogens whose impact on human health goes beyond their ability to infect humans, since they destroy a third of all food crops annually [5]. Indeed, food production is facing unprecedented challenges in terms of increased demand for improved quality and quantity of agricultural crops, due to the growth of global population. Phytopathogenic fungi are constantly challenging agriculture causing significant crop losses in the main high calorie cultures – rice, wheat, maize, soybean, potatoes – with consequent economic damages. In 2019 the Food and Agriculture Organization of the United Nations estimated that between 20% to 40% of global crop production are lost to plants pathogens, with a cost for the global economy of around \$220 billion (www.fao.org). Hypothetically, if all the aforementioned crops were affected simultaneously, approximately 61% of the world’s population would be in need of food [5].

Furthermore, many other crops can be affected, such as apples, grapevine, pears, citrus, strawberries, cherries, tomatoes and more. For instance, *Penicillium expansum* is a plant pathogen affecting pears, strawberries, tomatoes, rice, and corn. This fungus metabolites include neurotoxins that are harmful when consumed. Also, *P. expansum* is particularly known for causing blue mold of apples, one of the major post-harvest apple diseases with relevant economic consequences [6,7]. Fruits and vegetables rotting is often caused by *Aspergillus niger*, while foot and root diseases in cereals (maize, wheat, and barley) are induced by infections of different *Fusarium* species (e.g. *F. graminearum* and *F. culmorum*). Significant post-harvest losses are also caused by black spots on several fruits and vegetables (e.g. potatoes, apples, pears, strawberries, and blueberries). This kind of necrotic lesions are the result of infection by the filamentous ascomycete *Alternaria alternata*, one of the most devastating phytopathogenic fungi [8], which is also responsible for some human infections, especially in immunocompromised patients [9]. Interestingly, *A. alternata* displayed competitive exclusion in presence of another important pathogen, *Botrytis cinerea*, through the production of bioactive metabolites such as alteichin and alternariol 4-methyl ether [10]. *B. cinerea* is, in turn, the cause of

gray mold diseases in over 500 plant species, being grapevine one of the most economically relevant [11]. *B. cinerea* has been classified as the second plant pathogen worldwide in terms of economic impact [12], causing losses up to \$100 billion [13]. These effects are worsened by the spread of multiple fungicide resistance mechanisms. Indeed, *B. cinerea* displayed resistance to all seven Fungicide Resistance Action Committee (FRAC) codes with single modes of action, due to various target gene mutations [14].

However, the first place among destructive phytopathogenic fungi belongs to *Pyricularia oryzae*, also known as *Magnaporthe oryzae*, which is responsible for rice blast, a highly destructive disease widespread in Europe, Asia, Central and South America, Sub-Saharan Africa, and Australia [12]. Rice blast has been extensively studied due to the importance of rice production and consumption, and because of its vast distribution and destructiveness across the world. Indeed, blast disease can cause yield losses of up to 30%, or even complete harvest loss in favorable conditions of temperature and humidity [15]. According to a survey conducted in 2010, annual yield losses due to blast disease alone would be sufficient to feed 60 million people [16]. The devastating effects of blast disease are even worsened by the progressive withdrawal of fungicides from the market, that led to the repeated use of a small portfolio of antifungal agents. For instance, in Europe there are only four classes of fungicides for the treatment of rice blast, namely: strobilurins (quinone outside inhibitors, QoI) and demethylation inhibitors (DMI) as synthetic fungicides, together with sulphur and *Bacillus subtilis* QST713 used in biological agriculture. As a consequence, the incidence of resistance phenomena has been growing in the last decades, thus frustrating the use of all the commercially available agrochemicals [17–20]. This is especially true for those fungicides acting with a single mode of action [21,22]. For instance, quinone outside inhibitors have been widely and effectively used worldwide for the treatment of rice blast since 1977 [23]. Despite their potential as fungicides, their use is now frustrated by the development of resistance mechanism, most often caused by a single nucleotide mutation (G143A, substitution of glycine at position 143 for alanine) on QoI molecular target (cytochrome *bc1* complex). This mutation is now widespread, and it has already been detected in more than 50 fungal plant pathogens, including of course *P. oryzae* [20]. The presence of strobilurin-resistant strains of *P. oryzae* has been recently reported also in Italy, the biggest European rice producer [24].

In this scenario, the identification of novel and environmentally friendly agrochemicals, able to bypass antimicrobial-resistance while not showing toxicity towards humans and animals is of utmost importance. Besides the

identification of new chemical entities, rational design of multi-target drugs and agrochemicals should be considered. Multi-target compounds have emerged as an attractive therapeutic solution for diseases with significant drug-resistance problems [25]. Indeed, scaffolds endowed with different biological activities could serve as starting point for the design of innovative antimicrobials with enhanced efficacy. In this context, Nature represents a scientific goldmine for the identification of different chemotypes and a limitless source of inspiration for the development of nature-inspired agrochemicals. Special attention has been directed toward bioactives produced by living organisms against pathogens or stress factors such as phytoalexins and phytoanticipins that combat herbivores, microbial pathogens, or competing plants.

These compounds are characterized by a wide range of activities (e.g. antimicrobial, antioxidant, anti-inflammatory, anticancer, immunomodulatory), showing different mechanisms of actions. They are, in other words, built-in multi-target directed ligands, which makes them appealing for the design of multi-mode antimicrobials. Moreover, nature-derived products are relatively broad-spectrum, bioefficacious, economical, and environmentally safe, being ideal candidates for use as agrochemicals.

During my PhD work, different classes of natural and nature-inspired compounds have been studied for their antimicrobial potential, including myxochelins, stilbenoids, strobilurins, and phenylamides, that will be described in the following sections.

1.2. Natural phytoalexins: an arsenal against bacterial and fungal pathogens

The beneficial effects of plant-derived natural compounds have been known since ancient times. Indeed, the use of medicinal plants for the preparation of drugs has been reported for the first time more than 5000 years ago [26]. Over the time, humankind learned to recognize healing properties of plants, at first empirically, then with the support of scientific knowledge about the single bioactives responsible for their beneficial effects on human health. Over the years, several compounds have been identified and classified, unveiling the wide structural variety of plant phytoalexins, and shedding light on their biosynthesis and their biological properties. Tannins, flavonoids, lignans, stilbenoids and phenolic acids are among the most deeply studied families of natural compounds over the last decades. Each class displays a wide range of

biological properties, revealing their multi-mode action, although in most cases the mechanisms of action behind the biological activity remain unknown. In the present PhD project, four classes of natural phytoalexins - myxochelins, stilbenoids, strobilurins and phenolamides – were deeply studied. Their structural features, together with their biological properties and – when known – their mechanisms of action are presented below.

1.2.1. Myxochelins

Due to their complex social lifecycle, involving multicellular surface motility, fruiting body formation, sporulation, and wolf-like predatory behavior, Gram negative myxobacteria, as other predatory bacteria, are prone to produce a variety of secondary metabolites [27–29]. This makes them a prolific source of natural bioactives, characterized by a broad variety of chemical scaffolds with different biological activities and other functions, such as pigments, signaling molecules and iron-chelating siderophores [27,30]. Myxobacteria production is, therefore, extremely promiscuous, and mostly undiscovered since the difficulty in the cultivation and/or genetic manipulation makes it more challenging to study this class of microorganisms. To date, approximately 7500 myxobacterial strains have been identified, together with around 70 distinct core structures yielded by their metabolic production [31]. Secondary metabolites production includes linear or cyclic polyketides (PKs), non-ribosomal polypeptides (NRPs), terpenoids, phenyl-propanoids, alkaloids [32], and two different iron transport metabolites, the hydroxamate-type nannochelins [33], and the catecholate-type hyalachelins [34] and myxochelins (**Figure 1.1**). Myxochelins are structurally characterized by two catechol motifs connected through an aminic spacer *via* amidic bond (**Figure 1.2**). The spacer is usually – but not always – derived by lysine and it can be decorated with a primary alcohol (myxochelin A) or a primary amine (myxochelin B) [33,35].

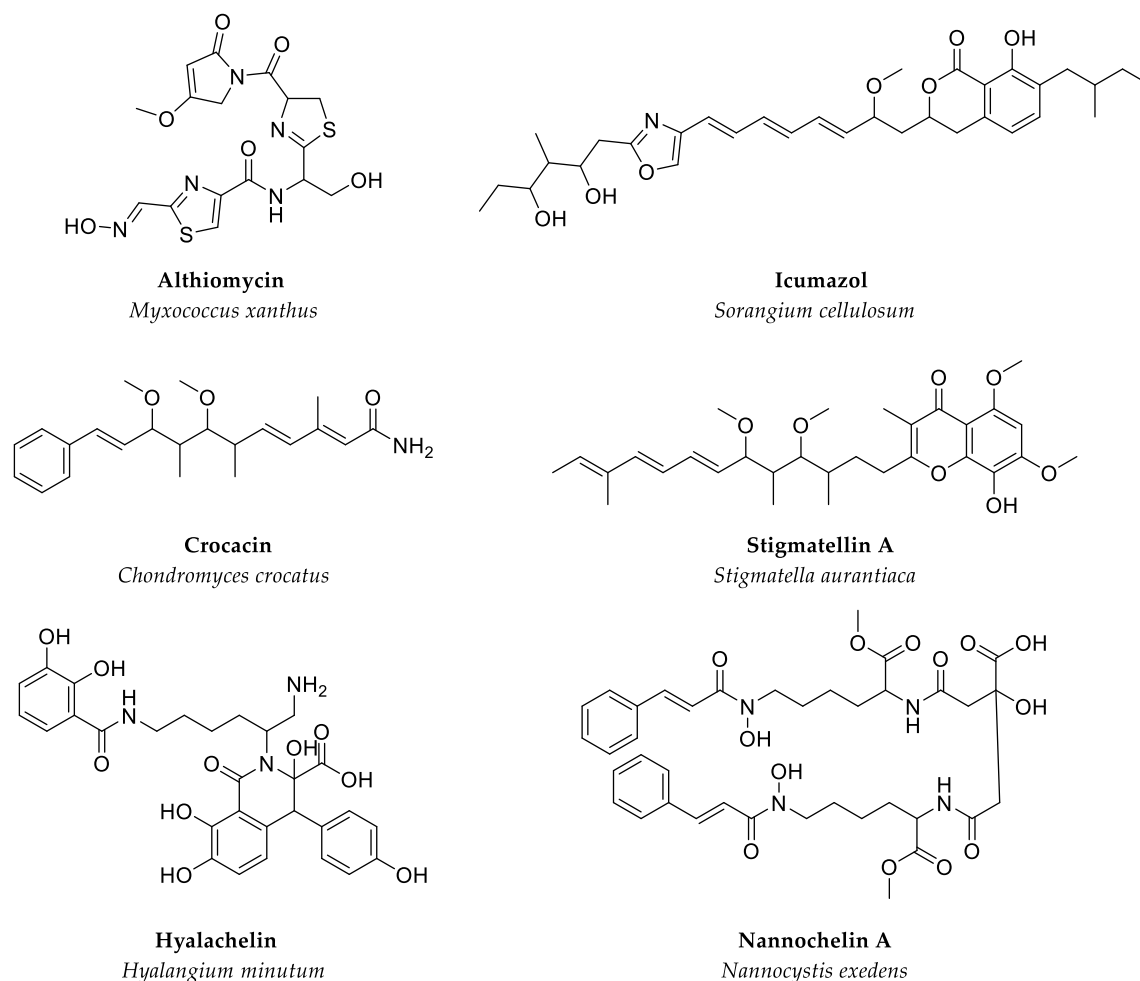


Figure 1.1. Examples of structurally diverse secondary metabolites from myxobacteria [29]

In pseudochelin A, one of the amidic bonds is replaced by a 4,5-dihydroimidazole moiety [36]. Also, analogues containing one or two nicotinic moieties in place of the catechol ring have been isolated in nature (myxochelins N1-N3) [37,38], as well as other non-catecholate type derivatives, some of which containing a rare 2-oxazolidinone motif (myxochelins P, O, Q) [38]. Myxochelin A was firstly isolated from *Angiococcus disciformis* strain An d30 in 1989, and it showed a weak antibacterial activity towards *S. aureus* [35]. Many other myxobacterial strains were used for the isolation of natural siderophores, as *Archangium* sp. SDU34 [38], *Pseudoalteromonas piscicida* S2040 [36], *Stigmatella aurantica* sg a15, *Sorangium cellulosum* So ce56 [39], *Myxococcus xanthus* DK 1622 [40], just to list a few. Other catecholate-type siderophores were isolated from *Azotobacter vinelandii*, namely azotochelin (1969) [41], bearing a carboxylic group on the central carbon chain, and the mono-catecholamide aminochelin (1988) [42,43] that is 2,3-dihydroxybenzoylputrescin, a bidentate siderophore bearing a free amino group (**Figure 1.3**).

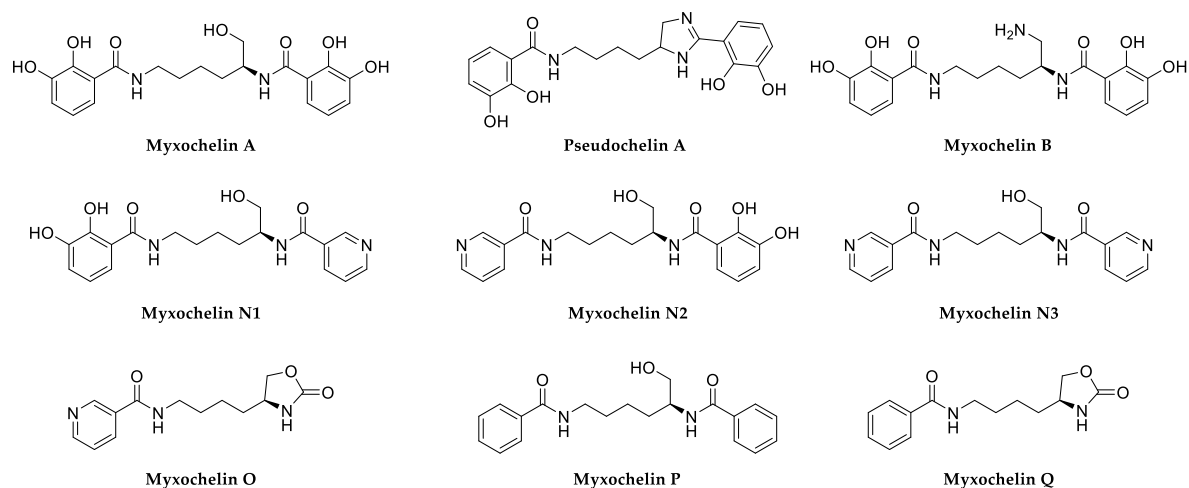


Figure 1.2. Natural myxochelins

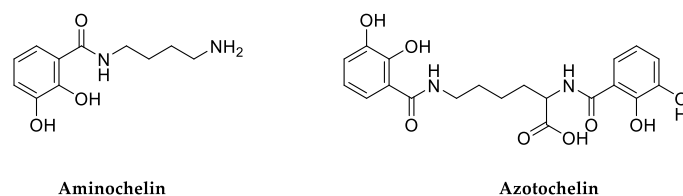


Figure 1.3. Aminochelin and azotochelin

The biosynthetic pathway leading to myxochelins was elucidated thanks to the *in vitro* reconstitution of myxochelin biosynthetic machinery of *Stigmatella aurantiaca* Sg a15 [44]. The process starts with the ATP-dependent activation of 2,3-dihydroxybenzoic acid (2,3-DHBA) mediated by the standalone adenylation domain MxcE. 2,3-DHBA is then transferred to the aryl-carrier protein (ArCP) domain of MxcF. Two units of 2,3-DHBA are subsequently condensed with the α - and ϵ - amino groups of lysine. The obtained PCP-thioester is reduced and released to afford an aldehydic intermediate which can undergo NAD(P)H-dependent reduction, giving myxochelin A, or reductive transamination by MxcL to produce myxochelin B (**Figure 1.4**) [38,45].

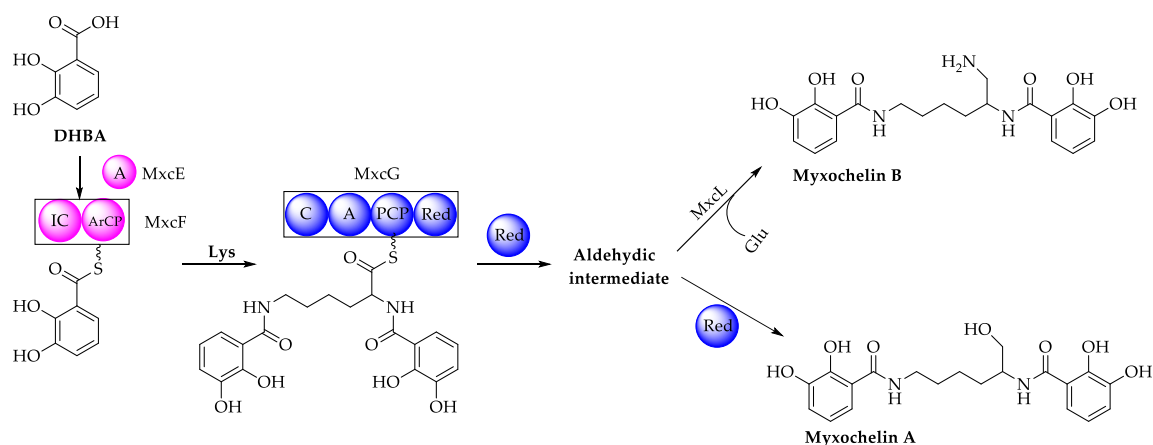


Figure 1.4. Myxochelin biosynthesis, modified from [45]

Iron chelation: potential target for new antifungal treatments

Myxochelins showed weak antibacterial activity towards *S. aureus* (MIC 25 $\mu\text{g/mol}$) [35], antifungal [36] and antineoplastic [46] activities, as well as inhibitory activity towards 5-lipoxygenase [47].

Their biological properties rely mostly on their ability to act as siderophores. Iron is an essential cofactor involved in many biological processes. Therefore, its cellular uptake is essential for all living organisms, including soil bacteria competing for scarce nutrients and space. Bacteria capture iron by secreting siderophores, which facilitate iron scavenging, transport, and uptake [48] by complexing insoluble iron (Fe^{3+}) and transporting it through specific membrane receptors. Once inside the cell, the complexed iron is released via reduction, ligand exchange or hydrolytic mechanisms leading to soluble Fe^{2+} species [49]. Siderophores are generally characterized by the presence of a high number of oxygen atoms, able to coordinate positively charged ions. Indeed, myxochelin A and B, and pseudochelin A present a 2,3-dihydroxybenzamide motif, whose iron-chelating properties have been known for a long time [50]. Moreover, the presence of the amidic group in the linker could further assist the iron chelation.

Iron homeostasis is crucial not only for bacteria, but also for other species as phytopathogenic fungi. For instance, blast disease, caused by the fungal phytopathogen *P. oryzae*, is spread by asexual spores (conidia) that infect the aerial parts of rice plant. The infective process involves the development of an infection cell – known as appressorium – which is able to firmly adhere on the plant surface, break the cuticle, and generate turgor pressure up to 8.0 MPa, leading eventually to the cuticle rupture and infection spread [16,51–54]. This

process requires the autophagic death of the conidial cell from which the infection originated, in order to allow appressorium maturation and infection [55]. Conidium apoptosis consists in an iron-dependent process known as ferroptosis, characterized by intracellular accumulation of iron and lipid peroxides [56,57]. Ferroptotic cell death involves an iron-dependent Fenton reaction [58,59], that generates free radicals, although the main source of lipid peroxides is represented by iron-dependent enzymes, such as lipoxygenases (LOXs) and NADPH oxidases (NOXs) [60]. Once inside the living host cells, colonization takes place through the production of invasive hyphae and the secretion of effector molecules to suppress plant immunity and aid infection [61].

In this perspective, iron depletion from the environment could be considered as an alternative strategy to counteract fungal infections, since it would prevent the iron-dependent processes that normally lead to the formation of lipid peroxides and eventually to conidial cells apoptosis. Therefore, natural siderophores such as myxochelins could be potentially employed to prevent plants infections from phytopathogenic fungi as, for instance, *P. oryzae*.

1.2.2. Stilbenoids

Stilbenoids, or polyhydroxystilbenes, are natural compounds produced by plant tissues. They are both constitutive product of plant secondary metabolism and phytoalexins, namely small bioactive molecules whose production is increased in presence of external stress factors, such as bacterial and fungal infections, UV radiations, or physical trauma [62,63]. These plant metabolites are produced by at least 72 species, including Pinaceae (e.g., *Picea abies* (L.) Karst. and *Pinus nigra* J.F. Arnold), Gnetaceae (e.g., *Gnetum parvifolium* (Warb.) W.C. Cheng and *G. africanum* Welw.), Fabaceae (*Arachis hypogaea* L. and *Robinia pseudoacacia* L.), Vitaceae (e.g., *Vitis vinifera* L.), Moraceae (e.g., *Morus alba* L. and *M. macroura* Miq.), and Polygonaceae (e.g., *Polygonum cuspidatum* Sieb. et Zucc. and *P. multiflorum* Thunb.) [64]. This means that the dietary intake of polyphenolic stilbenoids is quite common, since they can be found in various fruits, vegetables, and beverages as for example nuts, grapes, apples, red fruits, black olives, red rice, and red wines as well. Stilbenoids share most of phenylpropanoid biosynthetic pathway with flavonoids. This begins with the conversion of phenylalanine to cinnamate by phenylalanine ammonia lyase. CoA ligase then adds acetyl-CoA to the cinnamate, giving cinnamoyl-CoA. The only difference lies in the last enzymatic step, the aldol-type cyclization of the tetraketide intermediate performed by stilbene synthase (STS) [65].

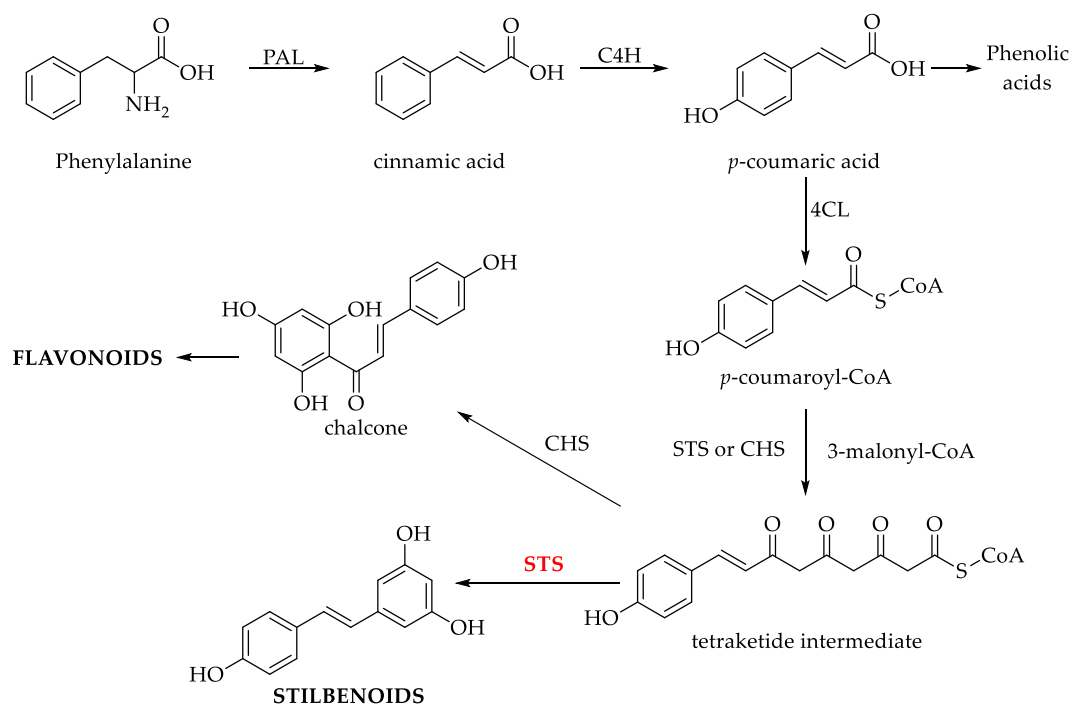


Figure 1.5. Stilbenoids biosynthesis, modified from [65]

Notably, STS genes are transcribed in response to various biotic and abiotic stress factors, consistently with the fundamental role of stilbenoids as secondary metabolites in plant protection [63]. It is noteworthy that stilbenoids are found in lignified stem tissues while they are entirely absent in the photosynthetic ones. In the latter, they seem to be detrimental for ion transport and associated with redox processes, suggesting their role in interfering with cellular mechanisms, thus leading to the protection of the plant during pathogen invasions [66]. Monomeric stilbenoids (e.g. resveratrol, piceatannol, pterostilbene, **Figure 1.6a**) share a common skeleton constituted by two phenolic moieties connected through a central carbon-carbon double bond. They differ in the number and position of functional groups, such as hydroxy, methoxy, prenyl, geranyl, or farnesyl groups. The ethylene bridge can be found in the *E* or *Z* configuration, but *trans* isomers are usually the most stable and common in nature. *Trans* to *cis* isomerization of resveratrol occurs upon exposure to both ultraviolet and visible light. Indeed, monomeric stilbenoids are usually sensitive to heat, light, air, and oxidative enzymes. Radical oxidative couplings of monomeric stilbenoids lead to the formation of oligomeric stilbenoids as viniferins (α -, δ -, ϵ -viniferin) and pallidol (**Figure 1.6b**). All these natural products can be isolated in nature as aglycones or glycosides [67].

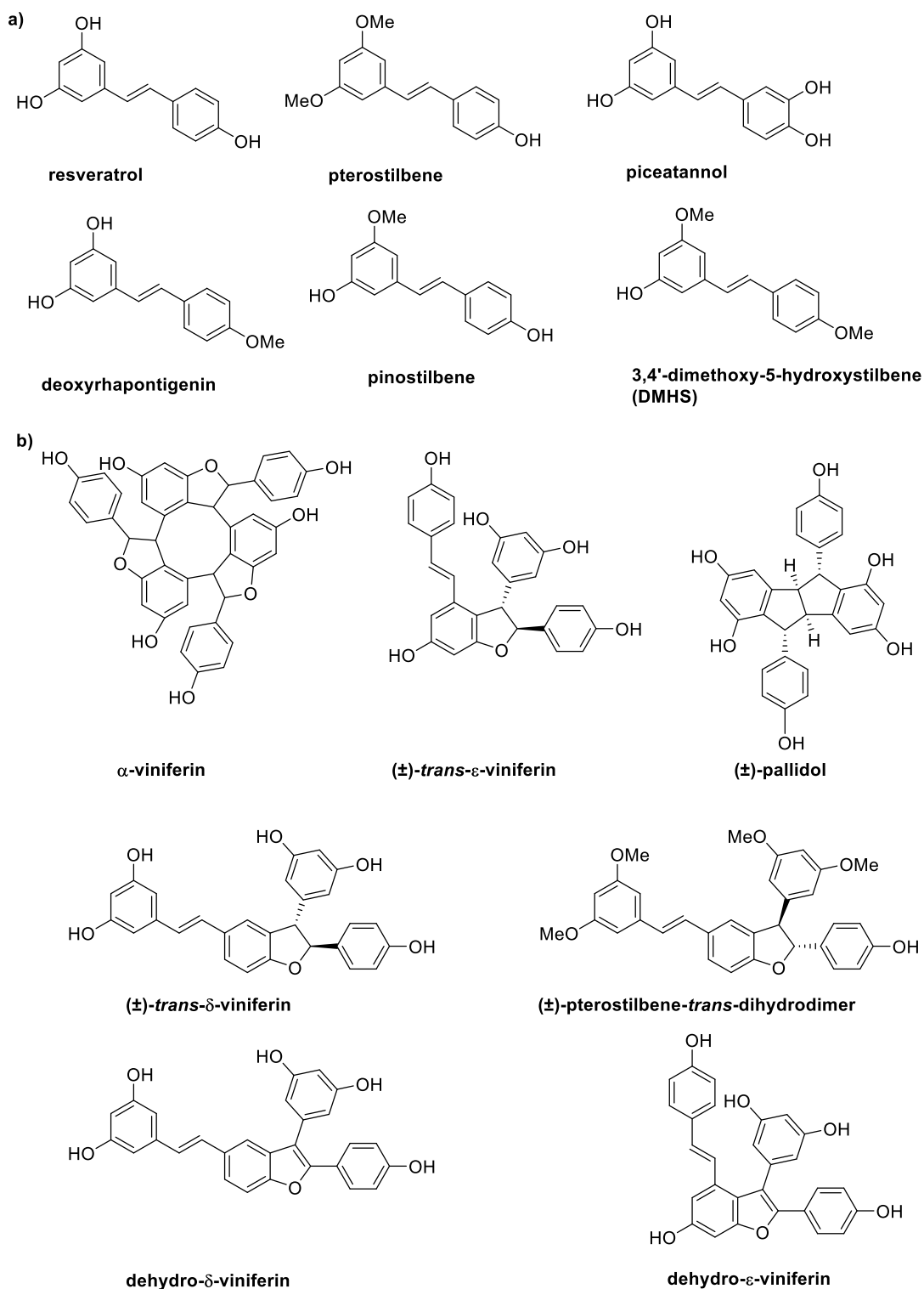


Figure 1.6. a) Monomeric stilbenoids; b) oligomers

Resveratrol is the most studied compound among monomeric stilbenoids. It was first isolated from the roots of white hellebore *Veratrum grandiflorum* in 1939 and then found in various other plants and fruits, such as grapes, apples, raspberries, and more [68]. Extensive experimental and preclinical studies have revealed its diverse health benefits, including cardioprotective, anticancer, anti-

inflammatory, anti-diabetic, antibacterial, antifungal, antiviral and neuroprotective properties [69–74]. Despite its therapeutic potential, resveratrol clinical applications remain limited due to high metabolism and poor bioavailability. However, resveratrol has been demonstrated to undergo different structural modifications that increase its biological properties. The methylation of two hydroxy groups by *O*-methyltransferase enzymes affords pterostilbene (*trans*-3,5-dimethoxy-4'-hydroxystilbene) which shows a higher bioavailability compared to resveratrol. This derivative, also isolated in different plant species such as *Pterocarpus marsupium*, *Vitis*, and *Vaccinium* species (blueberries), showed antifungal, antimicrobial, anticancer, antidiabetic and neuroprotective activities [72,75–77]. Resveratrol-3-*O*-glucoside, known as piceid, seems to preserve resveratrol from oxidation while it is stored in plant cell tissues [65]. Another interesting derivative is piceatannol, derived from resveratrol hydroxylation and easily found in berries, grapes, and white tea. Its catechol moiety leads to enhanced antioxidant properties compared to resveratrol, as well as to metal ions chelation.

As mentioned, the oxidative radical couplings of resveratrol and its derivatives afford chiral and three-dimensional polyphenolic compounds, collectively referred to as "oligomers" [78]. These are normally constituted by 2-8 units, and can be found in plants as well, sometimes even in larger amount compared to the corresponding monomer. In some cases, oligomers show improved biological activity compared to resveratrol, which may suggest that resveratrol acts more as a precursor for phytoalexins produced through oligomerization processes [79]. Different modes of oligomerization produce structurally different dimers, leading to high chemical diversity. The main radical couplings leading to the formation of dimeric stilbenoids are depicted in **Figure 1.7** and **Figure 1.8**. For instance, the 8-10' coupling represents the most common connectivity among natural resveratrol derivatives. The subsequent oxaconjugate addition or a vinylogous Friedel-Crafts reaction of the *para*-quinone methide affords ϵ -viniferin, which is found in nature as a mixture of enantiomers, whose proportions depend on the plant species [80]. Pallidol is obtained through the 8-8' coupling, leading to the formation of a dimeric intermediate with two *para*-quinone methides, followed by double Friedel-Crafts cyclization to afford the [3.3.0] bicyclic core of pallidol [66,81]. Another common product of resveratrol chemical or enzymatic oxidation is δ -viniferin, obtained through the 3-8' coupling [82]. Less common dimers are gnetin C and amurensin M, yielded by 8-12' and 12-12' coupling respectively [83,84]. These oligomers are found in nature as complex mixtures of stereo- and regioisomers. Rigorous extraction and purification procedures for identification and

biological evaluation are necessary to study these intriguing molecular structures.

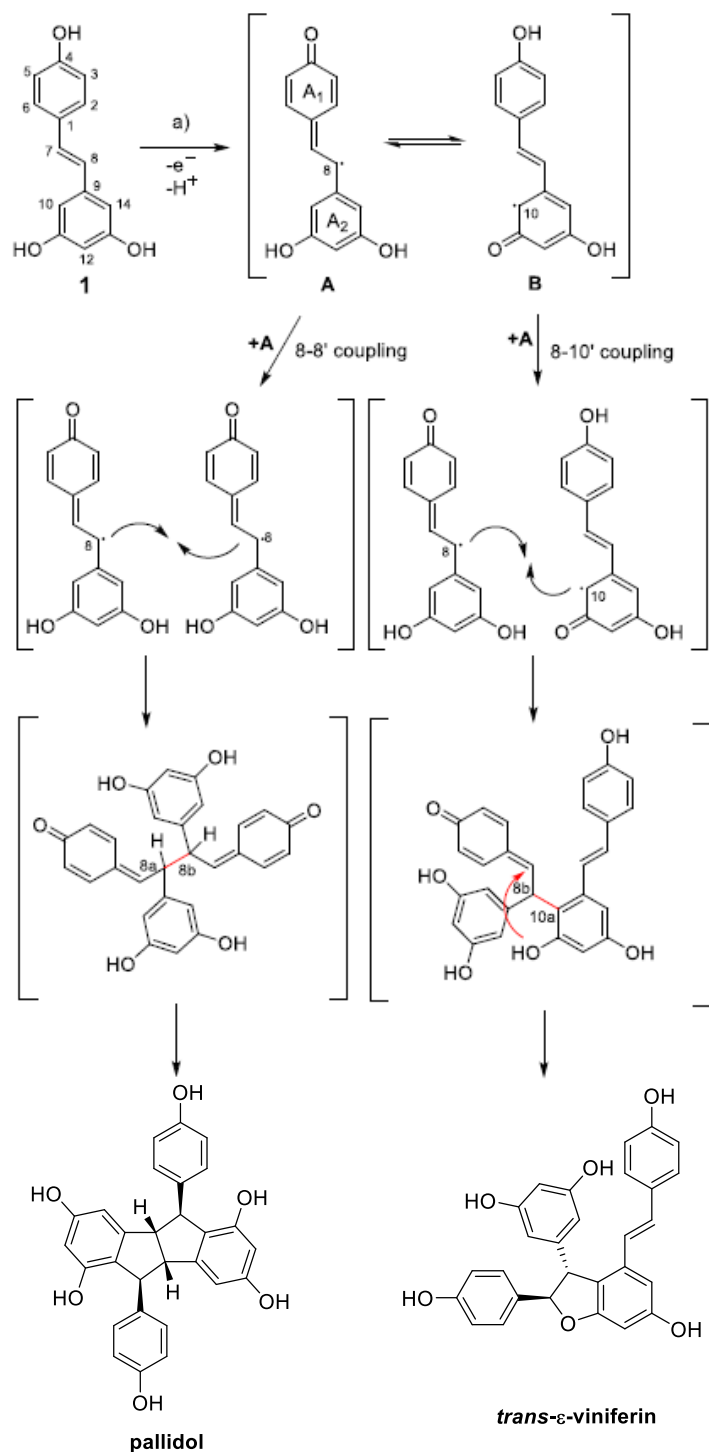


Figure 1.7. Proposed mechanism for 8-8' and 8-10' couplings

Viniferins (i.e., δ -viniferin, ϵ -viniferin) were discovered in the leaves and in the stem tissues of *Vitis vinifera*, are characterized by a 2,3-dihydrobenzofuran core. In 1999, the benzofuran derivative of ϵ -viniferin, viniferifuran or dehydro- ϵ -viniferin, was isolated from the corks of *Vitis vinifera* "Kyohou" [85]. It is worth

noting that a large number of natural products contain the 2,3-substituted benzofuran core, and these are endowed with multiple biological activities, such as antioxidant and anti-inflammatory properties, anticancer, antimicrobial, and immunomodulatory activities [86–89].

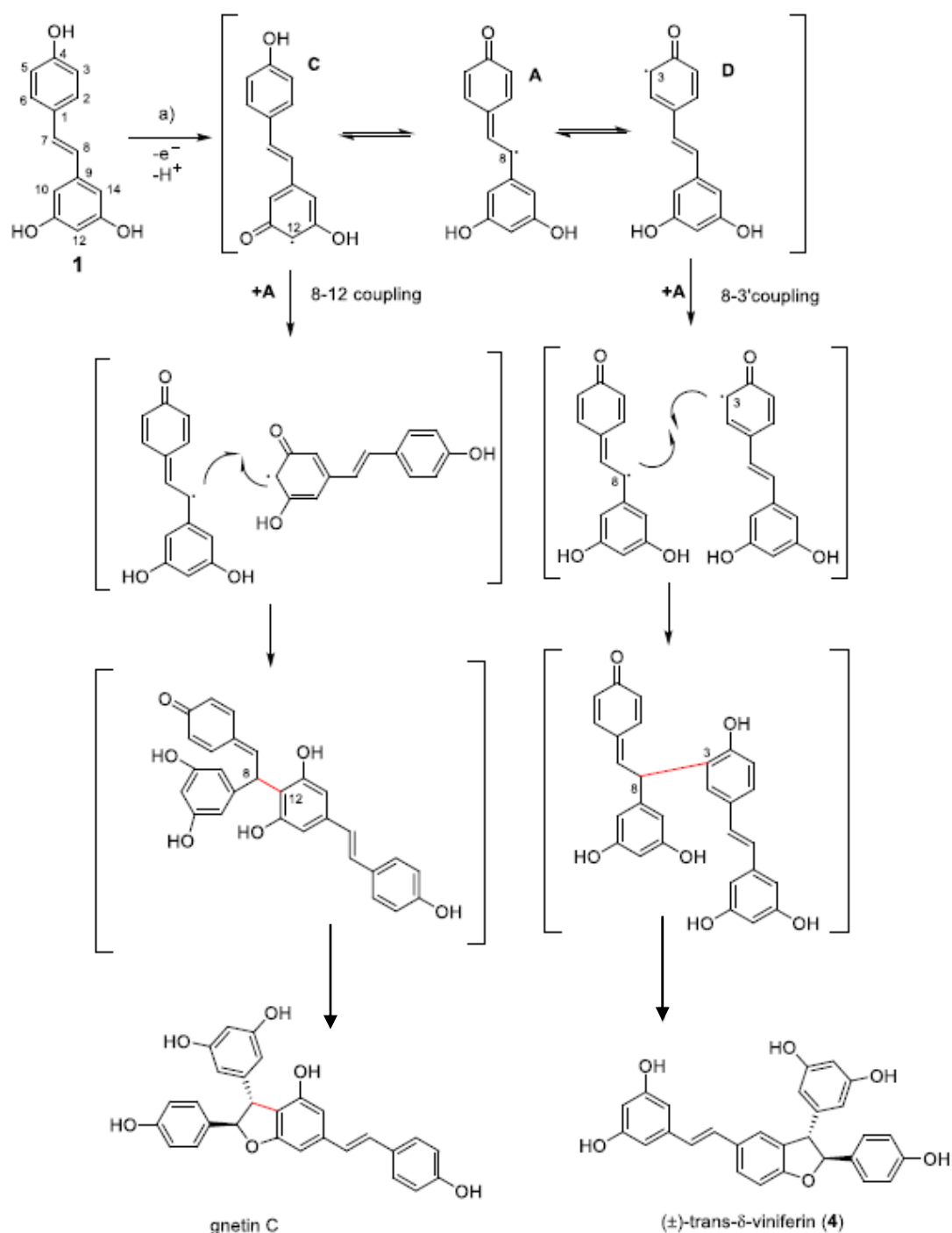


Figure 1.8. Proposed mechanism for 8-12 and 8-3' couplings

Dimers can undergo oligomerization in presence of other molecules of resveratrol. Higher order oligomers may derive either from an oxidative

coupling or an intramolecular Friedel-Crafts cyclization. Notably, most oligomers derive from convergent processes of dimerization of dimers and trimers. Usually, oligomerization is the result of intermolecular radical couplings and intramolecular Friedel-Crafts cyclization [66].

Biological activity of natural stilbenoids

Natural stilbenoids, and especially resveratrol, have been deeply studied in the last decades to elucidate their biological activities, which include antioxidant, antibacterial, antifungal, antiviral, antidiabetic, anti-cancer, neuroprotective, anti-inflammatory, and immunomodulatory properties [67]. Despite the high number of clinical studies highlighting the beneficial effects of this class of molecules, the elucidation of their mechanism(s) of action is far from being complete. Strategies for the identification of stilbenoids molecular targets will be discussed in the following chapters. Hereafter the main biological properties of stilbenoids are summarized.

Antioxidant activity

Natural polyphenolic stilbenoids are well known for their antioxidant properties. Their ability to scavenge reactive oxygen species (ROS) – which are capable of damaging DNA, lipids, carbohydrates, and proteins - is the basis of many of their beneficial effects, such as cardioprotective, neuroprotective, anticancer and antidiabetic activity. Stilbenoids scavenging activity can be exerted in multiple ways:

- hydrogen atom transfer (HAT), through which a phenol ring donates a hydrogen atom to a radical species $R\cdot$ becoming a free radical $ArO\cdot$, stabilized through electron delocalization on the aromatic ring. The weaker the O-H bond, the easier the H-transfer [90];
- single electron transfer (SET): in this case, the polyphenolic stilbenoid $ArOH$ transfers a single electron to a radical species, becoming $ArOH\cdot^+$. The process is driven by the ionization potential (IP) of the polyphenol: the lower the IP, the easier the electron transfer [91].

The antioxidant activity is affected by the position of hydroxyl groups: the *meta*-hydroxy group is less effective in radical scavenging than the *para*-hydroxy group. The methylation of hydroxyl groups compromises the antioxidant efficacy [92]. Moreover, stilbenoids show the ability to chelate metal ions necessary for the formation of hydroxyl radicals (iron, copper, manganese, magnesium), and to inhibit those enzymes involved in ROS formation, namely xanthine oxidase and protein kinase C. Notably, in oxidative conditions, the

presence of a catechol motif on the stilbenoid scaffold (see piceatannol) can lead to the formation of *ortho*-quinones, highly reactive species able to intervene in Dies-Alder type reactions, or to give nucleophilic addition with DNA and proteins [93]. Therefore, in some cases polyphenolic stilbenoids can show pro-oxidant activity.

Anti-inflammatory activity

Stilbenoids have been used for a long time for the treatment of infection-related disease (e.g. stomachache, arthritis, hepatitis, skin inflammation) [94]. Inflammation represents the physiological response to tissue injury and pathogens invasion, and it is characterized by the activation of immune cells (macrophages, leukocytes, neutrophils, and mast cells) leading to the release of inflammation mediators such as cytokines (TNF- α , interleukins), histamine, nitric oxide, leukotrienes, and prostaglandins. Inflammatory mediators activate several transcription factors, such as NF- κ B, NFAT (nuclear factor of activated T-cells), Nrf2 (nuclear factor erythroid 2-related factor 2), AP-1 (activator protein1), as well as several enzymes including IKK (I kappa B kinase), iNOS (inducible nitric oxide synthase), COX-2 (cyclooxygenase 2) and 5-LOX (lipoxygenase) [95]. The anti-inflammatory activity of stilbenoids relies indeed on the interference with activated transcription factors and enzymes. For instance, resveratrol was found to inhibit COX-2, NF- κ B nuclear translocation and transcriptional activity, MAPKs, AP-1 protein expression, STAT-1 (signal transducer and activator of transcription) activity and phosphorylation, cytokines, and matrix metalloproteinases production, while activating SIRT1, a human NAD-dependent acetylase promoting cell survival and cell repair and delaying cell apoptosis [94]. Almost the same inflammation mediators are affected by piceatannol and pterostilbene, which also inhibit iNOS, TNF- α , and several interleukins. Notably, the presence of the catechol motif on piceatannol seems to enhance the antioxidant and anti-inflammatory properties, due to the formation of semiquinone radicals, while complete methylation of hydroxyl groups leads to the loss of anti-inflammatory activity. Among oligostilbenoids, ϵ -viniferin was found to inhibit TNF- α and IL-6 [96], while α -viniferin showed significant anti-inflammatory properties inhibiting COX-2 and interfering with ERK-mediated STAT-1 activation, PGE2 production, NO release, and NF- κ B activation [97,98].

Anti-cancer activity

Chemo-preventive and anti-cancer properties of resveratrol and derivatives have been widely studied in the last decades and, in most cases, they have been

associated with polyphenolic stilbenoids ability to scavenge ROS. Moreover, different cellular mechanisms have been discovered, including, among others:

- inhibition of tumor-associated macrophages (TAMs), that are activated by cancer cells to stimulate the production of inflammatory cytokines;
- interference with the vascular endothelial grow factor (VEGF) pathway, leading to the inhibition of angiogenetic processes;
- inhibition of the production of pro-inflammatory interleukins, as TGF- α , IL-1, IL-6, IL-8, CXCR4, CXCL12 and monocyte-chemotactic protein 1 (MCP-1), also through inhibition of tumor-related fibrosis [68,99,100];
- inhibition of specific cytochrome P450 isoforms, hindering cancer initiation process;
- induction of phase II metabolism of carcinogens, facilitating their elimination from the body [101,102];
- activation of Nfr-2 transcription factor, followed by Nfr-2translocation into the nucleus and induction of antioxidant gene expression. This leads to increased apoptosis and reduced cancer cells proliferation [103].

In the last decades, the role of natural stilbenoids in specific cancer types has been deeply investigated. For instance, it has been demonstrated that resveratrol inhibits cancer cell growth in ER-positive and negative breast cancer by interfering with G1/S and G2/M stages of cell cycle. Moreover, it showed the ability to inhibit breast cancer cells migration and invasion by inducing apoptosis [104]. Stilbenoids showed encouraging results also towards prostatic cancer, whose aggressiveness is strongly dependent on the increased expression of metastasis-associated protein 1 (MTA1), due to their ability to interfere with it, by inhibiting its expression, disrupting MTA1/histone deacetylase complex, reducing MTA1-mediated inflammation, cell survival and metastasis [105]. Pterostilbene displayed superior MTA1 inhibitory activity compared to resveratrol, suggesting that resveratrol analogues with improved pharmacokinetics have higher pharmacological potency. Moreover, it was found that resveratrol dimer gnetin C downregulates MTA1 more potently than resveratrol and pterostilbene [106]. Also piceatannol showed promising activity in breast and prostate cancer through inhibition of matrix metalloproteinase (MMP)-9, and metastasis reduction [107]. Other oligomers, as α -viniferin and ϵ -viniferin, showed anti-epithelial mesenchymal transition (EMT) effects in TGF- β 1 or IL-1 β non-small cell lung cancer [108].

Antibacterial activity

As previously highlighted, one of the main functions of stilbenoids in nature is plant protection. Plant phytoalexins are specifically produced in presence of

microbial infections with the function of resisting pathogens, which makes them intriguing potential antimicrobial agents. The antimicrobial properties of resveratrol have been comprehensively summarized by Vestergaard and Ingmer in a review published in 2019. The authors described resveratrol's ability to bind ATP synthase, leading to reduced cellular energy and inhibited cell proliferation. Resveratrol also suppresses the gene encoding the filamentous temperature-sensitive protein (FtsZ), crucial in bacterial cell division, and it has been associated with membrane damage on certain bacterial species [109]. Moreover, resveratrol displayed the ability to cleave DNA, thanks to its *para* hydroxy group and the extensive electron conjugation conferred by the presence of the olefinic bridge [110]. Studies on other monomeric stilbenoids emphasized the impact of the number and position of hydroxyl groups in enhancing antibacterial activity. In a recent work published by our group, the antibacterial activity of natural monomeric and dimeric stilbenoids was assessed on a panel of nine foodborne pathogens (*L. monocytogenes*, *S. aureus*, *E. faecium*, *E. faecalis*, *P. aeruginosa*, *E. coli*, *S. enterica*, *P. hauseri*). Notably, among the tested monomers pterostilbene and its regioisomer DMHS (**Figure 1.6a**) displayed good antibacterial activity (MICs of 4 $\mu\text{g/mL}$ and 64 $\mu\text{g/mL}$, respectively) against *S. aureus*, while *gram* negative *P. aeruginosa* showed reduced susceptibility to all the tested compounds, probably due to the presence of the outer cellular membrane constituted by lipopolysaccharide. Resveratrol, in contrast, did not show antibacterial activity, suggesting that the partial methylation of hydroxyl groups is essential for achieving the biological activity, maybe due to a more efficient penetration inside the cell or due to slower metabolization, resulting in higher bioavailability. Among dimers, δ -viniferin, pallidol, ϵ -viniferin and dehydro- δ -viniferin displayed relevant activity on *S. aureus*, with MIC values of 16, 64, 16 and 2 $\mu\text{g/mL}$, respectively, which were much lower than that of the parent compound resveratrol (512 $\mu\text{g/mL}$). Nevertheless, the bioactivity against *P. aeruginosa* was still modest (MICs 128–256 $\mu\text{g/mL}$). Further investigations with TEM analysis clarified that the antibacterial effect of the most active compounds was due to severe cell membrane damage, resulting in the disruption of the phospholipid bilayer and leakage of intracellular content. However, it is not likely that the bactericidal activity is attributable exclusively to one specific mechanism, and additional targets might exist in the cell (e.g. inhibition of the metabolic activity, DNA cleavage, inhibition of biofilm formation) [72,110]. Interestingly, also for resveratrol oligomers, the partial methylation of hydroxyl groups seems to have an impact on the biological activity. Righi and co-workers exploited the protein secretome of *Botrytis cinerea* to perform the biotransformation of a mixture of resveratrol and pterostilbene, achieving a variety of unusually methoxylated

compounds, whose antibacterial activity was assessed on *P. aeruginosa* and methicillin-resistant *S. aureus*. While no activity was displayed towards *P. aeruginosa*, the results on *S. aureus* shed light on the positive impact of a partially methylated substitution pattern. Most of the produced compounds showed antibacterial activity, being *O*-dimethyl-*trans*- δ -viniferins the most active compounds, with MICs values of 4 and 2 μ M respectively (**Figure 1.9**). It is noteworthy that the MIC of the corresponding fully hydroxylated compound δ -viniferin was only 35 μ M. On the other hand, a higher degree of methylation caused a significant loss of activity, as for pterostilbene dihydrodimer. Therefore, both the number and the position of the methoxy groups are relevant in determining the antibacterial activity [111,112].

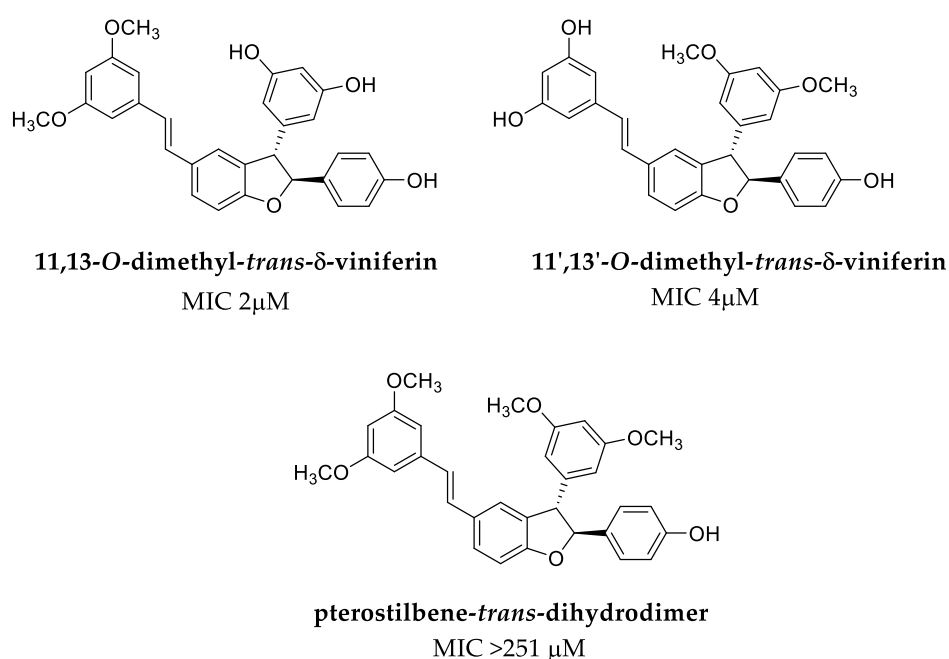


Figure 1.9. Partially methylated dimers, from Righi and co-workers [111].

Multiple cellular mechanisms seem to be involved in oligomers antibacterial activity. To give an example, δ -viniferin was associated with ABC transporters downregulation and inhibition of DNA gyrase [113], while ϵ -viniferin, α -viniferin, and vitisin A have shown antibiofilm activity [114–116]. Compounds like (-)-hopeaphenol and benzofuran-containing resveratrol dimers were found to act as antivirulence agents by inhibiting the type 3 secretion system (T3SS) in *gram*-negative pathogens [117,118]. Nevertheless, the understanding of stilbenoids' mechanisms of action is still incomplete, and further studies in this field are needed to exploit the whole potential of this class of phytoalexins for the production of new effective antibacterial agents.

Antifungal activity

Stilbenoids' antifungal activity was first described in 1977 by Langcake and Pryce, who highlighted the higher antifungal effect of α -viniferin and ϵ -viniferin against *B. cinerea*, compared to that of resveratrol, suggesting that the latter should not be considered a phytoalexin, but rather a biosynthetic precursor of viniferins. Nonetheless, the antifungal activity of resveratrol and its analogues was evaluated in several studies in the past decades, showing the antifungal potential of monomeric stilbenoids toward different phytopathogenic fungi (including *Pyricularia oryzae*, *Plasmopara viticola*, *Cladosporium cucumerinum*, *Sphaeropsis sapinea* and *Phytophthora capsici*, *P. colocasiae*, *Botrytis cinerea*, among others) [119–121]. Although resveratrol lacks activity towards human fungal pathogen *C. albicans*, it displayed synergistic anticandidal activity when administered in combination with azoles (i.e. ketoconazole and itraconazole). Besides reducing azoles dosage, resveratrol was able to increase azoles susceptibility in different *Candida* strains, including three fluconazole-resistant strains [122]. Antifungal activity against *Candida albicans* was found for pterostilbene, that inhibits *in vitro* biofilm formation [123]. Other mechanisms of action have been proposed, including the inhibition of fungal tyrosinases [124,125] and fungal cell respiration [126]. Moreover, a positive correlation between antifungal activity and hydrophobicity has been identified, suggesting, for instance, that the methyl groups of pterostilbene confer increased biological activity due to higher LogP and increased diffusion through the cytoplasmatic membrane [127,128]. In a recent work from our group, a panel of eight monomeric and dimeric stilbenoids was assayed on 19 wild strains of filamentous fungi and yeasts, showing moderate antifungal activity. 3'-Hydroxy-pterostilbene and piceatannol, as well as dimeric stilbenoids (\pm)-*trans*- δ -viniferin and pallidol resulted active on mycotoxigenic fungi. The biological activity varied depending on the fungal strain (higher activity against *Aspergillus* spp., *Penicillium* spp. and *F. verticillioides*), and on the chemical structure of the tested compounds, although it was not possible to draw a direct correlation between structural features and bioactivity [73,129]. All this considered, the design of novel derivatives with improved bioactivity, as well as of hybrid compounds containing the privileged stilbenoid scaffold need to be further explored.

1.2.3. Strobilurins

Among secondary metabolites produced by living organisms, strobilurins represent an extremely important class of molecules, due to the wide

application they found as fungicides worldwide. Indeed, strobilurins are the first example of natural fungicides belonging to the class of quinone outside inhibitors (QoI), which act on the *bc1* complex (or complex III) of the mitochondrial respiratory chain. Strobilurins interaction with their target prevents the electron transport in complex III, inhibiting cell respiration and eventually causing fungal cell death [130,131]. The *bc1* complex is a key intermediate in the chain of respiratory enzymes that catalyzes the electron transfer from hydroquinone to cytochrome *c*, converting the energy of this redox reaction into a chemiosmotic membrane potential, thanks to the translocation of $2e^-$ and $4H^+$ across the membrane (**Figure 1.10**). There are two quinone reaction site: the Q_o center, where hydroquinone oxidation takes place, while $2e^-$ are transferred by a high-potential route via the FeS protein and cytochrome *c*₁ to reduce cytochrome *c*; the Q_i center, that receives $2e^-$ from the Q_o site, through a low-potential route paved by cytochromes *b_H* and *b_L* and eventually catalyzes quinone reduction. Strobilurins bind the Q_o center, without displacing quinone, but probably causing conformational rearrangements leading to changes in the ubiquinone relative position at the Q_o site and inhibition of the electron transfer to FeS protein [132]. This process blocks the generation of ATP, leading to cell death. Most of the QoIs, including strobilurins, carry a β -methoxyacrylate (MOA) as a structural fragment and were therefore termed at first MOA-inhibitors [130,133].

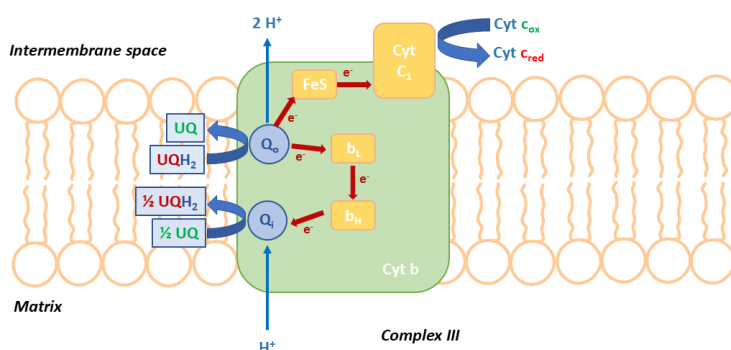


Figure 1.10. Schematic model of cytochrome *bc1* complex, from [134]. Three catalytic subunits can be distinguished: (i) cytochrome *b* (*cyt b*) with two *b*-type haems (*b_H* and *b_L*), (ii) the Rieske iron–sulfur protein (FeS) and (iii) cytochrome *c1* (*cyt c1*) with one *c*-type haem. Ubiquinone binding sites Q_i and Q_o , are shown in blue. Red arrows show the electrons pathways.

Strobilurin A and strobilurin B were first isolated in 1977 from the medium and mycelium of the basidiomycete *Strobilurus tenacellus* by Anke and coworkers [23]. Later, many other derivatives were isolated from different fungal strains, as myxothiazol, oudemasins and other strobilurins (C, D, E, F1, F2, G, H, etc., **Figure 1.11**). These compounds are characterized by the presence of the β -methoxyacrylate fragment (as ester or amide) linked to an α - or β - carbon to the

phenylpentadienyl chain or a similar aliphatic backbone. Differences rely on the number of double bonds within the backbone, and on the substitution pattern on the aromatic ring and/or on the aliphatic chain [135].

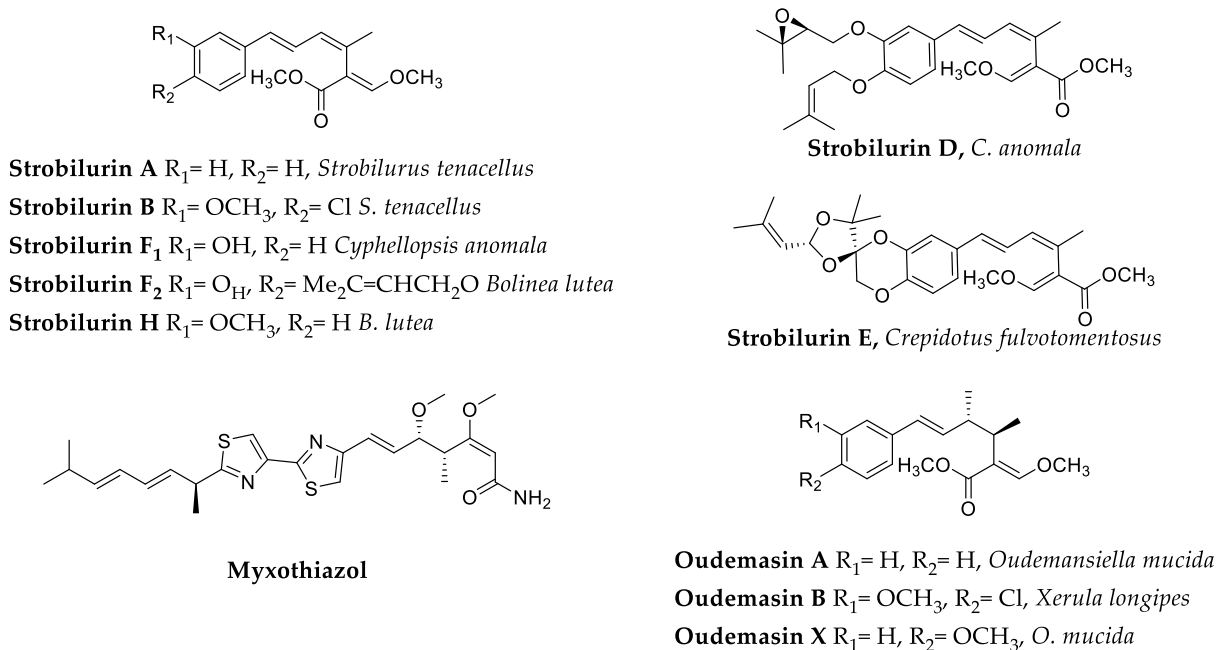


Figure 1.11. Strobilurins and other derivatives isolated from various fungal strains.

The β -methoxyacrylate (BMA) is a key portion of the toxicophore responsible for the interaction with the molecular target (cyt *bc1* complex). On the other hand, the phenylpentadienyl portion confers lipophilicity to the molecule, allowing the transport of the pharmacophore into the quinone center and its insertion on the Q_o center cavity [136]. Moreover, the β -methoxyacrylate portion does not seem to affect the stability – and particularly, the photostability - of the whole molecule, which depends most on the structural features of the backbone. Due to its ability to interfere with the redox processes involved in cellular respiration, β -methoxyacrylate confers activity towards a broad spectrum of species, not only fungi, but also insects, acarids and nematodes. Nevertheless, strobilurins showed relatively low toxicity for terrestrial animals. For instance, strobilurin A showed antifungal activity against a large variety of strains, including *Candida albicans*, *C. crusei*, *C. parapoilosis*, *C. tropicalis*, *Cryptococcus neoformans*, *Trichophyton mentagrophytes*, *Epidermophyton floccosum*, and *Microsporum canis*, displaying good potency *in vitro* (MIC values between 0.1 – 12.8 mg/ml). However, when employed in greenhouse studies, it is almost inactive, probably due to its low photochemical stability and its high volatility, that prevents its use as pesticide in agriculture [135]. Such disadvantages are common to almost all the MOA inhibitors and prompted scientists – both in

academia and industry – to improve strobilurin structure to achieve higher stability and potency. Due to their high fungicidal potential, strobilurins not only have been deeply studied, but they also have become a milestone in the crop-protection fungicides market. However, the spread of resistance phenomena keeps hampering their application. In most cases, fungal resistance is given by a point mutation in the gene encoding for cyt *bc1* complex, which leads to a single amino acid substitution as, for example: from phenylalanine to leucine at position 129 (F129L), from glycine to arginine at position 137 (G137R), or from glycine to alanine at position 143 (G143A). The latter is a well-known mutation that hinders QoI interaction with the target, due to the presence of the methyl group of alanine that introduces a severe steric hindrance at the central aromatic ring of synthetic QoIs [137]. G143A mutation has been already detected in approximately 50 different pathogens, including *P. oryzae* [24,138]. Its alarming incidence constantly prompts scientists to find new ways to improve strobilurins biological activity, besides their stability.

Development of synthetic strobilurins for crop protection

The British ICI and the German BASF groups were pioneers in the development of strobilurin synthetic analogues [139]. Although working separately, in the '80s they both proposed, β -methoxyacrylate stilbene (MOAS) as synthetic strobilurin with improved photostability and high potency (IC_{50} 0.04 μ M, that for strobilurin A is 0.11 μ M). As depicted in **Figure 1.12**, MOAS is characterized by the β -methoxyacrylate group, the benzene ring, substituting the original triene system, and an aliphatic side chain. MOAS showed increased stability and efficacy, and thus immediately became the lead compound for synthetic strobilurin analogues.

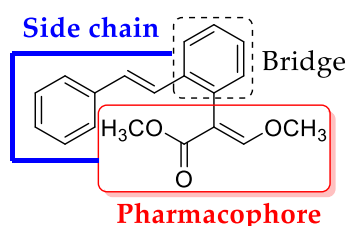


Figure 1.12. Methoxyacrylate stilbene (MOAS) lead structure.

Methoxyacrylate stilbene tolerates different variations in the side chain, as well as various β -methoxyacrylate bioisosters. Synthetic strobilurins bearing heterocycles and ether bridges between two aromatic rings, with improved photostability and lower volatility (such as azoxystrobin, picoxystrobin, pyraclostrobin, and trifloxystrobin, **Figure 1.13**) were designed and commercialized, and they have been largely employed in crop protection in the

past decades for different cultures (e.g. cereals, rice, wine, potato, peanut, and many others).

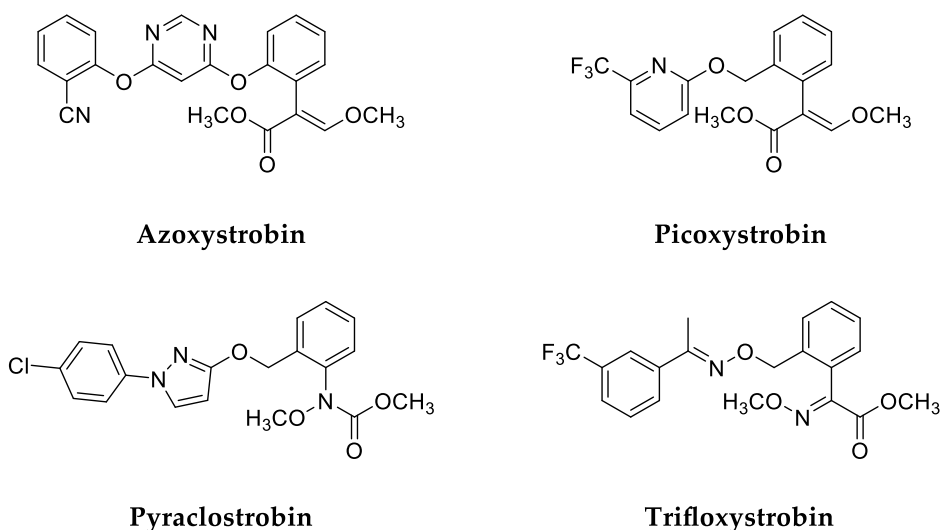


Figure 1.13. Commercial strobilurins

Another example of these attempts is represented by the structural modifications of enoxastrobin, a broad spectrum QoI developed by the Rohm and Haas Company. Tu and co-workers introduced modifications aimed at stabilizing the *E*-styryl bridge through the introduction of oxime ethers featuring heterocyclic moieties (**Figure 1.14**) balancing some physicochemical properties (e.g. lipophilicity and solubility) for optimal uptake and bioavailability. In particular, benzothiophene, benzofuran, and indole analogs were developed [140].

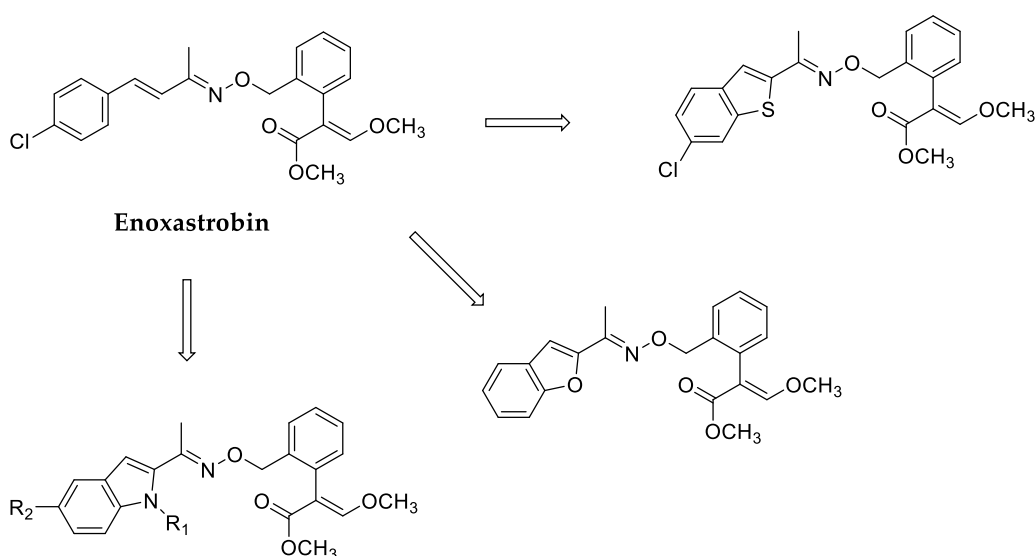


Figure 1.14. Enoxastrobin structural modifications

Once identified the most efficient modifications to improve stability, synthetic efforts focused on the modification of the strobilurin scaffold to bypass resistance phenomena. For this purpose, different approaches were employed in the past years, including biorational or chemorational design, fragment-based drug design (FBDD), and bioisosteric replacement. The combination of the β -methoxyacrylate group with other moieties known for their fungicidal properties was certainly one of the most investigated strategies. In this context, the combination of the key structural features of well-established fungicides with a different mode of action seems a promising approach for the development of innovative antifungal agents able to overcome drug resistance. For instance, various research groups proposed novel strobilurin-like fungicides containing the 1,2,4-triazole ring, a bioactive moiety with a broad-spectrum antifungal activity, due to its ability to inhibit ergosterol biosynthesis preventing cell membrane formation [141]. For instance, Chaudhary and co-workers developed a series of triazole-containing strobilurins that showed antifungal activity comparable to that of azoxystrobin when tested on a panel of phytopathogenic fungi (*F. oxysporum*, *M. oryzae*, *D. oryzae*, *C. neoformans*, *A. fumigatus*). In **Figure 1.15** are reported the most active compound of the series, whose MIC values ranged between 16 and 64 $\mu\text{g/mL}$, close to those of azoxystrobin [142]. A similar work was developed by Liu and co-workers, who combined the strobilurin pharmacophore with 1,2,4-triazole and a furan or a thiophene ring (**Figure 1.15**). Some of the obtained compounds showed antifungal activity higher than that of azoxystrobin when tested on *Physalospora piricola*, *Cercospora arachidicola* Hori, *Rhizotonia cerealis* and *Sclerotinia sclerotiorum* [143].

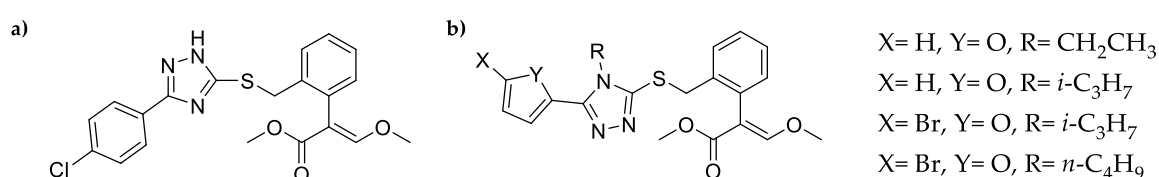


Figure 1.15. a) Lead structures from Chaudhary and co-workers [142]; b) most active compounds proposed by Liu et al. [143]

In coumoxystrobin BMA is connected to α -benzopyrone bicycle typical of coumarins. These are a large family of secondary metabolites produced by plants, fungi, and other microorganisms, which are well known for their biological activities, including antifungal properties [144]. Coumoxystrobin was developed by the Shenyang Research Institute of Chemical Industry and in a recent study it proved to be effective in preventing and curing infections by different strains of *M. oryzae*, with mean $\text{EC}_{50} = 0.0163 \pm 0.0036 \mu\text{g/ml}$ [145]. A

bioisosteric substitution of the coumarin skeleton was proposed by Liu et al., (**Figure 1.16**) who developed a series of quinoline-2(1H)-one containing analogues of coumoxystrobin, employing the Intermediate Derivatization Method for the development of novel agrochemicals, and tested them on a panel of ten phytopathogenic fungi [146]. Indeed, some of the presented quinoline bioisosters displayed *in vitro* inhibitory activity on mycelium growth comparable or even higher – depending on the plant pathogen – than that of the reference compound coumoxystrobin [147].

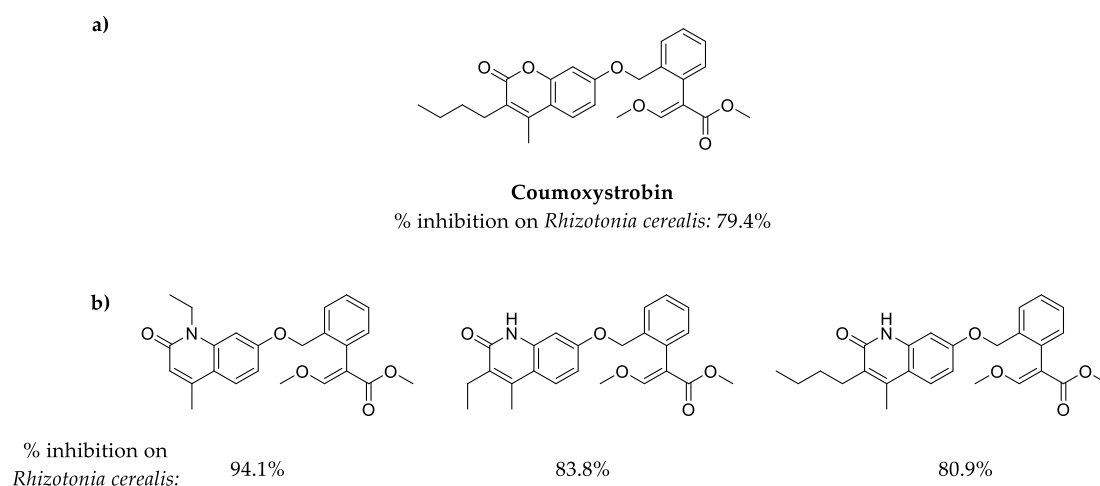
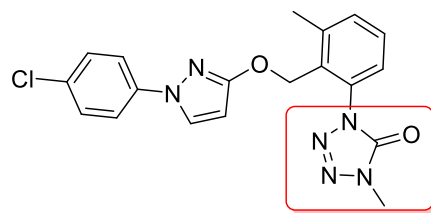


Figure 1.16. a) Structure of coumoxystrobin; b) quinoline-containing bioisosters proposed by Liu et al. [147].

However, it is likely that in presence of the β -methoxyacrylate moiety, such innovative fungicides would adopt the same binding mode of the traditional QoI, which involves interactions with Phe128, Tyr131, Phe274, and Glu271, and the formation of an H-bond between the methoxy group of the BMA moiety and the backbone nitrogen of Glu271. Therefore, when a fungal pathogen develops resistance mechanisms involving a single aminoacid mutation in cyt *bc1* complex (e.g. G143A), even well-designed multi-target agents can lose their antifungal activity, due to the hindered interaction with the molecular target. In this perspective, a convenient strategy for the design of novel agrochemical is represented by the bioisosteric substitution of the BMA toxicophore, to achieve a fruitful binding with the target. A relevant example is represented by metyltetraprole, a new QoI now commercially available with the brand name Pavecto®, whose development was presented in 2020 by Matsuzaki and co-workers. The authors proposed that the optimization of the pharmacophore could reduce the steric hindrance between the methyl group of alanine and the aromatic bridge of QoI by changing the angle and position of the latter, and possibly preventing steric clashes.



Metyltetraprole

Figure 1.17. Structure of metyltetraprole. Tetrazolinone pharmacophore is highlighted in the red box.

Therefore, they proposed as an alternative pharmacophore the tetrazolinone ring, smaller and more rigid than BMA, but still equipped with the carbonyl group required for the interaction with the target. Notably, metyltetraprole (**Figure 1.17**) retained the fungicidal activity when tested on G143A mutant species, paving the way for a new generation of QoIs non-susceptible to fungal resistance [148,149].

1.2.4. Phenolic acids and phenylamides

Plant phytoalexins include a large number of phenolic compounds, including phenolic acids and phenylamides. Hydroxybenzoic, phenylacetic and phenylpropionic acids can be found in edible plants or can be generated by human metabolism after the dietary intake of other phenolic compounds (e.g. flavan-3-ols, flavonols, flavones and anthocyanins) [150]. They display antioxidant [151] and antiproliferative activities and inhibit platelet aggregation [152]. For instance, gallic acid (**Figure 1.18**) can be found in common plants such as guava (*Psidium guajava*), grapes (*Vitis vinifera*), pomegranate (*Punica granatum*), avocado (*Persea americana*), blackcurrant (*Ribes nigrum*), and mango (*Mangifera indica*). Gallic acid is well known for its antioxidant activity [153,154], but other beneficial effects are reported and include anti-inflammatory, anti-platelet, and antineoplastic properties [155]. Antimicrobial activity towards different species (*Salmonella typhimurium*, *Escherichia coli*, *Staphylococcus aureus*, *Listeria innocua*, *Helicobacter pylori*, *Campylobacter* spp., and *Pseudomonas*) was highlighted as well [156]. Other widespread benzoic acids are 2,5-dihydroxy benzoic acid, or gentisic acid, which can be found in citrus fruits (*Citrus* spp.), sesame (*Sesamum indicum*), olive (*Olea europaea*), rose gum (*Eucalyptus grandis*), and Jerusalem artichoke (*Helianthus tuberosus*), and 3,4- dihydroxy benzoic acid, protocatechuic acid, present in garlic, onion, mulberry (*Morus alba*), Japanese pepper (*Zanthoxylum piperitum*), mandarin (*Satsuma mandarin*), sharp-leaf

galangal (*Alpinia oxyphylla*), and buckwheat (*Fagopyrum* spp.). Also in these cases, different biological properties have been identified, as anti-inflammatory, antigenotoxic, hepatoprotective, neuroprotective, antimicrobial, besides antioxidant activity [157]. Vanillic acid (3-methoxy, 4-hydroxy benzoic acid), together with vanillin, is a widely used dietary flavoring agent, which has also been employed as an additive for food preservation, due to its antioxidant and antimicrobial properties towards pathogenic species as *E. coli* and *S. aureus* [158]. Cueva and co-workers evaluated the antimicrobial activity of variously substituted benzoic, phenylacetic and phenylpropionic acids towards gram-positive *S. aureus* and gram-negative *P. aeruginosa*. The latter resulted non-susceptible to the tested compounds, while for *S. aureus* the inhibitory activity changed based on the substitution pattern on the aromatic ring, with inhibition percentage ranging from 33% to 97% [159].

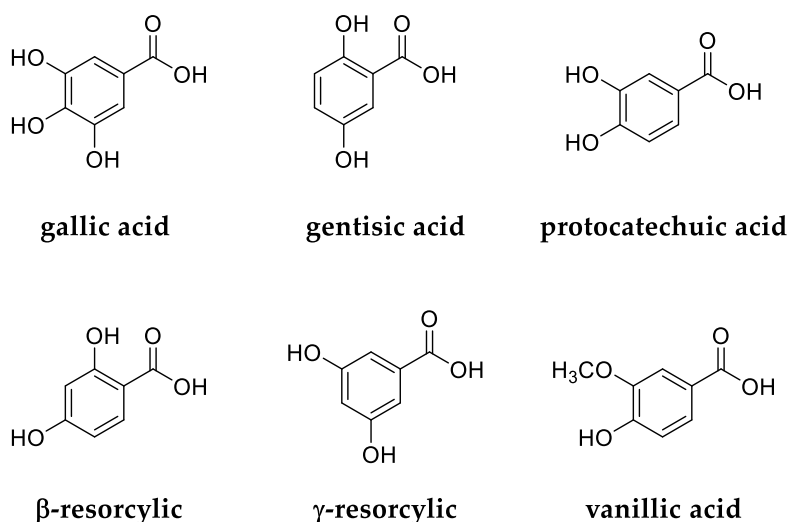


Figure 1.18. Hydroxybenzoic acids

Hydroxycinnamic acids are also produced in plants metabolism along the same biosynthetic pathway as phenylpropanoids, coumarins, lignans, flavonoids, anthocyanins, and stilbenes, and they play a relevant role in plant protection, growth and development [160]. The term “cinnamic” comes from *Cinnamomum zeilanicum*, the cinnamon spice, that has been used since ancient times as a flavoring agent, antiseptic and insecticide. Indeed, nature-derived cinnamic acids as coumaric, caffeic, ferulic, or sinapic acid (**Figure 1.19**) show different biological properties that include, as for hydroxybenzoic acids, antioxidant [161,162], anticancer [163] and antimicrobial activities [164,165].

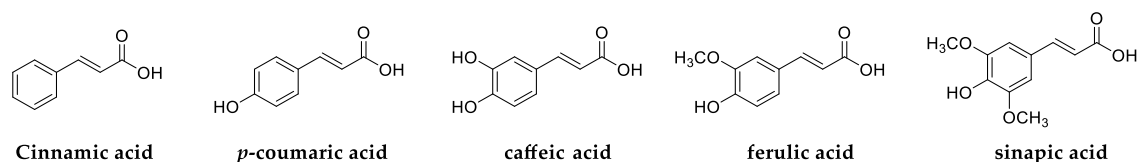


Figure 1.19. Cinnamic acids

Plant metabolism also provides hydroxybenzoyl- and hydroxycinnamoyl-amides, collectively named phenylamides, that are specifically produced in small quantities in presence of biotic or abiotic stress. These compounds result from the conjugation of acids (*e.g.*, benzoic, cinnamic, caffeic, ferulic and *p*-coumaric acid) with aryl-monoamines such as tyramine, tryptamine, and serotonin [166]. Obviously, also their biosynthesis exploits the phenylpropanoid pathway, involving phenylalanine deamination, giving *trans*-cinnamic acid, followed by its esterification with Coenzyme A (CoA). The final condensation with endogenous amines is catalyzed by different cinnamoyl transferases (CTs), acting on biogenic amines (originated from amino acid metabolism) and various cinnamoyl CoA-thioesters [167]. Notably, it has been demonstrated that genes encoding for CTs – as for example agmatine hydroxycinnamoyl transferases (OsAHT1/2) and tryptamine hydroxycinnamoyl transferases (OsTBT1/2) - are induced in rice plants during *P. oryzae* infection [168], leading to the presence of several phenylamides in rice leaves infected by blast fungus *P. oryzae* and rice brown spot fungus *Bipolaris oryzae*, as *N-p*-coumaroylserotonin (CouSer), *N*-feruloyltryptamine (FerTry), and *N*-feruloylserotonin (FerSer) [169,170]. Georgiev et al. reported the biological activity of caffeoyl-, sinapoyl-, feruloyl-, and cinnamoyl- amides towards *S. pyogenes*, *S. aureus*, *B. subtilis*, *L. monocytogenes* and the fungus *C. albicans*. [171]. Notably, for sinapoyl-tyramine, feruloyl-tryptamine, and feruloyl-dopamine (**Figure 1.20**), antibacterial activity against *S. aureus* was higher than that of the corresponding acid (MIC 62.5 µg/ml versus 125 µg/ml for sinapic acid and ferulic acid).

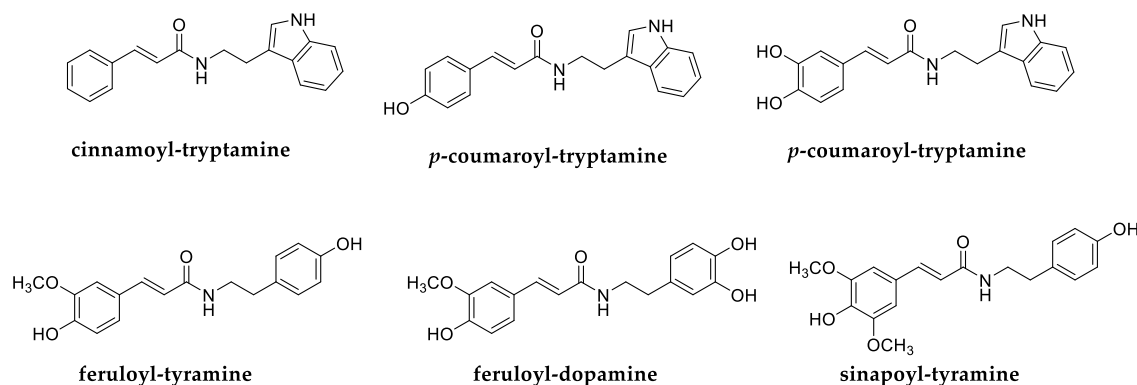


Figure 1.20. Natural phenylamides

Moreover, nature-derived hydroxybenzoyl amides have been synthesized by different research groups showing relevant biological properties. For instance, a set of amides derived from vanillic acid and different aliphatic and aromatic amines were prepared by Oliveira and co-workers and they showed inhibitory activity towards *S. aureus*. Also, all the tested compounds displayed antifungal activity and 14 α -demethylase was proposed as possible target [172]. Amides derived from gallic acid and the isomer 2,3,4-trihydroxybenzoic acid were found to be effective as antivirals against HIV and HCV viruses [173]. It is worth noting that the term “phenylamides” also indicates a group of synthetic fungicides (as benalaxyl, metalaxyl, furalaxyl, and oxadixyl) acting on RNA polymerase I, labelled by the Fungicides Resistance Action Committee as “high risk” for resistance development (www.frac.info). All this considered, natural phenolic acids and phenylamides represent a useful starting point for the design of new antibacterial and/or antifungal agents. Structural modification might afford enhanced bioactivity, reduced risk of resistance development, besides improved chemo-physical properties, as improved hydro-lipophilic balance, leading to higher cell penetration.

1.3. Bibliography

1. Naghavi, M.; Ikuta, K.S.; Swetschinski, L.R.; Robles Aguilar, G.; Sharara, F.; Mestrovic, T.; Gray, A.P.; Davis Weaver, N.; Wool, E.E.; Han, C.; et al. Global mortality associated with 33 bacterial pathogens in 2019: a systematic analysis for the Global Burden of Disease Study 2019. *Lancet* **2022**, *400*, 2221–2248, doi:10.1016/S0140-6736(22)02185-7.
2. Marr, A.K.; Gooderham, W.J.; Hancock, R.E. Antibacterial peptides for therapeutic use: obstacles and realistic outlook. *Curr. Opin. Pharmacol.* **2006**, *6*, 468–472, doi:10.1016/j.coph.2006.04.006.
3. Murray, C.J.; Ikuta, K.S.; Sharara, F.; Swetschinski, L.; Robles Aguilar, G.; Gray, A.; Han, C.; Bisignano, C.; Rao, P.; Wool, E.; et al. Global burden of bacterial antimicrobial resistance in 2019: a systematic analysis. *Lancet* **2022**, *399*, 629–655, doi:10.1016/S0140-6736(21)02724-0.
4. Kirk, M.D.; Pires, S.M.; Black, R.E.; Caipo, M.; Crump, J.A.; Devleeschauwer, B.; Döpfer, D.; Fazil, A.; Fischer-Walker, C.L.; Hald, T.; et al. World Health Organization Estimates of the Global and Regional Disease Burden of 22 Foodborne Bacterial, Protozoal, and Viral Diseases, 2010: A Data Synthesis. *PLoS Med.* **2015**, *12*, 1–21, doi:10.1371/journal.pmed.1001921.
5. Fisher, M.C.; Henk, D.A.; Briggs, C.J.; Brownstein, J.S.; Madoff, L.C.; McCraw, S.L.; Gurr, S.J. Emerging fungal threats to animal, plant and ecosystem health. *Nature* **2012**, *484*, 186–194, doi:10.1038/nature10947.
6. Morales, H.; Marín, S.; Rovira, A.; Ramos, A.J.; Sanchis, V. Patulin accumulation in apples by *Penicillium expansum* during postharvest stages. *Lett. Appl. Microbiol.* **2007**, *44*, 30–35, doi:10.1111/j.1472-765X.2006.02035.x.
7. Luciano-Rosario, D.; Keller, N.P.; Jurick, W.M. *Penicillium expansum*: biology, omics, and management tools for a global postharvest pathogen causing blue mould of pome fruit. *Mol. Plant Pathol.* **2020**, *21*, 1391–1404, doi:10.1111/mpp.12990.
8. Tanahashi, M.; Nakano, T.; Akamatsu, H.; Kodama, M.; Otani, H.; Osaki-Oka, K. *Alternaria alternata* apple pathotype (A. mali) causes black spot of European pear. *Eur. J. Plant Pathol.* **2016**, *145*, 787–795, doi:10.1007/s10658-016-0866-1.
9. Kpodzo, D.S.; Calderwood, M.S.; Ruchelsman, D.E.; Abramson, J.S.; Piris,

- A.; Winograd, J.M.; Kotton, C.N. Primary subcutaneous *Alternaria alternata* infection of the hand in an immunocompromised host. *Med. Mycol.* **2011**, *49*, 543–547, doi:10.3109/13693786.2011.555848.
10. Castaldi, S.; Zorrilla, J.G.; Petrillo, C.; Russo, M.T.; Ambrosino, P.; Masi, M.; Cimmino, A.; Istatico, R. *Alternaria alternata* Isolated from Infected Pears (*Pyrus communis*) in Italy Produces Non-Host Toxins and Hydrolytic Enzymes as Infection Mechanisms and Exhibits Competitive Exclusion against *Botrytis cinerea* in Co-Infected Host Fruits. *J. Fungi* **2023**, *9*, 326. doi:10.3390/jof9030326.
 11. Williamson, B.; Tudzynski, B.; Tudzynski, P.; Van Kan, J.A.L. *Botrytis cinerea*: The cause of grey mould disease. *Mol. Plant Pathol.* **2007**, *8*, 561–580, doi:10.1111/j.1364-3703.2007.00417.x.
 12. Dean, R.; Van Kan, J.A.L.; Pretorius, Z.A.; Hammond-Kosack, K.E.; Di Pietro, A.; Spanu, P.D.; Rudd, J.J.; Dickman, M.; Kahmann, R.; Ellis, J.; et al. The Top 10 fungal pathogens in molecular plant pathology. *Mol. Plant Pathol.* **2012**, *13*, 414–430, doi:10.1111/j.1364-3703.2011.00783.x.
 13. Hua, L.; Yong, C.; Zhanquan, Z.; Boqiang, L.; Guozheng, Q.; Shiping, T. Pathogenic mechanisms and control strategies of *Botrytis cinerea* causing post-harvest decay in fruits and vegetables. *Food Qual. Saf.* **2018**, *2*, 111–119, doi:10.1093/fqsafe/fyy016.
 14. Fernández-Ortuño, D.; Grabke, A.; Li, X.; Schnabel, G. Independent emergence of resistance to seven chemical classes of fungicides in *Botrytis cinerea*. *Phytopathology* **2015**, *105*, 424–432, doi:10.1094/PHYTO-06-14-0161-R.
 15. Kongcharoen, N.; Kaewsalong, N.; Dethoup, T. Efficacy of fungicides in controlling rice blast and dirty panicle diseases in Thailand. *Sci. Rep.* **2020**, *10*, 1–7, doi:10.1038/s41598-020-73222-w.
 16. Pennisi, E. Armed and dangerous. *Science.* **2010**, *327*, 804–805, doi:10.1126/science.327.5967.804.
 17. Hahn, M. The rising threat of fungicide resistance in plant pathogenic fungi: *Botrytis* as a case study. *J. Chem. Biol.* **2014**, *7*, 133–141, doi:10.1007/s12154-014-0113-1.
 18. Sang, H.; Lee, H.B. Molecular mechanisms of succinate dehydrogenase inhibitor resistance in phytopathogenic Fungi. *Res. Plant Dis.* **2020**, *26*, 1–7, doi:10.5423/RPD.2020.26.1.1.
 19. Müller, M.A.; Stammler, G.; May De Mio, L.L. Multiple resistance to DMI, QoI and SDHI fungicides in field isolates of *Phakopsora pachyrhizi*. *Crop Prot.* **2021**, *145*, 105618. doi:10.1016/j.cropro.2021.105618.

20. Fernández-ortuño, D.; Torés, J.A.; De Vicente, A.; Pérez-garcía, A. The QoI Fungicides, the Rise and Fall of a Successful Class of Agricultural Fungicides. *Fungicides* **2010**, 203-220. doi:10.5772/13205.
21. Perlin, D.S.; Rautemaa-Richardson, R.; Alastruey-Izquierdo, A. The global problem of antifungal resistance: prevalence, mechanisms, and management. *Lancet Infect. Dis.* **2017**, 17, e383–e392, doi:10.1016/S1473-3099(17)30316-X.
22. Fisher, M.C.; Hawkins, N.J.; Sanglard, D.; Gurr, S.J. health and food security. **2018**, 742, 739–742.
23. Anke, T.; Oberwinkler, F.; Steglich, W.; Schramm, G. The strobilurins - new antifungal antibiotics from the basidiomycete strobilurus tenacellus. *J. Antibiot. (Tokyo)*. **1977**, 30, 806–810, doi:10.7164/antibiotics.30.806.
24. Tenni, D.; Sinetti, A.; Waldner, M.; Torriani, S.F.F.; Romani, M. First report of QoI resistance in Italian population of *Pyricularia oryzae*. *J. Plant Dis. Prot.* **2021**, 128, 1705–1709, doi:10.1007/s41348-021-00494-3.
25. Löscher, W. Single-Target Versus Multi-Target Drugs Versus Combinations of Drugs With Multiple Targets: Preclinical and Clinical Evidence for the Treatment or Prevention of Epilepsy. **2021**, 12, 1–22, doi:10.3389/fphar.2021.730257.
26. Petrovska, B.B. Historical review of medicinal plants' usage. *Pharmacogn. Rev.* **2012**, 6, 1–5, doi:10.4103/0973-7847.95849.
27. Weissman, K.J.; Müller, R. Bioorganic & Medicinal Chemistry A brief tour of myxobacterial secondary metabolism. *Bioorg. Med. Chem.* **2009**, 17, 2121–2136, doi:10.1016/j.bmc.2008.11.025.
28. Wang, C.; Liu, X.; Zhang, P.; Wang, Y.; Li, Z.; Li, X.; Wang, R.; Shang, Z.; Yan, J.; He, H.; et al. *Bacillus licheniformis* escapes from *Myxococcus xanthus* predation by deactivating myxovirescin A through enzymatic glucosylation. *Environ. Microbiol.* **2019**, 21, 4755–4772, doi:10.1111/1462-2920.14817.
29. Bhat, M.A.; Mishra, A.K.; Bhat, M.A.; Banday, M.I.; Bashir, O.; Rather, I.A.; Rahman, S.; Shah, A.A.; Jan, A.T. Myxobacteria as a source of new bioactive compounds: A perspective study. *Pharmaceutics* **2021**, 13, doi:10.3390/pharmaceutics13081265.
30. Herrmann, J.; Fayad, A.A.; Muller, R. Natural products from myxobacteria: novel metabolites and bioactivities. *Nat. Prod. Rep.* **2017**, 34, 135–160, doi:10.1039/c6np00106h.
31. Garcia, R.O.; Krug, D.; Mu, R. Discovering Natural Products from

- Myxobacteria with Emphasis on Rare Producer Strains in Combination with Improved Analytical Methods. *Methods in Enzymology*, **2009**, *458*, 59–91, doi:10.1016/S0076-6879(09)04803-4.
32. Nett, M.; Gabriele, M.K. The chemistry of gliding bacteria. *Nat. Prod. Rep.* **2007**, 1245–1261, doi:10.1039/b612668p.
 33. Kunze, B.; Trowitzsch-kienast, W.; Reichenbach, H.; Hofle, G.; Reichenbach, H. Nannochelins A, B and C, new iron-chelating compounds from *Nannocystis exedens* (myxobacteria). Production, isolation, physico-chemical and biological properties. *Journal of Antibiotics*, **1992**, *45*(2), 147-150.
 34. Nadmid, S.; Plaza, A.;Lauro, G.; Garcia, R.; Bifulco, G.; Müller, R. Hyalachelins A – C, Unusual Siderophores Isolated from the Terrestrial Myxobacterium *Hyalangium minutum*. *Org. Lett.* **2014**, *16*, 4130-4133. dx.doi.org/10.1021/ol501826a
 35. Kunze, B.; Bedorfn, N.; Kohl, W.; Hofle, G.; Reichenbach, H. Myxochelin A, a new iron-chelating compound from *Angiococcus disciformis* (myxobacterales) - Production, isolation, physico-chemical and biological properties. *J. Antibiot. (Tokyo)*. **1989**, *62*(1), 14–17.
 36. Sonnenschein, E.C.; Stierhof, M.; Goralczyk, S.; Vabre, F.M.; Pellissier, L.; Hanssen, K.Ø.; de la Cruz, M.; Díaz, C.; de Witte, P.; Copmans, D.; et al. Pseudochelin A, a siderophore of *Pseudoalteromonas piscicida* S2040. *Tetrahedron* **2017**, *73*, 2633–2637, doi:10.1016/j.tet.2017.03.051.
 37. Frank, N.A.; Széles, M.; Akone, S.H.; Rasheed, S.; Hüttel, S.; Frewert, S.; Hamed, M.M.; Herrmann, J.; Schuler, S.M.M.; Hirsch, A.K.H.; et al. Expanding the myxochelin natural product family by nicotinic acid containing congeners. *Molecules* **2021**, *26*, doi:10.3390/molecules26164929.
 38. Wang, D.G.; Niu, L.; Lin, Z.M.; Wang, J.J.; Gao, D.F.; Sui, H.Y.; Li, Y.Z.; Wu, C. The Discovery and Biosynthesis of Nicotinic Myxochelins from an *Archangium* sp. SDU34. *J. Nat. Prod.* **2021**, *84*, 2744–2748, doi:10.1021/acs.jnatprod.1c00524.
 39. Gaitatzis, N.; Kunze, B.; Müller, R. Novel insights into siderophore formation in myxobacteria. *ChemBioChem* **2005**, *6*, 365–374, doi:10.1002/cbic.200400206.
 40. Krug, D.; Zurek, G.; Revermann, O.; Vos, M.; Velicer, G.J.; Müller, R. Discovering the hidden secondary metabolome of *Myxococcus xanthus*: A study of intraspecific diversity. *Appl. Environ. Microbiol.* **2008**, *74*, 3058–3068, doi:10.1128/AEM.02863-07.
 41. Wolff, W. The isolation, in *Values and personality: An existential psychology*

- of crisis*, **2005**, Grune & Stratton, *8*, 79–80, doi:10.1037/10647-016.
42. Page, W.J.; Tigerstrom, M. V. Aminochelin, a Catecholamine Siderophore Produced by *Azotobacter vinelandii*. *Microbiology* **1988**, *134*, 453–460, doi:10.1099/00221287-134-2-453.
 43. Khodr, H.H.; Hider, R.C.; Duhme-Klair, A.K. The iron-binding properties of aminochelin, the mono(catecholamide) siderophore of *Azotobacter vinelandii*. *J. Biol. Inorg. Chem.* **2002**, *7*, 891–896, doi:10.1007/s00775-002-0375-x.
 44. Gaitatzis, N.; Kunze, B.; Muller, R. In vitro reconstitution of the myxochelin biosynthetic machinery of *Stigmatella aurantiaca* Sg a15: Biochemical characterization of a reductive release mechanism from nonribosomal peptide synthetases. **2001**, *PNAS*, *98*(20), 11136-11141. doi:10.1073/pnas.201167098.
 45. Li, Y.; Weissman, K.J.; Müller, R. Myxochelin biosynthesis: Direct evidence for two- and four-electron reduction of a carrier protein-bound thioester. *J. Am. Chem. Soc.* **2008**, *130*, 7554–7555, doi:10.1021/ja8025278.
 46. Miyanaga, S.; Sakurai, H.; Saiki, I.; Onaka, H.; Igarashi, Y. Synthesis and evaluation of myxochelin analogues as antimetastatic agents. *Bioorganic Med. Chem.* **2009**, *17*, 2724–2732, doi:10.1016/j.bmc.2009.02.040.
 47. Schieferdecker, S.; König, S.; Pace, S.; Werz, O.; Nett, M. Myxochelin-Inspired 5-Lipoxygenase Inhibitors: Synthesis and Biological Evaluation. *ChemMedChem* **2017**, *12*, 23–27, doi:10.1002/cmdc.201600536.
 48. Kurth, C.; Kage, H.; Nett, M. Siderophores as molecular tools in medical and environmental applications. *Org. Biomol. Chem.* **2016**, *14*, 8212–8227, doi:10.1039/c6ob01400c.
 49. Górska, A.; Sloderbach, A.; Marszałł, M.P. Siderophore-drug complexes: Potential medicinal applications of the “Trojan horse” strategy. *Trends Pharmacol. Sci.* **2014**, *35*, 442–449, doi:10.1016/j.tips.2014.06.007.
 50. Avdeef, A.; Sofen, S.R.; Bregante, T.L.; Raymond, K.N. Coordination Chemistry of Microbial Iron Transport Compounds. Stability Constants for Catechol Models of Enterobactin. *J. Am. Chem. Soc.* **1978**, *100*, 5362–5370, doi:10.1021/ja00485a018.
 51. Dean, R.A.; Talbot, N.J.; Ebbole, D.J.; Farman, M.L.; Mitchell, T.K.; Orbach, M.J.; Thon, M.; Kulkarni, R.; Xu, J.R.; Pan, H.; et al. The genome sequence of the rice blast fungus *Magnaporthe grisea*. *Nature* **2005**, *434*, 980–986, doi:10.1038/nature03449.
 52. Wilson, R.A.; Talbot, N.J. Under pressure: Investigating the biology of

- plant infection by *Magnaporthe oryzae*. *Nat. Rev. Microbiol.* **2009**, *7*, 185–195, doi:10.1038/nrmicro2032.
53. Ebbole, D.J. *Magnaporthe* as a model for understanding host-pathogen interactions. *Annu. Rev. Phytopathol.* **2008**, *45*, 437–456, doi:10.1146/annurev.phyto.45.062806.094346.
 54. Couch, B.C.; Fudal, I.; Lebrun, M.H.; Tharreau, D.; Valent, B.; Van Kim, P.; Nottéghem, J.L.; Kohn, L.M. Origins of host-specific populations of the blast pathogen *Magnaporthe oryzae* in crop domestication with subsequent expansion of pandemic clones on rice and weeds of rice. *Genetics* **2005**, *170*, 613–630, doi:10.1534/genetics.105.041780.
 55. Bhadauria, V. Rice blast fungus transcriptomics. *Arch. Phytopathol. Plant Prot.* **2010**, *43*, 723–727, doi:10.1080/03235400802144488.
 56. Shen, Q.; Liang, M.; Yang, F.; Deng, Y.Z.; Naqvi, N.I. Ferroptosis contributes to developmental cell death in rice blast. *New Phytol.* **2020**, *227*, 1831–1846, doi:10.1111/nph.16636.
 57. Dixon, S.J.; Lemberg, K.M.; Lamprecht, M.R.; Skouta, R.; Zaitsev, E.M.; Gleason, C.E.; Patel, D.N.; Bauer, A.J.; Cantley, A.M.; Yang, W.S.; et al. Ferroptosis: An iron-dependent form of nonapoptotic cell death. *Cell* **2012**, *149*, 1060–1072, doi:10.1016/j.cell.2012.03.042.
 58. Dixon, S.J. The role of iron and reactive oxygen species in cell death. **2014**, *10*, 9–17, doi:10.1038/nchembio.1416.
 59. Yang, W.S.; Stockwell, B.R. Ferroptosis: Death by Lipid Peroxidation. *Trends Cell Biol.* **2016**, *26*, 165–176, doi:10.1016/j.tcb.2015.10.014.
 60. Seok, W.; Kim, K.J.; Gaschler, M.M.; Patel, M.; Shchepinov, M.S. Peroxidation of polyunsaturated fatty acids by lipoxygenases drives ferroptosis. *PNAS*, **2016**, *113*(34), E4966–E4975. doi:10.1073/pnas.1603244113.
 61. Giraldo, M.C.; Dagdas, Y.F.; Gupta, Y.K.; Mentlak, T.A.; Yi, M.; Martinez-Rocha, A.L.; Saitoh, H.; Terauchi, R.; Talbot, N.J.; Valent, B. Two distinct secretion systems facilitate tissue invasion by the rice blast fungus *Magnaporthe oryzae*. *Nat. Commun.* **2013**, *4*, 1996. doi:10.1038/ncomms2996.
 62. Niesen, D.B.; Hessler, C.; Seeram, N.P. Beyond resveratrol: A review of natural stilbenoids identified from 2009-2013. *J. Berry Res.* **2013**, *3*, 181–196, doi:10.3233/JBR-130062.
 63. Lu, D.; Zhao, W. Relevant Enzymes, Genes and Regulation Mechanisms in Biosynthesis Pathway of Stilbenes. *J. Bioprocess. Biotech.* **2012**, *2*(3), 1000119. doi:10.4172/2155-9821.1000119.

64. Valletta, A.; Iozia, L.M.; Leonelli, F. Impact of environmental factors on stilbene biosynthesis. *Plants* **2021**, *10*, 1–40, doi:10.3390/plants10010090.
65. Chong, J.; Poutaraud, A.; Hugueney, P. Metabolism and roles of stilbenes in plants. *Plant Sci.* **2009**, *177*, 143–155, doi:10.1016/j.plantsci.2009.05.012.
66. Keylor, M.H.; Matsuura, B.S.; Stephenson, C.R.J. Chemistry and Biology of Resveratrol-Derived Natural Products. **2015**, *115*, 8976–9027. doi:10.1021/cr500689b.
67. Akinwumi, B.C.; Bordun, K.A.M.; Anderson, H.D. Biological activities of stilbenoids. *Int. J. Mol. Sci.* **2018**, *19*, 1–25, doi:10.3390/ijms19030792.
68. Berretta, M.; Bignucolo, A.; Di Francia, R.; Comello, F.; Facchini, G.; Ceccarelli, M.; Iaffaioli, R.V.; Quagliariello, V.; Maurea, N. Resveratrol in cancer patients: From bench to bedside. *Int. J. Mol. Sci.* **2020**, *21*, doi:10.3390/ijms21082945.
69. Weiskirchen, S.; Weiskirchen, R. Resveratrol: How much wine do you have to drink to stay healthy? *Adv. Nutr.* **2016**, *7*, 706–718, doi:10.3945/an.115.011627.
70. Jayaprakash, J.S.; Gowda, D. V.; Kulkarni, P.K. Therapeutic application of resveratrol in human diseases. *Int. J. Res. Pharm. Sci.* **2020**, *11*, 1447–1456, doi:10.26452/ijrps.v11i2.2017.
71. Mattio, L.M.; Catinella, G.; Dallavalle, S.; Pinto, A. Stilbenoids: A natural arsenal against bacterial pathogens. *Antibiotics* **2020**, *9*, 1–40, doi:10.3390/antibiotics9060336.
72. Mattio, L.M.; Dallavalle, S.; Musso, L.; Filardi, R.; Franzetti, L.; Pellegrino, L.; D’Incecco, P.; Mora, D.; Pinto, A.; Arioli, S. Antimicrobial activity of resveratrol-derived monomers and dimers against foodborne pathogens. *Sci. Rep.* **2019**, *9*, 1–13, doi:10.1038/s41598-019-55975-1.
73. Mattio, L.; Catinella, G.; Iriti, M.; Vallone, L. Inhibitory activity of stilbenes against filamentous fungi. *Ital. J. Food Saf.* **2021**, *10*, 17–20, doi:10.4081/ijfs.2021.8461.
74. Mattio, L.M.; Catinella, G.; Pinto, A.; Dallavalle, S. Natural and nature-inspired stilbenoids as antiviral agents. *Eur. J. Med. Chem.* **2020**, *202*, 112541, doi:10.1016/j.ejmech.2020.112541.
75. Lin, W.S.; Leland, J.V.; Ho, C.T.; Pan, M.H. Occurrence, Bioavailability, Anti-inflammatory, and Anticancer Effects of Pterostilbene. *J. Agric. Food Chem.* **2020**, *68*, 12788–12799, doi:10.1021/acs.jafc.9b07860.
76. Kim, H.; Seo, K.H.; Yokoyama, W. Chemistry of Pterostilbene and Its Metabolic Effects. *J. Agric. Food Chem.* **2020**, *68*, 12836–12841,

doi:10.1021/acs.jafc.0c00070.

77. He, J.L.; Dong, X.H.; Li, Z.H.; Wang, X.Y.; Fu, Z.A.; Shen, N. Pterostilbene inhibits reactive oxygen species production and apoptosis in primary spinal cord neurons by activating autophagy via the mechanistic target of rapamycin signaling pathway. *Mol. Med. Rep.* **2018**, *17*, 4406–4414, doi:10.3892/mmr.2018.8412.
78. Matsuura, B.S.; Keylor, M.H.; Li, B.; Lin, Y.; Allison, S.; Pratt, D.A.; Stephenson, C.R.J. A Scalable Biomimetic Synthesis of Resveratrol Dimers and Systematic Evaluation of their Antioxidant Activities. *Angew. Comm.* **2015**, *54*, 3754–3757, doi:10.1002/anie.201409773.
79. Langcake, P.; Pryce, R.J. The production of resveratrol by *Vitis vinifera* and other members of the *Vitaceae* as a response to infection or injury. *Physiol. Plant Pathol.* **1976**, *9*, 77–86, doi:10.1016/0048-4059(76)90077-1.
80. Oshima, Y.; Ueno, Y.; Hisamichi, K.; Takeshita, M. Ampelopsins F and G, novel bridged plant oligostilbenes from *Ampelopsis brevipedunculata* var. *hancei* roots (*vitaceae*). *Tetrahedron* **1993**, *49*, 5801–5804, doi:10.1016/S0040-4020(01)87946-1.
81. Ducrot, P.H.; Kollmann, A.; Bala, A.E.; Majira, A.; Kerhoas, L.; Delorme, R.; Einhorn, J. Cyphostemmins A-B, two new antifungal oligostilbenes from *Cyphostemma crotalarioides* (*Vitaceae*). *Tetrahedron Lett.* **1998**, *39*, 9655–9658, doi:10.1016/S0040-4039(98)02207-2.
82. Breuil, A. C.; Adrian, M.; Pirio, N. ; Meunier, P. ; Bessis, R., Jeandet, P. Metabolism of stilbene phytoalexins by *Botrytis Cinerea*: characterization of a Resveratrol dehydrodimer, *Tetrahedron Lett.* **1998**, *39*, 537–540.
83. Lins, A.P.; Ribeiro, M.N.D.S.; Gottlieb, O.R.; Gottlieb, H.E. Gnetins: Resveratrol oligomers from *Gnetum* species. *J. Nat. Prod.* **1982**, *45*, 754–761, doi:10.1021/np50024a022.
84. Huang, K.S.; Lin, M.; Cheng, G.F. Anti-inflammatory tetramers of resveratrol from the roots of *Vitis amurensis* and the conformations of the seven-membered ring in some oligostilbenes. *Phytochemistry* **2001**, *58*, 357–362, doi:10.1016/S0031-9422(01)00224-2.
85. Ito, J.; Takaya, Y.; Oshima, Y.; Niwa, M. New oligostilbenes having a benzofuran from *Vitis vinifera* “Kyohou.” *Tetrahedron* **1999**, *55*, 2529–2544, doi:10.1016/S0040-4020(99)00039-3.
86. Chand, K.; Rajeshwari; Hiremathad, A.; Singh, M.; Santos, M.A.; Keri, R.S. A review on antioxidant potential of bioactive heterocycle benzofuran: Natural and synthetic derivatives. *Pharmacol. Reports* **2017**, *69*, 281–295, doi:10.1016/j.pharep.2016.11.007.

87. Naik, R.; Harmalkar, D.S.; Xu, X.; Jang, K.; Lee, K. Bioactive benzofuran derivatives: Moracins A-Z in medicinal chemistry. *Eur. J. Med. Chem.* **2015**, *90*, 379–393, doi:10.1016/j.ejmech.2014.11.047.
88. Miao, Y.H.; Hu, Y.H.; Yang, J.; Liu, T.; Sun, J.; Wang, X.J. Natural source, bioactivity and synthesis of benzofuran derivatives. *RSC Adv.* **2019**, *9*, 27510–27540, doi:10.1039/c9ra04917g.
89. Khanam, H.; Shamsuzzaman Bioactive Benzofuran derivatives: A review. *Eur. J. Med. Chem.* **2015**, *97*, 483–504, doi:10.1016/j.ejmech.2014.11.039.
90. Mustafa, S.K.; Oyouni, A.A.W.A.; Aljohani, M.M.H.; Ayaz Ahmad, M. Polyphenols more than an antioxidant: Role and scope. *J. Pure Appl. Microbiol.* **2020**, *14*, 47–61, doi:10.22207/JPAM.14.1.08.
91. Quideau, S.; Deffieux, D.; Douat-Casassus, C.; Pouységu, L. Plant polyphenols: Chemical properties, biological activities, and synthesis. *Angew. Chemie - Int. Ed.* **2011**, *50*, 586–621, doi:10.1002/anie.201000044.
92. He, S.; Yan, X. From Resveratrol to Its Derivatives: New Sources of Natural Antioxidant. *Curr. Med. Chem.* **2013**, *20*, 1005–1017, doi:10.2174/0929867311320080004.
93. Quideau, S.; Deffieux, D.; Douat-casassus, C.; Pouységu, L. Plant Polyphenols: Chemical Properties, Biological Activities, and Synthesis. *Angew. Chem. Int. Ed.* **2011**, *50*, 586–621, doi:10.1002/anie.201000044.
94. Dvorakova, M.; Landa, P. Anti-inflammatory activity of natural stilbenoids: A review. *Pharmacol. Res.* **2017**, *124*, 126–145, doi:10.1016/j.phrs.2017.08.002.
95. Newton, K.; Dixit, V.M. Signaling in innate immunity and inflammation. *Cold Spring Harb. Perspect. Biol.* **2012**, *4*, a006049, doi:10.1101/cshperspect.a006049.
96. Vion, E.; Page, G.; Bourdeaud, E.; Paccalin, M.; Guillard, J.; Rioux Bilan, A. Trans ϵ -viniferin is an amyloid- β disaggregating and anti-inflammatory drug in a mouse primary cellular model of Alzheimer's disease. *Mol. Cell. Neurosci.* **2018**, *88*, 1–6, doi:10.1016/j.mcn.2017.12.003.
97. Chung, E.Y.; Kim, B.H.; Lee, M.K.; Yun, Y.P.; Lee, S.H.; Min, K.R.; Kim, Y. Anti-inflammatory effect of the oligomeric stilbene α -viniferin and its mode of the action through inhibition of cyclooxygenase-2 and inducible nitric oxide synthase. *Planta Med.* **2003**, *69*, 710–714, doi:10.1055/s-2003-42787.
98. Ha, D.T.; Long, P.T.; Hien, T.T.; Tuan, D.T.; An, N.T.T.; Khoi, N.M.; Oanh, H.; Hung, T.M. Anti-inflammatory effect of oligostilbenoids from *Vitis*

- heyneana* in LPS-stimulated RAW 264.7 macrophages via suppressing the NF- κ B activation. *Chem. Cent. J.* **2018**, *12*, 1–9, doi:10.1186/s13065-018-0386-5.
99. Talib, W.H.; Alsayed, A.R.; Farhan, F.; Al Kury, L.T. Resveratrol and Tumor Microenvironment: Mechanistic Basis and Therapeutic Targets. *Mol. Rev.* **2020**, *25*, 1–25.
 100. Kalluri, R.; Zeisberg, M. Fibroblasts in cancer. *Nat. Rev. Cancer* **2006**, *6*, 392–401, doi:10.1038/nrc1877.
 101. Chang, T.K.H.; Lee, W.B.K.; Ko, H.H. *Trans*-resveratrol modulates the catalytic activity and mRNA expression of the procarcinogen-activating human cytochrome P450 1B1. *Can. J. Physiol. Pharmacol.* **2000**, *78*, 874–881, doi:10.1139/y00-067.
 102. Chun, Y.J.; Oh, Y.K.; Kim, B.J.; Kim, D.; Kim, S.S.; Choi, H.K.; Kim, M.Y. Potent inhibition of human cytochrome P450 1B1 by tetramethoxystilbene. *Toxicol. Lett.* **2009**, *189*, 84–89, doi:10.1016/j.toxlet.2009.05.005.
 103. Alavi, M.; Farkhondeh, T.; Aschner, M.; Samarghandian, S. Resveratrol mediates its anti-cancer effects by Nrf2 signaling pathway activation. *Cancer Cell Int.* **2021**, *21*, 1–9, doi:10.1186/s12935-021-02280-5.
 104. Bhardwaj, A.; Sethi, G.; Vadhan-Raj, S.; Bueso-Ramos, C.; Takada, Y.; Gaur, U.; Nair, A.S.; Shishodia, S.; Aggarwal, B.B. Resveratrol inhibits proliferation, induces apoptosis, and overcomes chemoresistance through down-regulation of STAT3 and nuclear factor- κ B-regulated antiapoptotic and cell survival gene products in human multiple myeloma cells. *Blood* **2007**, *109*, 2293–2302, doi:10.1182/blood-2006-02-003988.
 105. Kumar, A.; Dhar, S.; Campanelli, G.; Butt, N.A.; Schallheim, J.M.; Gomez, C.R.; Levenson, A.S. MTA1 drives malignant progression and bone metastasis in prostate cancer. *Mol. Oncol.* **2018**, *12*, 1596–1607, doi:10.1002/1878-0261.12360.
 106. Kumar, A.; Dholakia, K.; Sikorska, G.; Martinez, L.A.; Levenson, A.S. Mta1-dependent anticancer activity of gnetin c in prostate cancer. *Nutrients* **2019**, *11*, 90–95, doi:10.3390/nu11092096.
 107. Jayasooriya, R.G.P.T.; Lee, Y.G.; Kang, C.H.; Lee, K.T.; Choi, Y.H.; Park, S.Y.; Hwang, J.K.; Kim, G.Y. Piceatannol inhibits MMP-9-dependent invasion of tumor necrosis factor- α -stimulated DU145 cells by suppressing the Akt-mediated nuclear factor- κ B pathway. *Oncol. Lett.* **2012**, *5*, 341–347, doi:10.3892/ol.2012.968.
 108. Chiou, W.; Huang, C.; Lin, Z.; Hong, L.; Lai, Y.; Chen, J.; Huang, H. α -

- Viniferin and ϵ -Viniferin Inhibited TGF- β 1-Induced Epithelial-Mesenchymal Transition, Migration and Invasion in Lung Cancer Cells through Downregulation of Vimentin Expression. *Nutrients*, **2022**, *14*(11), 2294, <https://doi.org/10.3390/nu14112294>.
109. Vestergaard, M.; Ingmer, H. Antibacterial and antifungal properties of resveratrol. *Int. J. Antimicrob. Agents* **2019**, *53*, 716–723, doi:10.1016/j.ijantimicag.2019.02.015.
 110. Ma, D.S.L.; Tan, L.T.H.; Chan, K.G.; Yap, W.H.; Pusparajah, P.; Chuah, L.H.; Ming, L.C.; Khan, T.M.; Lee, L.H.; Goh, B.H. Resveratrol-potential antibacterial agent against foodborne pathogens. *Front. Pharmacol.* **2018**, *9*, 1–16, doi:10.3389/fphar.2018.00102.
 111. Righi, D.; Huber, R.; Koval, A.; Marcourt, L.; Schnee, S.; Le Floch, A.; Ducret, V.; Perozzo, R.; De Ruvo, C.C.; Lecoultre, N.; et al. Generation of Stilbene Antimicrobials against Multiresistant Strains of *Staphylococcus aureus* through Biotransformation by the Enzymatic Secretome of *Botrytis cinerea*. *J. Nat. Prod.* **2020**, *83*, 2347–2356, doi:10.1021/acs.jnatprod.0c00071.
 112. Huber, R.; Marcourt, L.; Héritier, M.; Luscher, A.; Guebey, L.; Schnee, S.; Michellod, E.; Guerrier, S.; Wolfender, J.L.; Scapozza, L.; et al. Generation of potent antibacterial compounds through enzymatic and chemical modifications of the trans- δ -viniferin scaffold. *Sci. Rep.* **2023**, *13*, 1–21, doi:10.1038/s41598-023-43000-5.
 113. Mora-Pale, M.; Bhan, N.; Masuko, S.; James, P.; Wood, J.; Mccallum, S.; Linhardt, R.J.; Dordick, J.S.; Koffas, M.A.G. Antimicrobial mechanism of resveratrol-trans-dihydrodimer produced from peroxidase-catalyzed oxidation of resveratrol. *Biotechnol. Bioeng.* **2015**, *112*, 2417–2428, doi:10.1002/bit.25686.
 114. Yadav, M.K.; Mailar, K.; Masagalli, J.N.; Chae, S.; Song, J.; Choi, W.J. Ruthenium Chloride-Induced Oxidative Cyclization of Trans- Resveratrol to (\pm)- ϵ -Viniferin and Antimicrobial and Antibiofilm Activity Against *Streptococcus pneumoniae*. *Front. Pharmacol.* **2019**, *10*, 1–15, doi:10.3389/fphar.2019.00890.
 115. Yim, N.H.; Ha, D.T.; Trung, T.N.; Kim, J.P.; Lee, S.M.; Na, M.K.; Jung, H.J.; Kim, H.S.; Kim, Y.H.; Bae, K.H. The antimicrobial activity of compounds from the leaf and stem of *Vitis amurensis* against two oral pathogens. *Bioorganic Med. Chem. Lett.* **2010**, *20*, 1165–1168, doi:10.1016/j.bmcl.2009.12.020.
 116. Cho, H.S.; Lee, J.H.; Ryu, S.Y.; Joo, S.W.; Cho, M.H.; Lee, J. Inhibition of *Pseudomonas aeruginosa* and *Escherichia coli* O157:H7 biofilm formation by

- plant metabolite ϵ -viniferin. *J. Agric. Food Chem.* **2013**, *61*, 7120–7126, doi:10.1021/jf4009313.
117. Zetterström, C.E.; Hasselgren, J.; Salin, O.; Davis, R.A.; Quinn, R.J.; Sundin, C.; Elofsson, M. The resveratrol tetramer (-)-hopeaphenol inhibits type III secretion in the gram-negative pathogens *Yersinia pseudotuberculosis* and *Pseudomonas aeruginosa*. *PLoS One* **2013**, *8*, 1–12, doi:10.1371/journal.pone.0081969.
 118. Sundin, C.; Zetterström, C.E.; Vo, D.D.; Brkljača, R.; Urban, S.; Elofsson, M. Exploring resveratrol dimers as virulence blocking agents – Attenuation of type III secretion in *Yersinia pseudotuberculosis* and *Pseudomonas aeruginosa*. *Sci. Rep.* **2020**, *10*, 1–11, doi:10.1038/s41598-020-58872-0.
 119. Adrian, M.; Jeandet, P. Effects of resveratrol on the ultrastructure of *Botrytis cinerea* conidia and biological significance in plant/pathogen interactions. *Fitoterapia* **2012**, *83*, 1345–1350, doi:10.1016/j.fitote.2012.04.004.
 120. Jeandet, P.; Douillet-Breuil, A.C.; Bessis, R.; Debord, S.; Sbaghi, M.; Adrian, M. Phytoalexins from the vitaceae: Biosynthesis, phytoalexin gene expression in transgenic plants, antifungal activity, and metabolism. *J. Agric. Food Chem.* **2002**, *50*, 2731–2741, doi:10.1021/jf011429s.
 121. Kumar, S.N.; Nambisan, B. Antifungal activity of diketopiperazines and stilbenes against plant pathogenic fungi in vitro. *Appl. Biochem. Biotechnol.* **2014**, *172*, 741–754, doi:10.1007/s12010-013-0567-6.
 122. Wang, J.; Zhang, X.; Gao, L.; Wang, L.; Song, F.; Zhang, L.; Wan, Y. The synergistic antifungal activity of resveratrol with azoles against *Candida albicans*. *Lett. Appl. Microbiol.* **2021**, *72*, 688–697, doi:10.1111/lam.13458.
 123. Li, D.D.; Zhao, L.X.; Mylonakis, E.; Hu, G.H.; Zou, Y.; Huang, T.K.; Yan, L.; Wang, Y.; Jiang, Y.Y. In vitro and in vivo activities of pterostilbene against *Candida albicans* biofilms. *Antimicrob. Agents Chemother.* **2014**, *58*, 2344–2355, doi:10.1128/AAC.01583-13.
 124. Schouten, A.; Wagemakers, L.; Stefanato, F.L.; Van der Kaaij, R.M.; Van Kan, J.A.L. Resveratrol acts as a natural profungicide and induces self-intoxication by a specific laccase. *Mol. Microbiol.* **2002**, *43*, 883–894, doi:10.1046/j.1365-2958.2002.02801.x.
 125. Seppänen, S.K.; Syrjälä, L.; Von Weissenberg, K.; Teeri, T.H.; Paajanen, L.; Pappinen, A. Antifungal activity of stilbenes in in vitro bioassays and in transgenic *Populus* expressing a gene encoding pinosylvin synthase. *Plant Cell Rep.* **2004**, *22*, 584–593, doi:10.1007/s00299-003-0728-0.

126. Hart, J.H. Role of Phytostilbenes in Decay and Disease Resistance. *Annu. Rev. Phytopathol.* **1981**, *19*, 437–458, doi:10.1146/annurev.py.19.090181.002253.
127. Caruso, F.; Mendoza, L.; Castro, P.; Cotoras, M.; Aguirre, M.; Matsuhira, B.; Isaacs, M.; Rossi, M.; Viglianti, A.; Antonioletti, R. Antifungal activity of resveratrol against *Botrytis cinerea* is improved using 2-furyl derivatives. *PLoS One* **2011**, *6*, 2–11, doi:10.1371/journal.pone.0025421.
128. Houillé, B.; Papon, N.; Boudesocque, L.; Bourdeaud, E.; Besseau, S.; Courdavault, V.; Enguehard-Gueiffier, C.; Delanoue, G.; Guérin, L.; Bouchara, J.P.; et al. Antifungal activity of resveratrol derivatives against *Candida* Species. *J. Nat. Prod.* **2014**, *77*, 1658–1662, doi:10.1021/np5002576.
129. Chalal, M.; Klinguer, A.; Echairi, A.; Meunier, P.; Vervandier-Fasseur, D.; Adrian, M. Antimicrobial activity of resveratrol analogues. *Molecules* **2014**, *19*, 7679–7688, doi:10.3390/molecules19067679.
130. Von Jagow, G.; Ljungdahl, P.O.; Graf, P.; Ohnishi, T.; Trumpower, B.L. An inhibitor of mitochondrial respiration which binds to cytochrome *b* and displaces quinone from the iron-sulfur protein of the cytochrome *bc1* complex. *J. Biol. Chem.* **1984**, *259*, 6318–6326, doi:10.1016/s0021-9258(20)82143-7.
131. Thierbach, G.; Reichenbach, H. Myxothiazol, a new antibiotic interfering with respiration. *Antimicrob. Agents Chemother.* **1981**, *19*, 504–507, doi:10.1128/AAC.19.4.504.
132. Brandt, U.; Schagger, H.; Von Jagow, G. Characterisation of binding of the methoxyacrylate inhibitors to mitochondrial cytochrome *c* reductase. *Eur. J. Biochem.* **1988**, *173*, 499–506, doi:10.1111/j.1432-1033.1988.tb14026.x.
133. Di Rago, J.P.; Coppée, J.Y.; Colson, A.M. Molecular Basis for Resistance to Myxothiazol, Mucidin (Strobilurin A), and Stigmatellin. *J. Biol. Chem.* **1989**, *264*, 14543–14548, doi:10.1016/s0021-9258(18)71712-2.
134. Musso, L.; Fabbrini, A.; Dallavalle, S. Natural Compound-Derived Cytochrome *bc1* Complex Inhibitors as Antifungal Agents. *Molecules*, **2020**, *25*, 4582, doi:10.3390/molecules25194582.
135. Zakharychev, V. V.; Kovalenko, L. V. Natural compounds of the strobilurin series and their synthetic analogues as cell respiration inhibitors. *Usp. Khim.* **1998**, *67*, 604–605, doi:10.1070/rc1998v067n06abeh000426.
136. Wiggins, T.E. The relationship between structure and activity of the methoxyacrylate toxophore. *Biochem. Soc. Trans.* **1993**, *21*(1), S1, doi:https://doi.org/10.1042/bst021001s.

137. Fisher, N.; Meunier, B. Re-examination of inhibitor resistance conferred by Qo-site mutations in cytochrome b using yeast as a model system. *Pest Manag. Sci.* **2005**, *61*, 973–978, doi:10.1002/ps.1066.
138. Fernández-ortuño, D.; Torés, J.A.; De Vicente, A.; Pérez-garcía, A. The QoI Fungicides, the Rise and Fall of a Successful Class of Agricultural Fungicides. *Fungicides* **2010**, 203-220. doi:10.5772/13205.
139. Sauter, H. Strobilurins and other complex III inhibitors. In *Modern Crop Protection Compounds*; Kramer, W., Schimer, U., Eds.; 2012; pp. 584–627.
140. Tu, S.; Xu, L.H.; Ye, L.Y.; Wang, X.; Sha, Y.; Xiao, Z.T.; Xiao, Z.Y. Synthesis and Fungicidal Activities of Novel Indene-Substituted Oxime Ether Strobilurins. *J. Agric. Food Chem.* **2008**, *56*, 5247–5253.
141. Worthington, P. Sterol biosynthesis inhibiting triazole fungicides. In *Bioactive Heterocyclic Compound Classes: Agrochemicals*; Lamberth, C., Dinges, J., Eds.; **2012**; pp. 129–145.
142. Chaudhary, P.M.; Tupe, S.G.; Jorwekar, S.U.; Sant, D.G.; Deshpande, S.R.; Maybhate, S.P.; Likhite, A.P.; Deshpande, M. V. Synthesis and antifungal potential of 1,2,3-triazole and 1,2,4-triazole thiol Substituted Strobilurin Derivatives. *Indian Journ. of Chem.* **2015**, *54*, 908–917.
143. Liu, Y.; Liu, M.; Zhang, D.; Hua, X.; Wang, B.; Zhou, S.; Li, Z. Design, synthesis and fungicidal activity of novel strobilurin-1,2,4-triazole derivatives containing furan or thiophene rings. *Chem. Res. Chinese Univ.* **2016**, *32*, 952–958, doi:10.1007/s40242-016-6253-9.
144. Annunziata, F.; Pinna, C.; Dallavalle, S.; Tamborini, L.; Pinto, A. An overview of coumarin as a versatile and readily accessible scaffold with broad-ranging biological activities. *Int. J. Mol. Sci.* **2020**, *21*, 1–83, doi:10.3390/ijms21134618.
145. Xin, W.; Mao, Y.; Lu, F.; Li, T.; Wang, J.; Duan, Y.; Zhou, M. In vitro fungicidal activity and in planta control efficacy of coumoxystrobin against *Magnaporthe oryzae*. *Pestic. Biochem. Physiol.* **2020**, *162*, 78–85, doi:10.1016/j.pestbp.2019.09.004.
146. Kalkhambkar, R.G.; Aridoss, G.; Kulkarni, G.M.; Bapset, R.M.; Kadakol, J.C.; Premkumar, N.; Jeong, Y.T. Synthesis and biological studies of some new acrylic acid ethyl esters of quinolinone. *Monatshefte fur Chemie* **2012**, *143*, 1075–1086, doi:10.1007/s00706-011-0692-2.
147. Liu, M.; Liu, Y.; Zhou, S.; Zhang, X.; Yu, S.; Li, Z. Synthesis and antifungal activities of novel strobilurin derivatives containing quinolin-2(1H)-one moiety. *Chem. Res. Chinese Univ.* **2016**, *32*, 600–606, doi:10.1007/s40242-016-6041-6.

148. Matsuzaki, Y.; Yoshimoto, Y.; Arimori, S.; Kiguchi, S.; Harada, T.; Iwahashi, F. Discovery of metyltetraprole: Identification of tetrazolinone pharmacophore to overcome QoI resistance. *Bioorganic Med. Chem.* **2020**, *28*, 115211, doi:10.1016/j.bmc.2019.115211.
149. Suemoto, H.; Matsuzaki, Y.; Iwahashi, F. Metyltetraprole, a novel putative complex III inhibitor, targets known QoI-resistant strains of *Zymoseptoria tritici* and *Pyrenophora teres*. *Pest Manag. Sci.* **2019**, *75*, 1181–1189, doi:10.1002/ps.5288.
150. Aura, A.M. Microbial metabolism of dietary phenolic compounds in the colon. *Phytochem. Rev.* **2008**, *7*, 407–429, doi:10.1007/s11101-008-9095-3.
151. Stevenson, D.E.; Hurst, R.D. Polyphenolic phytochemicals - Just antioxidants or much more? *Cell. Mol. Life Sci.* **2007**, *64*, 2900–2916, doi:10.1007/s00018-007-7237-1.
152. Rechner, A.R.; Kroner, C. Anthocyanins and colonic metabolites of dietary polyphenols inhibit platelet function. *Thromb. Res.* **2005**, *116*, 327–334, doi:10.1016/j.thromres.2005.01.002.
153. Kroes, B.H.; Van Den Berg, A.J.J.; Quarles Van Ufford, H.C.; Van Dijk, H.; Labadie, R.P. Anti-inflammatory activity of gallic acid. *Planta Med.* **1992**, *58*, 499–504, doi:10.1055/s-2006-961535.
154. Badhani, B.; Sharma, N.; Kakkar, R. Gallic acid: A versatile antioxidant with promising therapeutic and industrial applications. *RSC Adv.* **2015**, *5*, 27540–27557, doi:10.1039/c5ra01911g.
155. Wianowska, D.; Olszowy-Tomczyk, M. A Concise Profile of Gallic Acid—From Its Natural Sources through Biological Properties and Chemical Methods of Determination. *Molecules* **2023**, *28*, doi:10.3390/molecules28031186.
156. Sorrentino, E.; Succi, M.; Tipaldi, L.; Pannella, G.; Maiuro, L.; Sturchio, M.; Coppola, R.; Tremonte, P. Antimicrobial activity of gallic acid against food-related *Pseudomonas* strains and its use as biocontrol tool to improve the shelf life of fresh black truffles. *Int. J. Food Microbiol.* **2018**, *266*, 183–189, doi:10.1016/j.ijfoodmicro.2017.11.026.
157. Abedi, F.; Razavi, B.M.; Hosseinzadeh, H. A review on gentisic acid as a plant derived phenolic acid and metabolite of aspirin: Comprehensive pharmacology, toxicology, and some pharmaceutical aspects. *Phyther. Res.* **2020**, *34*, 729–741, doi:10.1002/ptr.6573.
158. Mourtzinos, I.; Konteles, S.; Kalogeropoulos, N.; Karathanos, V.T. Thermal oxidation of vanillin affects its antioxidant and antimicrobial properties. *Food Chem.* **2009**, *114*, 791–797,

doi:10.1016/j.foodchem.2008.10.014.

159. Cueva, C.; Moreno-Arribas, M.V.; Martín-Álvarez, P.J.; Bills, G.; Vicente, M.F.; Basilio, A.; Rivas, C.L.; Requena, T.; Rodríguez, J.M.; Bartolomé, B. Antimicrobial activity of phenolic acids against commensal, probiotic and pathogenic bacteria. *Res. Microbiol.* **2010**, *161*, 372–382, doi:10.1016/j.resmic.2010.04.006.
160. Ververidis, F.; Trantas, E.; Douglas, C.; Vollmer, G.; Kretzschmar, G.; Panopoulos, N. Biotechnology of flavonoids and other phenylpropanoid-derived natural products. Part I: Chemical diversity, impacts on plant biology and human health. *Biotechnol. J.* **2007**, *2*, 1214–1234, doi:10.1002/biot.200700084.
161. Shahidi, F.; Chandrasekara, A. Hydroxycinnamates and their in vitro and in vivo antioxidant activities. *Phytochem. Rev.* **2010**, *9*, 147–170, doi:10.1007/s11101-009-9142-8.
162. Kikuzaki, H.; Hisamoto, M.; Hirose, K.; Akiyama, K.; Taniguchi, H. Antioxidant Properties of Ferulic Acid and Its Related Compounds. *J. Agric. Food Chem.* **2002**, *50*, 2161–2168.
163. Caparica, R.; Julio, A.; Rolim Baby, A.; De Almeida, T. S.; Guilherme Costa, J. In vitro cytotoxicity assessment of ferulic, caffeic and p-coumaric acids on human renal cancer cells. *Biomed. Biophar. Res.* **2020**, *17*(1), 63–74, doi:10.19277/bbr.17.1.225.
164. Guzman, J.D. *Natural cinnamic acids, synthetic derivatives and hybrids with antimicrobial activity*; 2014; Vol. 19; ISBN 5753509509.
165. Boz, H. p-Coumaric acid in cereals: presence, antioxidant and antimicrobial effects. *Int. J. of Food Scie. and Techn.* **2015**, *50*, 2323–2328, doi:10.1111/ijfs.12898.
166. Edreva, A.M.; Velikova, V.B.; Tsonev, T.D. Phenylamides in plants. *Russ. J. Plant Physiol.* **2007**, *54*, 287–301, doi:10.1134/S1021443707030016.
167. Facchini, P.J.; Hagel, J.; Zulak, K.G. Hydroxycinnamic acid amide metabolism: Physiology and biochemistry. *Can. J. Bot.* **2002**, *80*, 577–589, doi:10.1139/b02-065.
168. Fang, H.; Zhang, F.; Zhang, C.; Wang, D.; Shen, S.; He, F.; Tao, H.; Wang, R.; Wang, M.; Wang, D.; et al. Function of hydroxycinnamoyl transferases for the biosynthesis of phenolamides in rice resistance to *Magnaporthe oryzae*. *J. Genet. Genomics* **2022**, *49*, 776–786, doi:10.1016/j.jgg.2022.02.008.
169. Ishihara, A.; Hashimoto, Y.; Tanaka, C.; Dubouzet, J.G.; Nakao, T.; Matsuda, F.; Nishioka, T.; Miyagawa, H.; Wakasa, K. The tryptophan

pathway is involved in the defense responses of rice against pathogenic infection via serotonin production. *Plant J.* **2008**, *54*, 481–495, doi:10.1111/j.1365-313X.2008.03441.x.

170. Ishihara, A.; Nakao, T.; Mashimo, Y.; Murai, M.; Ichimaru, N.; Tanaka, C.; Nakajima, H.; Wakasa, K.; Miyagawa, H. Probing the role of tryptophan-derived secondary metabolism in defense responses against *Bipolaris oryzae* infection in rice leaves by a suicide substrate of tryptophan decarboxylase. *Phytochemistry* **2011**, *72*, 7–13, doi:10.1016/j.phytochem.2010.11.001.
171. Georgiev, L.; Chochkova, M.; Ivanova, G.; Najdenski, H.; Ninova, M. Milkova, T. Radical scavenging and antimicrobial activities of cinnamoyl amides of biogenic monoamines. *RISG*, **2012**, *89*.
172. Santos Oliveira, A.J.D.M.; De Castro, R.D.; Pessôa, H.D.L.F.; Wadood, A.; De Sousa, D.P. Amides Derived from Vanillic Acid: Coupling Reactions, Antimicrobial Evaluation, and Molecular Docking. *Biomed Res. Int.* **2019**, *2019*, doi:10.1155/2019/9209676.
173. Leyssen, P.; Quesada, E.; Jos, M.; Paeshuyse, J.; Balzarini, J.; Neyts, J.; Sanf, A. Linear and branched alkyl-esters and amides of gallic acid and other (mono-, di- and tri-) hydroxy benzoyl derivatives as promising anti- HCV inhibitors. *Eur. J. Med. Chem.* **2015**, *92*, 656–671, doi:10.1016/j.ejmech.2015.01.033.

Chapter 2: Aim of the research project

Despite the considerable advances in the treatment of microbial infections, to date bacterial and fungal pathogens still represent a serious threat for humankind, affecting both public health and agricultural crops. Moreover, in the past decades, the overuse and misuse of antibiotics has led to the progressive adaptation of microbial pathogens to the available treatments. Antimicrobial resistance is an ever-growing phenomenon that urgently needs to be addressed through the identification of innovative bioactive molecules able to bypass pathogens resistance mechanisms, without toxic effects against humans and animals. In the search for novel, resistance-breaking antimicrobials, the rational design of multi-target drugs and agrochemicals should be considered as a strategic tool. Synergistic combinations of bioactive scaffolds able to inhibit multiple targets simultaneously, is expected to provide improved antimicrobial activity, while mitigating the risk of resistance [1]. In this context, the potential of phytoalexins could play a key role. Natural phytoalexins are often endowed with a plethora of biological activities, mediated by different mechanisms of actions and can therefore be referred to as “built-in multi-target directed ligands”. This intrinsic multi-mode activity makes them appealing for the design of hybrid compounds as innovative antimicrobials. In this perspective, a full comprehension of phytoalexins biological activities and mechanisms of action, most of which have not been elucidated yet, would allow their profitable employment for the development of new multi-target drugs and agrochemicals.

The aim of the present Ph.D. project was indeed the identification of naturally occurring bioactive scaffolds for the design of novel, nature-inspired antimicrobial agents.

Four classes of phytoalexins were considered in this project, namely: myxochelins, phenolamides, stilbenoids, and strobilurins. Chemo-enzymatic procedures were developed for the preparation of the most interesting natural compounds and their analogues, whose activities against fungal phytopathogens and bacterial pathogens were evaluated thanks to the collaboration with the research groups of Prof. Andrea Kunova (Department of Food, Environmental and Nutritional Sciences, DeFENS, University of Milan) and Prof. Piera Anna Martino (Department of Biomedical, Surgical and Dental Sciences, DSBCO, One Health Unit, University of Milan), to perform structure-activity relationship (SAR) studies. The investigation was not strictly limited to the antimicrobial activity of natural phytoalexins. Indeed, microbial infections usually stimulate immune response in the host cells, leading to the production of ROS and cytokines. Therefore, the antioxidant and anti-inflammatory properties of certain classes of phytoalexins (i.e. stilbenoids) were also evaluated, to investigate their immunomodulatory activity.

The assessment of antioxidant and anti-inflammatory activities was possible thanks to the collaboration with Prof. Hanne Frøkiær (Department of Veterinary and Animal Sciences, University of Copenhagen).

To further expand the study, a part of the present work was devoted to the identification of stilbenoids' molecular targets in bacterial pathogens. The development of stilbenoids-based affinity probes was accomplished during an 8-months stint abroad, at the Molecular Sciences Institute of the University of Bordeaux, under the supervision of Prof. Stéphane Quideau, and it will be discussed in detail in **Chapter 5.1**. To this purpose, we applied the affinity-based protein profiling (Af-BPP) approach, which represents a valuable tool for target identification studies [2]. This strategy involves the preparation of small molecules chemical probes to identify affinity-based interactions between a selected compound and proteins in cells or cell lysates [3–5].

In the second part of my PhD project I focused on the design of hybrid compounds obtained by merging different bioactive scaffolds, aiming at achieving enhanced biological activity while at the same time bypassing pathogens resistance mechanisms. The rational design of hybrid compounds involved the selection and combination of both natural and synthetic scaffolds, such as stilbenoid skeleton and strobilurins' pharmacophore (β -methoxyacrylate) on one side, and the pharmacophore from succinate dehydrogenase inhibitors (SDHI), a class of synthetic agrochemicals, on the other.

In parallel, we applied a different approach for the identification of novel bioactive scaffolds, namely the target-based virtual screening of libraries of nature-derived and synthetic compounds. This strategy, whose results will be described in detail in **Chapter 7**, aimed at the identification of novel scaffolds for the treatment of *P. oryzae* infections, and it was developed with the support of Prof. Ivano Eberini and his colleagues from the Department of Pharmacological and Biomolecular Sciences (DiSFeB), University of Milan.

In the following chapters the investigation of phytoalexins' biological properties, as well as the strategies adopted for the identification and the design of new antimicrobial agents will be described.

2.1. Bibliography

1. Ramsay, R.R.; Popovic-Nikolic, M.R.; Nikolic, K.; Uliassi, E.; Bolognesi, M.L. A perspective on multi-target drug discovery and design for complex diseases. *Clin. Transl. Med.* **2018**, *7*(1), 3-17, doi:10.1186/s40169-017-0181-2.
2. Kempf, K.; Capello, Y.; Melhem, R.; Lescoat, C.; Kempf, O.; Cornu, A.; Fremaux, I.; Chaignepain, S.; Groppi, A.; Nikolski, M.; et al. Systemic Convergent Multitarget Interactions of Plant Polyphenols Revealed by Affinity-Based Protein Profiling of Bone Cells Using C-Glucosidic Vesical(ag)in-Bearing Chemoproteomic Probes. *ACS Chem. Biol.* **2023**, *18*, 2495–2505, doi:10.1021/acscchembio.3c00440.
3. Barglow, K.T.; Cravatt, B.F. Activity-Based Protein Profiling for the Functional Annotation of Enzymes. *Nat. Methods* **2007**, *4*, 822–827.
4. Keller, L.J.; Babin, B.M.; Lakemeyer, M.; Bogyo, M. ScienceDirect Activity-based protein profiling in bacteria: Applications for identification of therapeutic targets and characterization of microbial communities. *Curr. Opin. Chem. Biol.* **2020**, *54*, 45–53, doi:10.1016/j.cbpa.2019.10.007.
5. Wright, M.H.; Sieber, S.A. Chemical proteomics approaches for identifying the cellular targets of natural products. *Nat. Prod. Rep.* **2016**, *33*, 681–708, doi:10.1039/c6np00001k.

Chapter 3: Study of natural siderophores as potential antifungal agents targeting ferroptosis

3. Synthesis of natural siderophores and their analogues as antifungal agents targeting ferroptosis.

Abstract

The rice-blast fungus, *Pyricularia oryzae*, is one of the major threats limiting rice production worldwide. Recently, it was reported that an iron-dependent form of regulated cell death, known as ferroptosis, is involved in fungal pathogenicity during plant-fungal interactions. Hence, inhibition of ferroptosis by interfering with iron homeostasis potentially constitutes an innovative strategy to address fungal plant infections. In this study, we established that a series of benzamides, containing a chelating catechol moiety, suppress the formation/maturation of appressoria, specialized cells necessary for host infection of the rice blast fungus *P. oryzae*. Our results confirmed a strong correlation between the ability to chelate iron and the inhibition of infection-related morphogenesis of rice blast fungus. Thus, our results may pave the way for the development of targeted strategies for *P. oryzae* management.

3.1 Introduction

The increased demand for improved quality and quantity of agricultural crops due to the growth of the global population, together with the climatic changes related to global warming, have generated unprecedented challenges to food production [1]. Fungi are among the most significant agents of plant diseases, affecting all the 168 crops listed as important in human nutrition by the Food and Agricultural Organization (FAO) [2], and causing crop losses between 10% and 23% and another 10–20% post-harvest yearly [3,4]. The fungicide global market, which is projected to grow by around 5% per year, is mainly covered by three classes of single-site fungicides: azoles, strobilurins and succinate dehydrogenase inhibitors [4]. The widespread use of antifungal treatments that target a single cellular process has led to the global emergence of fungicide resistance [5,6]. Rice (*Oryza sativa* L.) is the staple diet of over 3 billion people around the world, particularly in Asia, where nearly half of the population depends on rice as their main food source. Rice production is severely affected by the fungus *Pyricularia oryzae*, the causal agent of the rice blast disease [7–9]. Yield loss due to rice blast ranges annually from approximately 10 to 30% in the various rice-producing countries and can reach up to 50 to 100% during severe disease epidemics [10,11]. Strobilurin-resistant strains of *P. oryzae* have recently spread in Asia and Europe, including Italy [12], which is the largest rice

producer in Europe. Since among the registered antifungals the most used treatments against rice blast in Europe are strobilurins alone or in mix with demethylation inhibitors or sulphur (Fitogest, fitogest.imagelinenetwork.com) [13], new strategies for the management of this fungal pathogen need to be urgently developed.

Recent studies have highlighted that ferroptosis, an iron-dependent programmed cell death, plays a key role in *P. oryzae* infection development [14]. Ferroptosis mechanism was described in **Section 1.2.1**, and it basically involves the development of a specialized infection cell (appressorium) from the asexual spores (conidia) formed by *Pyricularia oryzae* on aerial hyphae. For the appressorium maturation from conidium germination tube, and subsequent infection of rice plant tissues, the death of conidial cells is necessary. Conidial death is characterized by the iron-dependent accumulation of lipid hydroperoxides to lethal levels [15,16]. Recent evidence demonstrated that the major source of lipid peroxides are iron-dependent enzymes such as lipoxygenases (LOXs) and NADPH oxidases (NOXs) [17, 18]. The uncovered correlation between appressorium development and iron homeostasis evidenced iron sequestration by chelating molecules as a promising new strategy to prevent *P. oryzae* infection. Siderophores are small molecular weight chelators able to transport the insoluble iron (Fe^{3+}) into the cell via cell membrane-specific receptor proteins. Siderophores have already found applications in different fields such as microbiology, agriculture, ecology, and bioremediation. Moreover, siderophores have been indicated to play a role in plant growth promotion (PGP) and biocontrol against different fungal pathogens and various studies show PGP and biocontrol activity of siderophore-producing bacteria, such as *Pseudomonas* or *Bacillus* [19]. In agriculture, siderophores are used to increase the yield of various plant species by improving plants iron uptake, while acting against harmful phytopathogens, and proving to be a viable and eco-friendly alternative to pesticides [20]. For instance, improved growth of tomato plants was observed after combined addition of Fe^{3+} and siderophore pyoverdine to soil [21]. As described in **Section 1.2.1**, diverse microorganisms including bacteria and fungi are known to produce a variety of siderophores, especially under competitive conditions, when nutrient availability is a limiting factor [22]. Therefore, the use of siderophores could play a role in the biocontrol of pathogens, as their growth and metabolic activity are inhibited or slowed down by iron sequestering [23]. There are three main classes of natural iron chelating moieties: phenols and catechols (e.g., enterobactin, cacillibactin, aminochelin, azotochelin, and myxochelins), hydroxamates (e.g., coelichelin) and α -hydroxycarboxylic acids

[24]. Among these, catechol siderophores are particularly attractive because of their extremely high affinity for Fe^{3+} due to the presence of the 2,3-dihydroxybenzamide motifs [25], [26].

Aiming at evaluating the potential of natural catechol-type siderophores in interfering with ferroptosis-mediated virulence of *P. oryzae*, we prepared a collection of catechol-containing natural siderophores, namely Aminochelin (1), Azotochelin (2) and Myxochelin (3) (**Figure 3.1**) and congeners, all featuring a lysine or putrescine-derived core structure and one or two catechol groups connected by amide bonds.

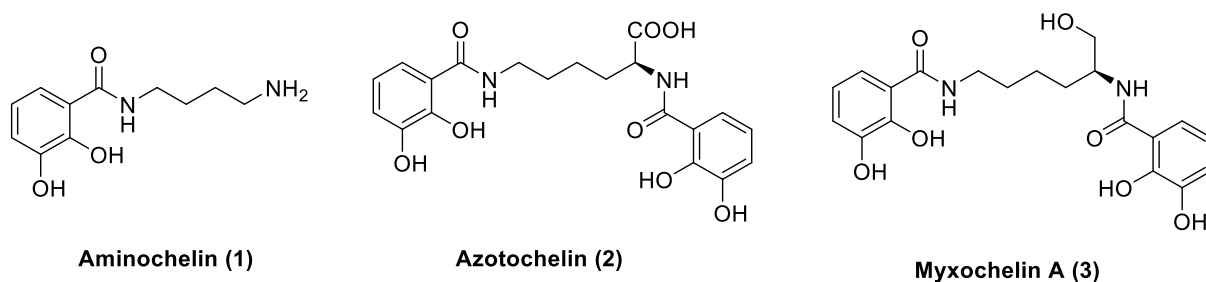


Figure 3.21. Structures of the selected catechol-containing siderophores

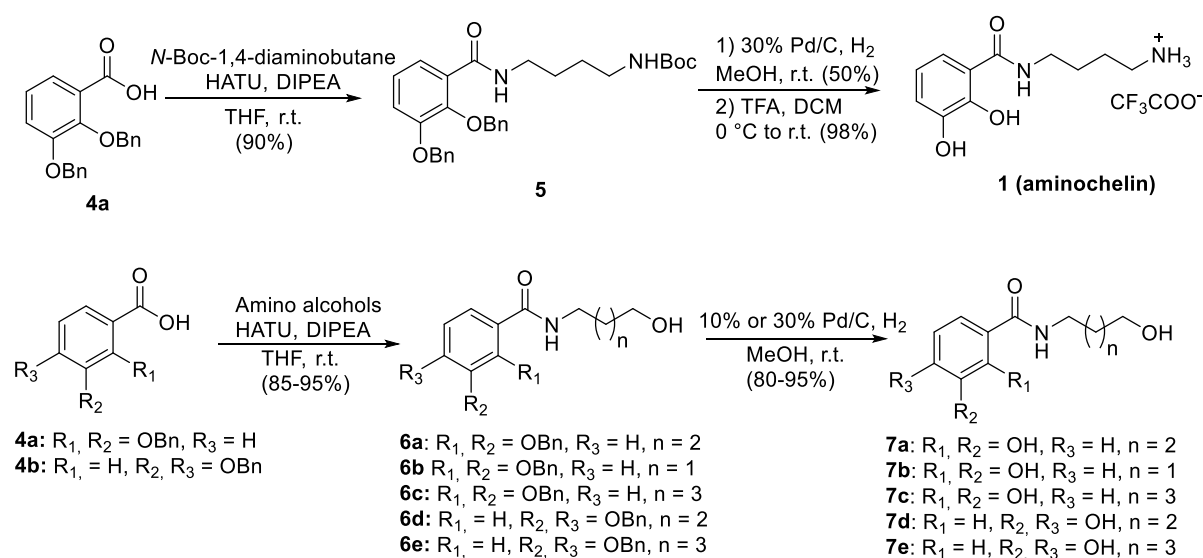
3.2 Results and discussion

Synthesis of natural siderophores 1, 2 and 3, and their analogues

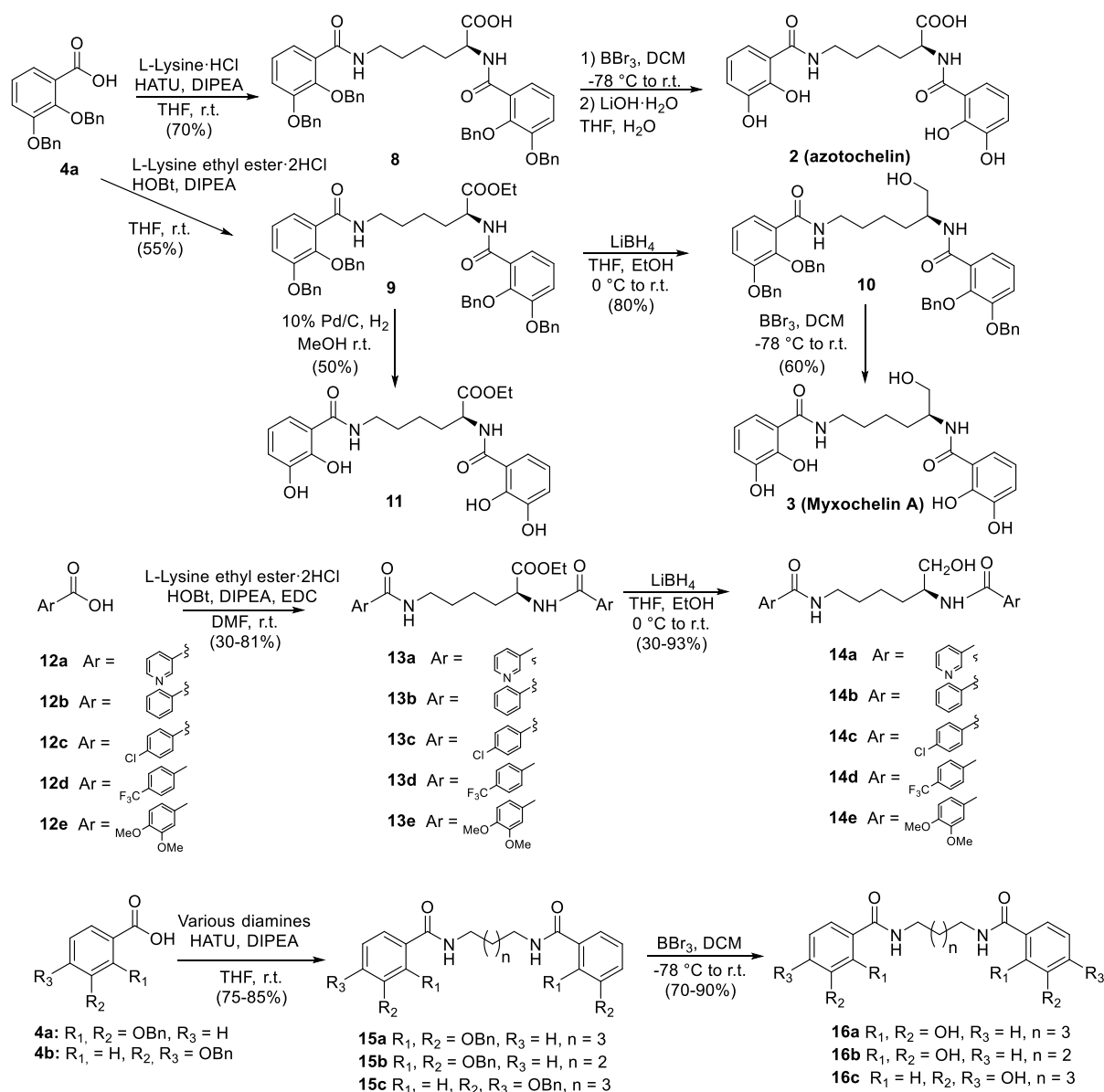
For the preparation of catechol-bearing natural compounds 1-3, protected 2,3-dihydroxybenzoic acid **4a** [27] was used as a key precursor. Aminochelin **1** was synthesized by reaction of **4a** with *N*-Boc-1,4-diaminobutane using HATU and DIPEA in THF. The protecting groups were removed by hydrogenation (30% Pd/C catalyst), followed by treatment with TFA in dichloromethane (**Scheme 3.1**). The analogue containing a hydroxy group in place of the amino group on the side chain was obtained following a similar procedure. Coupling of **4a** with 4-aminobutanol gave **6a**, which was then hydrogenated to provide **7a**. Compounds containing a side chain 1C-shorter (**7b**) and 1C-longer (**7c**) than **7a** were also prepared. The analogues containing the 3,4-dihydroxy-substituted moiety (**7d** and **7e**) in place of the 2,3-substituted one were prepared starting from the protected 3,4-dihydroxybenzoic acid **4b**. Azotochelin (**2**) was prepared via amide coupling between **4a** and L-lysine, followed by deprotection of the phenolic groups. In this case, the use of BBr_3 resulted to be more advantageous than hydrogenation, which did not give a complete deprotection. The reaction of **4a** with L-lysine ethyl ester gave compound **9**, which was reduced with LiBH_4 to obtain compound **10**. Removal of benzyl-protecting groups by BBr_3

afforded Myxochelin A. Myxochelin A analogues **14a-e** were prepared following the same synthetic pathway reported above (Scheme 3.2). Compounds **14a-b**, known as Myxochelin N and P, respectively, have been recently found in a natural source [28].

Finally, the reaction of the acid **4a** with pentane-1,5-diamine, followed by removal of the protecting group by BBr_3 in dichloromethane, gave diamide **16a**, which contained the same skeleton of azotochelin and myxochelin A, however lacking the substituent on the connecting chain. The same approach was followed to obtain compounds **16b-c**.



Scheme 3.1. Synthesis of natural compound **1** and analogues



Scheme 3.2. General synthetic pathway for natural compounds 2-3 and analogues.

Biological activity evaluation

Iron chelation colorimetric test.

The chelating ability of the synthesized compounds was evaluated by the Chrome azurol S (CAS) assay. The tested compounds were dissolved in a 9:1 mixture of H₂O: DMSO (1 mg/ml concentration). 100 μ L of the solution of the tested compounds and 100 μ L of CAS Reagent were added in the same well of the 96 Microwell plate (final concentration 0.5 mg/ml) and allowed to react for 30 minutes. The results are shown in **Figure 3.1**. The first five measures (E1 to

E5) represent the positive control of EDTA at increasing concentrations (from 0.25 to 2 mg/mL). The sixth one shows the results of the negative control (N.C.), namely the blank solution of H₂O: DMSO 9:1. The results evidenced that the 2,3-dihydroxysubstituted benzamides have a significant chelating capability, comparable to the reference compound EDTA (see compounds **2**, **3**, **7a-c**, **9**, **16a-b**) with the exception of aminochelin **1**. Conversely, 3,4-dihydroxybenzamides, characterized by a higher distance between the catechol group and the amide moiety, had a lower chelating activity (**7d-e**, **16c**). As expected, compounds **14a-e**, lacking the catechol group, did not show any significant ability to chelate iron.

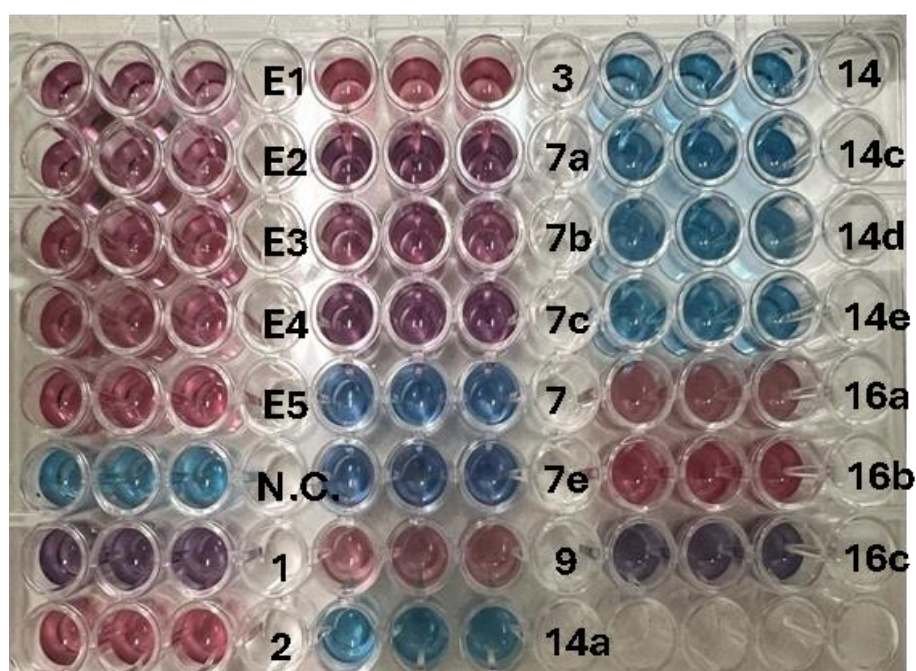


Figure 3.22. Chrome azurol S (CAS) assay. Evaluation of the chelating activity of the synthesized compounds. The assay was performed in triplicate.

Inhibition of spore germination and appressorium formation

The synthesized compounds were tested at a 1000 μ M concentration to evaluate the effect on spore germination and appressorium formation. While myxochelin A (**3**) showed ca. 50% inhibition of conidium germination and none of the germinated spores developed appressoria, aminochelin (**1**) did not inhibit significantly the germination, but ca. 40% of germinated spores were without appressoria. Azotochelin (**2**) inhibited appressorium formation only by 25%. The lower activity of compounds **1** and **2** could be explained by the presence of the amino- and carboxylic groups on the aliphatic chain, which can potentially be charged, affecting the penetration of the compounds into the conidia. For

this reason, we prepared various-length analogs of compound **1** in which the amino group was replaced by a non-protonatable alcohol group, and the side chain had a variable number of carbons. The obtained derivatives **7a** and **7b** showed statistically significant inhibition of appressorium formation without affecting the germination, compared to the parent compound. Surprisingly, compound **7c** showed an almost complete inhibition of germination, probably mediated by a different mechanism of action. Noteworthy, the germinated conidia did not develop appressoria. Shifting the catechol system from carbons 2,3 to carbons 3,4 caused a reduction in activity for the compound bearing a 4C side chain (**7d**), and almost completely abolished the activity of longer analogue **7e**, with a 5C side chain (percentage of appressoria inhibition 50% and 18%, respectively). As regards compound **2**, the corresponding ester (**9**) showed no activity. Considering that the natural compound containing the alcohol group in the same position (compound **3**, myxochelin A) showed considerable activity, a series of analogs (**14a-e**) were prepared by changing the aromatic systems, leaving however the central chain unchanged. In all cases, except for **14d**, the activity decreased sharply confirming the key role of the catechol moiety. Finally, to evaluate the effect of the hydroxymethyl group on the linker chain, compounds **16a-c** were prepared. Whereas **16b** and **16c** showed good inhibition of the appressorium formation, **16a** showed a complete conidia germination inhibition, precluding the investigation of the appressorium maturation at the tested concentration. Consequently, **16a** was tested at two additional 10-fold diluted concentrations (110 and 10 μM) together with the most active compounds identified as appressorium development inhibitors (**16b-c**, **7a-c**, myxochelin A **3**). Gratifyingly, compounds **16a** together with **7a** showed a significant activity (>65%) at 100 μM , with compound **7a** retaining a 37% inhibition of appressoria formation even at 10 μM concentrations. Overall, a good correlation between the chelating activity and the inhibition of appressorium formation was found, with the only exception of compound **9**, which showed good chelating ability but low activity on appressorium, and compound **14d**, which had significant activity on the appressorium formation despite the lack of the catechol chelating group.

These results confirm a link between iron-dependent cell death and the pathogen's developmental stages, supporting the hypothesis that ferroptosis contributes to conidial cell death during *P. oryzae* infection-related morphogenesis.

Figure 3.3. Activity of compounds on the germination (light grey) and appressoria formation (dark grey) of *Pyricularia oryzae* spores. A solution 2% methanol (MeOH) in water was used as a solvent (at 1000 μ M concentration). Error bars represent the standard deviation. The different letters indicate statistically significant differences among means ($P > 0.05$) calculated by the Tukey post hoc test.

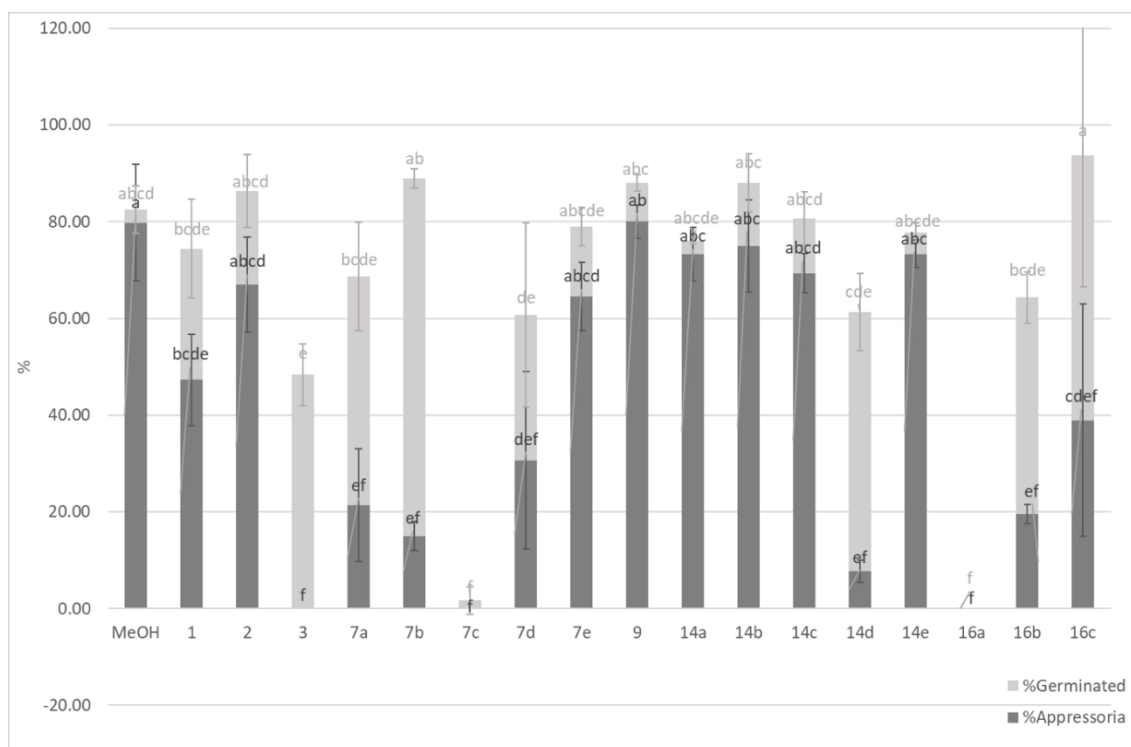
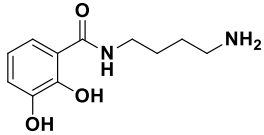
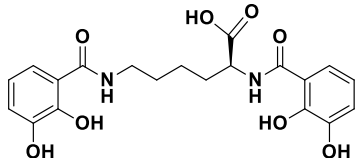
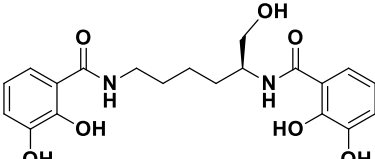
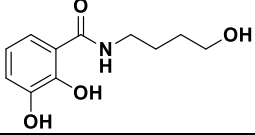
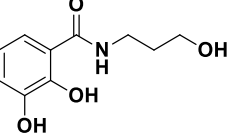
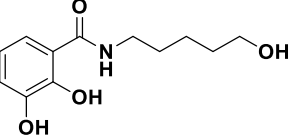
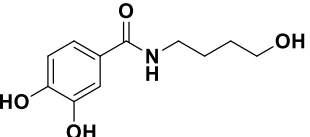
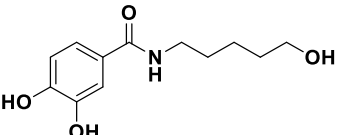
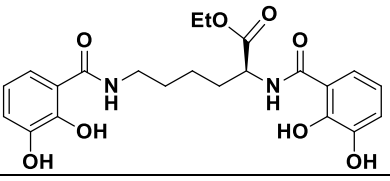
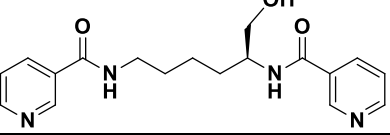
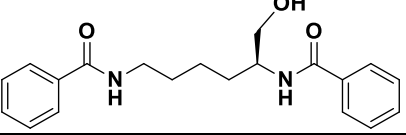
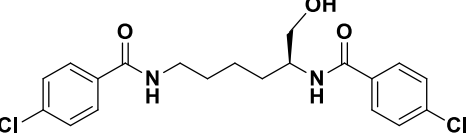
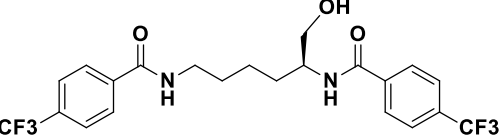
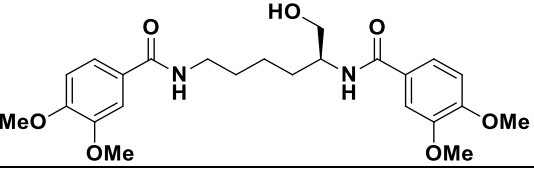
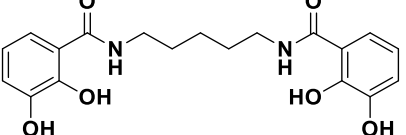


Table 3.1. Inhibition of spore germination and appressorium formation by the tested compounds (at 1000 μ M concentration). Mean % inhibition with standard deviation in brackets are listed. ^a N.I. = no inhibition; ^b N.A. = not assessed, as no germination occurred.

Compound	Germination Inhibition (%)	Appressorium formation inhibition (%)
1 	18.98	47.6
2 	3.72	24.72
3 	46.3	100

7a		N.I. ^a	64.37
7b		N.I. ^a	80
7c		72.87	98.85
7d		N.I. ^a	47.23
7e		4.57	12.95
11		N.I. ^a	1.49
14a		7.69	5.58
14b		N.I. ^a	10
14c		5.1	16.8
14d		24.28	90.09
14e		N.I. ^a	N.I. ^a
16a		38.02	100

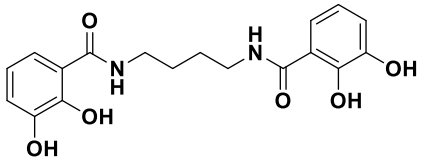
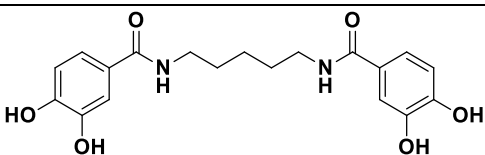
16b		N.I. ^a	78.91
16c		20	90.45

Table 3.1. Inhibition of the appressorium formation by the selected compounds tested at three different concentrations. Mean % inhibition with standard deviation in brackets are listed. N.A. = not assessed, as no germination occurred.

	Myxochelin	7a	7b	7c	16a	16b	16c
	A						
1000 μ M	100	64.37	82.1	98.85	100	78.91	90.45
100 μ M	7.41	55.64	10.3	4.81	54.81	40	<2
10 μ M	4.81	25.44	<2	2.2	21.76	4.36	<2

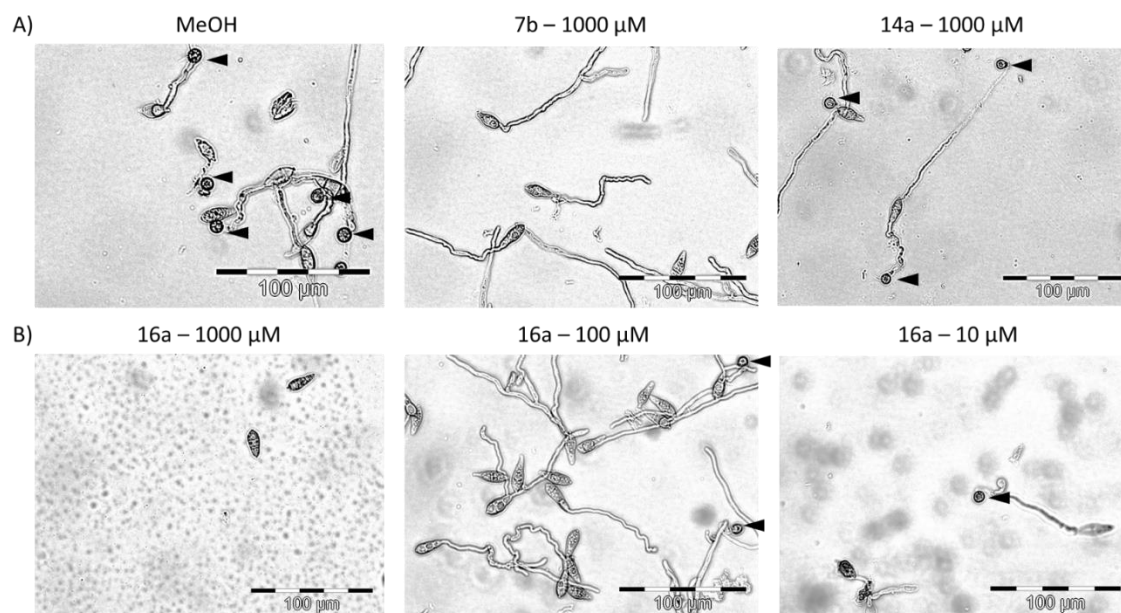


Figure 3.4. Germination and appressorium formation (black arrowheads) of spores of *Pyricularia oryzae* treated with tested compounds. A) Appressorium formation in control (2% MeOH). No appressoria were formed after treatment with **7b** (1000 μ M). Normal appressorium formation after treatment with **14a** (1000 μ M). B) Dose-dependent germination and appressorium formation after treatment with **16a**. No germination was observed at the concentration 1000 μ M, germination with few appressoria at the concentration 100 μ M and abundant appressorium formation at the concentration 10 μ M. The scale bar equals to 100 μ M.

3.3. Conclusions

Fungi are hugely devastating pathogens, affecting the most important crops for human nutrition. The destructive impacts fungi are having on the world's food supply must be addressed to address the greatest threats to food security. There is emerging evidence that ferroptosis may play an important and multifaceted role in the infection process various pathogens, including plant-pathogenic fungi. Ferroptotic cell death is a prerequisite for *P. oryzae* infection in rice and modulates the consequential infection-related morphogenesis. Therefore, ferroptosis inhibition can be a promising strategy to prevent *P. oryzae* infection and disease development. To this aim, we synthesized a small library of natural or nature derived siderophores to investigate their effect on the ferroptosis-mediated early development of conidia. The synthesized compounds were tested to evaluate both the chelating activity and the inhibition of conidia germination and appressorium development. The results showed a good correlation between the ability to chelate iron and the suppression of virulence of the rice blast fungus. In general, better chelating activity resulted in higher inhibition of appressoria development. In particular, compound **16a** and **7a** showed a significant activity (>65%) at 100 μM , with compound **7a** retaining a 37% inhibition of appressoria formation even at 10 μM concentration.

In conclusion, the reported findings not only contribute to the understanding of the *P. oryzae* rice infection process but also highlight the broader implications of ferroptosis in the context of fungal diseases and agriculture. The study's results could pave the way for future research and the development of targeted strategies for blast disease management in rice and other important cereal crops.

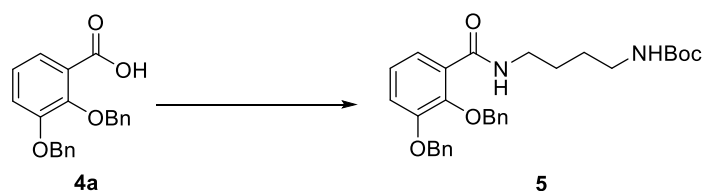
3.4. Materials and Methods

Chemistry

All reagents and solvents were purchased from commercial suppliers and used without further purification. All reactions requiring anhydrous conditions were performed under a positive nitrogen flow (after vacuuming the flask), and all glassware was oven dried. TLC analyses were performed using commercial silica gel 60 F₂₅₄ aluminum sheets. Spots were revealed under UV lamp ($\lambda = 254$ or 365 nm). Development reagents such as ninhydrin (1.5 g of ninhydrin, 3.0 mL of acetic acid in 100 mL of ethanol) and KMnO_4 were used occasionally as needed.

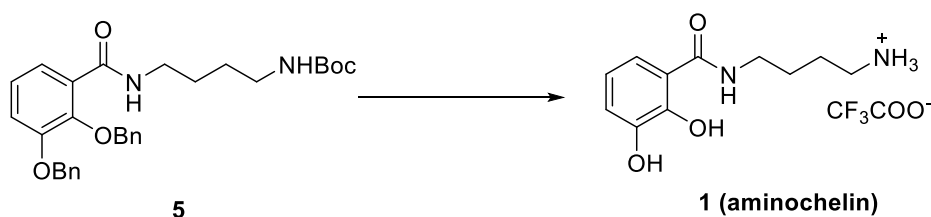
Isolation and purification of the products was performed by flash column chromatography on silica gel 60 (230-400 mesh). For thin layer chromatography (TLC) purification Analtech UNIPLATE™UV254 glass sheets with a 1.5 mm layer of silica gel 60 F₂₅₄ were used. The NMR spectra were acquired either using a Bruker AV600 (¹H, 600 MHz, ¹³C, 150 MHz) spectrometer or a Bruker NMR Avance™ NEO 400 MHz spectrometer (¹H, 400 MHz, ¹³C 100 MHz). TMS was used as an internal standard and chemical shifts (δ) are expressed in ppm. The coupling constants (*J*) are reported in Hz. For the NMR analysis we used CDCl₃ and CD₃OD-*d*₄ as deuterated solvents. All the spectra were recorded at room temperature (298.15K). ¹H-NMR signals are indicated with the following abbreviations: s (singlet), d (doublet), t (triplet), q (quartet), dd (doublet of doublets), m (multiplet), bs (broad singlet).

Synthesis of tert-butyl (4-(2,3-bis(benzyloxy)benzamido)butyl)carbamate (5).



To a solution of 2,3-bis(benzyloxy)benzoic acid **4a** (0.27 g, 0.8 mmol) in THF (20 mL), HATU (0.34 g, 0.88 mmol) and DIPEA (0.36 mL, 2.0 mmol) were added, and the mixture was stirred for 30 min at room temperature. Then, *N*-Boc-1,4-diaminobutane (0.18 g, 0.8 mmol) was added and the mixture was stirred for 3 hours at room temperature. After the completion of the reaction, the solvent was evaporated and EtOAc was added. The organic layer was washed with sat. NH₄Cl and brine, dried with Na₂SO₄, filtered, and evaporated. The residue was purified by flash column chromatography (Hex/EtOAc 6:4) to provide **5** as a white amorphous solid (90% yield). The NMR spectra matched with those reported in the literature [29].

Synthesis of Aminochelin (1)



To a solution of **5** (0.35 g, 0.70 mmol) in MeOH (30 mL), 30% Pd/C was added (0.105 g). The new mixture was degassed three times (vacuum/N₂) and then reacted under H₂ (1 atm) overnight at room temperature. After reaction completion, the mixture was filtered through celite and washed with MeOH. The filtrate was evaporated and the residue was purified by flash column chromatography (DCM/MeOH 99:1) to provide *tert*-butyl (4-(2,3-dihydroxybenzamido)butyl)carbamate (50% yield).

¹H NMR (400 MHz, CD₃OD-*d*₄): δ = 7.21 (1H, dd, *J* = 8.0 Hz *J* = 1.2 Hz), 6.92 (1H, dd, *J* = 8.0 Hz *J* = 1.6 Hz), 6.70 (1H, t, *J* = 8.0 Hz), 3.38 (2H, t, *J* = 6.8 Hz), 3.08 (2H, t, *J* = 6.8 Hz), 1.66 – 1.50 (4H, m), 1.42 (9H, s)

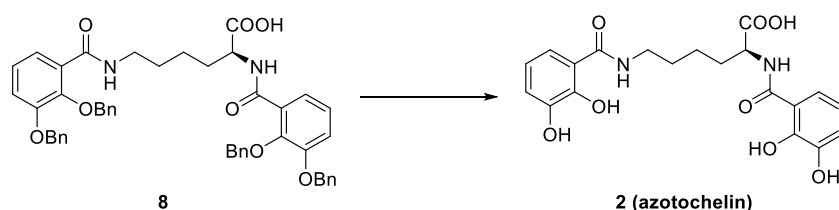
¹³C NMR (100 MHz, CD₃OD-*d*₄): δ = 170.1, 157.2, 148.9, 146.0, 118.2, 118.1, 117.2, 115.4, 78.5, 39.6, 38.8, 27.4 (3C), 27.1, 26.3.

To a cold at 0 °C solution of the above compound (0.067 g, 0.19 mmol) in DCM (3.0 mL), TFA was added (0.29 mL, 3.8 mmol) and the reaction was stirred overnight at room temperature. After the completion of the reaction, the solvent was evaporated to provide compound **1** as a white amorphous solid (98% yield).

¹H NMR (400 MHz, DMSO-*d*₆): δ = 8.76 (1H, t, *J* = 5.6 Hz), 8.54 (1H, s), 7.68 (3H, br. s), 6.84 (1H, d, *J* = 8.8 Hz), 6.37 (1H, d, *J* = 8.8 Hz), 3.82 (3H, s), 3.37 – 3.34 (2H, m), 2.84 – 2.81 (2H, m), 1.59 – 1.56 (4H, m)

¹³C NMR (100 MHz, DMSO-*d*₆): δ = 170.1, 158.5 (q, *J* = 31 Hz), 152.0, 151.2, 140.7, 118.5, 117.7 (q, *J* = 298 Hz), 104.7, 100.7, 56.6, 39.1, 38.7, 26.4, 25.1.

Synthesis of Azotochelin (2)



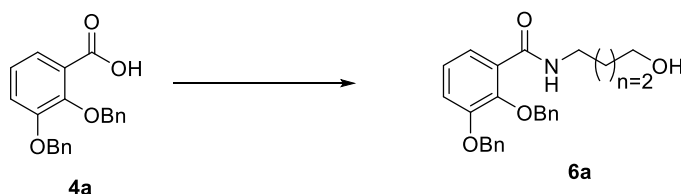
To a cold at -78 °C solution of compound **8** (0.26 g, 0.33 mmol) in DCM (23 mL), BBr₃ (1.45 mL, 1.45 mmol, 1.0 M in DCM, 1.1 equiv. per bond) was added dropwise and the reaction was kept for another 1 h at the same temperature and then overnight at room temperature. Then, the solution was cooled at 0 °C, neutralized with MeOH, and H₂O was added. The organic phase was extracted twice with EtOAc. The combined organic extracts were washed with brine, dried with Na₂SO₄, filtered, and evaporated. The residue was purified by flash

column chromatography (DCM/MeOH/AcOH 9.8:0.2:0.1) to provide the azotochelin methyl ester as a white amorphous solid (50% yield). Subsequently, LiOH·H₂O (0.020 g, 0.49 mmol) was added in a solution of azotochelin methyl ester (0.060 g, 0.14 mmol) in THF/H₂O (1.8/0.7 mL) and the new solution was refluxed for 4 h. After the completion of the reaction, the solvent was evaporated and EtOAc was added. The organic layer was washed with HCl 1N and brine, dried with Na₂SO₄, filtered, and evaporated. The residue was purified by flash column chromatography (DCM/MeOH/AcOH 9:1:0.1) to provide compound **2** as foam (70% yield).

¹H NMR (400 MHz, CD₃OD): δ = 7.31 (1H, dd, *J* = 8.0 Hz *J* = 1.2 Hz), 7.18 (1H, dd, *J* = 8.0 Hz *J* = 1.2 Hz), 6.93 (1H, dd, *J* = 8.0 Hz *J* = 1.6 Hz), 6.91 (1H, dd, *J* = 8.0 Hz *J* = 1.6 Hz), 6.72 (1H, t, *J* = 8.0 Hz), 6.68 (1H, t, *J* = 8.0 Hz), 4.63 – 4.59 (1H, m), 3.39 (2H, t, *J* = 6.8 Hz), 2.08 – 2.00 (1H, m), 1.96 – 1.86 (1H, m), 1.73 – 1.65 (2H, m), 1.57 – 1.50 (2H, m)

¹³C NMR (100 MHz, CD₃OD): δ = 176.1, 171.5, 170.9, 150.2, 149.8, 147.3, 147.2, 119.7 (2C), 119.5 (2C), 119.4, 118.6, 117.0, 116.8, 54.1, 40.2, 32.4, 30.0, 24.4. [30]

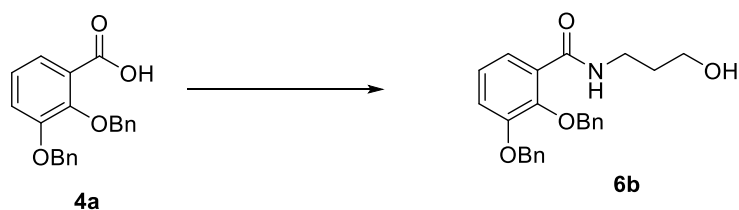
Synthesis of 2,3-bis(benzyloxy)-N-(4-hydroxybutyl)benzamide (6a)



To a solution of 2,3-bis(benzyloxy)benzoic acid **4a** (0.50 g, 1.5 mmol) in THF (20 mL), HATU (0.62 g, 1.64 mmol) and DIPEA (2.5 mL, 2.2 mmol) were added, and the mixture was stirred for 30 min at room temperature. Then, 4-amino-1-butanol (0.15 mL, 1.6 mmol) was added, and the new mixture was stirred for 3 h at room temperature. After reaction completion, the solvent was evaporated and EtOAc was added. The organic layer was washed with sat. NH₄Cl and brine, dried with Na₂SO₄, filtered, and evaporated. Purification by flash column chromatography (Hex/EtOAc 2:8) and evaporation of the solvent afforded the title compound as a yellow oil (95% yield).

¹H NMR (400 MHz, CDCl₃): δ = 8.05 (1H, br. s), 7.77 – 7.73 (1H, m), 7.51 – 7.37 (10H, m), 7.18 – 7.17 (2H, m), 5.18 (2H, s), 5.11 (2H, s), 3.60 (2H, t, *J* = 6.0 Hz), 3.36 – 3.11 (2H, m), 1.52 – 1.44 (4H, m). The spectroscopic data matched with those reported in the literature [31].

Synthesis of 2,3-bis(benzyloxy)-N-(3-hydroxypropyl)benzamide (6b)

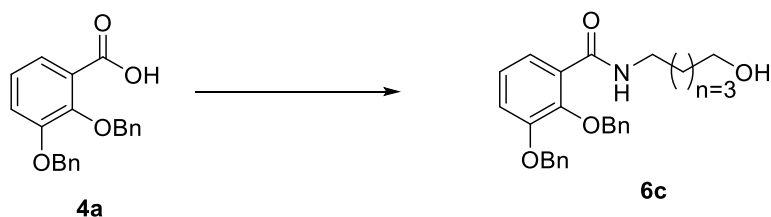


Following the procedure reported for **6a**, compound **6b** was obtained from acid **4a** (0.50 g, 1.5 mmol) and 3-amino-1-propanol (0.12 mL, 1.6 mmol), after purification by flash column chromatography (Hex/EtOAc 2:8) and evaporation of the solvent as a white amorphous solid (95% yield).

¹H NMR (400 MHz, CDCl₃): δ = 8.11 (1H, t, *J* = 3.6 Hz), 7.74 – 7.72 (1H, m), 7.48 – 7.33 (10H, m), 7.17 – 7.16 (2H, m), 5.17 (2H, s), 5.10 (2H, s), 3.50 (2H, q, *J* = 5.8 Hz), 3.42 – 3.39 (2H, m), 1.54 – 1.50 (2H, m)

¹³C NMR (100 MHz, DMSO-*d*₆): δ = 165.9, 151.0, 148.1, 137.6, 137.4, 128.9 (4C), 128.3 (2C), 128.0 (4C), 127.9, 121.2, 113.8, 113.7, 70.7, 70.4, 61.0, 39.4, 30.5, 26.4. The spectroscopic data matched with those reported in the literature [31].

Synthesis of 2,3-bis(benzyloxy)-N-(5-hydroxypentyl)benzamide (6c)

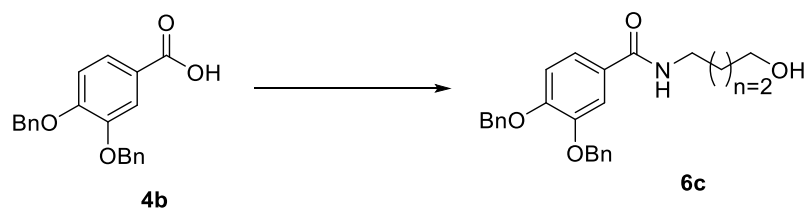


Following the procedure reported for **6a**, compound **6c** was obtained from acid **4a** (0.21 g, 0.63 mmol) and 5-amino-1-pentanol (0.081 mL, 0.69 mmol) after purification by flash column chromatography (Hex/EtOAc 2:8) and evaporation of the solvent as a yellow oil (95% yield).

¹H NMR (400 MHz, CDCl₃): δ = 8.05 (1H, br. s), 7.76 – 7.73 (1H, m), 7.50 – 7.37 (10H, m), 7.18 – 7.17 (2H, m), 5.18 (2H, s), 5.11 (2H, s), 3.59 (2H, t, *J* = 6.4 Hz), 3.31 (2H, q, *J* = 6.0 Hz), 1.56 – 1.49 (2H, m), 1.41 – 1.28 (4H, m)

¹³C NMR (100 MHz, CD₃OD-*d*₄): δ = 166.9, 152.0, 146.3, 136.8 (2C), 128.6, 128.4 (2C), 128.2 (2C), 128.1 (2C), 128.0, 127.8, 127.6 (2C), 124.1, 121.4, 116.8, 75.7, 70.9, 61.3, 39.4, 31.8, 28.7, 23.0

Synthesis of 3,4-bis(benzyloxy)-N-(4-hydroxybutyl)benzamide (6d)

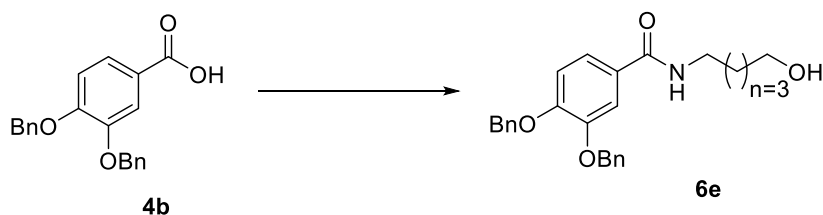


Following the procedure reported for **6a**, **6d** was obtained from acid **4b** (0.25 g, 0.75 mmol) and 4-amino-1-butanol (0.077 mL, 0.82 mmol) after purification by flash column chromatography (Hex/EtOAc 1:9) and evaporation of the solvent as a white amorphous solid (94% yield).

¹H NMR (400 MHz, CDCl₃): δ = 7.49 – 7.26 (12H, m), 6.89 (1H, d, *J* = 8.4 Hz), 5.18 (4H, s), 3.68 (2H, t, *J* = 6.0 Hz), 3.45 (2H, t, *J* = 6.4 Hz), 1.73 – 1.61 (4H, m)

¹³C NMR (100 MHz, DMSO-*d*₆): δ = 165.9, 151.0, 148.1, 137.6, 137.4, 128.9 (4C), 128.3 (2C), 128.0 (4C), 127.9, 121.2, 113.8, 113.7, 70.8, 70.4, 61.0, 39.4, 30.5, 26.4

Synthesis of 3,4-bis(benzyloxy)-N-(5-hydroxypentyl)benzamide (6e)

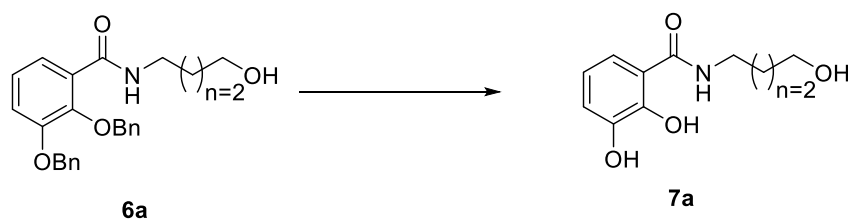


Following the procedure reported for **6a**, **6e** was obtained from acid **4b** (0.25 g, 0.75 mmol) and 5-amino-1-pentanol (0.088 mL, 0.82 mmol) after purification by flash column chromatography (Hex/EtOAc 1:9) and evaporation of the solvent as a white amorphous solid (85% yield).

¹H NMR (400 MHz, DMSO-*d*₆): δ = 8.29 (1H, t, *J* = 5.2 Hz), 7.58 (1H, d, *J* = 2.0 Hz), 7.48 – 7.31 (11H, m), 7.12 (1H, d, *J* = 8.4 Hz), 5.20 (2H, s), 5.17 (2H, s), 4.36 (1H, t, *J* = 4.8 Hz), 3.40 (2H, q, *J* = 5.2 Hz), 3.23 (2H, q, *J* = 6.0 Hz), 1.55 – 1.42 (4H, m), 1.36 – 1.30 (2H, m).

¹³C NMR (100 MHz, DMSO-*d*₆): δ = 165.9, 151.0, 148.1, 137.6, 137.4, 128.9 (2C), 128.8 (2C), 128.3 (2C), 128.0 (4C), 127.9, 121.2, 113.8, 113.7, 70.8, 70.4, 61.1, 39.7, 32.7, 29.6, 23.5.

Synthesis of 2,3-dihydroxy-N-(4-hydroxybutyl)benzamide (7a)

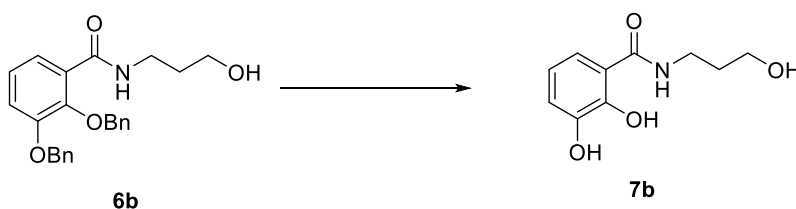


To a solution of **6a** (0.23 g, 0.57 mmol) in MeOH (33 mL), 10% Pd/C was added. The new mixture was degassed three times (vacuum/N₂) and then reacted under H₂ (1 atm) overnight at room temperature. After the completion of the reaction, the mixture was filtered through celite and washed with MeOH. After purification by flash column chromatography (Hex/EtOAc/MeOH 5:5:0.5) and evaporation of the solvent the title compound was obtained as a white amorphous solid (80% yield).

¹H NMR (400 MHz, CD₃OD): δ = 7.22 (1H, dd, J = 8.0 Hz J = 1.4 Hz), 6.94 (1H, dd, J = 8.0 Hz J = 1.4 Hz), 6.73 (1H, t, J = 8.0 Hz), 3.62 (2H, t, J = 6.4 Hz), 3.42 (2H, t, J = 6.8 Hz), 1.74 – 1.59 (4H, m)

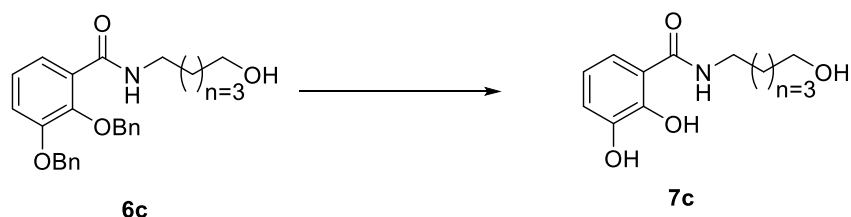
¹³C NMR (100 MHz, CD₃OD): δ = 170.1, 148.9, 145.9, 118.1 (2C), 117.2, 115.4, 61.2, 38.9, 29.6, 25.6. The spectroscopic data matched with those reported in the literature [31].

Synthesis of 2,3-dihydroxy-N-(3-hydroxypropyl)benzamide (7b)



To a solution of **6b** (0.27 g, 0.68 mmol) in MeOH (33 mL), 30% Pd/C was added (0.027 g). The new mixture was degassed three times (vacuum/N₂) and then reacted under H₂ (1 atm) overnight at r.t. After the completion of the reaction, the mixture was filtered through celite and washed with MeOH. The filtrate was evaporated, and the residue was purified by flash column chromatography (DCM/MeOH 96:4) to provide the amide **7b** as oil (60% yield). The spectroscopic data matched with those reported in the literature [31].

Synthesis of 2,3-dihydroxy-N-(5-hydroxypentyl)benzamide (7c)

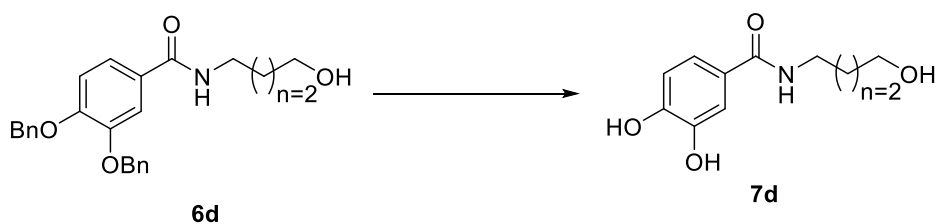


Following the procedure reported for **7a**, compound **7c** was obtained from **6c** (0.23 g, 0.57 mmol) and 10% Pd/C after purification by flash column chromatography (Hex/EtOAc/MeOH 5:5:0.5) and evaporation of the solvent as a white amorphous solid (80% yield).

¹H NMR (400 MHz, CD₃OD): δ = 7.23 (1H, dd, J = 8.0 Hz J = 1.6 Hz), 6.94 (1H, dd, J = 8.0 Hz J = 1.2 Hz), 6.73 (1H, t, J = 8.0 Hz), 3.58 (2H, t, J = 6.8 Hz), 3.40 (2H, t, J = 7.2 Hz), 1.70 – 1.57 (4H, m), 1.50 – 1.42 (2H, m)

¹³C NMR (100 MHz, CD₃OD): δ = 170.0, 148.9, 145.9, 118.1 (2C), 117.2, 115.4, 61.4, 39.1, 31.9, 28.8, 23.0.

Synthesis of 3,4-dihydroxy-N-(4-hydroxybutyl)benzamide (7d)

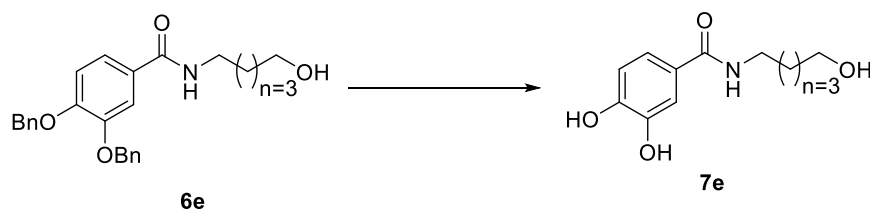


Following the procedure reported for **7a**, **7d** was obtained from **6d** (0.28 g, 0.69 mmol) and 10% Pd/C after purification by flash column chromatography (EtOAc/MeOH 9.5:0.5) and evaporation of the solvent as a white amorphous solid (95% yield).

¹H NMR (400 MHz, CD₃OD): δ = 7.29 (1H, d, J = 2.0 Hz), 7.21 (1H, dd, J = 8.0 Hz J = 2.0 Hz), 6.80 (1H, d, J = 8.4 Hz), 3.61 (2H, t, J = 6.4 Hz), 3.38 (2H, t, J = 6.8 Hz), 1.72 – 1.58 (4H, m)

¹³C NMR (100 MHz, CD₃OD): δ = 168.9, 148.6, 144.9, 125.9, 119.1, 114.4, 114.3, 61.2, 39.3, 29.6, 25.7 [32].

Synthesis of 3,4-dihydroxy-N-(5-hydroxypentyl)benzamide (7e)

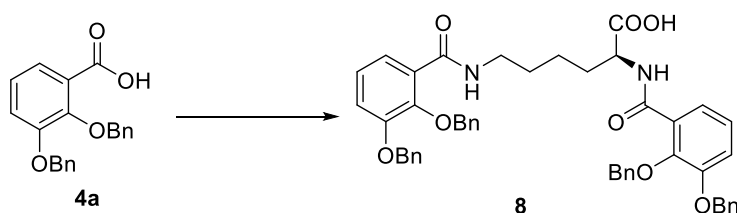


Following the procedure reported for **7a**, **7e** was obtained from **6e** (0.19 g, 0.45 mmol) and 10% Pd/C after purification by flash column chromatography (Hex/EtOAc/MeOH 3:7:0.5) and evaporation of the solvent as a white amorphous solid (85% yield).

¹H NMR (400 MHz, CD₃OD): δ = 7.30 (1H, d, J = 2.0 Hz), 7.22 (1H, dd, J = 8.4 Hz, J = 2.0 Hz), 6.81 (1H, d, J = 8.4 Hz), 3.58 (2H, t, J = 6.8 Hz), 3.35 (2H, t, J = 7.2 Hz), 1.67 – 1.55 (4H, m), 1.48 – 1.41 (2H, m)

¹³C NMR (100 MHz, CD₃OD): δ = 168.9, 148.6, 144.9, 125.9, 119.0, 114.4, 114.3, 61.4, 39.5, 31.9, 29.0, 23.0.

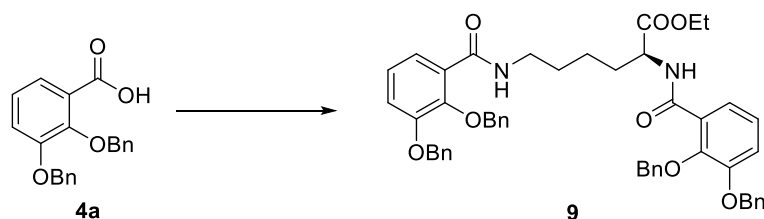
Synthesis of N₂,N₆-bis(2,3-bis(benzyloxy)benzoyl)-L-lysine (8)



To a solution of 2,3-bis(benzyloxy)benzoic acid **4a** (0.30 g, 0.9 mmol) in THF (5 mL), was added HATU (0.38 g, 0.99 mmol) and DIPEA (0.24 mL, 1.35 mmol) and the new mixture was stirred for 30 min at room temperature. Then, the mixture was set at 0 °C and a solution at 0 °C of L-lysine hydrochloride (0.080 g, 0.44 mmol) and NaOH (0.054 g, 0.44 mmol) in H₂O (1.8 mL) was added and the new mixture was stirred overnight at rt. After the completion of the reaction, the solvent was evaporated and EtOAc was added. The organic layer was washed with HCl 1N and brine, dried with Na₂SO₄, filtered, and evaporated. The residue was purified by flash column chromatography (DCM/MeOH/AcOH 9.6:0.4:0.1) to provide compound **8** as an oil (70% yield).

¹H NMR (400 MHz, CDCl₃): δ = 8.54 (1H, d, J = 6.8 Hz), 7.92 (1H, d, J = 5.6 Hz), 7.77 – 7.72 (2H, m), 7.49 – 7.14 (24H, m), 5.16 (6H, s), 5.08 (2H, s), 4.55 – 4.50 (1H, m), 3.17 – 3.12 (2H, m), 1.76 – 1.67 (1H, m), 1.44 – 1.35 (1H, m), 1.26 – 1.14 (2H, m). The spectroscopic data matched with those reported in the literature [33].

Synthesis of Ethyl *N*²,*N*⁶-bis(2,3-bis(benzyloxy)benzoyl)-*L*-lysinate (**9**)

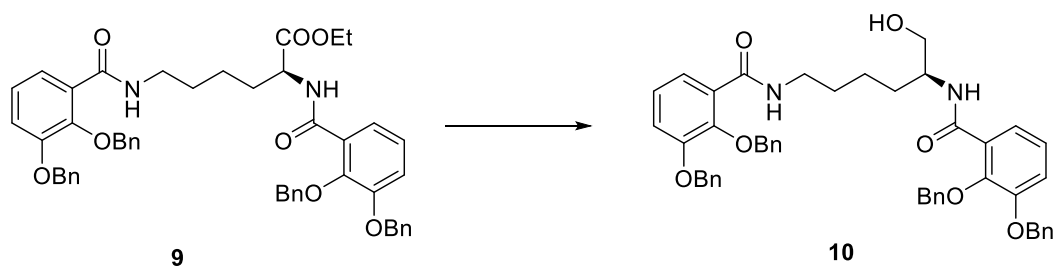


In a round bottom-flask 2,3-bis(benzyloxy)benzoic acid (**4a**) (600 mg, 1.8 mmol, 2eq) and L-lysine ethyl ester dichlorohydrate (221.8 mg, 0.9 mmol, 1eq) were dissolved in dry DMF (7.8 ml, 0.2M) under nitrogen atmosphere. DIPEA (0.35 ml, 2.02 mmol, 2.25eq), EDC·HCl (378.4 mg, 1.97 mmol, 2.2eq) and HOBT·H₂O (266.7 mg, 1.97 mmol, 2.2eq) were added and the obtained reaction mixture was stirred at room temperature overnight. After this time, the reaction mixture was diluted with DCM and the organic layer was washed with 0.02M HCl, NaHCO₃ 5% and brine. The organic layers were dried over sodium sulfate, filtered and the solvent was evaporated under reduced pressure. The crude product was purified by flash column chromatography (Hex/AcOEt 1:1 → Hex/AcOEt 3:7). To obtain the title compound as a yellow sticky solid in 55% yield.

¹H-NMR (400 MHz, CDCl₃): δ = 8.46 (1H, d, *J* = 7.5 Hz), 7.86 (1H, t, *J* = 5.0 Hz), 7.78 – 7.70 (2H, m), 7.53 – 7.46 (4H, m), 7.45 – 7.35 (9H, m), 7.35 – 7.30 (5H, m), 7.28 – 7.25 (2H, m), 7.20 – 7.13 (4H, m), 5.32 (2H, s), 5.20 (1H, d, *J* = 10.1), 5.17 (4H, s), 5.12 (1H, d, *J* = 10.1 Hz), 5.08 (2H, s), 4.64 – 4.56 (1H, m), 4.19 (2H, q, *J* = 7.3 Hz), 3.20 – 3.09 (2H, m), 1.73 – 1.60 (1H, m), 1.49 – 1.37 (1H, m), 1.31 – 1.20 (2H, m), 1.27 (3H, t, *J* = 7.3 Hz), 1.19 – 1.09 (2H, m).

¹³C-NMR (150 MHz, CDCl₃): δ = 172.3 (2C), 171.1, 154.5 (2C), 152.0 (2C), 137.3 (2C), 136.4 (2C), 132.6 (2C), 128.6 (4C), 128.3 (4C), 128.1 (6C), 127.9 (2C), 127.5 (4C), 124.8 (2C), 118.5 (2C), 115.4 (2C), 75.7 (2C), 71.0 (2C), 56.6, 53.4, 45.0 (3C), 35.3, 27.0, 14.7.

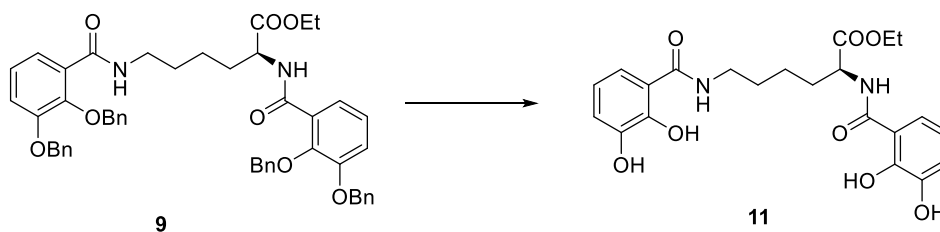
Synthesis of (*S*)-*N,N'*-(6-hydroxyhexane-1,5-diyl)bis(2,3-bis(benzyloxy) benzamide) (**10**)



In a round-bottom flask ethyl *N*²,*N*⁶-bis(2,3-bis(benzyloxy)benzoyl)-L-lysinate (**9**) (145 mg, 0.18 mmol, 1eq) was dissolved in dry THF (1.12 ml, 0.16 M) under an argon atmosphere and cooled in an ice bath. LiBH₄ (6 mg, 0.27 mmol, 1.5 eq) in EtOH dry (1.68 ml, 0.16M) was added and the reaction mixture was stirred at 4 °C for 15 min. The reaction mixture was then warmed to room temperature and stirred overnight. After this time, the reaction was quenched with NH₄Cl sat. and stirred for 15 min. Then the organic solvents were evaporated under reduced pressure. The aqueous layer was extracted with ethyl acetate, the organic layer was dried over sodium sulfate, filtered and the solvents were evaporated under reduced pressure. The crude product was purified by flash column chromatography (DCM/MeOH 95:5). The product was obtained as a transparent sticky oil in 80% yield.

¹H-NMR (400 MHz, CDCl₃): δ = 8.13 (1H, d, *J* = 7.5 Hz), 7.93 (1H, t, *J* = 6.1 Hz), 7.79 – 7.70 (2H, m), 7.51 – 7.46 (4H, m), 7.45 – 7.30 (18H, m), 7.20 – 7.11 (4H, m), 5.22 – 5.15 (5H, m), 5.11 – 5.05 (3H, m), 4.01 – 3.88 (1H, m), 3.57 (1H, dd, *J* = 3.3 Hz *J* = 11.4 Hz), 3.44 (1H, dd, *J* = 6.2 Hz *J* = 11.4 Hz), 3.31 – 3.09 (2H, m), 1.45 – 1.20 (4H, m), 1.19 – 1.04 (4H, m).

Synthesis of Ethyl *N*²,*N*⁶-bis(2,3-dihydroxybenzoyl)-L-lysinate (**11**)



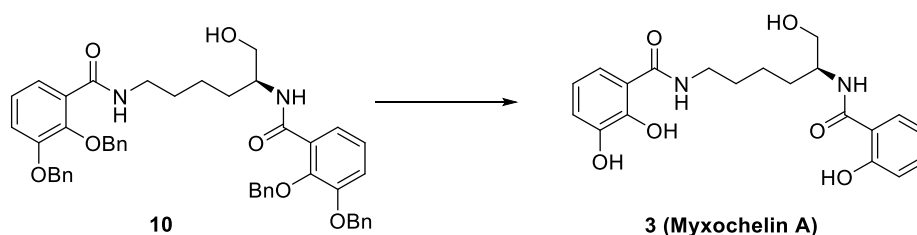
In a round-bottom flask ethyl *N*²,*N*⁶-bis(2,3-bis(benzyloxy)benzoyl)-L-lysinate (**9**) (90 mg, 0.11 mmol,) was dissolved in methanol (18.3 ml, 0.006M) and the catalyst (10% Pd/C, 50% in weight) was added. After creating vacuum inside the flask, the system was put under H₂ atmosphere, and the reaction was stirred at room temperature overnight. After reaction completion, the catalyst was removed by filtration on celite, and the organic solvent was evaporated under reduced pressure. The crude product was purified by flash column chromatography (Hex/AcOEt 1:1). The product was obtained as a white solid in 50% yield.

¹H-NMR (400 MHz, CD₃OD): δ = 7.33 (1H, dd, *J* = 1.5 Hz *J* = 8.1 Hz), 7.20 (1H, dd, *J* = 1.4 Hz *J* = 8.0 Hz), 6.96 (1H, dd, *J* = 1.4 Hz *J* = 7.8 Hz), 6.93 (1H, dd, *J* = 1.5 *J* = 8.0 Hz), 6.77 – 6.67 (2H, m), 4.63 (1H, dd, *J* = 5.4 Hz *J* = 8.0 Hz), 4.20 (2H, q, *J*

= 7.3 Hz), 3.41 (2H, t, $J = 6.9$ Hz), 2.09 – 1.85 (2H, m), 1.75 – 1.64 (2H, m), 1.60–1.47 (2H, m), 1.26 (3H, t, $J = 7.3$ Hz).

$^{13}\text{C-NMR}$ (100 MHz, CD_3OD): $\delta = 172.4, 170.1, 169.7, 148.9, 148.4, 145.9, 145.8, 118.4, 118.3, 118.2$ (x2C), 118.1, 117.2, 115.5, 115.4, 61.0, 52.6, 38.7, 30.7, 28.5, 23.0, 13.1.

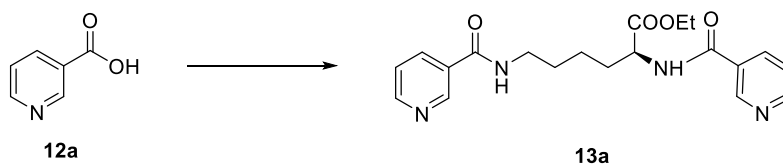
Synthesis of (*S*)-*N,N'*-(6-hydroxyhexane-1,5-diyl)bis(2,3-dihydroxybenzamide) (**3**)



In a round-bottom flask (*S*)-*N,N'*-(6-hydroxyhexane-1,5-diyl)bis(2,3-bis(benzyloxy) benzamide) (**10**) (41.3 mg, 0.05 mmol, 1eq) was dissolved in DCM dry (3.9 ml, 0.01M), then the solution was cooled in a dry ice/acetone bath until the temperature reached -78 °C. BBr_3 (1M, in DCM, 0.24 ml, 4,4 eq) was added dropwise and the reaction was stirred at -78 °C for 1 h. The reaction was then warmed to room temperature and stirred overnight. After reaction completion, methanol was added to neutralize the excess of BBr_3 , and the solvents were evaporated under reduced pressure. The residue was taken up with ethyl acetate and washed with HCl 1N and Brine. The organic layer was dried over sodium sulfate, filtered and the solvents were evaporated under reduced pressure. The crude product was purified by flash column chromatography (DCM/MeOH 95:5). The product was obtained as a slightly orange sticky solid in 60% yield.

$^1\text{H-NMR}$ (600 MHz, CD_3OD): $\delta = 7.29$ (1H, dd, $J = 1.3$ Hz $J = 8.1$ Hz), 7.19 (1H, dd, $J = 1.3$ Hz $J = 8.1$ Hz), 6.98 – 6.90 (2H, m), 6.76 – 6.67 (2H, m), 4.22 – 4.16 (1H, m), 3.70 – 3.60 (2H, m), 3.41 (2H, t, $J = 7.4$ Hz), 1.83 – 1.61 (4H, m), 1.60 – 1.43 (2H, m). Spectroscopic data are in accordance with those reported in literature [34].

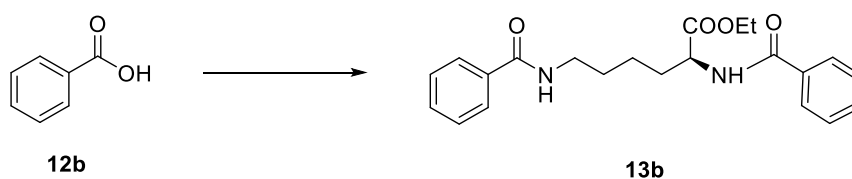
Ethyl N2,N6-dinicotinoyl-L-lysinate (13a)



In a round bottom-flask nicotinic acid (**12a**) (295.5 mg, 2.4 mmol, 2eq) and L-lysine ethyl ester dichlorohydrate (296.6 mg, 1.2 mmol, 1eq) were dissolved in dry DMF (10.4 ml, solution 0,2M) under nitrogen atmosphere. DIPEA (0.47 ml, 2.7 mmol, 2,25 eq), 1-(3-dimethylaminopropyl)-3-ethylcarbodiimide hydrochloride (EDC·HCl, 506.1 mg, 2.6 mmol, 2,2 eq) and hydroxybenzotriazole monohydrate (356.7 mg, 2.6 mmol, HOBT·H₂O, 2,2 eq) were added and the obtained reaction mixture was stirred at room temperature overnight. Then, the reaction mixture was diluted with DCM and the organic layer was washed with 0.02M HCl, 5% NaHCO₃ and brine. The organic layers were dried over sodium sulfate, filtered and the solvent was evaporated under reduced pressure. The crude product was purified by flash column chromatography (DCM/MeOH 95:5) to obtain the title compound as a transparent sticky solid in 81% yield.

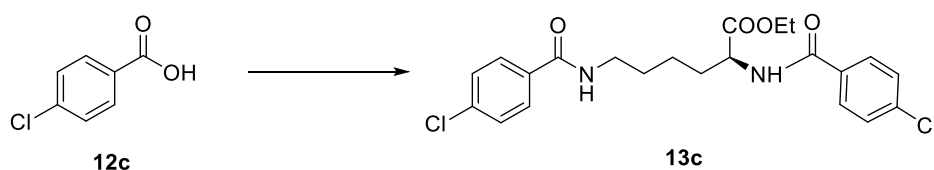
¹H-NMR (600 MHz, CDCl₃): δ = 9.15 – 9.02 (2H, m), 8.80 – 8.69 (2H, m), 8.20 – 8.08 (2H, m), 7.44 – 7.34 (2H, m), 7.17 (1H, d, J = 7.4 Hz), 6.84 – 6.72 (1H, m), 4.84 – 4.77 (1H, m), 4.27 (2H, q, J = 6.9 Hz), 3.60 – 3.47 (2H, m), 2.11 – 1.87 (2H, m), 1.86 – 1.67 (2H, m), 1.63 – 1.47 (2H, m), 1.33 (3H, t, J = 6.9 Hz).

Synthesis of Ethyl N2,N6-dibenzoyl-L-lysinate (13b)



The compound was prepared from benzoic acid (**12b**) (293.1, 2.4 mmol, 2eq) following the procedure described for **13a**. The crude product was purified by flash column chromatography (CyHex/AcOEt 7:3 → 1:1), affording product **13b**, which was obtained in 36% yield and directly used for the next step.

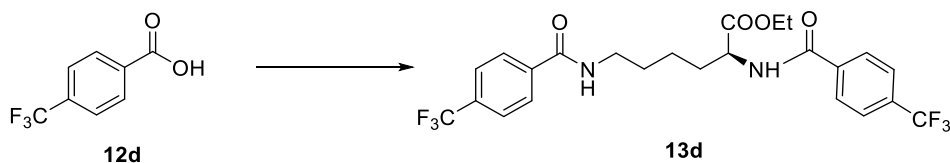
Synthesis of Ethyl N^2,N^6 -bis(4-chlorobenzoyl)-L-lysinate (**13c**)



The compound was prepared from 4-chlorobenzoic acid (375.8 mg, 2.4 mmol, **12c**) (2eq) following the procedure described for **13a**. The crude product was purified by flash column chromatography (DCM/MeOH 98:2). A second purification (Hex/AcOEt 6:4 \rightarrow AcOEt 100%) was needed. The product was obtained as a white yellow solid in 30% yield.

$^1\text{H-NMR}$ (600 MHz, CDCl_3): δ = 7.79 – 7.73 (2H, m), 7.72 – 7.67 (2H, m), 7.44 – 7.39 (2H, m), 7.38 – 7.35 (2H, m), 6.91 (1H, d, J = 7.6 Hz), 6.42 (1H, br. s), 4.83 – 4.75 (1H, m), 4.27 (2H, q, J = 7.1 Hz), 3.59 – 3.50 (1H, m), 2.08 – 1.99 (1H, m), 1.93 – 1.85 (1H, m), 1.84 – 1.76 (1H, m), 1.75 – 1.66 (1H, m), 1.60 – 1.45 (2H, m), 1.32 (3H, t, J = 7.1 Hz).

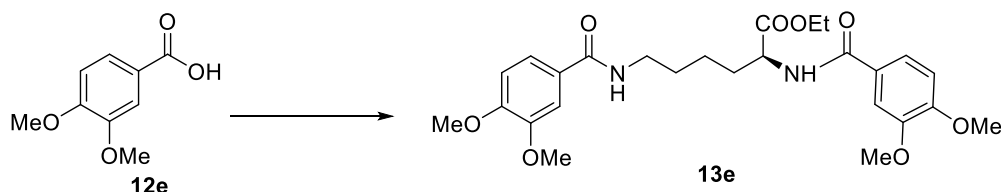
Synthesis of Ethyl N^2,N^6 -bis(4-(trifluoromethyl)benzoyl)-L-lysinate (**13d**)



The compound was prepared from **12d** (456.3, 2.4 mmol, 2eq) following the procedure described for **13a**. The crude product was purified by flash column chromatography (DCM/MeOH 98:2). The product was obtained as a white/yellow solid in 35% yield.

$^1\text{H-NMR}$ (600 MHz, CD_3OD): δ = 8.01 – 7.96 (2H, m), 7.95 – 7.90 (2H, m), 7.77 – 7.69 (4H, m), 4.63 – 4.57 (1H, m), 4.20 (2H, q, J = 7.1 Hz), 3.51 – 3.36 (2H, m), 2.08 – 1.98 (1H, m), 1.96 – 1.86 (1H, m), 1.78 – 1.64 (2H, m), 1.61 – 1.49 (2H, m), 1.27 (3H, t, J = 7.1 Hz).

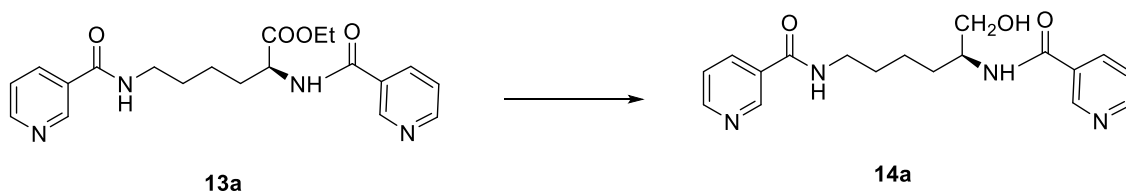
Synthesis of Ethyl N^2,N^6 -bis(3,4-dimethoxybenzoyl)-L-lysinate (**13e**)



The compound was prepared from 2,3-dimethoxybenzoic acid (**12e**) (437.2 mg, 2.4 mmol, 2eq) following the procedure described for **13a**. The crude product was purified by flash column chromatography (AcOEt 100%) to obtain the title compound as a white solid in 40% yield.

¹H-NMR (600 MHz, CDCl₃): δ = 7.46 – 7.42 (2H, m), 7.36 (1H, dd, *J* = 1.7 Hz *J* = 8.1 Hz), 7.26 (1H, dd, *J* = 2.0 Hz *J* = 8.4 Hz), 6.87 – 6.81 (2H, m), 6.79 (1H, d, *J* = 8.4 Hz), 6.38 – 6.28 (1H, m), 4.86 – 4.77 (1H, m), 4.27 (2H, q, *J* = 7.1 Hz), 3.94 (3H, s), 3.93 (3H, s), 3.92 (6H, s), 3.58 – 3.43 (2H, m), 2.08 – 2.00 (1H, m), 1.94 – 1.85 (1H, m), 1.83 – 1.67 (2H, m), 1.61 – 1.47 (2H, m), 1.33 (3H, t, *J* = 7.1 Hz).

Synthesis of (S)-N,N'-(6-hydroxyhexane-1,5-diyl)dinicotinamide (**14a**)

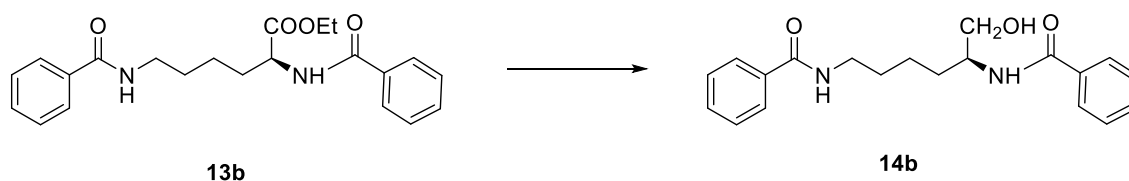


In a round-bottom flask ethyl N²,N⁶-dinicotinoyl-L-lysinate (**13a**) (90.1 mg, 0.23 mmol, 1eq) was dissolved in dry THF (1.5 ml, 0.16 M) under an argon atmosphere and cooled in an ice bath. LiBH₄ (7.7 mg, 0.35 mmol, 1.5 eq) in dry EtOH (2.2 ml, 0.16M) was added and the reaction mixture was stirred at 4 °C for 15 min., then warmed to room temperature and stirred overnight. After this time, the reaction was quenched with a saturated solution of NH₄Cl and stirred for 15 min. The organic solvent was evaporated under reduced pressure. The aqueous layer was extracted with ethyl acetate, and the organic layer was dried over sodium sulfate, filtered, and evaporated under reduced pressure. The crude product was purified by flash column chromatography (DCM/MeOH 9:1) to obtain a white solid in 51% yield.

¹H-NMR (400 MHz, CH₃OH): δ = 8.98 (1H, dd, *J* = 2.3 Hz *J* = 0.7 Hz), 8.95 (1H, dd, *J* = 2.3 *J* = 0.8), 8.69 – 8.64 (2H, m), 8.26 – 8.22 (1H, m), 8.22 – 8.18 (1H, m), 7.55 – 7.48 (2H, m), 4.23 – 4.11 (1H, m), 3.71 – 3.61 (2H, m), 3.48 – 3.38 (2H, t, *J* = 6.5 Hz), 1.84 – 1.60 (4H, m), 1.59 – 1.44 (2H, m)

¹³C-NMR (100 MHz, CH₃OH): δ = 166.6, 166.3, 151.1 (2C), 147.8, 147.7, 135.6, 135.4, 130.9, 130.7, 123.7, 123.6, 63.7, 52.0, 39.4, 30.2, 28.8, 23.2.

Synthesis of (S)-N,N'-(6-hydroxyhexane-1,5-diyl)dibenzamide (14b)

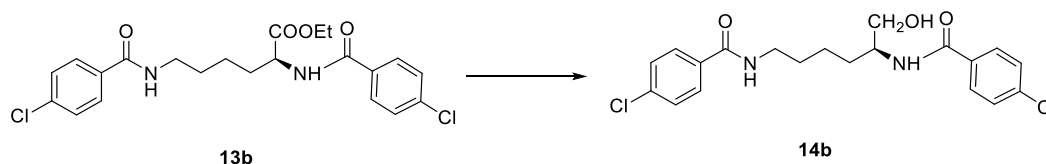


The compound was obtained following the procedure reported for **14a**. The crude product was purified by flash column chromatography (DCM/MeOH 98:2). The product was obtained as a white solid in 50% yield.

¹H-NMR (600 MHz, CH₃OH): δ = 7.86 – 7.82 (2H, m), 7.81 – 7.77 (2H, m), 7.57 – 7.50 (2H, m), 7.47 – 7.40 (4H, m), 4.20 – 4.12 (1H, m), 3.70 – 3.60 (2H, m), 3.49 – 3.37 (2H, m), 1.82 – 1.61 (4H, m), 1.59 – 1.45 (2H, m)

¹³C-NMR (150MHz, CD₃OD): δ = 169.1, 169.0, 134.6, 134.5, 131.1 (x2C), 128.1 (x4C), 126.9 (x2C), 126.8 (x2C), 63.8, 51.8, 39.3, 30.3, 29.0, 23.2.

Synthesis of (S)-N,N'-(6-hydroxyhexane-1,5-diyl)bis(4-chlorobenzamide) (14c)

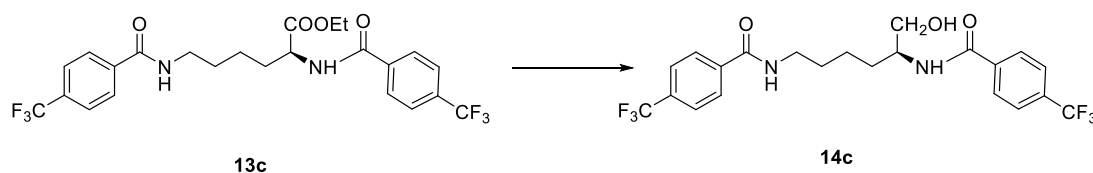


The compound was obtained following the procedure reported for **14a**. The crude product was purified by flash column chromatography (DCM/MeOH 95:5) The product was obtained as a white solid in 30% yield.

¹H-NMR (600 MHz, CD₃OD): δ = 7.84 – 7.73 (4H, m), 7.49 – 7.40 (4H, m), 4.20 – 4.10 (1H, m), 3.69 – 3.60 (2H, m), 3.47 – 3.36 (2H, m), 1.82 – 1.60 (4H, m), 1.58 – 1.44 (2H, m)

¹³C-NMR (100 MHz, CD₃OD): δ = 167.9, 137.2, 133.2, 131.1, 128.7, 126.9, 63.8, 51.8, 39.4, 30.3, 29.1, 23.1.

Synthesis of (S)-N,N'-(6-hydroxyhexane-1,5-diyl)bis(4-(trifluoromethyl)benzamide) (14d)

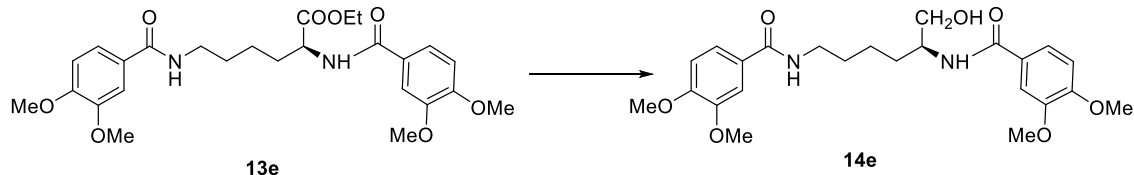


The compound was obtained following the procedure reported for **14a**. The product was obtained as a white powder in 93% yield. No further purification was needed.

¹H-NMR (400 MHz, CD₃OD): δ = 7.99 – 7.9 (4H, m), 7.75 – 7.68 (4H, m), 4.24 – 4.09 (1H, m), 3.70 – 3.60 (2H, m), 3.53 – 3.36 (2H, m), 1.87 – 1.61 (4H, m), 1.60 – 1.45 (2H, m)

¹³C-NMR (100 MHz, CD₃OD): δ = 167.7, 167.4, 138.3, 138.1, 132.5 (q, J_{C-F} = 31.9, C-CF₃, 2C), 127.7 (2C), 127.6 (2C), 125.0 (m, 4C), 123.8 8 (q, J_{C-F} = 272.0 Hz, CF₃, 2C), 63.7, 52.0, 39.3, 30.2, 28.8, 23.1.

Synthesis of (S)-N,N'-(6-hydroxyhexane-1,5-diyl)bis(3,4-dimethoxybenzamide) (14e)

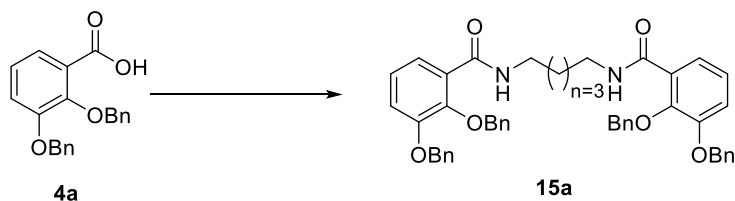


The compound was obtained following the procedure reported for **14a** as a transparent sticky solid in 61% yield. No further purification was needed.

¹H-NMR (600 MHz, CD₃OD): δ = 7.48 – 7.42 (2H, m), 7.41 – 7.36 (2H, m), 6.97 – 6.90 (2H, m), 4.19 – 4.11 (1H, m), 3.89 (6H, s), 3.87 (3H, s), 3.86 (3H, s), 3.65-3.60 (2H, m), 3.50 – 3.41 (1H, m), 3.40 – 3.34 (1H, m), 1.82 – 1.59 (4H, m), 1.58 – 1.43 (2H, m)

¹³C-NMR (100 MHz, CD₃OD): δ = 168.4, 152.0, 148.7, 126.8, 120.3, 110.4, 64.0, 55.1, 51.7, 39.2, 30.3, 29.0, 23.1.

Synthesis of N,N'-(pentane-1,5-diyl)bis(2,3-bis(benzyloxy)benzamide) (15a)

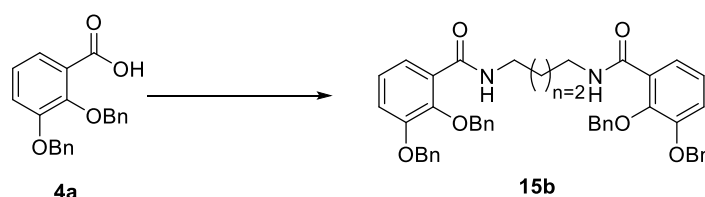


To a solution of 2,3-bis(benzyloxy)benzoic acid **4a** (0.20 g, 0.6 mmol) in THF (7.0 mL), HATU (0.24 g, 0.66 mmol) and DIPEA (0.16 mL, 0.90 mmol) were added, and the mixture was stirred for 30 min at room temperature. Then, 1,5-diaminopentane (0.35 mL, 0.30 mmol) was added and the new mixture was stirred overnight at room temperature. After the completion of the reaction, the solvent was evaporated and EtOAc was added. The organic layer was washed with sat. NH₄Cl and brine, dried with Na₂SO₄, filtered, and evaporated. The residue was purified by flash column chromatography (Hex/EtOAc 1:1) to provide **15a** after evaporation of the solvent as oil (80% yield).

¹H NMR (400 MHz, CDCl₃): δ = 7.95 (2H, t, *J* = 5.2 Hz), 7.77 – 7.73 (2H, m), 7.50 – 7.38 (20H, m), 7.18 – 7.16 (4H, m), 5.18 (4H, s), 5.09 (4H, s), 3.21 (4H, q, *J* = 6.0 Hz), 1.31 – 1.24 (4H, m), 1.16 – 1.10 (2H, m)

¹³C NMR (100 MHz, CDCl₃): δ = 165.1 (2C), 151.7 (2C), 146.8 (2C), 136.4 (4C), 128.7 (16C), 128.3 (2C), 127.7 (2C), 127.4 (2C), 124.4 (2C), 123.4 (2C), 117.0 (2C), 71.3 (4C), 39.5 (2C), 28.9 (2C), 24.41 [35].

Synthesis of *N,N'*-(butane-1,4-diyl)bis(2,3-bis(benzyloxy)benzamide) (**15b**)

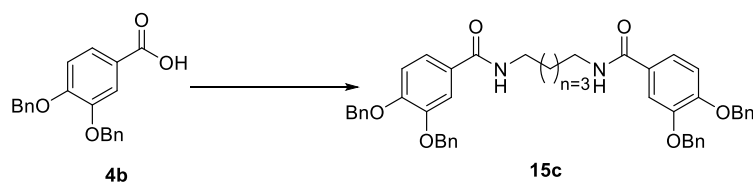


Following the procedure reported for **15a**, **15b** was obtained from 2,3-bis(benzyloxy)benzoic acid **4a** and 1,4-diaminobutane (0.11 g, 1.2 mmol) after purification by flash column chromatography (Hex/EtOAc 6:4) and evaporation of the solvent as a white amorphous solid (85% yield).

¹H NMR (400 MHz, CDCl₃): δ = 7.89 (2H, t, *J* = 5.2 Hz), 7.78 – 7.76 (2H, m), 7.50 – 7.17 (24H, m), 5.18 (4H, s), 5.08 (4H, s), 3.24 – 3.16 (4H, m), 1.26 – 1.23 (4H, m)

¹³C NMR (100 MHz, CDCl₃): δ = 165.0 (2C), 151.7 (2C), 146.8 (2C), 136.5 (2C), 136.4 (2C), 128.7 (16C), 128.3 (2C), 127.7 (2C), 127.4 (2C), 124.4 (2C), 123.4 (2C), 117.0 (2C), 76.4 (2C), 71.3 (2C), 39.3 (2C), 26.7 (2C)

Synthesis of *N,N'*-(pentane-1,5-diyl)bis(3,4-bis(benzyloxy)benzamide) (15c)

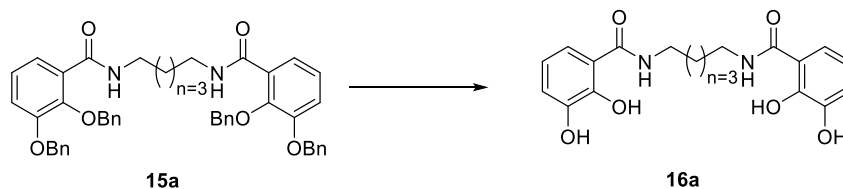


Following the procedure reported for **15a**, **15c** was obtained from 3,4-bis(benzyloxy)benzoic acid **4b** (0.20 g, 0.60 mmol) and 1,5-diaminopentane (0.35 mL, 0.30 mmol) after purification by flash column chromatography (DCM/MeOH 98:2) and evaporation of the solvent as a white amorphous solid (75% yield).

¹H NMR (400 MHz, DMSO-*d*₆): δ = 8.28 (2H, t, *J* = 5.6 Hz), 7.57 (2H, d, *J* = 2.0 Hz), 7.47 – 7.30 (22H, m), 7.10 (2H, d, *J* = 8.4 Hz), 5.19 (4H, s), 5.16 (4H, s), 3.24 (4H, q, *J* = 6.0 Hz), 1.58 – 1.51 (4H, m), 1.38 – 1.32 (2H, m)

¹³C NMR (100 MHz, DMSO-*d*₆): δ = 165.9 (2C), 151.0 (2C), 148.1 (2C), 137.6 (2C), 137.4 (2C), 128.9 (8C), 128.3 (4C), 128.0 (8C), 127.9 (2C), 121.2 (2C), 113.8 (2C), 113.7 (2C), 70.7 (2C), 70.4 (2C), 39.7 (2C), 29.4 (2C), 24.5.

Synthesis of *N,N'*-(pentane-1,5-diyl)bis(2,3-dihydroxybenzamide) (16a)

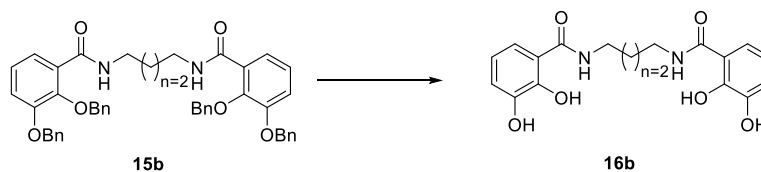


To a cold solution of **15a** (0.13 g, 0.18 mmol) at -78 °C in DCM (12 mL), BBr₃ (0.79 mL, 0.79 mmol, 1.0 M in DCM, 1.1 equiv. per bond) was added dropwise and the reaction was kept for another 1 h at the same temperature and then overnight at room temperature. Then, the solution was cooled at 0 °C, neutralized with MeOH and H₂O was added. The organic phase was extracted twice with EtOAc. The combined organic extracts were washed with brine, dried with Na₂SO₄, filtered, and evaporated. The residue was purified by flash column chromatography (DCM/MeOH 96:4) to provide amide **16a** after evaporation of the solvent as a white amorphous solid (75% yield).

¹H NMR (400 MHz, CDCl₃): δ = 7.04 (2H, d, *J* = 10.8 Hz), 6.87 (2H, d, *J* = 10.8 Hz), 6.74 (2H, t, *J* = 10.8 Hz), 6.42 (2H, br. s), 3.48 (4H, q, *J* = 8.8 Hz), 1.76 – 1.66 (4H, m), 1.53 – 1.43 (2H, m)

^{13}C NMR (100 MHz, CDCl_3): δ = 170.1 (2C), 148.8 (2C), 145.9 (2C), 118.1 (4C), 117.2 (2C), 115.4 (2C), 38.96 (2C), 28.70 (2C), 23.98 [35].

Synthesis of N,N' -(butane-1,4-diyl)bis(2,3-dihydroxybenzamide) (**16b**)

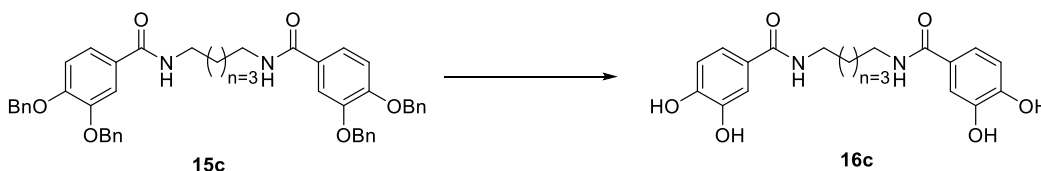


Following the procedure reported for **16a**, **16b** was obtained from **15b** (0.10 g, 0.14 mmol) after purification by flash column chromatography (DCM/MeOH 98:2) and evaporation of the solvent as a white amorphous solid (90% yield).

^1H NMR (400 MHz, $\text{DMSO}-d_6$): δ = 12.8 (2H, br. s), 7.28 (2H, br. s), 7.28 (2H, t, J = 5.6 Hz), 7.28 (2H, dd, J = 8.0 Hz J = 0.8 Hz), 6.91 (2H, dd, J = 8.0 Hz J = 0.8 Hz), 6.68 (2H, t, J = 8.0 Hz), 3.35 – 3.32 (4H, m), 1.62 – 1.56 (4H, m)

^{13}C NMR (100 MHz, $\text{DMSO}-d_6$): δ = 170.2 (2C), 150.2 (2C), 146.7 (2C), 119.2 (2C), 118.3 (2C), 117.5 (2C), 115.4 (2C), 30.1 (2C), 26.9 (2C).

Synthesis of N,N' -(pentane-1,5-diyl)bis(3,4-dihydroxybenzamide) (**16c**)



Following the procedure reported for **16a**, **16c** was obtained from **15c** (0.10 g, 0.14 mmol) after purification by flash column chromatography (DCM/MeOH 85:15) and evaporation of the solvent as a white amorphous solid (70% yield).

^1H NMR (400 MHz, CD_3OD): δ = 7.28 (2H, d, J = 2.0 Hz), 7.18 (2H, dd, J = 8.4 Hz J = 2.0 Hz), 6.78 (2H, d, J = 8.4 Hz), 3.36 – 3.33 (4H, m), 1.67 – 1.60 (4H, m), 1.46 – 1.39 (2H, m)

^{13}C NMR (100 MHz, CD_3OD): δ = 168.9 (2C), 148.6 (2C), 144.9 (2C), 125.9 (2C), 119.1 (2C), 114.4 (2C), 114.3 (2C), 39.4 (2C), 28.9 (2C), 24.0.

Evaluation of iron-chelating properties and biological activity

Chromule azurol S (CAS) assay

CAS Reagent. 100mL graduated glass cylinder was previously washed with HCl 6M. 6mL of 10mM solution of hexadecyltrimethylammonium bromide (HDTMA) (22 mg in 6 mL distilled water) was poured into the cylinder and diluted to 40 mL with distilled water. While stirring, 1.5 mL of 1 mM ferric iron solution (2.7 mg of $\text{FeCl}_3 \cdot 6\text{H}_2\text{O}$ in 10 mL HCl 1M) was added, whereupon 7.5 mL of 2 mM Chrome Azurol S (CAS) solution (9.1 mg in 7.5 mL distilled water) was added slowly.

In a separate flask 2.5M solution of piperazine (4.31mg in 20 mL distilled water) was prepared and cooled to 0 °C and 6.25 mL of concentrated HCl (37%) was added carefully. The piperazine solution was added to the CAS/ Fe^{3+} solution in the cylinder, and then brought to a final volume of 100 mL with distilled water. Lastly, sulfosalicylic acid (102 mg) was added. The final blue solution was stored in plastic falcon and away from light.

Compounds. Tested compounds were dissolved in H_2O : DMSO 9:1 in order to get a final concentration of 1mg/mL. 100 μL of CAS Reagent and then 100 μL of the tested compound solution were added into the same well of the 96 Microwell plate and allowed to react for 30 minutes. The assay was done in triplicate. EDTA was selected as positive control, whereas the negative control (N.C.) was the blank solution of H_2O : DMSO 9:1.

Fungal Strains

In this study, four strains of *P. oryzae* were used: two strains sensitive to quinone outside inhibitor (QoI) fungicides (WT): A252 and TA102, and two strains resistant to QoI (RES): PO21_01 and PO21_07. The strains belong to a vast collection of *P. oryzae* monoconidial isolates maintained at the Laboratory of Plant Pathology, University of Milan. The strains were maintained as single-spore isolates on malt-agar medium (MA: 20 g/L malt extract, Oxoid, U.K.; 15 g/L agar, Oxoid, U.K.) at 4 °C.

Collection of spores

The individual fungal strains were inoculated on MA medium and incubated in the growth chamber at 24°C in the dark for 12-14 days. Then, 2 ml of sterile water were added to the mycelium and the formed conidia were scraped from the whole mycelium surface with the help of the glass spatula. The spore

suspension was collected and filtered through two layers of sterile gauze into an Eppendorf tube to remove mycelium. The whole amount was applied on a piece of sterile filter paper (4 x 4 cm) and left air-dry under the hood. The filter paper containing the spores was cut into small pieces and stored in a freezer at -20°C until use.

Inhibition of spore germination and appressorium formation

Three to five pieces of filter paper containing the spores were put in an Eppendorf with 1 ml of sterile water and vortexed for 10 minutes to release the spores. The spore concentration was estimated using the Thoma haemocytometer and adjusted to a concentration of 2×10^4 conidia/ml. The tested compounds were dissolved in methanol and were added to 100 μ l of conidial suspension to obtain final concentrations of 1000 – 100 – 10 μ M and 2% of methanol. Conidia treated with 2% methanol were considered a control. Twenty μ l of conidial suspension in three replicates were applied on a microscopic cover slide in a wet chamber and incubated for 24 hours at 24°C in the dark. The germination of 100 randomly chosen conidia for each treatment and replica was determined. The conidia were assigned into one of four germination classes: NG = not germinated, G = germinated, A = germinated with appressorium, and ANM = germinated with not mature appressorium.

The percentage of spore germination was calculated according to the formula: $\text{Germ (\%)} = \Sigma(\text{G}+\text{A}+\text{ANM})/n \times 100$, where n = total number of spores observed per replica. The inhibition of spore germination was calculated as $\text{IG (\%)} = (\text{GermC} - \text{GermT}) / \text{GermC} \times 100$, where GermC was % germination in the control (solvent), and GermT was % germination in the treated sample. Inhibition of appressoria formation was calculated as $\text{IA (\%)} = (\text{GermT} - \text{AT}) / \text{GermT} \times 100$, where AT was % of appressoria in the treated sample.

Statistical analysis

The statistical analyses were performed using R software, version 4.2.2.22 The percentage data of the inhibition of spore germination and appressorium formation were square root arcsine transformed and submitted to ANOVA, followed by Tukey's post hoc test for multiple comparison ($P = 0.05$), using the TukeyC package.

3.5. Bibliography

1. Fróna, D.; Szenderák, J.; Harangi-Rákos, M. The challenge of feeding the world. *Sustain.* **2019**, *11*, 5816, doi:10.3390/su11205816.
2. Savary, S.; Willocquet, L.; Pethybridge, S.J.; Esker, P.; McRoberts, N.; Nelson, A. The global burden of pathogens and pests on major food crops. *Nat. Ecol. Evol.* **2019**, *3*, 430–439, doi:10.1038/s41559-018-0793-y.
3. Steinberg, G.; Gurr, S.J. Fungi, fungicide discovery and global food security. *Fungal Genet. Biol.* **2020**, *144*, 103476, doi:10.1016/j.fgb.2020.103476.
4. Stukenbrock, E.; Gurr, S. Address the growing urgency of fungal disease in crops. *Nature* **2023**, *617*, 31–34.
5. Perlin, D.S.; Rautemaa-Richardson, R.; Alastruey-Izquierdo, A. The global problem of antifungal resistance: prevalence, mechanisms, and management. *Lancet Infect. Dis.* **2017**, *17*, e383–e392, doi:10.1016/S1473-3099(17)30316-X.
6. Fisher, M.C.; Hawkins, N.J.; Sanglard, D.; Gurr, S.J. Worldwide emergence of resistance to antifungal drugs challenges human health and food security. *Science (80-.)*. **2018**, *360*, 739–742.
7. Wilson, R.A.; Talbot, N.J. Under pressure: Investigating the biology of plant infection by *Magnaporthe oryzae*. *Nat. Rev. Microbiol.* **2009**, *7*, 185–195, doi:10.1038/nrmicro2032.
8. Kato, H. Rice Blast Disease. *R. Soc. Chem.* **2001**, 23–25.
9. Hosseini-Moghaddam, M.S.; Soltani, J. An investigation on the effects of photoperiod, aging and culture media on vegetative growth and sporulation of rice blast pathogen *Pyricularia oryzae*. *Prog. Biol. Sci.* **2013**, *3*, 135–143.
10. Skamnioti, P.; Gurr, S.J. Against the grain: safeguarding rice from rice blast disease. *Trends Biotechnol.* **2009**, *27*, 141–150, doi:10.1016/j.tibtech.2008.12.002.
11. Devanna, B.N.; Jain, P.; Solanke, A.U.; Das, A.; Thakur, S.; Singh, P.K.; Kumari, M.; Dubey, H.; Jaswal, R.; Pawar, D.; et al. Understanding the Dynamics of Blast Resistance in Rice-*Magnaporthe oryzae* Interactions. *J. Fungi* **2022**, *8*, 584, doi:10.3390/jof8060584.
12. Tenni, D.; Sinetti, A.; Waldner, M.; Torriani, S.F.F.; Romani, M. First report of QoI resistance in Italian population of *Pyricularia oryzae*. *J. Plant Dis. Prot.* **2021**, *128*, 1705–1709, doi:10.1007/s41348-021-00494-3.

13. Pinna, C.; Laurenzi, T.; Forlani, F.; Palazzolo, L.; Nolan, C. B.; Christodoulou, M.S.; Cortesi, P.; Pinto, A.; Eberini, I.; Kunova, A.; Dallavalle, S. Exploration of Novel Scaffolds Targeting Cytochrome b of *Pyricularia oryzae*. *Int. J. Mol. Sci.* **2023**, *24*, 2705, <https://doi.org/10.3390/ijms24032705>.
14. Shen, Q.; Liang, M.; Yang, F.; Deng, Y.Z.; Naqvi, N.I. Ferroptosis contributes to developmental cell death in rice blast. *New Phytol.* **2020**, *227*, 1831–1846, doi:10.1111/nph.16636.
15. Stockwell, B.R.; Friedmann Angeli, J.P.; Bayir, H.; Bush, A.I.; Conrad, M.; Dixon, S.J.; Fulda, S.; Gascón, S.; Hatzios, S.K.; Kagan, V.E.; et al. Ferroptosis: A Regulated Cell Death Nexus Linking Metabolism, Redox Biology, and Disease. *Cell* **2017**, *171*, 273–285, doi:10.1016/j.cell.2017.09.021.
16. Yang, W.S.; Stockwell, B.R. Ferroptosis: Death by Lipid Peroxidation. *Trends Cell Biol.* **2016**, *26*, 165–176, doi:10.1016/j.tcb.2015.10.014.
17. Yang, W.S.; Kim, K.J.; Gaschler, M.M.; Patel, M.; Shchepinov, M.S.; Stockwell, B.R. Peroxidation of polyunsaturated fatty acids by lipoxygenases drives ferroptosis. *Proc. Natl. Acad. Sci. U. S. A.* **2016**, *113*, E4966–E4975, doi:10.1073/pnas.1603244113.
18. Liang, M.; Ye, H.; Shen, Q.; Jiang, X.; Cui, G.; Gu, W.; Zhang, L.H.; Naqvi, N.I.; Deng, Y.Z. Tangeretin inhibits fungal ferroptosis to suppress rice blast. *J. Integr. Plant Biol.* **2021**, *63*, 2136–2149, doi:10.1111/jipb.13175.
19. De Serrano, L.O. Biotechnology of siderophores in high-impact scientific fields. *Biomol. Concepts* **2017**, *8*, 169–178, doi:10.1515/bmc-2017-0016.
20. Hamid, B.; Zaman, M.; Farooq, S.; Fatima, S.; Sayyed, R.Z.; Baba, Z.A.; Sheikh, T.A.; Reddy, M.S.; Enshasy, H. El; Gafur, A.; et al. Bacterial plant biostimulants: A sustainable way towards improving growth, productivity, and health of crops. *Sustain.* **2021**, *13*, 1–24, doi:10.3390/su13052856.
21. Nagata, T.; Oobo, T.; Aozasa, O. Efficacy of a bacterial siderophore, pyoverdine, to supply iron to *Solanum lycopersicum* plants. *J. Biosci. Bioeng.* **2013**, *115*, 686–690, doi:10.1016/j.jbiosc.2012.12.018.
22. Kramer, J.; Özkaya, Ö.; Kümmerli, R. Bacterial siderophores in community and host interactions. *Nat. Rev. Microbiol.* **2020**, *18*, 152–163, doi:10.1038/s41579-019-0284-4.
23. Pecoraro, L.; Wang, X.; Shah, D.; Song, X.; Kumar, V.; Shakoob, A.; Tripathi, K.; Ramteke, P.W.; Rani, R. Biosynthesis Pathways, Transport Mechanisms and Biotechnological Applications of Fungal Siderophores. *J.*

Fungi **2022**, *8*, 21, doi:10.3390/jof8010021.

24. Wilson, B.R.; Bogdan, A.R.; Miyazawa, M.; Hashimoto, K.; Tsuji, Y. Siderophores in Iron Metabolism: From Mechanism to Therapy Potential. *Trends Mol. Med.* **2016**, *22*, 1077–1090, doi:10.1016/j.molmed.2016.10.005.
25. Bijlsma, J.; de Bruijn, W.J.C.; Hageman, J.A.; Goos, P.; Velikov, K.P.; Vincken, J.P. Revealing the main factors and two-way interactions contributing to food discolouration caused by iron-catechol complexation. *Sci. Rep.* **2020**, *10*, 1–12, doi:10.1038/s41598-020-65171-1.
26. Nguyen, M.; Meunier, B.; Robert, A. Catechol-Based Ligands as Potential Metal Chelators Inhibiting Redox Activity in Alzheimer's Disease. *Eur. J. Inorg. Chem.* **2017**, *2017*, 3198–3204, doi:10.1002/ejic.201700385.
27. Leydier, A.; Lin, Y.; Arrachart, G.; Turgis, R.; Lecerclé, D.; Favre-Reguillon, A.; Taran, F.; Lemaire, M.; Pellet-Rostaing, S. EDTA and DTPA modified ligands as sequestering agents for uranyl decorporation. *Tetrahedron* **2012**, *68*, 1163–1170, doi:10.1016/j.tet.2011.11.065.
28. Wang, D.G.; Niu, L.; Lin, Z.M.; Wang, J.J.; Gao, D.F.; Sui, H.Y.; Li, Y.Z.; Wu, C. The Discovery and Biosynthesis of Nicotinic Myxochelins from an *Archangium* sp. SDU34. *J. Nat. Prod.* **2021**, *84*, 2744–2748, doi:10.1021/acs.jnatprod.1c00524.
29. D'Amato, A.; Ghosh, P.; Costabile, C.; Della Sala, G.; Izzo, I.; Maayan, G.; De Riccardis, F. Peptoid-based siderophore mimics as dinuclear Fe³⁺chelators. *Dalt. Trans.* **2020**, *49*, 6020–6029, doi:10.1039/d0dt00689k.
30. Schnabelrauch, M.; Wittmann, S.; Rahn, K.; Möllmann, U.; Reissbrodt, R.; Heinisch, L. New synthetic catecholate-type siderophores based on amino acids and dipeptides. *BioMetals* **2000**, *13*, 333–348, doi:10.1023/A:1009297610755.
31. Zhang, Q.; Jin, B.; Wang, X.; Lei, S.; Shi, Z.; Zhao, J.; Liu, Q.; Peng, R. The mono(Catecholamine) derivatives as iron chelators: Synthesis, solution thermodynamic stability and antioxidant properties research. *R. Soc. Open Sci.* **2018**, *5*, 171492, doi:10.1098/rsos.171492.
32. Guo, W.; Kong, X.; Zhu, T.; Gu, Q.; Li, D. Penipyrols A-B and peniamidones A-D from the mangrove derived *Penicillium solitum* GWQ-143. *Arch. Pharm. Res.* **2015**, *38*, 1449–1454, doi:10.1007/s12272-014-0513-3.
33. Dubme, A.-K.; Hider, R.C.; Khodrb, H.H. Synthesis and Iron-Binding Properties of Protochelin, the Tris(catecholamide) Siderophore of *Azotobacter vinelandii*. *Chem. Ber.* **1997**, *130*, 969–973.

34. Schieferdecker, S.; Nett, M. A fast and efficient method for the preparation of the 5-lipoxygenase inhibitor myxochelin A. *Tetrahedron Lett.* **2016**, *57*, 1359–1360, doi:10.1016/j.tetlet.2016.02.047.
35. Miyanaga, S.; Sakurai, H.; Saiki, I.; Onaka, H.; Igarashi, Y. Synthesis and evaluation of myxochelin analogues as antimetastatic agents. *Bioorganic Med. Chem.* **2009**, *17*, 2724–2732, doi:10.1016/j.bmc.2009.02.040.

Chapter 4: Biocatalyzed synthesis of phenolamides and evaluation of their antimicrobial activity.

Published article:

“Biocatalyzed synthesis of vanillamides and evaluation of their antimicrobial activity.” - *J. Agric. Food Chem.* **2022**, *70*, 1, 223–228.

DOI :<https://doi.org/10.1021/acs.jafc.1c06213>

Authors:

Cecilia Pinna,¹ Piera Anna Martino,² Gabriele Meroni,² Valerio Massimo Sora,² Lucia Tamborini,³ Sabrina Dallavalle,¹ Martina L. Contente,¹ and Andrea Pinto¹

Affiliations:

¹Department of Food, Environmental and Nutritional Sciences (DeFENS), University of Milan, 20133 Milan, Italy.

²Department of Biomedical, Surgical and Dental Sciences (DSBCO), One Health Unit, University of Milan, 20133 Milan, Italy.

³Department of Pharmaceutical Sciences (DISFARM), University of Milan, 20133 Milan, Italy.

Abstract

A series of vanillamides were easily synthesized, exploiting an acyltransferase from *Mycobacterium smegmatis* (MsAcT). After their evaluation as antimicrobial agents against a panel of Gram-positive and Gram-negative bacteria, three compounds were demonstrated to be 9-fold more effective toward *Pseudomonas aeruginosa* than the vanillic acid precursor. Taking into consideration the scarce permeability of the Gram-negative bacteria cell envelope when compared to Gram-positive strains or yeasts, these molecules can be considered the basis for the generation of new nature-inspired antimicrobials. To increase the process productivity and avoid any problem related to the poor water solubility of the starting material, a tailored flow biocatalyzed strategy in pure toluene was set up. While a robust immobilization protocol exploiting glyoxyl-agarose was employed to increase the stability of MsAcT, in-line work-up procedures were added downstream the process to enhance the system automation and reduce the overall costs.

KEYWORDS: *vanillamides, antimicrobial agents, MsAcT, biocatalyzed reactions, enzyme immobilization, flow chemistr*

4.1 Introduction

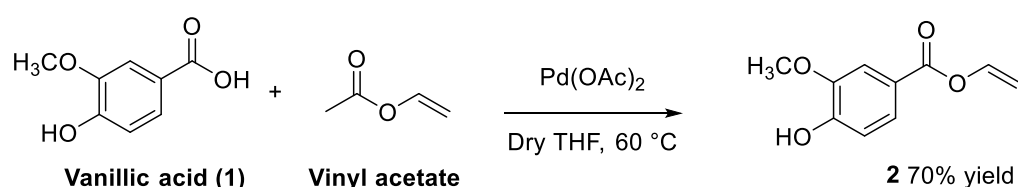
Microorganisms are frequently associated with a variety of diseases in a wide range of infections. During the past years, a significant increase in antimicrobial resistance, prolonged treatment times, therapy toxicity, and related costs was observed [1]. Well-known multidrug-resistant strains, such as the methicillin-resistant *Staphylococcus epidermidis* (MRSE), *Staphylococcus aureus* (MRSA), and vancomycin-resistant *Enterococcus faecalis* (VRE), among the Gram-positive bacteria, and *Escherichia coli*, *Klebsiella pneumoniae*, and *Pseudomonas aeruginosa*, considering the Gram-negative ones, have appeared to be the main source of community- and hospital-associated severe infections [2]. Among the causes, the abuse of antimicrobials and interrupted therapies in humans or animals seem to play a key role, thus making antimicrobial resistance a global threat worldwide [3–5]. Natural products typically produced by living organisms (e.g., plants, bacteria, fungi, sponges, and animals) against pathogens or stress factors have been successfully used for treating several illnesses and represent a great source of inspiration for the development of novel bioactive molecules [6,7]. The chemical diversity of natural compounds as well as the wide range of activities (anticancer, antimicrobial, immunomodulatory, antioxidant, and anti-inflammatory, among others) have attracted the attention of many researchers during the years. In this context, identifying natural antimicrobial agents, understanding their mechanism of action, and optimizing their structure–activity relationship are important tasks. As described in **Chapter 1**, many phenolic compounds derived from plants exhibit antimicrobial properties and therefore have the potential to be applied as new varieties of antimicrobial agents. In this work, we focused our attention on benzoic acids and particularly on vanillic acid. Aiming at improving the chemophysical properties and the stability profile of vanillic acid, a small collection of differently *N*-substituted vanillamides was prepared to be tested as antimicrobial agents [2,8]. In tune with the increasing emphasis placed today on sustainable processing in chemistry, a biocatalytic approach exploiting the efficient and selective acyl transferase from *Mycobacterium smegmatis* (MsAcT) [9,10] was set up and optimized. While batch strategies [11–13] have been employed to generate a sufficient amount of compounds to assess their antibacterial activities, a tailored flow-intensified process was developed for the best hits [14,15]. We recently exploited the immobilized MsAcT (imm-MsAcT) for the flow synthesis of esters and amides both in water and organic solvents, starting from primary alcohols or amines and short chain esters [16–19]. The first immobilization attempts involved the use of carbon nanotubes to exploit the MsAcT perhydrolase properties [20,21]. A better catalyst activity and stability for the condensation

reactions (i.e., esterification and amidation reactions) have been observed using hydrophilic supports; among them, glyoxyl-agarose showed the best results (i.e., recovered activity: 73%; enzymatic loading: 1 mg_{MsAcT}/ g_{matrix}; reusability: 100 cycles) [18]. In the present work, the catalytic power of MsAcT was demonstrated using vinyl vanillate (i.e., vinyl 4-hydroxy-3-methoxybenzoate **2**, **Scheme 4.3**) and several primary amines in pure toluene, thus guaranteeing a good solubility of the hydrophobic substrates while achieving highly productive protocols. It is worth noting that conventional chemical methods for the preparation of vanillamides usually require energy-consuming procedures, harsh reaction conditions, the use of unstable coupling agents, and an anhydrous environment, generating a significant amount of waste [22]. In this scenario, biocatalytic approaches can be considered an alternative to classical chemistry and their combination with flow facilities represents a powerful tool to enhance productivity while reducing the process-related costs.

4.2 Results and discussion

Batch Biotransformations and Vanillamide Antimicrobial Activity Evaluation.

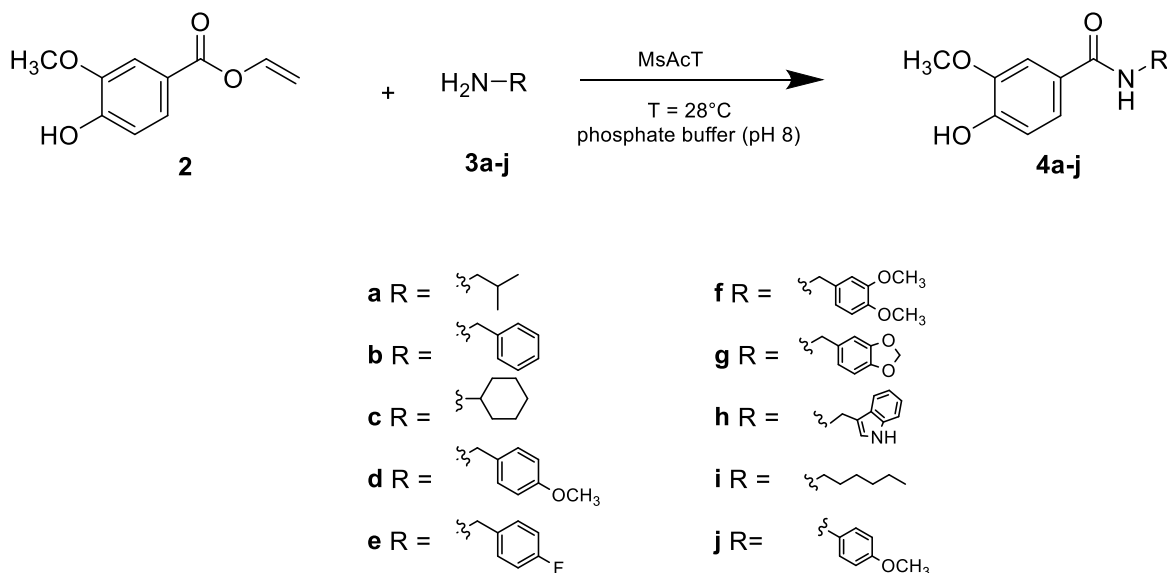
In previous works, it was already demonstrated that vinyl esters are more efficient acyl donors than the ethyl ones for MsAcT-mediated transesterifications, so activated vinyl vanillate was prepared through a Pd(II)-catalyzed transvinylation reaction starting from vanillic acid (**Scheme 4.1**) [12,18,19].



Scheme 4.3. Preparation of vinyl vanillate **2**

Using the newly formed ester and several primary amines, batch reactions were subsequently carried out for the preparation of a variety of different vanillamides (**Figure 4.3**). Following our previously optimized reaction conditions [11–13] a high substrate loading (0.25 M for the acyl donor and 0.5 M for the amines), free MsAcT (1 mg/mL), and phosphate buffer (0.1 M, pH 8.0) were employed. Unlike the biotransformations described so far, where water-immiscible liquid acyl donors were employed, creating a more favorable-to-solubilization biphasic environment, vinyl vanillate is a solid compound slightly soluble in buffer media. Adding cosolvents (e.g., 10–20% (v/v) DMSO) or decreasing the substrate concentration (0.05 and 0.1 M) did not show any

further improvement in the solubility. Although the reactions were characterized by modest-to good yields (15–40%) and prolonged reaction times (24 h), mainly due to the poor solubility of vinyl vanillate, the desired products **4a-j** were obtained in a sufficient amount to assay their potential antimicrobial activity (**Table 4.2**).



Scheme 4.4. Batch preparation of vanillamides in water media

According to the literature, vanillic acid has been reported to have antimicrobial activity against *Bacillus cereus*, *E. coli*, *S. aureus*, *P. aeruginosa*, and *Salmonella typhi* with MICs in the range of 2000–583 $\mu\text{g/ml}$ [23,24]. Therefore, compounds **4a–4j** have been submitted to antibacterial screening against a panel of Gram-positive and Gram-negative bacteria. **Table 4.2** shows the results of MICs against target microorganisms. Interestingly, all the amide derivatives exhibited better activity than the vanillic acid precursor. It was reported that compounds such as geraniol, octanol, citronellol, and polyphenols showed antimicrobial activity through microbial membrane disruption [8,25–27]. This suggests that the increased lipophilicity of the generated molecules in combination with the polyphenolic moiety may have strengthened their antimicrobial activity through their membrane-disrupting properties. Compounds **4b**, **4c**, and **4h** were the most potent, being 9-fold more effective against *P. aeruginosa* than the vanillic acid precursor (64 and 583 $\mu\text{g/mL}$, respectively). Taking into account the stronger cell envelope of Gram-negative strains and their lower sensitivity to polyphenolic compounds when compared to Gram-positive bacteria or yeasts [27], these molecules can be considered promising prototypes for the development of antimicrobial agents active against Gram-negative bacteria. To

maximize the productivity of the best hits, a tailored flow process was developed.

Table 4.2. Microbial Evaluation of Compounds **4a–4j**

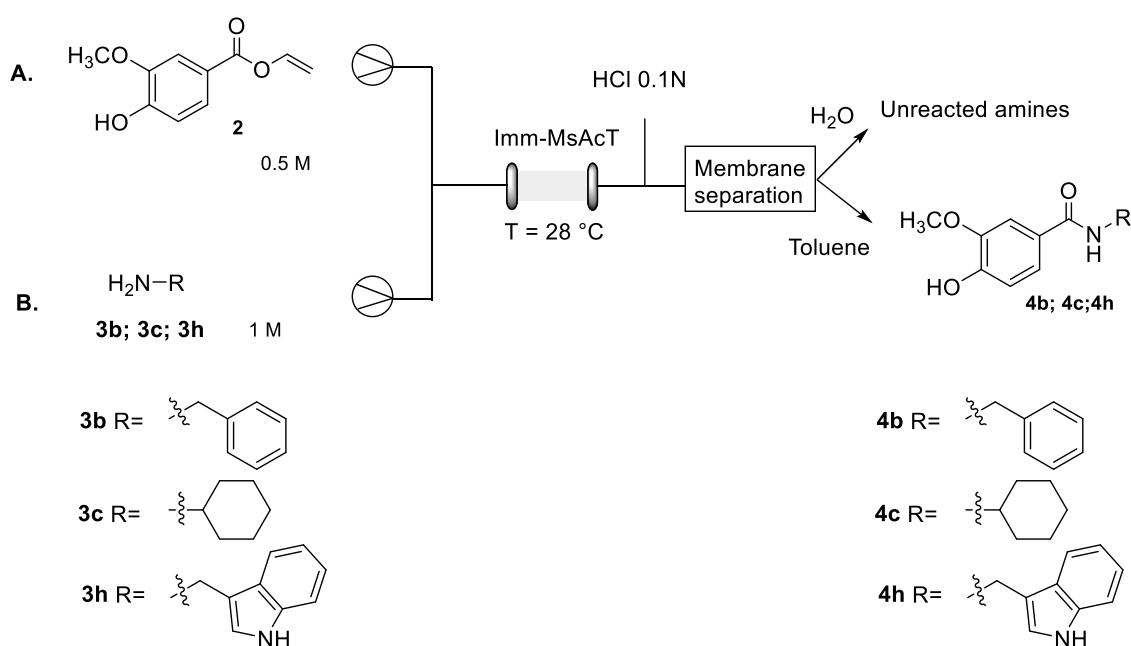
Compound	<i>Ec</i> ^a	<i>Se</i> ^b	<i>Pa</i> ^c	<i>Sa</i> ^d
	MIC (μg/mL)	MIC (μg/mL)	MIC (μg/mL)	MIC (μg/mL)
4a	256	128	128	256
4b	256	128	64	256
4c	128	128	64	256
4d	128	128	128	256
4e	128	128	128	256
4f	128	128	128	256
4g	128	128	128	256
4h	256	128	64	128
4i	128	128	128	256
4j	128	128	128	256

^a*Ec* = *E. coli*. ^b*Se* = *S. enterica* Enteritidis. ^c*Pa* = *P. aeruginosa*. ^d*Sa* = *S. aureus*.

Flow-Intensified Process for the Synthesis of **4b**, **4c**, and **4h**.

To enhance the MsAcT stability, the enzyme was immobilized onto glyoxyl-agarose, selected as the best carrier after an in-depth study previously performed by our group [18]. Among the different hydrophilic supports (i.e., agarose, cellulose, silica, and epoxy resins), aldehyde-agarose immobilization allowed not only for the highest recovered activity (i.e., 73%) with low enzymatic loading (1 mg/g_{matrix}) but also the easy catalyst integration in flow chemistry reactors (packedbed reactor, PBR), ensuring controlled fluid dynamics, acceptable residence times, and process efficiency [28]. To overcome the solubility limitations observed with water medium biotransformations, pure toluene, a well-tolerated organic solvent from MsAcT [19], was employed as reaction medium. Batch reactions were first set up to check the stability of imm-MsAcT while monitoring the reaction outcome by HPLC. Although improvements in the conversion were observed (**4b**: 30%; **4c**: 40%; **4h**: 50%), prolonged reaction times (16 h) were still necessary. A continuous process was then set up (**Scheme 4.5**). Using a 1.2 mL bioreactor, different residence times were evaluated (i.e., 15, 30, and 60 min). As previously demonstrated for different MsAcT-mediated condensation reactions in flow mode [16,17,29,30] due to the high local concentration of the biocatalyst, the efficient mixing as well as the increased catalyst stability improved yields and shorter reaction times were observed when compared with batch transformations. In particular, using 0.25 M **2** and 2 equivalents of the amines (**3b**, **3c**, and **3h**), the desired amides **4b**, **4c**, and **4h** were obtained with very good conversions (68–75%) in

only 15 min of residence time. To enhance the system automation and the overall sustainability, work-up procedure was added downstream the process. An in-line extraction was performed by adding an inlet of HCl and using a liquid–liquid separator. In this way, also the unreacted amines have been collected as salt form. After basification and extraction in toluene, they could be reused as a fresh substrate into the system. To evaluate the performance of our bioreactor over time, the preparation of amide **4b** was selected and 50 mL of the corresponding solution was collected (10 h of continuous operations). Pure **4b** (2.6 g) was obtained after column chromatography (Table 4.3).



Scheme 4.5. Flow-based preparation of **4b**, **4c**, and **4h**. (A) Solution of vinyl vanillate **2** (0.5 M) in toluene. (B) Solution amine **3b**, **3c**, or **3h** (1 M) in toluene.

Table 4.3. Continuous Preparation of **4b** in a Flow Reactor (Reactor Volume, 1.2 mL; Residence Time, 15 min)

m. c. ^a (%)	Isolated yield (%) ^b	Productivity (g/h)	Catalyst Productivity (mmol/mg _{enzyme} h)
75	70	0.26 g	0.45

4.3 Conclusions

In summary, a series of vanillamides have been synthesized using a facile enzymatic strategy and tested for their antimicrobial activity against a panel of Gram-positive and Gram-negative microorganisms. All the generated molecules exhibited better antibacterial action than the vanillic acid precursor, attributable to the increased lipophilicity as well as the enhanced membrane-disrupting

under a nitrogen atmosphere. After stirring for 30 min at room temperature, 10% (w/w) sulfuric acid in THF (500 μ L) was added and the temperature increased to 60 $^{\circ}$ C overnight. After cooling to room temperature, the reaction mixture was filtered through Celite, and the solvent was evaporated. The crude mixture was purified by column chromatography (cyclohexane/EtOAc, 7:3), giving the desired product as a white solid (70% yield).

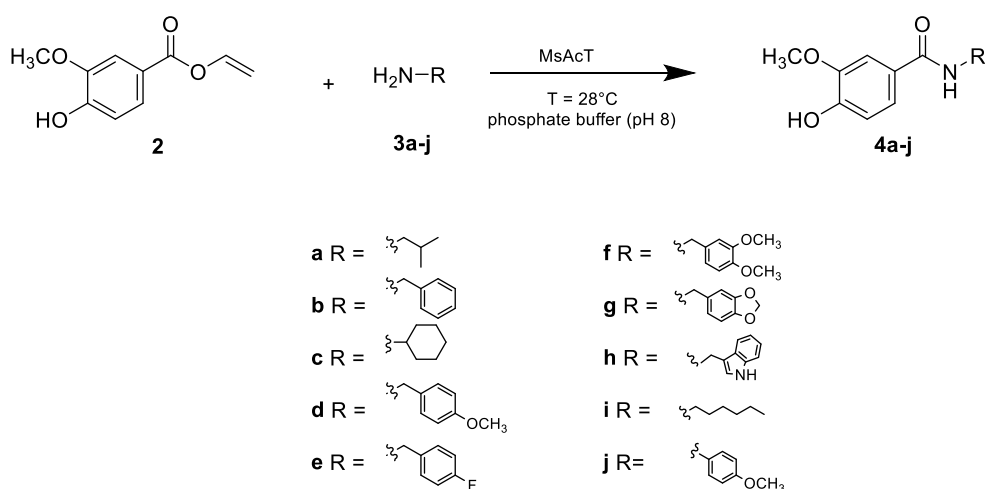
$^1\text{H NMR}$ (600 MHz, CDCl_3): δ 7.75 (dd, $J = 1.8, 8.2$ Hz, 1H), 7.59 (d, $J = 1.8$ Hz, 1H), 7.50 (dd, $J = 6.2, 14$ Hz, 1H), 6.99 (d, $J = 8.2$ Hz, 1H), 6.09 (s, 1H), 5.05 (dd, $J = 1.6, 14$ Hz, 1H), 4.65 (dd, $J = 1.6, 6.2$ Hz, 1H), 3.95 (s, 3H)

$^{13}\text{C NMR}$ (150 MHz, CDCl_3): δ 163.4, 150.7, 146.3, 141.5, 124.9, 120.9, 114.2, 112.0, 97.8, 56.1.

Enzyme Preparation and Immobilization.

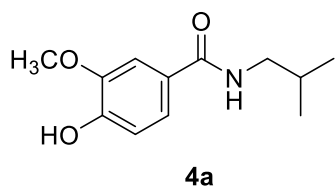
MsAcT was expressed and purified as previously reported [12]. The enzyme was immobilized onto glyoxyl-agarose [18] and its activity was assayed as previously described [18,28].

General Procedure for the Biocatalyzed Batch Synthesis of Vanillyl Amides (4a–4j)



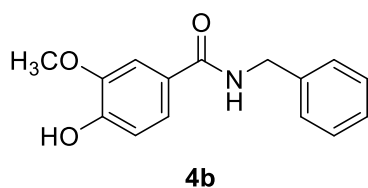
Using Free MsAcT. In 10 mL screw cap tubes, a solution of 0.25 M (1 mmol, 194.2 mg) vinyl vanillate (**2**) in phosphate buffer (0.1 M, pH 8.0) and 10% (v/v) DMSO was prepared. The required amines (**3a–3j**) (0.5 M; 2 mmol) were then added together with free MsAcT (1 mg/mL). The obtained reaction mixture (final volume: 4 mL) was gently stirred at 28 $^{\circ}$ C for 24 h. After this time, dichloromethane (10 mL) and 0.5 M HCl (6 mL) were added. The aqueous phase was extracted three times with dichloromethane. The organic phases were washed with brine, dried over Na_2SO_4 , and filtered, while the solvent was

evaporated under reduced pressure. The crude product was purified by flash chromatography (cyclohexane/EtOAc, 7:3 to 1:1), giving the desired products.



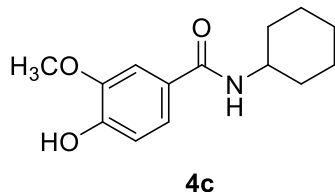
4-Hydroxy-N-isobutyl-3-methoxybenzamide (4a).

Colorless sticky solid; 25% yield. $^1\text{H NMR}$ (600 MHz, CDCl_3): δ 7.47 (s, 1H), 7.17 (d, $J = 8.1$ Hz, 1H), 6.91 (d, $J = 8.1$ Hz, 1H), 6.16–6.04 (m, 1H), 5.90 (br s, 1H), 3.9 (s, 3H), 3.30–3.25 (m, 2H), 1.93–1.85 (m, $J = 6.7$ Hz, 1H), 0.98 (d, $J = 6.7$, 6H). Spectroscopic data matched with those reported in the literature [8].



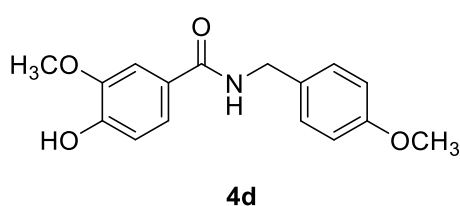
N-Benzyl-4-hydroxy-3-methoxybenzamide (4b).

Yellow oil; 15% yield. $^1\text{H NMR}$ (600 MHz, CDCl_3): δ 7.49 (d, $J = 1.8$ Hz, 1H), 7.38–7.34 (m, 3H), 7.32–7.28 (m, 2H), 7.20 (dd, $J = 1.8, 8.2$ Hz, 1H), 6.90 (d, $J = 8.2$ Hz, 1H), 6.41–6.30 (m, 1H), 5.90 (br s, 1H), 4.63 (d, $J = 5.4$ Hz, 2H), 3.9 (s, 3H). Spectroscopic data matched with those reported in the literature [8].



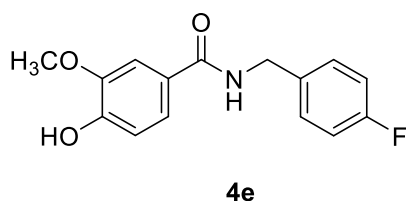
N-Cyclohexyl-4-hydroxy-3-methoxybenzamide (4c).

White solid; 18% yield. $^1\text{H NMR}$ (600 MHz, CDCl_3): δ 7.44 (s, 1H), 7.16 (d, $J = 8.3$ Hz, 1H), 6.90 (d, $J = 8.3$ Hz, 1H), 5.98–5.88 (m, 1H), 3.90 (s, 3H), 2.02 (d, $J = 11.3$ Hz, 2H), 1.74 (d, $J = 13.2$ Hz, 2H), 1.64 (d, $J = 13.2$, 1H), 1.47–1.37 (m, 2H), 1.28–1.15 (m, 4H). Spectroscopic data matched with those reported in the literature [8].



4-Hydroxy-3-methoxy-N-(4-methoxybenzyl)benzamide (4d).

Yellow wax; 27% yield. $^1\text{H NMR}$ (600 MHz, CDCl_3): δ 7.49 (d, $J = 1.9$ Hz, 1H), 7.30–7.27 (m, 1H), 7.19 (dd, $J = 1.9, 8.2$ Hz, 1H), 6.90–6.87 (m, 3H); 6.29–6.22 (m, 1H), 5.90 (bs, 1H), 4.56 (d, $J = 5.4$ Hz, 2H), 3.94 (s, 3H), 3.80 (s, 3H). Spectroscopic data matched with those reported in the literature [8].

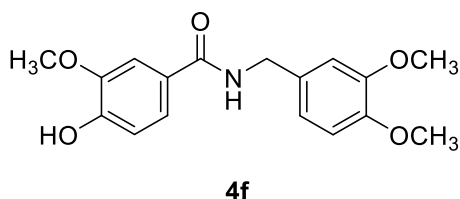


N-(4-Fluorobenzyl)-4-hydroxy-3-

methoxybenzamide (4e).

Orange solid; 40% yield. $^1\text{H NMR}$ (600 MHz, CDCl_3): δ 7.49 (d, $J = 1.8$ Hz, 1H), 7.34–7.30 (m, 2H), 7.20 (dd, $J = 1.8, 8.2$ Hz, 1H), 7.06–7.01 (m, 2H), 6.90 (d, $J = 8.2$ Hz, 1H), 6.38–6.31 (m, 1H), 5.90 (br s, 1H), 4.60 (d, $J =$

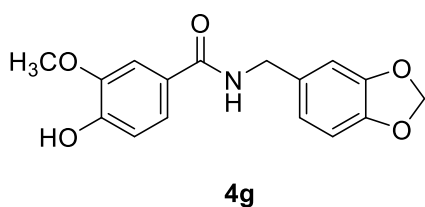
5.7 Hz, 2H), 3.94 (s, 3H). Spectroscopic data matched with those reported in the literature [8].



***N*-(3,4-Dimethoxybenzyl)-4-hydroxy-3-**

methoxybenzamide (4f). Orange solid; 30% yield. $^1\text{H NMR}$ (600 MHz, CDCl_3): δ 7.49 (d, J = 1.8 Hz, 1H), 7.19 (dd, J = 1.8, 8.2 Hz, 1H), 6.92–6.88 (m, 3H), 6.84 (d, J = 8.2 Hz, 1H), 6.30–6.25 (m, 1H), 5.90 (br s, 1H), 4.57 (d, J =

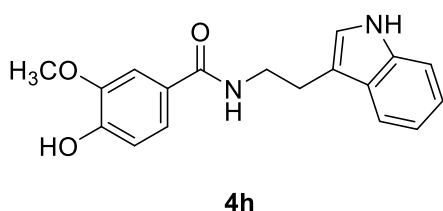
5.5 Hz, 2H), 3.95 (s, 3H), 3.88 (s, 3H). Spectroscopic data matched with those reported in the literature [8].



***N*-(Benzo[d][1,3]dioxol-5-ylmethyl)-4-**

hydroxy-3-methoxybenzamide (4g). Yellow sticky solid; 27% yield. $^1\text{H NMR}$ (600 MHz, CDCl_3): δ 7.48 (d, J = 1.7 Hz, 1H), 7.19 (dd, J = 1.7, 8.2 Hz, 1H), 6.89 (d, J = 8.2 Hz, 1H), 6.84 (s,

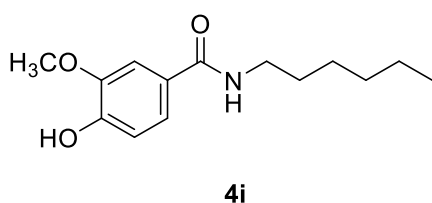
1H), 6.80 (d, J = 7.9 Hz, 1H), 6.76 (d, J = 7.9 Hz, 1H), 6.43–6.30 (m, 1H), 5.94 (s, 2H), 4.52 (d, J = 5.6 Hz, 2H), 3.93 (s, 3H). Spectroscopic data matched with those reported in the literature [8].



***N*-(2-(1H-Indol-2-yl)ethyl)-4-hydroxy-3-**

methoxybenzamide (4h). White spongy solid; 40% yield. $^1\text{H NMR}$ (600 MHz, CDCl_3): δ 8.09 (s, 1H), 7.65 (d, J = 7.8 Hz, 1H), 7.46–7.36 (m, 2H), 7.22 (t, J = 7.8 Hz, 1H), 7.13 (t, J = 7.8 Hz, 1H), 7.07 (s, 1H), 7.04 (dd, J = 8.2, 1.8 Hz, 1H),

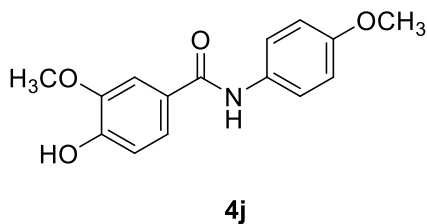
6.48 (d, J = 8.2 Hz, 1H), 6.23–6.10 (m, 1H), 6.10 (bs, 1H), 3.89 (s, 3H), 3.78 (q, J = 6.1 Hz, 2H), 3.09 (t, J = 6.6 Hz, 2H); $^{13}\text{C NMR}$ (150 MHz, CDCl_3): δ 167.2, 148.8, 146.8, 136.7, 127.6, 127.1, 122.5, 122.3, 119.8, 119.8, 119, 114.0, 113.4, 111.5, 110.5, 56.3, 40.6, 25.5.



***N*-Hexyl-4-hydroxy-3-methoxybenzamide (4i).**

White solid; 50% yield. $^1\text{H NMR}$ (600 MHz, CDCl_3): δ 7.46 (d, J = 1.0 Hz, 1H), 7.17 (dd, J = 1.0, 8.3 Hz), 6.90 (d, J = 8.3 Hz, 1H), 6.16–6.04 (m, 1H), 5.98 (br s, 1H), 3.93 (s, 1H), 3.43 (q, J =

6.7 Hz, 2H), 1.60 (q, J = 7.2 Hz, 2H), 1.43–1.28 (m, 6H), 0.89 (t, J = 6.7 Hz, 3H); $^{13}\text{C NMR}$ (150 MHz, CDCl_3): δ 167.3, 148.8, 146.9, 127.3, 119.6, 114.0, 110.7, 56.3, 40.4, 31.7, 29.9, 26.9, 22.8, 14.2.



4-Hydroxy-3-methoxy-N-(4-methoxyphenyl)benzamide (4j). White solid; 5% yield.

$^1\text{H NMR}$ (300 MHz, CDCl_3): δ 7.72 (s, 1H), 7.55–7.49 (m, 3H), 7.32 (dt, $J = 8.2, 1.9$ Hz, 1H), 6.99–6.89 (m, 3H), 3.96 (s, 3H), 3.82 (s, 3H).

Spectroscopic data matched with those reported in the literature [8].

Bacterial Strains and Culture Conditions.

E. coli ATCC 25922 (*Ec*), *Salmonella enterica* Enteritidis ISM 8324 (*Se*), *P. aeruginosa* IMV1 (*Pa*), and *S. aureus* ATCC 6538 (*Sa*) were plated on Tryptic Soy Agar + 5% sheep blood (Microbiol, Italy) and incubated aerobically at 37 °C for 24 h.

Determination of the Minimum Inhibitory Concentration.

The minimum inhibitory concentration (MIC) was determined using the microdilution assay, according to the Clinical and Laboratory Standards Institute (CLSI) guidelines. All the strains were grown on Tryptic Soy Broth (TSB, Oxoid, Milan, Italy) and three or four isolated colonies were suspended in fresh sterile saline solution to reach an initial concentration of 1.5×10^8 CFU/mL (equivalent to 0.5 MacFarland standard). One hundred microliters of the 1:100 diluted cell suspension was dispensed into each well of a 96-well microtiter plate. The strains were exposed to 2-fold dilution series of each vanillamide. After incubation for 24 h at 37 °C, the MICs were determined as the lowest dilution of molecules that was able to inhibit visible bacterial growth.

Biocatalyzed Batch Synthesis of Vanillyl Amides (4b, 4c, and 4h) with Imm-MsAcT.

In 10 mL screw cap tubes, 0.25 M vinyl vanillate (**2**) (48.5 mg, 0.25 mmol) was dissolved in toluene. Amine **3b**, **3c**, or **3h** (0.5 M) and immobilized MsAcT (50 mg, 1 mg/g_{agarose}) were added, and the reaction mixture was gently stirred overnight at 28 °C. After this time, the reaction output was evaluated by HPLC (see below).

HPLC Analysis.

Mobile phase: (A) H_2O + 0.05% TFA; (B) CAN + 0.05% TFA; gradient conditions: 0–4 min 80% (A)/20% (B), 4–8 min 65% (A)/35% (B); 8–12 min 50% (A)/50% (B); 12–16 min 35% (A)/65% (B); 16–20 min 20% (A)/80% (B); 20–24 min 20% (A)/80% (B); flow rate: 1.0 mL/min; λ : 254 nm. Injection volume: 10 μL . Reaction samples (150 μL) were diluted with a solution of 1:50 $\text{H}_2\text{O}/\text{ACN}$ + 0.05% TFA (1.90 mL). Retention times (t_{R}): vinyl vanillate (**2**) = 15.8 min; benzylamine (**3b**) = 2.3 min;

N-benzyl-4-hydroxy-3-methoxybenzamide (**4b**) = 21.2 min; *N*-cyclohexyl-4-hydroxy-3-methoxybenzamide (**4c**) = 20.9 min; tryptamine (**3h**) = 2.2 min; *N*-(2-(1H-indol-2-yl)ethyl)-4-hydroxy-3-methoxybenzamide (**4h**) = 20.5 min.

Intensified Flow Process

An Omnifit glass column (6.6 mm i.d.) was filled with 1.5g of imm-MsAcT (1 mg/g_{agarose}). A 1 M amine solution (**3b**, **3c**, or **3h**) and 0.5 M vinyl vanillate (**2**) both in toluene were prepared. The two solutions were mixed in a T-piece and the resulting flow stream (0.5 M amine and 0.25 M acyl donor) was directed into the column packed with imm-MsAcT (packed-bed reactor volume: 1.2 mL). The flow rate was 0.04 mL/min for each pump. An in-line extraction was performed using a Zaiput liquid/liquid separator and an inlet of 1 N HCl (flow rate: 0.19 mL/min), which was mixed to the exiting reaction flow stream using a T junction. Both the organic and aqueous phases were analyzed by HPLC using the above reported conditions. The desired amides were obtained with the following molar conversions: **4b**, 75%; **4c**, 68%; **4h**, 72%. For the gram-scale preparation of amide **4b**, the system was left operating for 10 h; the organic phase was collected, and the solvent was evaporated under reduced pressure. Purification through column chromatography (cyclohexane/EtOAc, 7:3 to 1:1) was performed, yielding 2.6 g of the desired product (70% isolated yield).

4.5 Bibliography

1. Li, B.; Webster, T.J. Bacteria antibiotic resistance: New challenges and opportunities for implant-associated orthopedic infections. *J. Orthop. Res.* **2018**, *36*, 22–32, doi:10.1002/jor.23656.
2. Teng, P.; Huo, D.; Nimmagadda, A.; Wu, J.; She, F.; Su, M.; Lin, X.; Yan, J.; Cao, A.; Xi, C.; et al. Small Antimicrobial Agents Based on Acylated Reduced Amide Scaffold. *J. Med. Chem.* **2016**, *59*, 7877–7887, doi:10.1021/acs.jmedchem.6b00640.
3. Hammerum, A.M.; Heuer, O.E. Human health hazards from antimicrobial-resistant escherichia coli of animal origin. *Clin. Infect. Dis.* **2009**, *48*, 916–921, doi:10.1086/597292.
4. Allen, H.K.; Donato, J.; Wang, H.H.; Cloud-Hansen, K.A.; Davies, J.; Handelsman, J. Call of the wild: Antibiotic resistance genes in natural environments. *Nat. Rev. Microbiol.* **2010**, *8*, 251–259, doi:10.1038/nrmicro2312.
5. Lee, H.H.; Molla, M.N.; Cantor, C.R.; Collins, J.J. Bacterial charity work leads to population-wide resistance. *Nature* **2010**, *467*, 82–85, doi:10.1038/nature09354.
6. Singh, P.A.; Desai, S.D.; Singh, J. A Review on Plant Antimicrobials of Past Decade. *Curr. Top. Med. Chem* **2018**, *18*, 812–833.
7. Anand, U.; Jacobo-Herrera, N.; Altemimi, A.; Lakhssassi, N. A comprehensive review on medicinal plants as antimicrobial therapeutics: Potential avenues of biocompatible drug discovery. *Metabolites* **2019**, *9*, 1–13, doi:10.3390/metabo9110258.
8. Santos Oliveira, A.J.D.M.; De Castro, R.D.; Pessôa, H.D.L.F.; Wadood, A.; De Sousa, D.P. Amides Derived from Vanillic Acid: Coupling Reactions, Antimicrobial Evaluation, and Molecular Docking. *Biomed Res. Int.* **2019**, *2019*, 1-11, doi:10.1155/2019/9209676.
9. Mathews, I.; Soltis, M.; Saldajeno, M.; Ganshaw, G.; Sala, R.; Weyler, W.; Cervin, M.A.; Whited, G.; Bott, R. Structure of a novel enzyme that catalyzes acyl transfer to alcohols in aqueous conditions. *Biochemistry* **2007**, *46*, 8969–8979, doi:10.1021/bi7002444.
10. De Leeuw, N.; Torrelo, G.; Bisterfeld, C.; Resch, V.; Mestrom, L.; Straulino, E.; van der Weel, L.; Hanefeld, U. Ester Synthesis in Water: *Mycobacterium smegmatis* Acyl Transferase for Kinetic Resolutions. *Adv. Synth. Catal.* **2018**, *360*, 242–249, doi:10.1002/adsc.201701282.
11. Contente, M.L.; Roura Padrosa, D.; Molinari, F.; Paradisi, F. A strategic

- Ser/Cys exchange in the catalytic triad unlocks an acyltransferase-mediated synthesis of thioesters and tertiary amides. *Nat. Catal.* **2020**, *3*, 1020–1026, doi:10.1038/s41929-020-00539-0.
12. Contente, M.L.; Pinto, A.; Molinari, F.; Paradisi, F. Biocatalytic *N*-Acylation of Amines in Water Using an Acyltransferase from *Mycobacterium smegmatis*. *Adv. Synth. Catal.* **2018**, *360*, 4814–4819, doi:10.1002/adsc.201801061.
 13. Perdomo, I.C.; Gianolio, S.; Pinto, A.; Romano, D.; Contente, M.L.; Paradisi, F.; Molinari, F. Efficient Enzymatic Preparation of Flavor Esters in Water. *J. Agric. Food Chem.* **2019**, *67*, 6517–6522, doi:10.1021/acs.jafc.9b01790.
 14. Tamborini, L.; Fernandes, P.; Paradisi, F.; Molinari, F. Flow Bioreactors as Complementary Tools for Biocatalytic Process Intensification. *Trends Biotechnol.* **2018**, *36*, 73–88, doi:10.1016/j.tibtech.2017.09.005.
 15. Benítez-Mateos, A.I.; Contente, M.L.; Roura Padrosa, D.; Paradisi, F. Flow biocatalysis 101: Design, development and applications. *React. Chem. Eng.* **2021**, *6*, 599–611, doi:10.1039/d0re00483a.
 16. Annunziata, F.; Contente, M.L.; Pinna, C.; Tamborini, L.; Pinto, A. Biocatalyzed flow oxidation of tyrosol to hydroxytyrosol and efficient production of their acetate esters. *Antioxidants* **2021**, *10*, 1–8, doi:10.3390/antiox10071142.
 17. Contente, M.L.; Tamborini, L.; Molinari, F.; Paradisi, F. Aromas flow: eco-friendly, continuous, and scalable preparation of flavour esters. *J. Flow Chem.* **2020**, *10*, 235–240, doi:10.1007/s41981-019-00063-8.
 18. Contente, M.L.; Farris, S.; Tamborini, L.; Molinari, F.; Paradisi, F. Flow-based enzymatic synthesis of melatonin and other high value tryptamine derivatives: A five-minute intensified process. *Green Chem.* **2019**, *21*, 3263–3266, doi:10.1039/c9gc01374a.
 19. Annunziata, F.; Contente, M.L.; Betti, D.; Pinna, C.; Molinari, F.; Tamborini, L.; Pinto, A. Efficient chemo-enzymatic flow synthesis of high value amides and esters. *Catalysts* **2020**, *10*, 1–8, doi:10.3390/catal10080939.
 20. Dinu, C.Z.; Zhu, G.; Bale, S.S.; Anand, G.; Reeder, P.J.; Sanford, K.; Whited, G.; Kane, R.S.; Dordick, J.S. Enzyme-based nanoscale composites for use as active decontamination surfaces. *Adv. Funct. Mater.* **2010**, *20*, 392–398, doi:10.1002/adfm.200901388.
 21. Dinu, C.Z.; Borkar, I. V.; Bale, S.S.; Campbell, A.S.; Kane, R.S.; Dordick, J.S. Perhydrolase-nanotube-paint sporicidal composites stabilized by intramolecular crosslinking. *J. Mol. Catal. B Enzym.* **2012**, *75*, 20–26,

doi:10.1016/j.molcatb.2011.11.003.

22. Pattabiraman, V.R.; Bode, J.W. Rethinking amide bond synthesis. *Nature* **2011**, *480*, 471–479, doi:10.1038/nature10702.
23. Ibrahim, H.A.; Soliman, H.S.M.; Hamed, F.M.; Marrez, D.A.; Othman, S.M. Antibacterial activity of vanillic acid and catechol produced by microbial biotransformation of caffeic acid. *J. Pharm. Sci. Res.* **2020**, *12*, 740–743.
24. Keman, D.; Soyer, F. Antibiotic-Resistant Staphylococcus aureus Does Not Develop Resistance to Vanillic Acid and 2-Hydroxycinnamic Acid after Continuous Exposure in Vitro. *ACS Omega* **2019**, *4*, 15393–15400, doi:10.1021/acsomega.9b01336.
25. Di Pasqua, R.; Betts, G.; Hoskins, N.; Edwards, M.; Ercolini, D.; Mauriello, G. Membrane toxicity of antimicrobial compounds from essential oils. *J. Agric. Food Chem.* **2007**, *55*, 4863–4870, doi:10.1021/jf0636465.
26. Kubo, I.; Muroi, H.; Kubo, A. Structural functions of antimicrobial long-chain alcohols and phenols. *Bioorganic Med. Chem.* **1995**, *3*, 873–880, doi:10.1016/0968-0896(95)00081-Q.
27. Xin, X.; Zhang, M.; Li, X.F.; Zhao, G. Biocatalytic Synthesis of Lipophilic Baicalin Derivatives as Antimicrobial Agents. *J. Agric. Food Chem.* **2019**, *67*, 11684–11693, doi:10.1021/acs.jafc.9b04667.
28. Benítez-Mateos, A.I.; Contente, M.L. Agarose vs. Methacrylate as material supports for enzyme immobilization and continuous processing. *Catalysts* **2021**, *11*, 814–824, doi:10.3390/catal11070814.
29. Szymańska, K.; Odrozek, K.; Zniszczoł, A.; Torrelo, G.; Resch, V.; Hanefeld, U.; Jarzębski, A.B. MsAcT in siliceous monolithic microreactors enables quantitative ester synthesis in water. *Catal. Sci. Technol.* **2016**, *6*, 4882–4888, doi:10.1039/c5cy02067k.
30. Padrosa, D.R.; Contente, M.L. Multi-gram preparation of cinnamoyl tryptamines as skin whitening agents through a chemo-enzymatic flow process. *Tetrahedron Lett.* **2021**, *86*, 153453, doi:10.1016/j.tetlet.2021.153453.

Chapter 5: In-depth investigation of natural stilbenoids' mode of action

5.1. Design and synthesis of stilbenoid-bearing affinity probes for target proteins identification in bacterial pathogens.

5.2. Immunomodulating activity of stilbenoids on bacteria-induced immune response.

General introduction

Due to their promising antimicrobial activity, stilbenoids represented a central theme of the present PhD project. Indeed, previous research works from our group allowed us to collect information concerning the antibacterial, antifungal, and antiviral activity of these phytoalexins [1–4]. With the aim of exploiting stilbenoids scaffold for the development of new antimicrobial agents, we saw the need to investigate the molecular mechanisms behind their bioactivity. In this perspective, the identification of stilbenoids molecular targets is of utmost importance, and it can be achieved by target-capture strategies such as affinity-based protein profiling (*Af*-BPP), whose application for target identification studies in bacterial pathogens will be described in the next section.

In our attempt to elucidate stilbenoids mode of action, we decided to investigate the beneficial properties of resveratrol and its monomeric and dimeric derivatives from a different perspective. In particular, the knowledge of the antioxidant and anti-inflammatory properties of stilbenoids – that are abundantly reported in literature – prompted us to investigate their role in cell protection. Indeed, it has been demonstrated that bacterial infections induce cytokine production in infected organisms, leading to inflammation spread. The immunomodulatory properties of resveratrol and its derivatives might therefore constitute an additional protective effect against bacterial infections. In other words, stilbenoids seem to combine the antibacterial activity (preventing bacterial infections) with immunomodulatory effects, leading to host cell protection during pathogens attack. To further investigate these aspects, a comprehensive study of monomeric and dimeric stilbenoids immunomodulating effects has been performed, and it will be discussed in section 5.2.

5.1. Design and synthesis of stilbenoid-bearing affinity probes for target proteins identification in bacterial pathogens.

The research activities described in this paragraph have been developed at the Molecular Sciences Institute (ISM) of the University of Bordeaux, Organic Synthesis and Natural Products division, under the supervision of Prof. Stéphane Quideau.

Abstract

Natural polyphenolic stilbenoids, such as resveratrol, piceatannol, and resveratrol dimer *trans*- δ -viniferin, have been widely studied for their biological activity against foodborne pathogens (e.g., *S. aureus*) [1]. However, despite the large number of studies reporting on their antibacterial potential, their exact mechanism of action has not been elucidated yet. In this perspective, the use of affinity-based probes constitutes a valuable tool for the identification of stilbenoid-protein interactions, that is, of stilbenoids molecular targets. In this work, biotinylated stilbenoid-based affinity probes were designed and prepared to be employed for *in vitro* proteins capture and identification in bacterial cell lysates. Moreover, “clickable” alkynylated stilbenoids were synthesized to be introduced in living cells for *in cellulo* protein capture. Natural stilbenoids were chemically modified and combined with a linker and a reporting group required for probes assembly. Probes incubation with cell lysates from *S. aureus* or with whole cells will allow for affinity-based interactions between stilbenoids and target proteins. The formed protein-probes complexes will be visualized by SDS page or recovered using streptavidin-coated magnetic beads, allowing for protein identification by proteomic and bioinformatic analyses. Hereafter, the design and synthesis of stilbenoid probes will be discussed in detail. Future planned activities will be presented as well, to give an outline of the experimental workflow for protein capture and of the possible implementations of the probes here described.

5.1.1. Introduction

As described in **Chapter 1**, several research works highlighted the multiple biological activities (i.e. antioxidant, anti-inflammatory, anticancer, antimicrobial, among others) of resveratrol and its derivatives and oligomers, suggesting, in some cases, possible molecular targets. However, the elucidation of stilbenoids mechanisms of action is far from being complete and still it is of utmost importance in the perspective of exploiting these phytoalexins for the

development of novel nature-inspired bioactives. For instance, in a recent work published by our group we demonstrated that stilbenoids antibacterial activity against foodborne pathogens was due to severe cell membrane damage [1]. However, it is not likely that the bactericidal activity is attributable exclusively to one specific mechanism, and additional targets might exist in the cell, whose identification would be helpful in improving stilbenoids bioactivity. In this perspective, affinity-based protein profiling (*Af*-BPP) represents a solid strategy for target identification studies [5]. *Af*-BPP consists in a set of chemical and proteomic approaches developed by Benjamin F. Cravatt and Matthew Bogyo at the end of the 20th century [6,7], that involves the use of small molecules chemical probes to identify affinity-based interactions between a selected compound and proteins (e.g. enzymes, receptors) in cells or cell lysates [8–10]. With this methodology, target proteins can be isolated from complex mixtures and identified through proteomic and chemoinformatic procedures. Molecular probes are usually constituted by three main components: an affinity function, or warhead (WH), responsible for the interaction with the putative molecular target(s); a reporter group (or tag), needed to allow labelled proteins visualization or enrichment; a linker that provides adequate distancing between the affinity function and the tag [8]. The profitable application of this technique relies on the critical design of the probe. The affinity function is the most important element since it is responsible for target recognition. For instance, it could be constituted by small natural molecules with a strong biological effect, as phytoalexins [11, 12]. The tag has a purification/detection function allowing for protein-probe complex isolation/visualization and protein identification. The most commonly used reporting group is biotin, which provides probe-protein complex separation from the reaction mixture using streptavidin-coated (magnetic) beads [13]. Otherwise, a fluorescent dye (e.g. rhodamine B) can be used as a tag to visualize protein-probe complexes on SDS-page. Finally, the linker is intended to ensure good solubility of the probe in biological environment, besides connecting the two functional portions providing an optimal distancing. Spacers of different nature are available, such as polyethylene glycol (PEG) chain [14], linear alkane chains [15] or even peptide chains [16]. Besides the nature of the spacer, accounting for the solubility of the probe, the size represents another parameter that must be chosen carefully. The affinity and reporting functions should be neither too close nor too far apart. The functionalization of the spacer offers numerous possibilities in terms of size, as long as it remains inert with respect to the other functions.

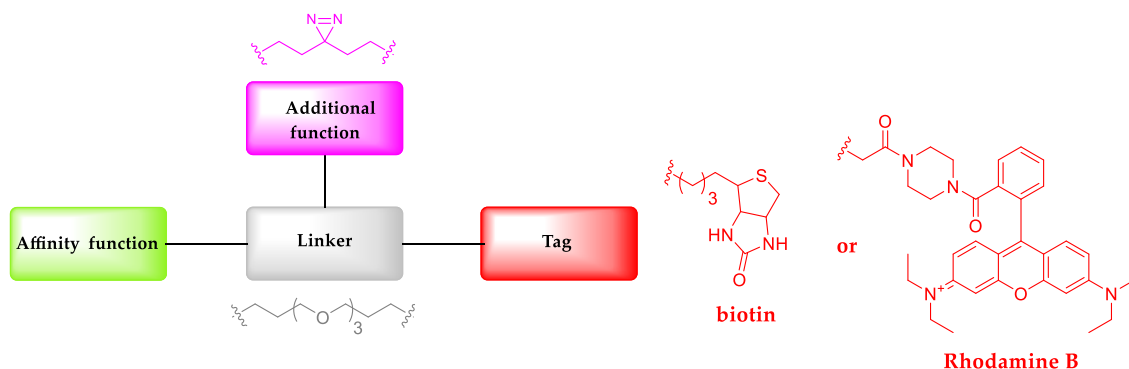
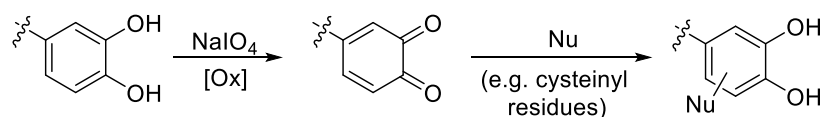


Figure 5.23. General structure of a molecular probe. Examples of tag, linker and additional function are shown: biotin or rhodamine B as reporting groups (red); a PEG-type linker (grey); a diazirine-containing chain (violet).

It is noteworthy that *Af*-BPP might suffer from non-specific interactions with other cellular components, that can interfere with the correct identification of target proteins. Limitations due to unspecific interferences could be overcome by introducing an additional function on the linker which is intended to provide a covalent bond with the target protein. This probe component should be initially non-reactive, meaning that it should not alter the affinity function behavior. Then, after the recognition step, it can be activated, for instance, by UV irradiation. Some examples of additional functions are benzophenone [17], aryl azide [18] or the “minimalist” photocrosslinkers diazirine (**Figure 5.1**) [19,20]. However, also in the need of providing a covalent bond, additional functions are not always needed. For instance, if the small molecule under investigation bears a catechol moiety, a covalent bond with target proteins could be achieved *via* oxidation with NaIO_4 . This leads to the formation of an *ortho*-quinone able to react with the nucleophilic sites on the protein (e.g. cysteinyl residues, **Scheme 5.1**) [21].



Scheme 5.6. Covalent bond formation via catechol oxidation with NaIO_4

It should be considered that the insertion of a linker bearing a bulky reporting group could significantly alter the biological activity and the cell permeability of the studied compound, limiting the application of *Af*-BPP approaches *in cellulo*. This issue could be addressed exploiting selective and reliable biorthogonal reactions, such as copper(I)-catalyzed azide-alkyne cycloaddition (CuAAC) [22]. The use of “clickable” probes involves the introduction on the warhead of a small and not-interfering moiety, namely a short-chained terminal

alkyne. The modified affinity function can then be incubated with whole cells and interact with target proteins. Finally, combination with the proper counterpart, namely a tag-bearing linker equipped with a terminal azide, will allow to perform protein enrichment or visualization, depending on the reporting group.

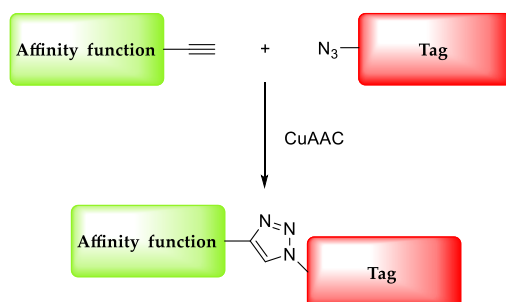


Figure 5.24. Schematic representation of a "clickable" probe

In this work, we employed the *Af*-BPP strategy aiming at clarifying the molecular mechanisms behind stilbenoids antibacterial activity against foodborne pathogens. After the biological evaluation of resveratrol, its hydroxylated derivative piceatannol, and resveratrol dimer *trans*- δ -viniferin (**Figure 5.25**), a small collection of biotinylated probes and "clickable" alkynylated stilbenoids were prepared to perform protein-capture procedures in cell lysates or living cells.

5.1.2. Results and discussion

Stilbenoids biological evaluation and design of stilbenoid-based chemical probes.

First, the antibacterial activity of resveratrol, its hydroxylated derivative piceatannol, and resveratrol dimer *trans*- δ -viniferin was assessed against Gram positive *S. aureus* and Gram negative *P. aeruginosa*. The latter resulted non sensitive to the tested compounds, while piceatannol showed modest activity towards *S. aureus* and a strong inhibitory activity (MIC 8 μ g/ml) was displayed by *trans*- δ -viniferin (**Figure 5.25**). Therefore, we decided to focus our studies mainly on the stilbenoid-protein interactions of *trans*- δ -viniferin in *S. aureus*.

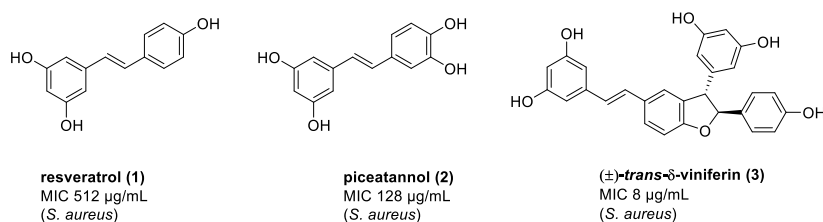


Figure 5.25. Chemical structures and MIC values of resveratrol, piceatannol and *trans*-δ-viniferin on *S. aureus*.

However, despite their modest or null biological activity, monomers were also employed for the development of molecular probes, in order to assess the feasibility of the whole process, as well as to provide a system to be used as a negative control (resveratrol-based probe). The profitable application of *Af*-BPP relies on the rational design of the probe. The warhead – i.e. the stilbenoid – shall preserve all the -OH groups possibly responsible for the interaction with target proteins. Indeed, in our design of biotinylated probes, stilbenoids functionalization did not interest free hydroxy groups. An amino-terminal PEG chain was selected as a suitable linker since it allows the formation of stable amidic bonds with the warhead and the tag.

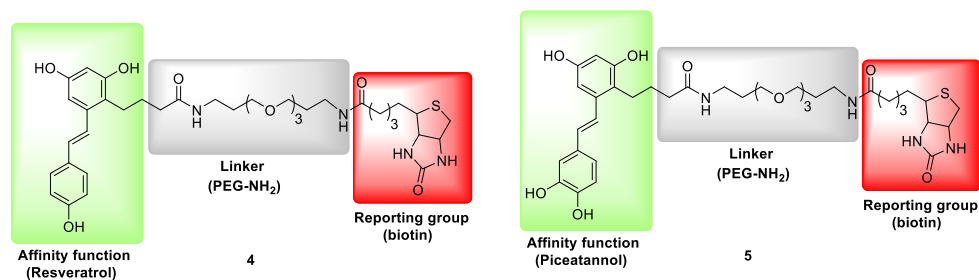


Figure 5.26. Monomer-based biotinylated probes.

Finally, biotin was engaged as a reporting group (**Figure 5.4**). As mentioned, the introduction of substantial structural modifications (i.e. the insertion of a bulky reporting group) may lead to the alteration of the biological activity and the cell permeability of the studied compound, thus limiting the application of *Af*-BPP *in cellulo*. The use of whole cells for protein-capture procedure is expected to preserve the native cellular environment where stilbenoid-target interactions naturally occur, avoiding the loss of important information during target investigation. Therefore, aiming at performing target identification studies in the most reliable system, we decided to exploit copper(I)-catalyzed azide-alkyne cycloaddition (CuAAC) for probe assembly. This strategy required the introduction on the warhead of a small and not-interfering reactive group, namely a short-chained terminal alkyne. Indeed, alkynylated stilbenoids were prepared to be incubated with whole cells. Combination with the proper

counterpart (a tag-bearing linker equipped with an azide) will eventually allow to perform protein enrichment or visualization. Both biotin and rhodamine B were considered as reporting groups for the azide counterpart. We envisioned a synthetic pathway for the preparation of biotin-PEG3-azide, while the same linker with rhodamine B was purchased (**Figure 5.27**).

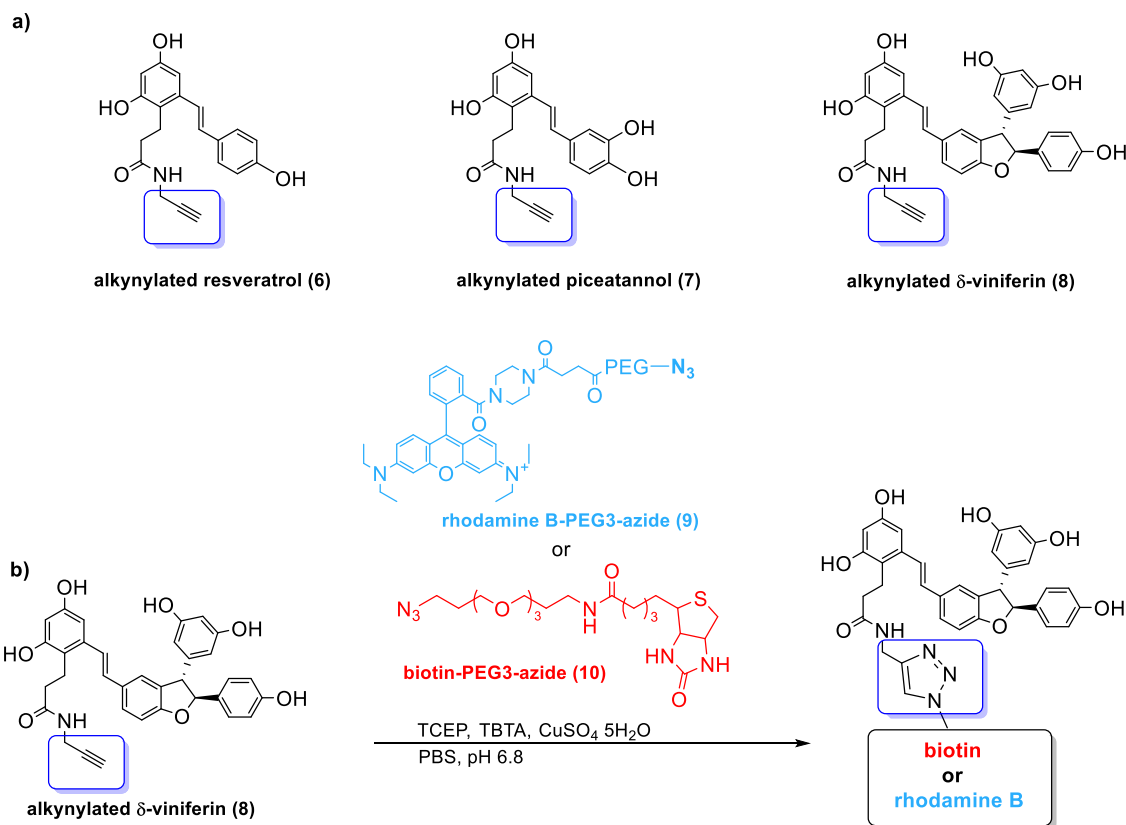
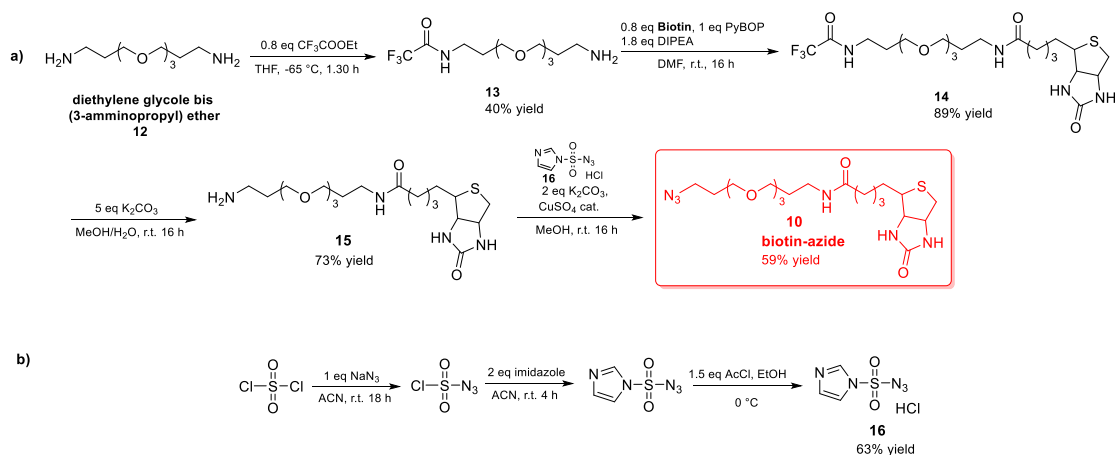


Figure 5.27. a) Alkylnylated stilbenoids; b) *trans*- δ -viniferin clickable probe assembly

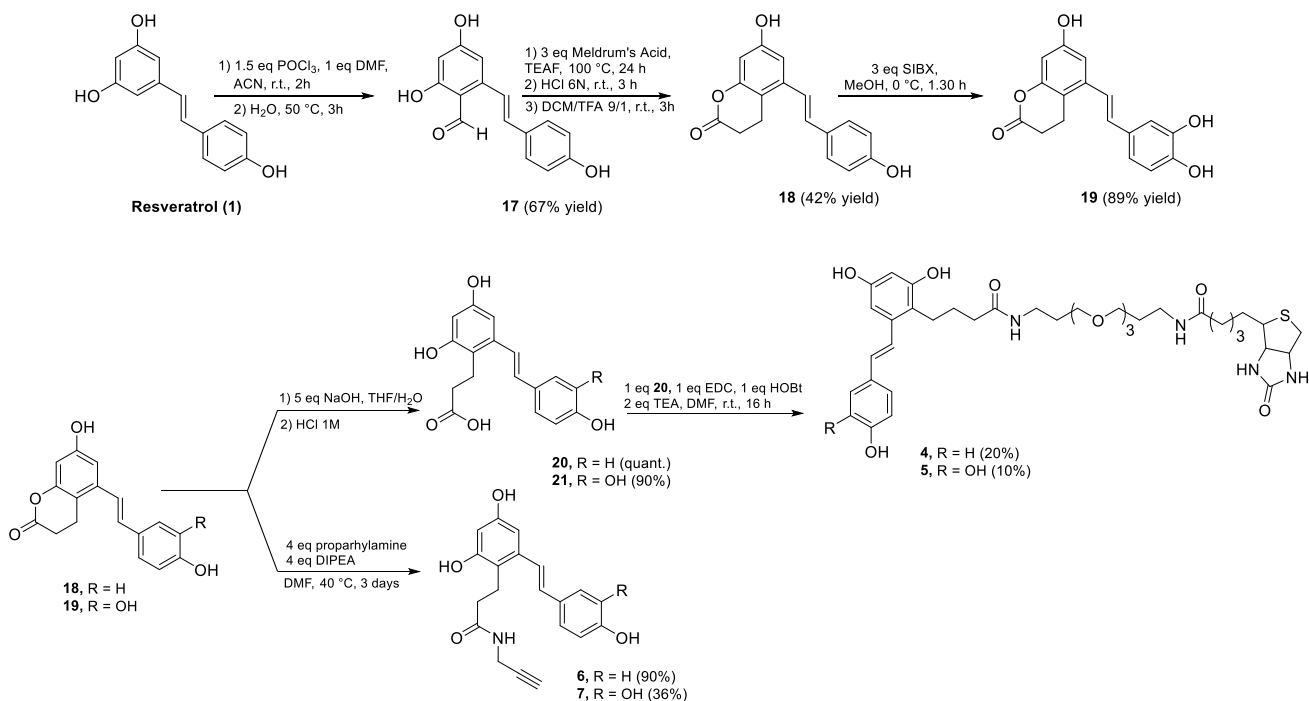
Synthesis of stilbenoid-bearing affinity probes and alkylnylated stilbenoids

Stilbenoid-based affinity probes were prepared by synthesizing the biotin-containing linker on one hand and functionalizing the natural stilbenoids on the other. Notably, the amino terminal linker could be easily converted into the corresponding azide, required for the assembly of clickable probes (**Scheme 5.2**). Similarly, stilbenoids functionalization involved the formation of a key lactone intermediate that could be either hydrolyzed into the corresponding acid and then combined with the biotin-containing linker or opened with propargylamine to afford the corresponding alkylnylated derivatives (**Scheme 5.3**). The preparation of the biotin linker involved the monoprotection of an

excess of diethylene glycol bis (3-aminopropyl) ether with ethyl trifluoroacetate at $-65\text{ }^{\circ}\text{C}$ for 1.30 h. The free aminic group was connected to biotin *via* amidic coupling in presence of PyBOP and DIPEA. Final deprotection with K_2CO_3 (5 eq) in a 1:1 mixture of water and methanol afforded the desired linker **15**, that could be converted into the corresponding azide (**10**) using diazo-transfer reagent **16** in presence of K_2CO_3 (2 eq) and cat. CuSO_4 (**Scheme 5.2**).

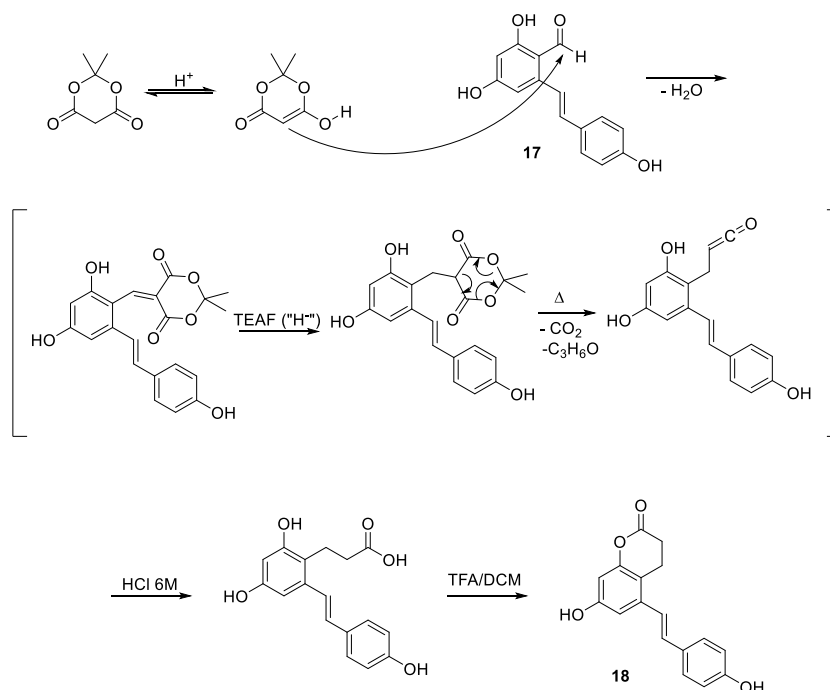


Scheme 5.2. a) Synthesis of amino- and azido-terminal biotin-bearing linker; b) synthesis of diazo-transfer reagent.



Scheme 5.3. Synthesis of monomers-based biotinylated probes and of alkynylated resveratrol and piceatannol.

Then, we moved to the synthesis of monomer-based probes **4** and **5** and terminal alkynes **6** and **7** (**Scheme 5.3**). Resveratrol-containing probes were prepared with the purpose of using them as a negative control during preliminary experiments in cell lysates. Briefly, starting from resveratrol, aldehydic intermediate **17** was obtained through a Vilsmeier-Haack reaction using 1.5 eq of POCl₃ in presence of DMF (1 eq). Aldehyde **17** was reacted with Meldrum's acid in a triethylammonium formate mixture (TEAF, Et₃N: HCOOH 9:3 *v/v*) at 100 °C for 24 h to afford the key six-membered lactone ring (**18**) [23,24]. In an acidic environment, Meldrum's acid tautomeric equilibrium is shifted towards the enolic form, that gives a nucleophilic attack on the aldehyde. After water elimination, the corresponding α - β unsaturated intermediate is obtained. At this point, TEAF mixture reduces the double bond [24] and the obtained intermediate undergoes a concerted retro cyclization, leading to decarboxylation and release of CO₂, acetone and a ketene. It is noteworthy that TEAF mixture acts first as a pH buffer and then as a reducing agent, releasing a hydride atom after decomposition of TEAF carboxylate due to heating [25–27]. The formed ketene is hydrolyzed with concentrated HCl (6M), and the obtained acid is treated with TFA to force cyclization into the desired lactone (**Scheme**).

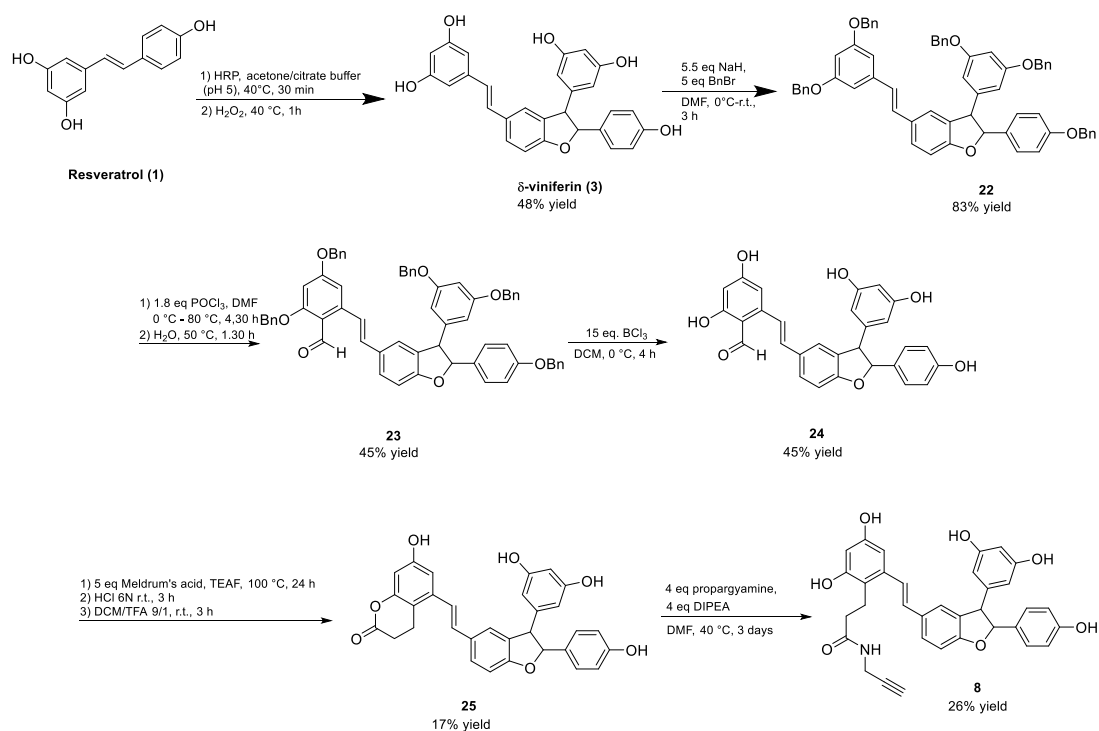


Scheme 5.4. Mechanism of the formation of lactone intermediate **18**

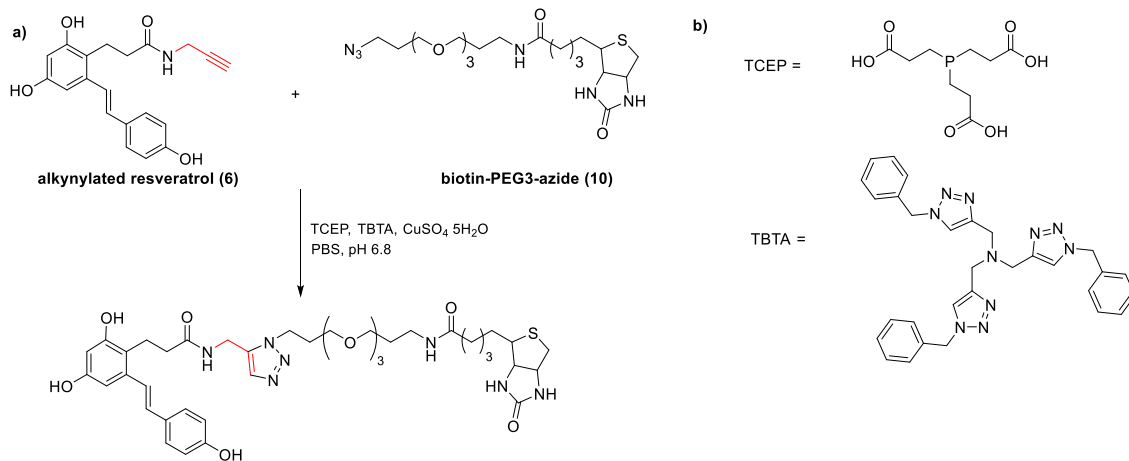
Piceatannol corresponding lactone **19** (Scheme 5.3.) was obtained through oxidative dearomatization with hypervalent iodine, SIBX (Stabilized 2-Iodoxybenzoic acid), leading to the formation of an *ortho*-quinone that is reduced with aqueous Na₂S₂O₄ to afford the desired catechol [28]. Lactone ring opening by nucleophilic attack by the free terminal amine of **15** was not successful. This lack of reactivity may be due the presence of the hydrophilic polyethylene glycol chain that, under reaction conditions (i.e. in presence of Et₃N and DMF as a solvent) would fold into a ball-like shape, thus reducing the availability of the amine. To overcome this limitation, lactones **18** and **19** were hydrolyzed into the corresponding carboxylic acid, and directly used for the amidic coupling with biotinylated linker **15** in presence of EDC and HOBT, affording monomers-containing biotinylated probes **4** and **5** in 10% to 20% yield. On the other hand, lactone rings opening with propargylamine (3 eq) in presence of DIPEA, in DMF at 40 °C for 72 h afforded “clickable” alkynylated resveratrol (**6**, 90% yield) and piceatannol (**7**, 36% yield). The same approach was applied for the preparation of alkynylated δ -viniferin. *Trans*- δ -viniferin (**3**) was prepared from resveratrol *via* oxidative radical coupling using a horseradish peroxidase (HRP) in presence of H₂O₂ (solution 30% *v/v*). In this case, direct formylation of the hydroxylated natural compound was not successful, and -OH protection with benzyl ethers was required to proceed with the synthesis. After Vilsmeier-Haack formylation on the O-benzylated derivative **22**, deprotection was achieved using BCl₃ in dichloromethane at 0 °C for 4 hours. Finally, lactone ring (**25**) was formed as previously described, and then opened with propargylamine affording the desired alkyne (**8**) (Scheme 5.5).

Clickable probes assembly

Once all probe portions were ready, a model click reaction with resveratrol-alkyne **6** and the biotinylated azide counterpart (**10**), was performed following the optimized reaction conditions proposed by Cravatt et al. [29], namely CuSO₄·5H₂O as a catalyst, tris(2-carboxyethyl) phosphine (TCEP) as a reducing agent and tris((1-benzyl-4-triazolyl) methyl) amine (TBTA) as a ligand. Reaction was performed in PBS at pH 6.8, mimicking the conditions that will be used during target identification assays on cell lysates (Scheme 5.6). After only 5 minutes, the desired probe was detected by mass spectroscopy (LRMS (ESI) calcd. for C₄₀H₅₅N₇O₉S²³Na: 832.3674, found 832.4).



Scheme 5.5. Preparation of alkylnated *trans*- δ -viniferin



Scheme 5.6. **a)** Copper (I) assisted alkyne azide cycloaddition (CuAAC) for the assembly of resveratrol-based probe. **b)** Structures of TCEP (tris(2-carboxyethyl) phosphine) and TBTA (Tris((1-benzyl-4-triazolyl) methyl) amine).

Experimental workflow for protein-capture procedures

With all probe components in hand, we are now ready to perform a first set of preliminary experiments. However, before setting up the experiments, the biological activity of stilbenoids alkynes and probes should be assessed, to verify that the structural modifications introduced on the natural compounds do not affect their antibacterial properties. This biological evaluation is now ongoing in the laboratories of Prof. Sébastien Vilain, from the École Nationale Supérieure de Technologie des Biomolécules (ENSTBB, Bordeaux INP).

The workflow for the application of stilbenoids-based biotinylated probes will involve their incubation with a protein mixture derived from *S. aureus* cell lysates, allowing affinity-based interactions within stilbenoids and their targets to occur. If required, an activation step to afford a covalent bond will be performed (e.g. oxidation with NaIO_4 for piceatannol-containing probes). The formed protein-probe complexes will be recovered using streptavidin-coated magnetic beads, and the bound protein will be isolated and identified by proteomic and bioinformatic techniques (Figure 5.28).

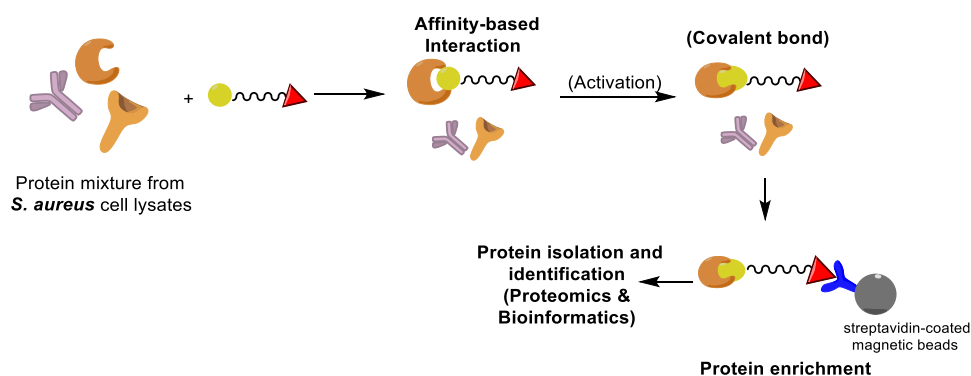


Figure 5.28. Experimental workflow for protein-capture procedure with biotinylated probes

For alkynylated stilbenoids the same protocol will be followed, except that an additional step – that is, click reaction – will be required for probe assembly. During preliminary experiments, rhodamine-bearing azide will be used as a counterpart, to allow the visualization of protein-probe complexes *via* SDS-page and the optimization of protein capture conditions. After the identification of optimal conditions, stilbenoids alkynes will be used to perform target identification studies directly on whole cells, using either rhodamine- or biotin-bearing azides as counterparts. After incubation with whole cells, possible probe activation, and cell lysis, click reaction with the selected azide will be

performed, affording the complete molecular probe, and allowing stilbenoid-target complexes detection or isolation (**Figure 5.29**).

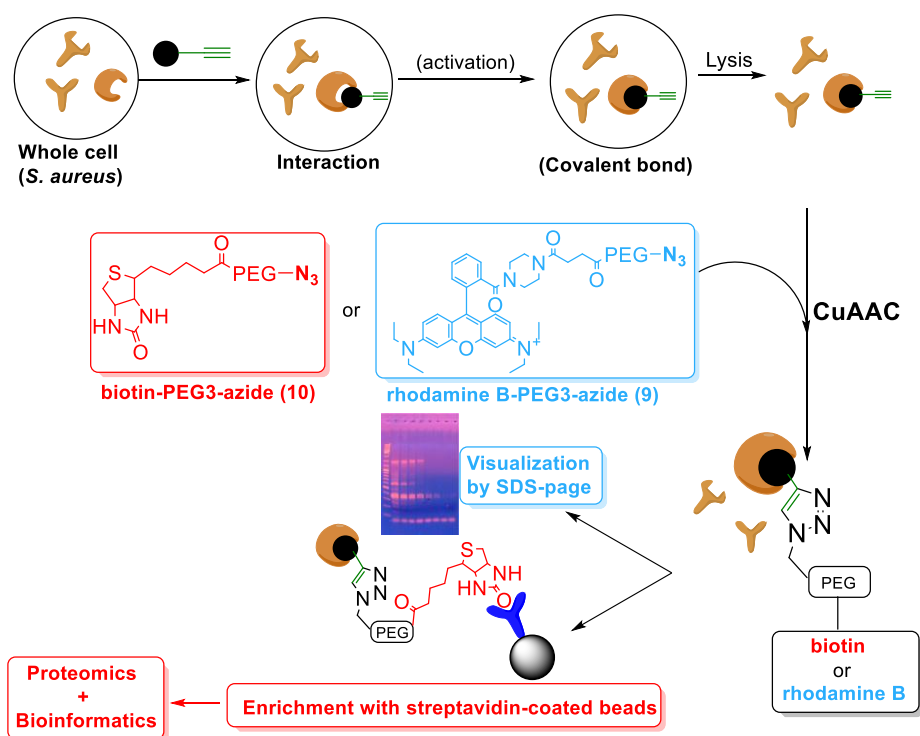
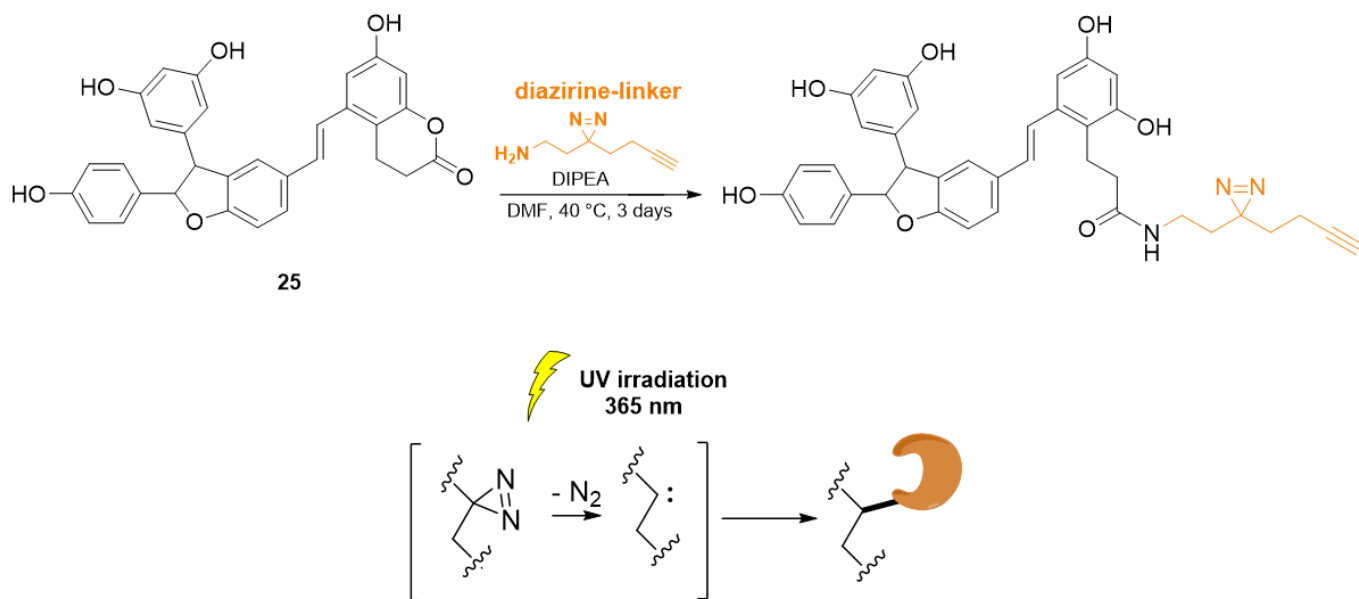


Figure 5.29. Schematic workflow for protein capture procedure with clickable stilbenoids in whole cells.

Further developments of the present project will concern the optimization of chemical probes, to achieve a covalent connection with the putative targets, thus excluding unspecific interactions and preserving the relevant ones during all the phases of the experiments. To afford covalent connections, probes can be activated in different ways, depending on the functions incorporated in their structures. As mentioned, if a catechol motif is present, activation can be easily achieved *via* oxidation with NaIO₄. However, for molecules lacking this function (e.g. δ -viniferin), the introduction of an additional function able to afford covalent bonds with target protein upon activation (e.g. UV irradiation) will be required. In this regard, we have been focusing on the “minimalist” photocrosslinker diazirine, due to its small size -allowing to minimize interference with protein binding- and the short irradiation time required for the generation of a highly reactive carbene species, minimizing unspecific protein binding. The synthesis of an alkyne-terminal diazirine-containing linker is currently under optimization, and it will be employed for the preparation of photoactivable clickable probes.



Scheme 5.7. Structure and functioning of diazirine photocrosslinkers.

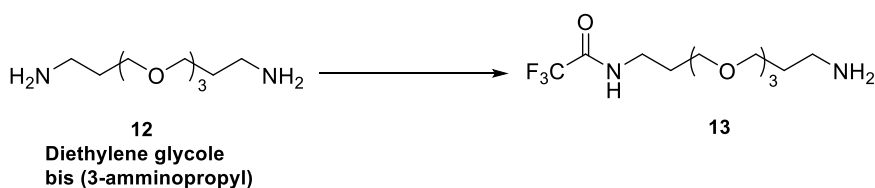
5.1.3 Conclusions

Due to their antibacterial potential, natural stilbenoids represent a valuable starting point for the development of novel sustainable antibacterial agents with increased bioactivity and able to bypass antibiotic resistance mechanisms developed by pathogens. However, to achieve a fruitful implementation of stilbenoid scaffolds, a precise knowledge of their molecular targets is required. Pursuing such knowledge, our idea was to apply an affinity-based protein profiling strategy, involving the use of chemical molecular probes, for target identification of monomeric and dimeric stilbenoids in *S. aureus*. Particular attention was directed toward *trans*- δ -viniferin, which showed the highest antibacterial activity among the tested compounds. Here we described the preparation of stilbenoids-based molecular probes; both biotinylated probes and clickable probes were considered in the study. This project is currently ongoing, and future activities will involve probes incubation with protein mixtures or whole cells from *S. aureus*, followed by protein isolation and identification, as well as structural implementation of the probes. Intriguingly, the same strategy could be applied for target identification or validation of other natural compounds with relevant bioactivities, thus representing a versatile tool for the investigation of natural phytoalexins biological properties.

5.1.4 Materials and Methods

All reactions were carried out under argon atmosphere using dry solvents under anhydrous conditions, unless otherwise noted. Dry dichloromethane (DCM) and tetrahydrofuran (THF) were obtained by distillation over Na/benzophenone under argon atmosphere. Dimethylformamide (DMF), acetonitrile (ACN) and toluene were purchased at the highest commercial quality in anhydrous and oxygen-free formulations. Ethyl acetate (EtOAc), diethyl ether (Et₂O), acetone, ethanol (EtOH), cyclohexane, *n*-pentane and petroleum ether (PET) were purchased at the highest commercial quality and used without further purification. Reagents were purchased at the highest commercial quality and used without further purification, unless otherwise noted. Yields refer to chromatographically and spectroscopically (¹H NMR) homogeneous materials, unless otherwise noted. Reactions were monitored by thin-layer chromatography (TLC) carried out on 0.25 mm Merck silica gel plates (60F-254). Merck silica gel (60, particle size 40-63 μm) was used for column chromatography. NMR spectra were recorded on the following instruments: Bruker DPX-300, Bruker Avance I 300 MHz, Bruker Avance 400 MHz, Bruker Avance III 600 MHz. NMR spectra were calibrated using residual undeuterated solvent as an internal reference (CDCl₃ (¹H): δ = 7.26 ppm; CDCl₃ (¹³C): δ = 77.16 ppm; DMSO-*d*₆ (¹H): 2.50 ppm; DMSO-*d*₆ (¹³C): 39.52 ppm; Acetone-*d*₆ (¹H): 2.05 ppm; Acetone-*d*₆ (¹³C): 29.84 ppm; CD₃CN (¹H): 1.94 ppm; CD₃CN (¹³C): 1.32 ppm; MeOD (¹H): 3.31 ppm; MeOD (¹³C): 49.00 ppm). The following abbreviations were used to describe the multiplicities: s = singlet, d = doublet, t = triplet, q = quartet, m = multiplet, br = broad signal. IR spectra were recorded between 4000 and 550 cm⁻¹ on a Bruker IFS55 (OPUS/IR 3.0.2) FT-IR spectrometer. High resolution mass spectrometry (HRMS) and low-resolution mass spectrometry (LRMS) analyses were obtained from the Centre d'Etude Structurale et d'Analyse des Molécules Organiques (CESAMO) at the Institut des Sciences Moléculaires (ISM, CNRS-UMR 5255, Talence, France). Reverse-phase HPLC analyses were carried out using C₁₈ Pyramid (250 x 21.4 mm) column on a Thermo Spectra system equipped with P1000 XR pumps, an AS3000 autosampler and an UV 6000 LP diode array detector. Effluent was monitored by UV/Vis detection at 230, 248 and 280 nm.

Synthesis of N-(3-(2-(2-(3-aminopropoxy)ethoxy)ethoxy)propyl)-2,2,2-trifluoroacetamide (13)



Commercially available 4,7,10-Trioxa-1,13-tridecanediamine **12** (1.00 g, 4.539 mmol, 1 eq) was dissolved in anhydrous THF (3 ml) under argon atmosphere and cooled to -65°C . To this solution, ethyl trifluoroacetate (513 mg, 3.631 mmol, 0.8 eq) was added dropwise over a period of 30 minutes. The resulting solution was stirred for 90 minutes at -65°C under argon atmosphere. After this time, the solution was slowly warmed up to room temperature. Solvent and volatiles were removed in *vacuo* and the residue was taken up in water (15 ml). The resulting aqueous solution was extracted with CH_2Cl_2 (6 x 10 ml). The organic layer was dried over Na_2SO_4 , filtered, and concentrated under reduced pressure. Flash column chromatography ($\text{CH}_2\text{Cl}_2/\text{MeOH}$, 98/2 \rightarrow 90/10 + 0.5% NH_4OH) afforded the desired product **13** (463.4 mg, 40% yield) as pale yellowish oil.

R_f : (DCM/MeOH/ NH_4OH , 9/1/0.03) = 0.28

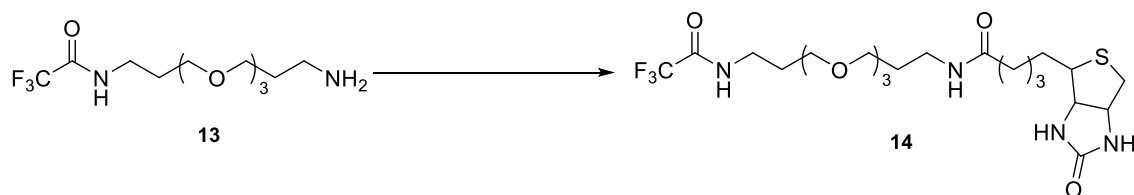
IR (ZnSe) ν_{max} 3363, 3066, 2876, 1714, 1564, 1483, 1350, 1208, 1188, 1155 cm^{-1}

^1H NMR (300 MHz, Chloroform-*d*): δ 8.70 (bs, 1H, NH), 3.65 – 3.51 (m, 12H), 3.49 – 3.40 (m, 2H), 2.79 (t, J = 6.4 Hz, 2H), 1.83 (qd, J = 6.0, 5.1 Hz, 2H), 1.71 (h, J = 6.5 Hz, 2H).

^{13}C -NMR (75 MHz, Chloroform-*d*): δ 157.2, 116.1, 70.5, 70.4, 70.0, 69.7, 69.7, 39.8, 38.2, 32.9, 28.0.

HRMS (ESI-TOF) calcd for $\text{C}_{12}\text{H}_{24}\text{F}_3\text{N}_2\text{O}_4$ $[\text{M}+\text{H}]^+$ 317.1683, found 317.1697

Synthesis of 4-(2-oxohexahydro-1H-thieno[3,4-d]imidazol-4-yl)-N-(1,1,1-trifluoro-2-oxo-7,10,13-trioxa-3-azahexadecan-16-yl)butanamide (14)



A solution of biotin (83.2 mg, 0.341 mmol, 1 eq) in anhydrous DMF (2.8 ml) was prepared under argon atmosphere. DIPEA (59 μ l, 0.341 mmol, 1 eq) was added and the obtained reaction mixture was stirred for 10 minutes. After this time, PyBOP (230.3 mg, 0.443 mmol, 1.3 eq) was added and resulting suspension was stirred at room temperature until it became clear (approx. 30 minutes). Finally, a solution of **13** (140 mg, 0.443 mmol, 1.3 eq) and DIPEA (77 μ l, 0.443 mmol, 1.3 eq) in DMF (1.4 ml) was added to the reaction mixture. The resulting mixture was stirred at room temperature for 16h under argon atmosphere. The resulting mixture was diluted with 70 ml of ethyl acetate. The organic layer was washed with sat. NH_4Cl (4 x 20 ml) and brine (2x 20 ml). The aqueous phase was extracted with ethyl acetate (3 x 20 ml). The combined organic layers were dried over Na_2SO_4 , filtered, and concentrated under *vacuum*. Flash column chromatography (DCM/MeOH, 95/5 \rightarrow 90/10 + 0.3% NH_4OH) afforded the desired product **14** (141 mg, 76% yield) as a pale-yellow wax.

R_f : (DCM/MeOH/ NH_4OH , 9/1/0.03) = 0.35

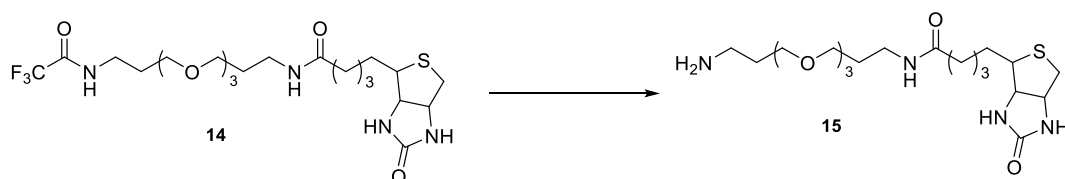
IR (ZnSe) ν_{max} 3285, 2928, 2871, 1697, 1649, 1555, 1460, 1209, 1188, 1156 cm^{-1}

^1H NMR (300 MHz, Methanol- d_4): δ 4.51 (m, 1H), 4.32 (dd, J = 7.9, 4.4 Hz, 1H), 3.69 – 3.58 (m, 8H), 3.54 (m, 4H), 3.40 (t, J = 6.9 Hz, 2H), 3.28 (t, J = 6.8 Hz, 2H), 3.25 – 3.18 (m, 1H), 2.95 (dd, J = 12.7, 5.0 Hz, 1H), 2.72 (d, J = 12.7 Hz, 1H), 2.21 (t, J = 7.3 Hz, 2H), 1.93 – 1.57 (m, 8H), 1.51 – 1.40 (m, 2H).

^{13}C -NMR (75 MHz, Chloroform- d): δ 175.9, 166.0, 158.8, 117.5, 71.5, 71.2, 69.9, 69.6, 63.3, 61.6, 57.0, 41.0, 38.3, 37.8, 36.8, 30.4, 29.8, 29.7, 29.5, 26.9

HRMS (ESI-TOF) calcd for $\text{C}_{22}\text{H}_{37}\text{F}_3\text{N}_4\text{O}_6\text{SNa}$ [$\text{M}+\text{Na}$] $^+$ 565.2278, found 565.2272.

Synthesis of N-(3-(2-(2-(3-aminopropoxy)ethoxy)ethoxy)propyl)-4-(2-oxohexahydro-1H-thieno[3,4-d]imidazol-4-yl)butanamide (15)



A solution of K_2CO_3 (318.4 mg, 2.3036 mmol, 5 eq) in a mixture of methanol (3.6 ml) and water (1.8 ml) was added dropwise to a solution of compound **14** in methanol (1.8 ml) previously prepared under argon atmosphere. The resulting mixture was stirred at room temperature for 16 hours. After complete consumption of the starting material, solvents were removed under *vacuum*, then the residue was dissolved in a mixture 3:1 of dichloromethane/methanol. Na_2SO_4 was added and the resulting suspension was filtered to remove the solids. The filtrate was concentrated under *vacuum*. Flash column chromatography (DCM/MeOH, 90:10 + 2% NH_4OH) afforded the desired product **15** as a yellow sticky solid in 73% yield.

R_f : (DCM/MeOH/ NH_4OH , 8/2/0.2) = 0.21

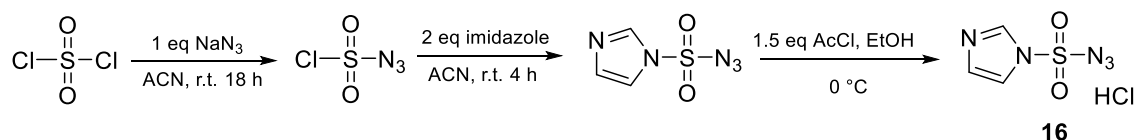
IR (ZnSe) ν_{max} 3313, 2933, 2876, 1682, 1556, 1466, 1202, 1180, 1132 cm^{-1} .

$^1\text{H NMR}$ (300 MHz, Methanol- d_4): δ 4.51 (ddd, $J = 7.9, 5.0, 1.0$ Hz, 1H), 4.32 (dd, $J = 7.9, 4.4$ Hz, 1H), 3.70 – 3.50 (m, 12H), 3.37 – 3.17 (m, 6H), 2.95 (dd, $J = 12.7, 5.0$ Hz, 1H), 2.82 – 2.68 (m, 3H), 2.22 (t, $J = 7.3$ Hz, 2H), 1.84 – 1.55 (m, 8H), 1.47 (q, $J = 7.5$ Hz, 2H).

$^{13}\text{C NMR}$ (75 MHz, Methanol- d_4): δ 176.0, 166.1, 71.4, 71.2, 71.1, 71.1, 70.4, 69.8, 63.4, 61.6, 57.0, 41.0, 40.1, 37.7, 36.8, 30.5, 29.8, 29.5, 29.4, 26.9.

HRMS (ESI-TOF) calcd for $\text{C}_{20}\text{H}_{39}\text{N}_4\text{O}_5\text{S}$ $[\text{M}+\text{H}]^+$ 447.2635, found 447.2632.

Synthesis of 1H-imidazole-1-sulfonyl azide hydrochloride (16)



A suspension of sodium azide (240.5 mg, 3.7 mmol, 1 eq) in anhydrous acetonitrile (4 ml) was prepared under argon atmosphere and cooled to 0 °C in an ice bath. Then, sulfonyl chloride (300 μl , 3.7 mmol, 1 eq) was added dropwise. The obtain reaction mixture was warmed up and stirred at room

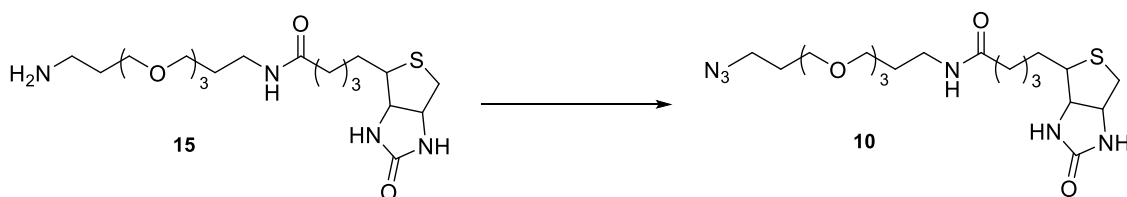
temperature for 18 hours, then cooled again to 0 °C. Imidazole (504 mg, 7.4 mmol, 2 eq) was added portion wise, reaction was led warm to room temperature and stirred for 4 hours. Ethyl acetate (8 ml) was added, and the organic phase was washed with water (2 x 8 ml) and sat. NaHCO₃, then dried over Na₂SO₄, filtered, and cooled to 0 °C. Finally, 1.5 ml of HCl in absolute ethanol (obtained by dropping 410 µl of acyl chloride in 1.5 ml of absolute ethanol) were added. Product **16** precipitated as a white needless solid, which was recovered after filtration on sintered glass in 63% yield (488 mg).

M.p. 99 – 102 °C (reported 100 - 102 °C). Data are consistent with the literature [30].

¹H NMR (300 MHz, Deuterium Oxide): δ 9.26 – 9.16 (m, 1H), 7.98 (t, *J* = 1.9 Hz, 1H), 7.56 (m, 1H).

¹³C NMR (76 MHz, Deuterium Oxide): δ 137.7, 124.9, 119.7.

Synthesis of *N*-(3-(2-(2-(3-azidopropoxy)ethoxy)ethoxy)propyl)-4-(2-oxohexahydro-1*H*-thieno[3,4-*d*]imidazol-4-yl)butanamide (**10**)



K₂CO₃ (43.3 mg, 0.313 mmol, 2 eq) and CuSO₄ (0.25 mg, 1 % mol) were added to a stirred solution of **15** (70 mg, 0.157 mmol, 1 eq) in methanol (8.5 ml). After stirring for 5 min, **16** (39.4 mg, 0.188 mmol, 1.2 eq) was added. The resulting mixture was stirred at room temperature for 16 hours. After complete consumption of the starting material, the solvent was evaporated, and the residual oil was diluted in 2.5 ml H₂O and 5 mL HCl 1N. The aqueous phase was extracted with ethyl acetate (6 x 8 m). The organic layer was dried over Na₂SO₄, filtered, and concentrated under reduced pressure to give compound **10** a yellowish oil (44 mg, 60 %).

R_f: (DCM/MeOH/NH₄OH, 9/1/0.1) = 0.33

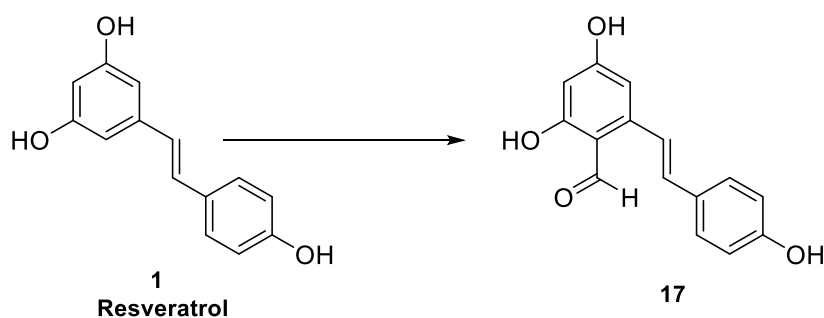
IR (ZnSe) ν_{max} 2933, 2876, 2090, 1682, 1556, 1466, 1202, 1180, 1132 cm⁻¹.

¹H NMR (300 MHz, Methanol-*d*₄): δ 4.50 (dd, *J* = 7.9, 4.9, 1H), 4.31 (dd, *J* = 7.9, 4.4 Hz, 1H), 3.67 – 3.49 (m, 13H), 3.40 (t, *J* = 6.8 Hz, 2H), 3.27 (t, *J* = 6.8 Hz, 2H), 2.93 (dd, *J* = 12.7, 5.0 Hz, 1H), 2.71 (d, *J* = 12.7 Hz, 1H), 2.20 (t, *J* = 7.3 Hz, 2H), 2.05 – 1.56 (m, 7H), 1.50 – 1.41 (m, 2H).

^{13}C NMR (76 MHz, Methanol- d_4): δ 176.08, 165.96, 71.44, 71.43, 71.20, 71.15, 69.85, 68.89, 63.58, 61.89, 56.88, 56.46, 40.91, 37.90, 36.70, 30.28, 30.09, 29.72, 29.41, 26.83.

HRMS (ESI-TOF) calcd for $\text{C}_{20}\text{H}_{36}\text{N}_6\text{O}_5\text{SNa}$ $[\text{M}+\text{Na}]^+$ 495.23601, found 495.23510

Synthesis of (E)-2,4-dihydroxy-6-(4-hydroxystyryl)benzaldehyde (17)



Resveratrol (2g, 8.76 mmol) was dissolved in 40 ml of anhydrous acetonitrile under argon atmosphere and the obtained solution was cooled to 0 °C. POCl_3 (1.2 ml, 13.14 mmol, 1.5 eq) was added, followed by DMF (680 μl , 8.76 mmol, 1 eq) and reaction mixture was allowed to warm up to room temperature and stirred for 2 hours. After this time, 160 ml of cold water were added. The obtained mixture was stirred at 50 °C for 3 hours, then extracted three times with ethyl acetate (30 ml). The organic layer was dried over Na_2SO_4 , filtered and the solvent was removed under reduced pressure. Flash column chromatography (cyclohexane/acetone 7/3) afforded the desired compound **17** as a yellow solid in 67% yield.

R_f : (CHX/EtOAc) = 0.2

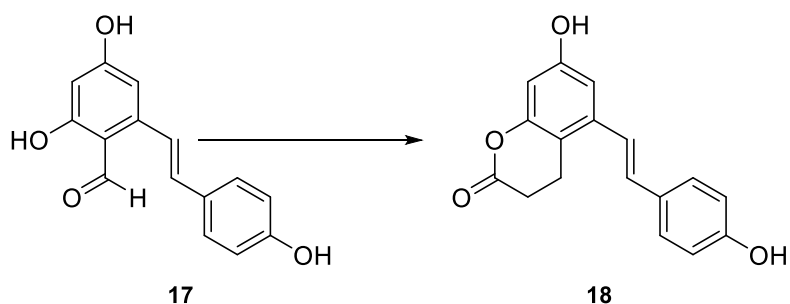
IR (ZnSe) ν_{max} 3457, 1634, 1602, 1513, 1455, 1375, 1243, 1170, 769 cm^{-1}

^1H NMR (300 MHz, Methanol- d_4): δ 10.20 (s, 1H), 7.51 (d, J = 16.0 Hz, 1H), 7.48 – 7.42 (m, 2H), 6.97 (d, J = 16.0 Hz, 1H), 6.83 – 6.79 (m, 2H), 6.58 (d, J = 2.2 Hz, 1H), 6.20 (d, J = 2.3 Hz, 1H).

^{13}C NMR (75 MHz, Methanol- d_4): δ 194.3, 167.2, 166.9, 159.2, 147.0, 136.0, 129.7, 129.5, 121.0, 116.6, 113.0, 107.5, 102.3.

HRMS (-ESI) m/z : $[\text{M} - \text{H}]^-$. Calcd for $\text{C}_{15}\text{H}_{11}\text{O}_4$ 255.0662; found, 255.0667.

Synthesis of (E)-7-hydroxy-5-(4-hydroxystyryl)chroman-2-one (18)



To a stirred solution of **17** (300 mg, 1.17 mmol) in 20 ml of a mixture 3:1 of triethylamine and formic acid was added Meldrum's acid (438.5 mg, 3.04 mmol, 2.6 eq). The resulting mixture was heated to 100°C and stirred for 24 hours. After complete consumption of the starting material, reaction mixture was cooled to room temperature and then to 0 °C. 25 ml of HCl 6N were carefully added and reaction mixture was stirred at room temperature for two hours, then extracted with ethyl acetate (5 x 15 ml). Organic layers were dried over Na₂SO₄, filtered and the solvent was removed under reduced pressure. The residue was dissolved in 20 ml of a mixture 9:1 of dichloromethane and trifluoroacetic acid. The obtained mixture was stirred at room temperature for 3 hours, then the solvents were removed. Flash column chromatography (cyclohexane/ethyl acetate 7/3 + 0.5% TFA) afforded the desired product **17** as a light brown solid in 42% yield.

R_f: (CHX/EtOAc 1/1 + 0.05% TFA) = 0.47

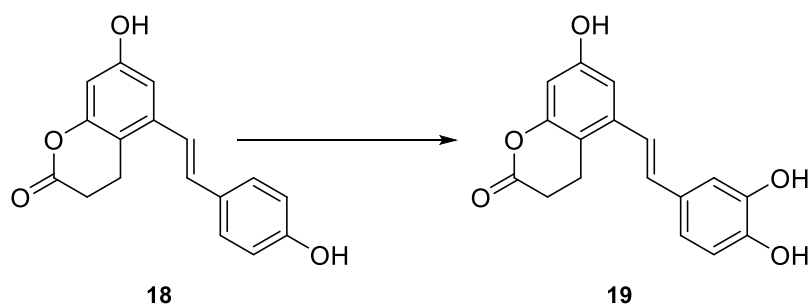
IR (ZnSe) ν_{\max} 3355, 2920, 1737, 1623, 1605, 1585, 1513, 1468, 1327, 1133, 962, 843 cm⁻¹

¹H NMR (300 MHz, Acetone-*d*₆): δ 7.51 – 7.46 (m, 2H), 7.19 (d, *J* = 16.2 Hz, 1H), 7.01 (d, *J* = 16.2 Hz, 1H), 6.95 (d, *J* = 2.4 Hz, 1H), 6.89 – 6.83 (m, 2H), 6.43 (d, *J* = 2.4 Hz, 1H), 3.09 (dd, *J* = 8.2, 6.2 Hz, 2H), 2.81 – 2.71 (m, 2H).

¹³C NMR (75 MHz, Acetone *d*₆): δ = 168.9, 158.5, 157.7, 154.3, 138.4, 132.3, 129.8, 129.1, 122.6, 116.4, 113.0, 108.8, 103.6, 29.6, 20.8.

HRMS (-ESI) *m/z*: [M - H]⁻. Calcd for C₁₇H₁₃O₄ 281.0819; found, 281.0830.

Synthesis of (E)-5-(3,4-dihydroxystyryl)-7-hydroxychroman-2-one (19)



Resveratrol lactone **18** (50 mg, 0.177 mmol, 1 eq) was dissolved in 5 ml of methanol at 0 °C. SIBX (150 mg, 0.531 mmol, 3 eq) was added and reaction mixture was stirred at 0 °C for 1 hour, then at room temperature for 30 minutes. After complete consumption of the starting material, reaction was quenched with 10 ml of a solution 0.15 M of Na₂S₂O₄. The aqueous phase was extracted with ethyl acetate (4 x 10 ml). The organic layer was then washed with sat. NaHCO₃, then dried over Na₂SO₄, filtered and the solvent was removed under reduced pressure, giving compound **19** in 89% yield.

R_f: (CHX/EtOAc 1/1) = 0.32

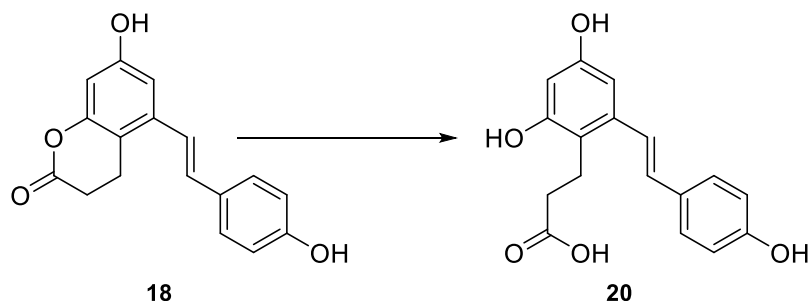
IR (ZnSe) ν_{max} 3375, 1737, 1608, 1518, 1440, 1281, 1132, 958 cm⁻¹

¹H NMR (300 MHz, Acetone-*d*₆): δ 7.13 (d, *J* = 2.0 Hz, 1H), 7.12 (d, *J* = 16.1 Hz, 1H), 6.99 – 6.91 (m, 3H), 6.83 (d, *J* = 8.2 Hz, 1H), 6.42 (d, *J* = 2.4 Hz, 1H), 3.08 (dd, *J* = 8.2, 6.2 Hz, 2H), 2.80 – 2.72 (m, 2H).

¹³C NMR (75 MHz, Acetone *d*₆): δ 168.8, 157.6, 154.2, 146.4, 146.1, 138.4, 132.6, 130.5, 122.7, 120.3, 116.3, 114.1, 113.0, 108.8, 103.6, 29.5, 20.79

HRMS (-ESI) *m/z*: [M - H]⁻. Calcd for C₁₇H₁₃O₅: 297.0768; found, 297.0755.

Synthesis of (E)-3-(2,4-dihydroxy-6-(4-hydroxystyryl)phenyl)propanoic acid (20)



Resveratrol lactone **18** (45 mg, 0.161 mmol, 1 eq) was dissolved in 5 ml of a THF/H₂O 9:1 mixture. NaOH (32.2 mg, 0.806 mmol, 5 eq) was added and reaction mixture was stirred at room temperature for 30 minutes. After

complete consumption of the starting material, HCl 1M was added dropwise to reach pH 2. The aqueous phase was extracted with ethyl acetate (5 x 5 ml). Organic layers were washed with brine, dried over Na₂S₂O₄, filtered, and the solvent was removed under *vacuum*, giving carboxylic acid **20** in quantitative yield.

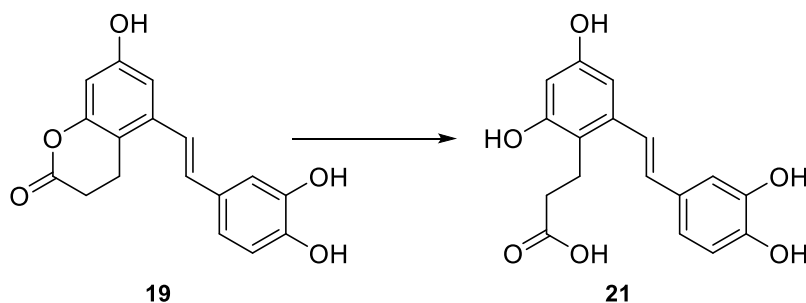
R_f: 0.18 (DCM/MeOH 9/1 + 0.05% TFA)

IR (ZnSe) ν_{max} 3320, 2627, 1623, 1605, 1585, 1468, 1327, 1191, 955, 836 cm⁻¹

¹H NMR (300 MHz, Acetone-*d*₆): δ 7.51 – 7.44 (m, 2H), 7.34 (d, *J* = 16.1 Hz, 1H), 6.93 (d, *J* = 16.1 Hz, 1H), 6.89 – 6.82 (m, 2H), 6.68 (d, *J* = 2.4 Hz, 1H), 6.38 (d, *J* = 2.4 Hz, 1H), 3.09 – 2.99 (m, 2H), 2.62 – 2.51 (m, 2H).

¹³C NMR (76 MHz, Acetone-*d*₆): δ 175.2, 157.9, 156.9, 156.8, 139.1, 130.7, 130.1, 128.6, 124.0, 117.5, 116.2, 104.4, 102.7, 34.7, 21.3.

Synthesis of (E)-3-(2-(3,4-dihydroxystyryl)-4,6-dihydroxyphenyl)propanoic acid (**21**)



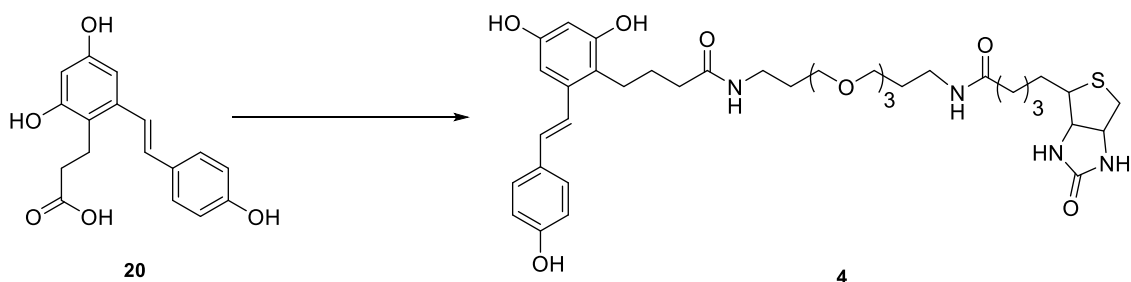
Piceatannol lactone **19** (40 mg, 0.402 mmol, 1 eq) was dissolved under argon atmosphere in 3.6 ml of THF, previously degassed with argon for 20 minutes. Then, a solution of NaOH (16.1 mg, 0.806 mmol, 3 eq) in 0.4 ml of water was added dropwise, and reaction mixture was stirred at room temperature for 10 minutes. After complete consumption of the starting material, HCl 1M was added dropwise to reach pH 2. The aqueous phase was extracted with ethyl acetate (5 x 5 ml). Organic layers were washed with brine, dried over Na₂S₂O₄, filtered, and the solvent was removed under *vacuum*, giving carboxylic acid **21** in 90% yield.

R_f: 0.22 (DCM/MeOH 95/5 + 0.05% TFA)

IR (ZnSe) ν_{max} 3333, 2589, 1623, 1605, 1544, 1468, 1200, 988, 842 cm⁻¹

¹H NMR (300 MHz, Acetone-*d*₆): δ 7.16 – 7.08 (m, 2H), 6.95 (m, 3H), 6.83 (d, *J* = 8.2 Hz, 1H), 6.42 (d, *J* = 2.4 Hz, 1H), 3.08 (m, 2H), 2.80 – 2.72 (m, 2H).

Synthesis of (E)-N-(3-(2-(2-((7-(2,4-dihydroxy-6-(4-hydroxystyryl)phenyl)-5-oxoheptyl)oxy)ethoxy)ethoxy)propyl)-4-(2-oxohexahydro-1H-thieno[3,4-d]imidazol-4-yl)butanamide (4)



A solution of **20** (12 mg, 0.04 mmol, 1 eq) in anhydrous DMF (1.5 ml) was prepared under argon atmosphere. A solution of biotin-linker **15** (35 mg, 0.08 mmol, 2 eq) in 0.5 ml of dry DMF was then added, followed by HOBt (10.5 mg, 0.08 mmol, 2 eq), TEA (21.8 μ l, 0.16 mmol, 4 eq) and EDC (14.9 mg, 0.08 mmol, 2 eq). Reaction mixture was stirred at room temperature for 22 hours. After complete consumption of the starting material, DMF was evaporated under *vacuum* and the crude product was purified by preparative TLC (0.25, DCM/MeOH 80/20) affording the desired probe **4** as a pale-yellow solid in 20% yield.

R_f: 0.77 (DCM/MeOH 8/2)

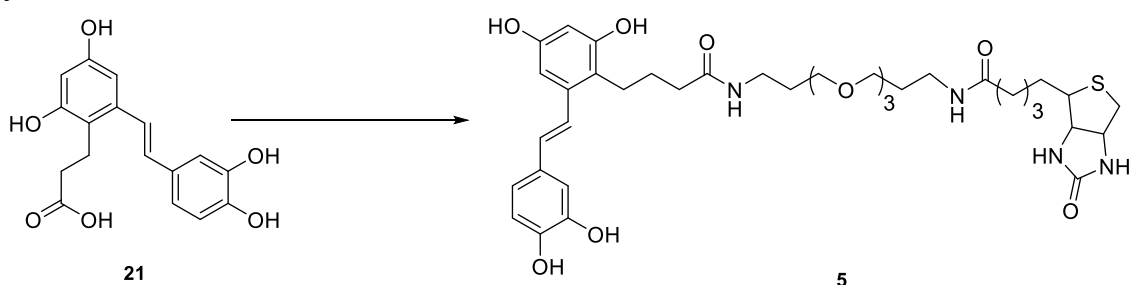
IR ν_{max} 3428, 2920, 2873, 1641, 1456, 1353, 1094, 1034, 945 cm^{-1}

¹H NMR (300 MHz, Methanol-*d*₄): δ 7.45 – 7.40 (m, 2H), 7.25 (d, *J* = 16.0 Hz, 1H), 6.87 (d, *J* = 16.0 Hz, 1H), 6.82 – 6.75 (m, 2H), 6.59 (d, *J* = 2.4 Hz, 1H), 6.25 (d, *J* = 2.4 Hz, 1H), 4.53 – 4.42 (m, 1H), 4.31 – 4.24 (m, 1H), 3.68 – 3.46 (m, 13H), 3.40 (t, *J* = 6.2 Hz, 2H), 3.29 – 3.12 (m, 6H), 3.00 (t, *J* = 7.3 Hz, 2H), 2.96 – 2.87 (m, 1H), 2.71 (m, 1H), 2.43 (t, *J* = 7.3 Hz, 2H), 2.19 (m, 3H), 1.88 – 1.50 (m, 5H), 1.44 (q, *J* = 7.4 Hz, 2H).

¹³C NMR (76 MHz, Methanol-*d*₄): δ 174.70, 174.58, 164.70, 157.01, 156.11, 155.92, 138.32, 129.75, 129.38, 127.65, 123.27, 116.87, 115.11, 103.01, 101.50, 70.09 (d, *J* = 1.5 Hz), 69.80, 69.74, 68.54, 68.46, 61.98, 60.22, 55.59, 39.63, 36.51, 36.45, 36.36, 35.46, 29.36, 28.99, 28.72, 28.39, 28.09, 25.48, 21.20.

HRMS (ESI-TOF) calcd for C₃₇H₅₂N₄O₉SNa [M+Na]⁺ 751.3347, found 751.3345.

Synthesis of (E)-N-(3-(2-(2-((7-(2-(3,4-dihydroxystyryl)-4,6-dihydroxyphenyl)-5-oxoheptyloxy)ethoxy)ethoxy)propyl)-4-(2-oxohexahydro-1H-thieno[3,4-d]imidazol-4-yl)butanamide (5)



A solution of **21** (30 mg, 0.095 mmol, 0.8 eq) in anhydrous DMF (1.5 ml) was prepared under argon atmosphere. A solution of biotin-linker **15** (53 mg, 0.118 mmol, 1 eq) in 0.5 ml of dry DMF was then added, followed by HOBt (16 mg, 0.118 mmol, 1 eq), TEA (33 μ l, 0.237 mmol, 2 eq) and EDC (22.7 mg, 0.118 mmol, 1 eq). Reaction mixture was stirred at room temperature for 18 hours. After complete consumption of the starting material, DMF was evaporated under *vacuum* and the crude product was purified by preparative TLC (0.25, DCM/MeOH 80/20) affording the desired probe **5** as a pale-yellow solid in 10% yield.

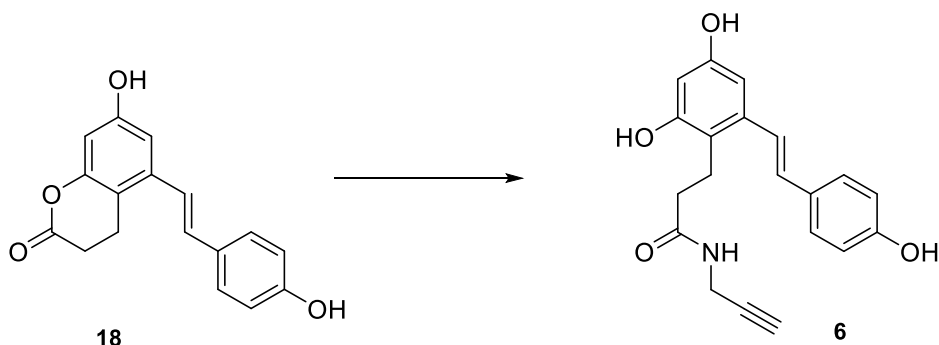
R_f: 0.76 (DCM/MeOH 8/2)

IR ν_{max} 3410, 2955, 2876, 1670, 1641, 1456, 1353, 1094, 1034, 945 cm^{-1}

¹H NMR (300 MHz, Methanol-*d*₄): δ 7.20 (d, *J* = 16.0 Hz, 1H), 7.06 (d, *J* = 2.0 Hz, 1H), 6.88 (dd, *J* = 8.2, 2.0 Hz, 1H), 6.82 (d, *J* = 16.0 Hz, 1H), 6.77 (d, *J* = 8.2 Hz, 1H), 6.59 (d, *J* = 2.4 Hz, 1H), 6.26 (d, *J* = 2.4 Hz, 1H), 4.54 – 4.42 (m, 1H), 4.28 (m, 1H), 3.73 – 3.45 (m, 10H), 3.41 (t, *J* = 6.1 Hz, 2H), 3.30 – 3.19 (m, 4H), 3.19 – 3.11 (m, 1H), 3.05 – 2.97 (m, 3H), 2.95 – 2.87 (m, 2H), 2.70 (d, *J* = 12.7 Hz, 1H), 2.44 (t, *J* = 7.3 Hz, 2H), 2.20 (t, *J* = 7.3 Hz, 2H), 1.68 (m, 10H), 1.51 – 1.37 (m, 2H).

¹³C NMR (76 MHz, Methanol-*d*₄): δ 174.68, 174.61, 164.70, 156.11, 155.91, 145.16, 138.25, 130.02, 129.95, 123.24, 119.07, 116.88, 115.05, 112.50, 102.94, 101.48, 70.08, 70.06, 69.78, 69.72, 68.54, 68.46, 61.98, 60.21, 55.58, 39.63, 36.55, 36.46, 36.39, 35.47, 29.36, 28.98, 28.69, 28.39, 28.09, 25.48, 21.17.

Synthesis of (E)-3-(2,4-dihydroxy-6-(4-hydroxystyryl)phenyl)-N-(prop-2-yn-1-yl)propenamide (6)



To a stirred solution of resveratrol lactone **18** (25 mg, 0.089 mmol, 1 eq) in anhydrous DMF (1.4 mL) propargylamine (22.5 μ L, 0.354 mmol, 4 eq) and DIPEA (59.7 μ L, 0.354 mmol, 4 eq) were added under argon atmosphere. The mixture was heated at 40 °C and stirred for 3 days. After this time, reaction was quenched with 2 ml of HCl 1N. The aqueous phase was extracted three times with ethyl acetate (10 ml) and combined layers were washed with NaCl sat. The organic layer was dried over Na₂SO₄, filtered, and concentrated under *vacuum*. The crude brown oil was purified by flash column chromatography (cyclohexane/ethyl acetate 30:70, v/v) afforded the desired product **6** as yellow solid in 90% yield.

R_f : 0.67 (100% EtOAc)

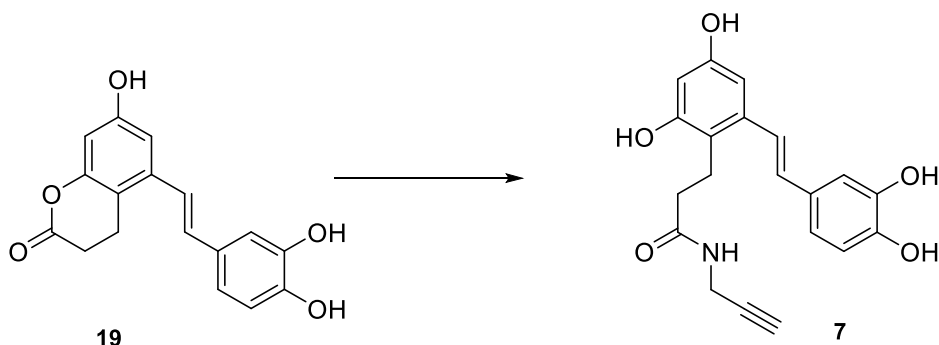
IR (ZnSe) ν_{max} 3355, 2920, 2270, 1665, 1585, 1513, 1468, 1133, 962, 843 cm⁻¹

¹H NMR (300 MHz, Methanol-*d*₄): δ 2.41 (t, *J* = 7.7 Hz, 2H), 2.52 (t, *J* = 2.0 Hz, 1H), 2.98 (t, *J* = 7.6 Hz, 2H), 3.94 – 3.87 (m, 2H), 6.23 (d, *J* = 2.2 Hz, 1H), 6.57 (d, *J* = 2.4 Hz, 1H), 6.74 – 6.81 (m, 2H), 6.85 (d, *J* = 16.0 Hz), 7.21 (d, *J* = 16.0 Hz, 1H), 7.40 (d, *J* = 8.3 Hz, 2H).

¹³C NMR (101 MHz, Methanol-*d*₄): δ 175.76, 158.37, 157.40, 157.27, 139.69, 131.25, 130.74, 129.00, 124.48, 118.12, 116.46, 104.46, 102.78, 80.58, 72.07, 37.35, 29.47, 22.43.

HRMS (ESI-TOF) calcd for C₂₀H₁₈NO₄ [M] 336.1241, found 336.1244.

Synthesis of (E)-3-(2-(3,4-dihydroxystyryl)-4,6-dihydroxyphenyl)-N-(prop-2-yn-1-yl)propanamide (7)



To a stirred solution of piceatannol lactone **19** (90 mg, 0.302 mmol, 1 eq) in anhydrous DMF (6.3 mL) propargylamine (77 μ L, 1.207 mmol, 4 eq) and DIPEA (204 μ L, 1.207 mmol, 4 eq) were added under Argon atmosphere. The mixture was heated at 40 $^{\circ}$ C and stirred for 3 days. Then, reaction was quenched with 7 ml of HCl 1N. The aqueous layer was extracted with ethyl acetate (5 \times 10 mL) and combined organic layers were washed with brine (2 \times 10 mL), dried over Na_2SO_4 , filtered, and concentrated under *vacuum*. The crude brown oil was purified by flash column chromatography (cyclohexane/ethyl acetate 10:90, v/v) affording the desired product **7** as yellow solid in 36% yield.

R_f : 0.67 (100% EtOAc)

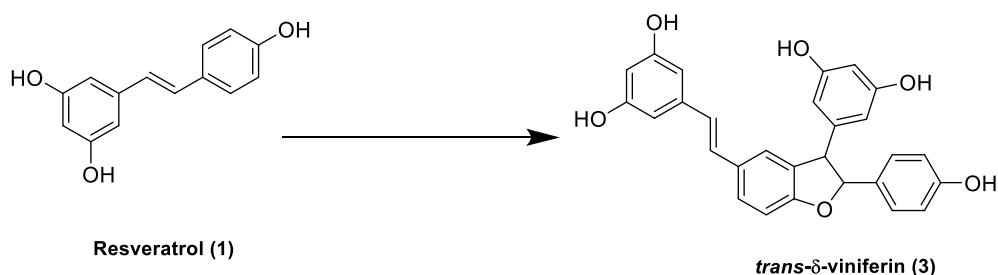
IR (ZnSe) ν_{max} 3305, 2899, 2256, 1684, 1563, 1513, 1133, 968, 890 cm^{-1}

^1H NMR (300 MHz, Methanol- d_4): δ 2.41 (dd, J = 8.6, 6.7 Hz, 2H), 2.52 (t, J = 2.6 Hz, 1H), 2.98 (dd, J = 8.7, 6.7 Hz, 2H), 3.91 (d, J = 2.6 Hz, 2H), 6.24 (d, J = 2.4 Hz, 1H), 6.56 (d, J = 2.6 Hz, 1H), 6.72 – 6.79 (m, 2H), 6.86 (dd, J = 8.3, 2.1 Hz, 1H), 7.04 (d, J = 2.1 Hz, 1H), 7.16 (d, J = 16.0 Hz, 1H).

^{13}C NMR (76 MHz, Methanol- d_4): δ 175.7, 157.3, 157.1, 146.4, 146.4, 139.6, 131.4, 131.3, 124.4, 120.4, 118.1, 116.4, 113.8, 104.4, 102.7, 80.5, 72.1, 37.3, 29.5, 22.3.

HRMS (ESI-TOF) calcd for $\text{C}_{20}\text{H}_{19}\text{NO}_5\text{Na}$ $[\text{M}+\text{Na}]^+$ 376.1155, found 376.1145.

Synthesis of (E)-5-(2-(3-(3,5-dihydroxyphenyl)-2-(4-hydroxyphenyl)-2,3-dihydrobenzofuran-5-yl)vinyl)benzene-1,3-diol, trans- δ -viniferin (3)



Resveratrol (1g, 4.381 mmol) was dissolved in 43.8 mL of a mixture 1:1 of acetone/citrate buffer (pH = 5) and aqueous solution of horseradish peroxidase (1.75 ml, 1 mg/ml) was added to the solution. The obtained reaction mixture was heated to 40 °C and stirred for 30 minutes. After this time, 0.66 ml of H₂O₂ (30% v/v) were added and reaction mixture was stirred at 40 °C for additional 1h. After reaction completion, acetone was evaporated. The aqueous phase was extracted with ethyl acetate (5 x 10 ml). Organic layers were washed with brine, dried over Na₂SO₄, filtered, and evaporated. Purification by flash chromatography (DCM/MeOH 95/5 \rightarrow 9/1) afforded the desired product 3 as a light brown amorphous solid in 48% yield.

R_f : (DCM/MeOH 9/1) = 0.28

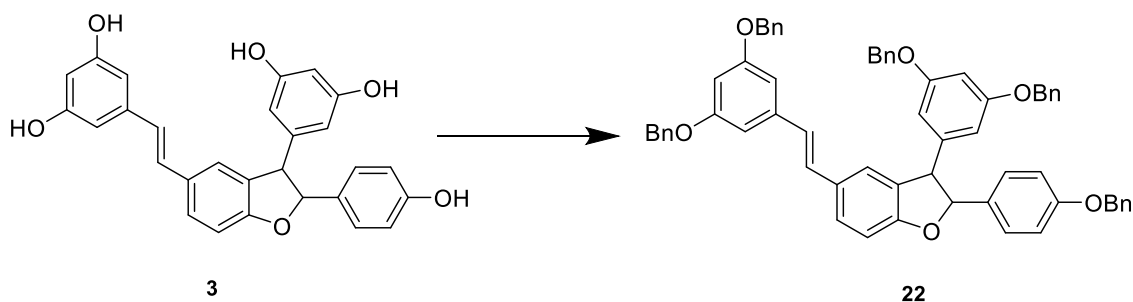
IR ν_{\max} 3339, 1740, 1601, 1367, 1230, 1217, 1153, 833 cm⁻¹

¹H NMR (300 MHz, Methanol-*d*₄): δ 7.38 (dd, *J* = 8.1, 2.0 Hz, 1H), 7.23 – 7.14 (m, 3H), 7.00 (d, *J* = 16.3 Hz, 1H), 6.87 (d, *J* = 8.3 Hz, 1H), 6.84 – 6.77 (m, 3H), 6.45 (d, *J* = 2.2 Hz, 2H), 6.22 (t, *J* = 2.2 Hz, 1H), 6.17 (t, *J* = 2.2 Hz, 1H), 6.15 (d, *J* = 2.2 Hz, 2H), 5.41 (d, *J* = 8.4 Hz, 1H), 4.42 (d, *J* = 8.4 Hz, 1H).

¹³C NMR (76 MHz, Methanol-*d*₄): δ 161.02, 159.94 (x2C), 159.63 (x2C), 158.72, 145.37, 141.17, 132.84, 132.39, 132.34, 129.37, 128.65 (x3C), 127.46, 124.16, 116.31 (x2C), 110.35, 107.73 (x2C), 105.82 (x2C), 102.72, 102.48, 94.91, 58.79.

LRMS (ESI) calcd for C₂₈H₂₁O₆ [M-H]⁻ 453.13436, found 453.1344.

Synthesis of (E)-2-(4-(benzyloxy)phenyl)-3-(3,5-bis(benzyloxy)phenyl)-5-(3,5-bis(benzyloxy)styryl)-2,3-dihydrobenzofuran (22)



A solution of trans- δ -viniferin **3** (650 mg, 1.43 mmol) in dry DMF was prepared under argon atmosphere and cooled to 0 °C. Then, NaH (60% dispersion in mineral oil, 314.6 mg, 7.866 mmol) was added and reaction mixture was stirred for 30 minutes. Finally, benzyl bromide (0.85 ml, 7.15 mmol) was added dropwise. Reaction mixture was allowed to warm up to room temperature and stirred for 3 hours. After completion, reaction was cooled again to 0 °C and quenched with 30 ml of sat. NH₄Cl, then diluted with additional 120 ml of water. The aqueous phase was extracted with EtOAc (4 x 30 ml). The combined organic layers were washed with HCl 1 M, water, and brine, dried over Na₂SO₄, filtered, and concentrated under reduced pressure. Flash chromatography (CHX/AcOEt 9:1) afforded the desired product as a light-yellow amorphous solid in 83% yield.

R_f: (CHX/AcOEt 9/1) = 0.44

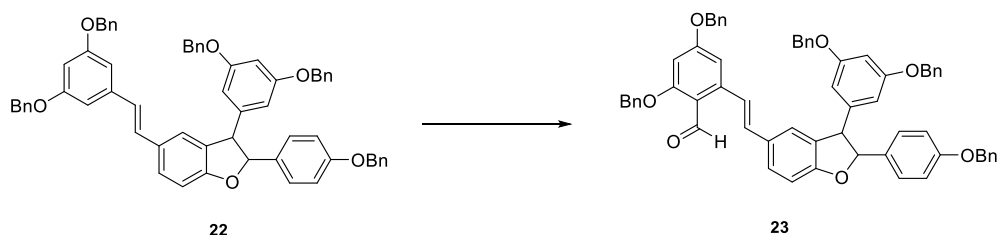
IR ν_{\max} 3032, 2922, 1591, 1512, 1487, 1453, 1376, 1344, 1296, 1237, 1156, 1056, 960.5, 828.9, 736.1, 695.9 cm⁻¹

¹H NMR (300 MHz, Chloroform-*d*): δ 7.48 – 7.22 (m, 29H), 7.16 (d, *J* = 1.8 Hz, 1H), 7.06–6.92 (m, 4H), 6.82 (d, *J* = 16.2 Hz, 1H), 6.73 (d, *J* = 2.2 Hz, 2H), 6.57 (t, *J* = 2.3 Hz, 1H), 6.53 (t, *J* = 2.2 Hz, 1H), 6.44 (d, *J* = 2.3 Hz, 2H), 5.51 (d, *J* = 8.1 Hz, 1H), 5.07 (s, 2H), 5.06 (s, 4H), 4.99 (s, 4H), 4.48 (d, *J* = 8.1 Hz, 1H).

¹³C NMR (76 MHz, Chloroform-*d*): δ 160.4 (x2C), 160.3 (x2C), 159.9, 159.0, 144.2, 139.9, 137.1 (x2C), 137.0, 136.8 (x2C), 133.0, 130.9, 130.7, 129.3, 128.7 (x10C), 128.2 (x2C), 128.1, 128.0 (x2C), 127.8 (x5C), 127.7 (x5C), 127.6 (x2C), 127.5, 126.3, 123.3, 115.1 (x2C), 109.8, 107.7 (x2C), 105.6 (x2C), 101.4, 100.9, 93.1, 70.3 (x4C), 70.2, 57.9.

HRMS (ESI) calcd for C₆₃H₅₂O₆²³Na 927.36561, found 927.36518.

Synthesis of (E)-2,4-bis(benzyloxy)-6-(2-(2-(4-(benzyloxy)phenyl)-3-(3,5-bis(benzyloxy)phenyl)-2,3-dihydrobenzofuran-5-yl)vinyl)benzaldehyde (23)



POCl_3 (0.16 ml, 1.690 mmol) was added to 9.6 ml of dry DMF (9.6 ml) at 0 °C in and the obtained solution was stirred for 20 minutes. Then, a solution of compound **22** (850 mg, 0.9391 mmol) in dry DMF (9.6 ml) was added at 0 °C. Reaction mixture was allowed to warm up to room temperature and then heated to 80 °C and stirred for 4.30 hours. After this time reaction mixture was cooled to room temperature and then to 0 °C with an ice bath. 30 ml of NaOH 1M were carefully added and the obtained suspension was stirred at 50 °C for 1.30 hours, then diluted with additional 180 ml of water and extracted with EtOAc (4 x 50 ml). The combined organic layers were washed with brine, dried over Na_2SO_4 , filtered, and concentrated under reduced pressure. Flash chromatography (CHX/AcOEt 95/5, then CHX/AcOEt/DCM 85/15/0.5) afforded unreacted compound **22** (13%) and the desired product **23** as a yellow sticky solid in 30% yield.

R_f : (CHX/AcOEt 85/15) = 0.33

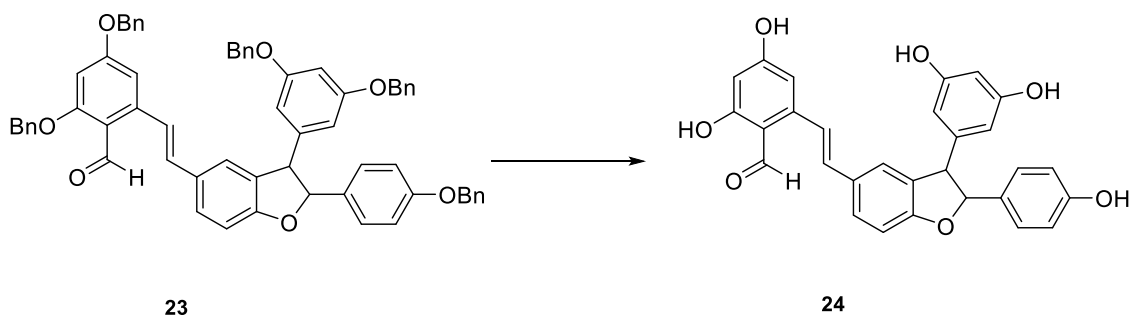
IR ν_{max} 3032, 2922, 1673, 1592, 1564, 1512, 1487, 1454, 1234, 1155, 737.2, 696.2 cm^{-1}

$^1\text{H NMR}$ (300 MHz, Chloroform-*d*): δ 10.63 (s, 1H), 8.03 (d, $J = 16.2$ Hz, 1H), 7.53 – 7.16 (m, 29H), 7.02 – 6.91 (m, 4H), 6.86 (d, $J = 2.2$ Hz, 1H), 6.58 (t, $J = 2.2$ Hz, 1H), 6.56 (d, $J = 2.2$ Hz, 1H), 6.46 (d, $J = 2.3$ Hz, 2H), 5.54 (d, $J = 7.8$ Hz, 1H), 5.16 (s, 2H), 5.14 (s, 2H), 5.10 (s, 2H), 5.01 (s, 4H), 4.51 (d, $J = 7.8$ Hz, 1H).

$^{13}\text{C NMR}$ (76 MHz, Chloroform-*d*): δ 190.7, 164.2, 163.7, 160.4 (x2C), 160.2, 159.0, 144.3, 143.4, 137.0, 136.8 (x2C), 136.1, 136.0, 133.2, 132.9, 131.0, 130.6, 128.9 (x2C), 128.8 (x2C), 128.8, 128.7 (x2C), 128.7 (x4C), 128.5, 128.4, 128.1 (x2C), 127.8 (x4C), 127.7 (x2C), 127.7, 127.6 (x2C), 127.5 (x4C), 125.3, 124.2, 116.6, 115.1 (x2C), 109.9, 107.6 (x2C), 104.7, 100.9, 99.1, 93.1, 70.9, 70.4, 70.2 (x2C), 70.1, 57.6.

HRMS (ESI) calcd for $\text{C}_{64}\text{H}_{51}\text{O}_7$ $[\text{M}-\text{H}]^-$ 931.36212, found 931.36403.

Synthesis of (E)-2-(2-(3-(3,5-dihydroxyphenyl)-2-(4-hydroxyphenyl)-2,3-dihydrobenzofuran-5-yl)vinyl)-4,6-dihydroxybenzaldehyde (24)



A solution of **23** (75 mg, 0.0804 mmol) in dry dichloromethane (3 ml) was prepared under argon atmosphere and cooled to 0 °C with an ice bath. BCl_3 (1.0 M in dichloromethane, 1.2 ml, 15 eq) was added dropwise over a period of 15 minutes. Reaction mixture was stirred at 0 °C for four hours. After this time, reaction was quenched, at 0 °C, with 10 ml of H_2O . The aqueous phase was extracted with ethyl acetate (4 x 10 ml). Organic layers were dried over Na_2SO_4 , filtered, and concentrated under reduced pressure. The crude product was purified by flash chromatography (DCM/MeOH 95/5) affording 17.7 mg of **24** as an orange sticky solid (45% yield).

R_f : (DCM/MeOH 9/1) = 0.56

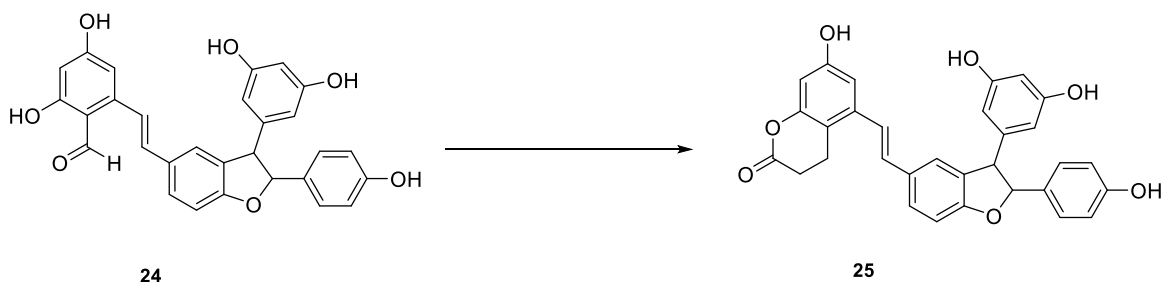
IR ν_{max} 3326, 2970, 1740, 1605, 1488, 1454, 1368, 1230, 1217, 814 cm^{-1}

^1H NMR (300 MHz, Methanol- d_4): δ 10.17 (s, 1H), 7.56 – 7.44 (m, 2H), 7.30 (s, 1H), 7.19 (d, J = 8.6 Hz, 2H), 7.00 (d, J = 15.9 Hz, 1H), 6.90 (d, J = 8.3 Hz, 1H), 6.80 (d, J = 8.6 Hz, 2H), 6.57 (d, J = 2.2 Hz, 1H), 6.21 (t, J = 2.2 Hz, 1H), 6.19 (d, J = 2.2 Hz, 1H), 6.14 (d, J = 2.2 Hz, 2H), 5.43 (d, J = 8.2 Hz, 1H), 4.43 (d, J = 8.2 Hz, 1H).

^{13}C NMR (76 MHz, Methanol- d_4): δ 193.0, 165.8, 165.5, 160.3, 158.6 (x2C), 157.3, 145.5, 144.0, 134.6, 131.4, 131.2, 130.3, 128.1, 127.3 (x2C), 123.5, 120.1, 114.9 (x2C), 111.6, 109.1, 106.4 (x2C), 106.2, 101.1, 101.0, 93.65, 57.26.

HRMS (ESI) calcd for $\text{C}_{29}\text{H}_{22}\text{O}_7$ [M-H] 481.12839, found 481.12928.

Synthesis of (E)-5-(2-(3-(3,5-dihydroxyphenyl)-2-(4-hydroxyphenyl)-2,3-dihydrobenzofuran-5-yl)vinyl)-7-hydroxychroman-2-one (25)



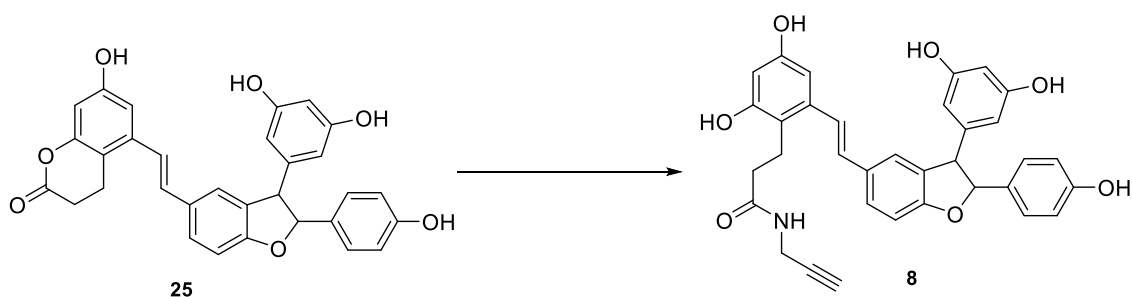
Meldrum's acid (35.8 mg, 0.2487 mmol, 3 eq) was added to a solution of **24** (40.0 mg, 0.0829 mmol, 1 eq) in 5.6 ml of TEAF (Et₃N/HCCOC 3/1). The obtained reaction mixture was heated to 100 °C and stirred for 18 hours. After complete consumption of the starting material, reaction mixture was cooled to room temperature, carefully added with 7 ml of HCl 6N and stirred at room temperature for additional 2 hours. After this time, the aqueous layer was extracted five times with 10 ml of ethyl acetate. Organic layers were dried over Na₂SO₄, filtered, and concentrated under reduced pressure. The crude product was dissolved in a 9:1 DCM/TFA mixture and stirred at room temperature for 3 hours. Flash chromatography (cyclohexane/acetone gradient 8/2 → 6/4) afforded the desired product as a pale-yellow sticky solid in 17% yield.

R_f: (CHX/Acetone 55/45) = 0.38

¹H NMR (300 MHz, Acetone-*d*₆): δ 8.37 (m, 5H), 7.52 (dd, *J* = 8.3, 1.9 Hz, 1H), 7.36 (s, 1H), 7.28 – 7.18 (m, 3H), 7.08 (d, *J* = 16.1 Hz, 1H), 6.97 (d, *J* = 2.4 Hz, 1H), 6.91 (d, *J* = 8.3 Hz, 1H), 6.87 (d, *J* = 8.6 Hz, 1H), 6.44 (d, *J* = 2.4 Hz, 1H), 6.31 (t, *J* = 2.2 Hz, 1H), 6.21 (d, *J* = 2.2 Hz, 2H), 5.49 (d, *J* = 7.9 Hz, 1H), 4.49 (d, *J* = 7.8 Hz, 1H), 3.07 (dd, *J* = 8.1, 6.1 Hz, 2H), 2.75 (dd, *J* = 8.0, 6.2 Hz, 2H).

¹³C NMR (75 MHz, Acetone-*d*₆): δ 168.7, 161.0, 159.8 (x2C), 158.5, 157.7, 154.3, 145.30, 138.4, 132.6, 132.5, 132.3, 131.6, 129.1, 128.6 (x3C), 124.3, 123.1, 116.2 (x2C), 113.1, 110.2, 108.9, 107.5 (x2C), 103.7, 102.4, 94.1, 57.8, 29.6, 20.8.

Synthesis of (E)-3-(2-(2-(3-(3,5-dihydroxyphenyl)-2-(4-hydroxyphenyl)-2,3-dihydrobenzofuran-5-yl)vinyl)-4,6-dihydroxyphenyl)-N-(prop-2-yn-1-yl)propanamide (8)



Compound **25** (7 mg, 0.0138 mmol, 1 eq) was dissolved in DMF (1 ml) under argon atmosphere. Propargylamine (3.5 μ l, 0.0551 mmol, 4 eq) and DIPEA (9.6 μ l, 0.0551 mmol, 4 eq) were added to the obtained solution, then reaction mixture was heated to 40 $^{\circ}$ C and stirred for 3 days. After complete consumption of the starting material, 2 ml of HCl 1M were added and the aqueous phase was extracted three times with ethyl acetate. Combined organic layers were washed with brine, dried over Na_2SO_4 , filtered, and concentrated under reduced pressure. Column chromatography (DCM/MeOH 95/5 \rightarrow 9/1) afforded compound **8** as a colorless sticky solid in 26% yield.

R_f (DCM/MeOH 9/1) = 0.30

$^1\text{H NMR}$ (300 MHz, Methanol- d_4): δ 7.47 (dd, J = 8.2, 1.9 Hz, 1H), 7.25 – 7.16 (m, 4H), 6.93 – 6.85 (m, 2H), 6.81 (d, J = 8.7 Hz, 2H), 6.56 (d, J = 2.4 Hz, 1H), 6.24 (d, J = 2.4 Hz, 1H), 6.20 (t, J = 2.2 Hz, 1H), 6.15 (d, J = 2.2 Hz, 2H), 5.40 (d, J = 8.1 Hz, 1H), 4.43 (d, J = 8.1 Hz, 1H), 3.89 (d, J = 2.6 Hz, 2H), 2.97 (t, J = 7.7 Hz, 2H), 2.51 (t, J = 2.6 Hz, 1H), 2.40 (d, J = 7.7 Hz, 2H).

$^{13}\text{C NMR}$ (75 MHz, Methanol- d_4): δ 174.4, 158.5 (x2C), 157.3, 156.0, 155.8, 144.1, 138.2, 131.6, 131.3, 130.8, 130.00, 127.3, 127.2 (x2C), 123.6, 123.3, 116.8, 114.9 (x2C), 114.8, 109.0, 106.3 (x2C), 103.3, 101.5, 101.1, 93.4, 79.2, 70.6, 57.4, 35.9, 29.2, 28.1.

5.2 Immunomodulating activity of stilbenoids on bacteria-induced immune response.

Published article:

“Investigation of the Effects of Monomeric and Dimeric Stilbenoids on Bacteria-Induced Cytokines and LPS-Induced ROS Formation in Bone Marrow-Derived Dendritic Cells.” - *Int. J. Mol. Sci.* **2023**, *24*, 2731.
<https://doi.org/10.3390/ijms24032731>

Authors:

Peter Riber Johnsen¹, Cecilia Pinna², Luce Mattio², Mathilde Bech Strube¹, Mattia Di Nunzio^{2,*}, Stefania Iametti², Sabrina Dallavalle², Andrea Pinto² and Hanne Frøkiær¹

Affiliations:

¹Department of Veterinary and Animal Sciences, University of Copenhagen, Ridebanevej 9, 1871 Frederiksberg, Denmark

²Department of Food, Environmental and Nutritional Sciences (DeFENS), University of Milan, Via Celoria 2, 20133 Milan, Italy

Abstract

Stilbenoids are anti-inflammatory and antioxidant compounds, with resveratrol being the most investigated molecule in this class. However, the actions of most other stilbenoids are much less studied. This study compares five monomeric (resveratrol, piceatannol, pterostilbene, 3,4'-dimethoxy-5-hydroxystilbene, and trimethoxy-resveratrol) and two dimeric (dehydro- δ -viniferin and *trans*- δ -viniferin) stilbenoids for their capability to modulate the production of bacteria-induced cytokines (IL-12, IL-10, and TNF- α), as well as lipopolysaccharide (LPS)-induced reactive oxygen species (ROS), in murine bone marrow-derived dendritic cells. All monomeric species showed dose-dependent inhibition of *E. coli*-induced IL-12 and TNF- α , whereas only resveratrol and piceatannol inhibited IL-10 production. All monomers, except trimethoxy-resveratrol, inhibited *L. acidophilus*-induced IL-12, IL-10, and TNF- α production. The dimer dehydro- δ -viniferin remarkably enhanced *L. acidophilus*-induced IL-12 production. The contrasting effect of resveratrol and dehydro- δ -viniferin on IL-12 production was due, at least in part, to a divergent inactivation of the

mitogen-activated protein kinases by the two stilbenoids. Despite having moderate to high total antioxidant activity, dehydro- δ -viniferin was a weak inhibitor of LPS-induced ROS formation. Conversely, resveratrol and piceatannol potently inhibited LPS-induced ROS formation. Methylated monomers showed a decreased antioxidant capacity compared to resveratrol, also depending on the methylation site. In summary, the immunomodulating effect of the stilbenoids depends on both specific structural features of tested compounds and the stimulating bacteria.

KEYWORDS: *monomeric stilbenoids; dimeric stilbenoids; immune modulating; ROS formation; dendritic cells.*

5.2.1. Introduction

Stilbenoids, such as resveratrol and its hydroxylated (e.g., piceatannol) and methylated (e.g., pterostilbene and 3,4'-dimethoxy-5-hydroxystilbene) derivatives, are a group of naturally occurring phenolic compounds endowed with several biological activities (see **Chapter 1**). The bioavailability of the different stilbenoid compounds differs substantially and may depend on multiple factors, such as solubility, lipophilicity, and metabolic and chemical stability [31]. Substitution of hydroxy with methoxy groups increases lipophilicity, so that pterostilbene is more bioavailable than resveratrol [32]. Furthermore, resveratrol-derived dimers, such as δ -viniferin and its dehydro analogue, are also characterized by different bioavailability and biological activities compared to their monomers. For these reasons, information on the relative potency of stilbenoids, including whether a relationship exists between the anti-inflammatory and antioxidant ability, is still fuzzy. Macrophages and dendritic cells constitute key cell types involved in inflammation and in the initiation of immune responses. In particular, dendritic cells play an essential role in the conduction of immune responses, e.g., by activating different subtypes of T-cells through the production of cytokines in response to signals provided by microbial organisms [33]. Regarding bacteria-induced cytokine production, it has been previously demonstrated that Gram-negative and Gram-positive bacteria induce responses through different pathways [34–36]. The antioxidant effect of stilbenoids has often been assumed to explain most of the other observed bioactivities, not least the anti-inflammatory effect [37]. However, stilbenoids have also demonstrated the ability to act on a broad range of cellular molecules involved in inflammatory signaling [38]. Most studies on the antioxidative or anti-inflammatory properties of stilbenoids were conducted on resveratrol, whereas only marginal attention has been placed on its

hydroxylated and methylated analogues [38]. Additionally, assessment of bioactivities has generally been performed in a limited experimental setup without considering that the modulation exerted by these molecules is dependent on the nature of the stimulating agent [34,35]. To our knowledge, no systematic study comparing the immune-modulating and antioxidant effects of the various stilbenoid subclasses has been conducted so far. Here, a comparative and inclusive study has been performed to assess the immune-modulating effect of monomeric (resveratrol, piceatannol, pterostilbene, 3,4'-dimethoxy-5-hydroxystilbene (DMHS), and trimethoxy resveratrol) and dimeric (dehydro- δ -viniferin and *trans*- δ -viniferin) stilbenoids [1] on the production of bacterially induced cytokines (IL-12, IL-10, and TNF- α) in murine bone marrow-derived dendritic cells (bmDCs). The study also included the possible effects on the lipopolysaccharide (LPS)-induced production of reactive oxygen species (ROS) in the same experimental system. In this frame, the relationship between the aforementioned effects and the antioxidant capacity of the individual molecules (as evaluated by ABTS and DPPH assays) was also investigated to provide a comprehensive vision of these systems.

5.2.2. Results

Methylation of Resveratrol Diminishes Its Inhibitory Effect on the *L. Acidophilus* NCFM-Induced Cytokine Response

Murine bmDCs stimulated with an increasing multiplicity of infection (MOI) of *L. acidophilus* NCFM responded with a dose-dependent production of IL-12, IL-10, and TNF- α (**Figure 5.30**). An increasing concentration of either stilbenoid resulted in a dose-dependent inhibition of all three cytokines, leading to at least a 70% decrease in their production at the highest stilbenoid concentration. Methylated analogues demonstrated a decreased inhibition capacity compared to resveratrol. More specifically, methylation of two hydroxy groups in resveratrol (i.e., DHMS and pterostilbene) resulted in a less decreased cytokine production, while methylation of all three hydroxy groups in resveratrol (i.e., trimethoxy-resveratrol) almost entirely abrogated the inhibitory capacity (**Figure 5.30**, panels D–F). The inhibitory effect on cytokine production relates to the substitution pattern. Whereas methylation of the two hydroxyl groups at C3 and C5 (pterostilbene, **Figure 5.30D**) gave only a slightly lower inhibition than resveratrol, methylation of the hydroxy groups at C3 and C4' (DMHS, **Figure 5.30E**) resulted in a substantially weakened inhibition of cytokine release (40 μ M DMHS gave \approx 50% inhibition of IL-12 production compared to \approx 81% inhibition for 40 μ M resveratrol).

Monomer Derivatives Show Potent IL-12 Inhibition but Weak Inhibition of IL-10 and TNF- α Production in bmDCs Stimulated with *E. Coli* Nissle 1917

Stimulation with increasing MOI (0.3–3) of the Gram-negative *E. coli* Nissle 1917 resulted in a dose-dependent increase for IL-10, a slight decrease for IL-12, and no effects on TNF- α production (

Figure 5.31A). All monomers significantly inhibited the *E. coli*-induced production of IL-12 in a dose-dependent manner (

Figure 5.31, panels B–F). Piceatannol was the most potent inhibitor of IL-12 production ($\approx 82\%$ at 40 μM ,

Figure 5.31C). Trimethoxy-resveratrol also displayed more potent inhibition of IL-12 than resveratrol (75% inhibition vs. $\approx 61\%$ for resveratrol, both at 40 μM ,

Figure 5.31, panel F vs. panel B). Only resveratrol and piceatannol displayed significant inhibition of IL-10 production, but only at high concentrations (30 μM and 40 μM ,

Figure 5.31, panels B, C). Only the trimethylated analogue and resveratrol showed potent inhibition of the *E. coli*-induced TNF- α production (

Figure 5.31, panels B, F).

Effect of Dimeric Stilbenoids on the Bacterially Induced Cytokine Response

The stilbenoid dimers dehydro- δ -viniferin and *trans*- δ -viniferin were used in the same molar concentration range of stilbenoid monomers (0–40 μM) to assess whether dimerization affected bacterially induced cytokine response. Dehydro- δ -viniferin enhanced *L. acidophilus* induced IL-12 response in a dose-dependent manner, whereas the IL-10 response showed a dose-dependent inhibition, and TNF- α gave a non-significant increase (**Figure 5.32A**). Treatment with *trans*- δ -viniferin did not affect the *L. acidophilus*-induced cytokine response pattern (**Figure 5.32B**). Neither dehydro- δ -viniferin nor *trans*- δ -viniferin affected the *E. coli*-induced production of any of the examined cytokines (**Figure 5.32**, panels C, D).

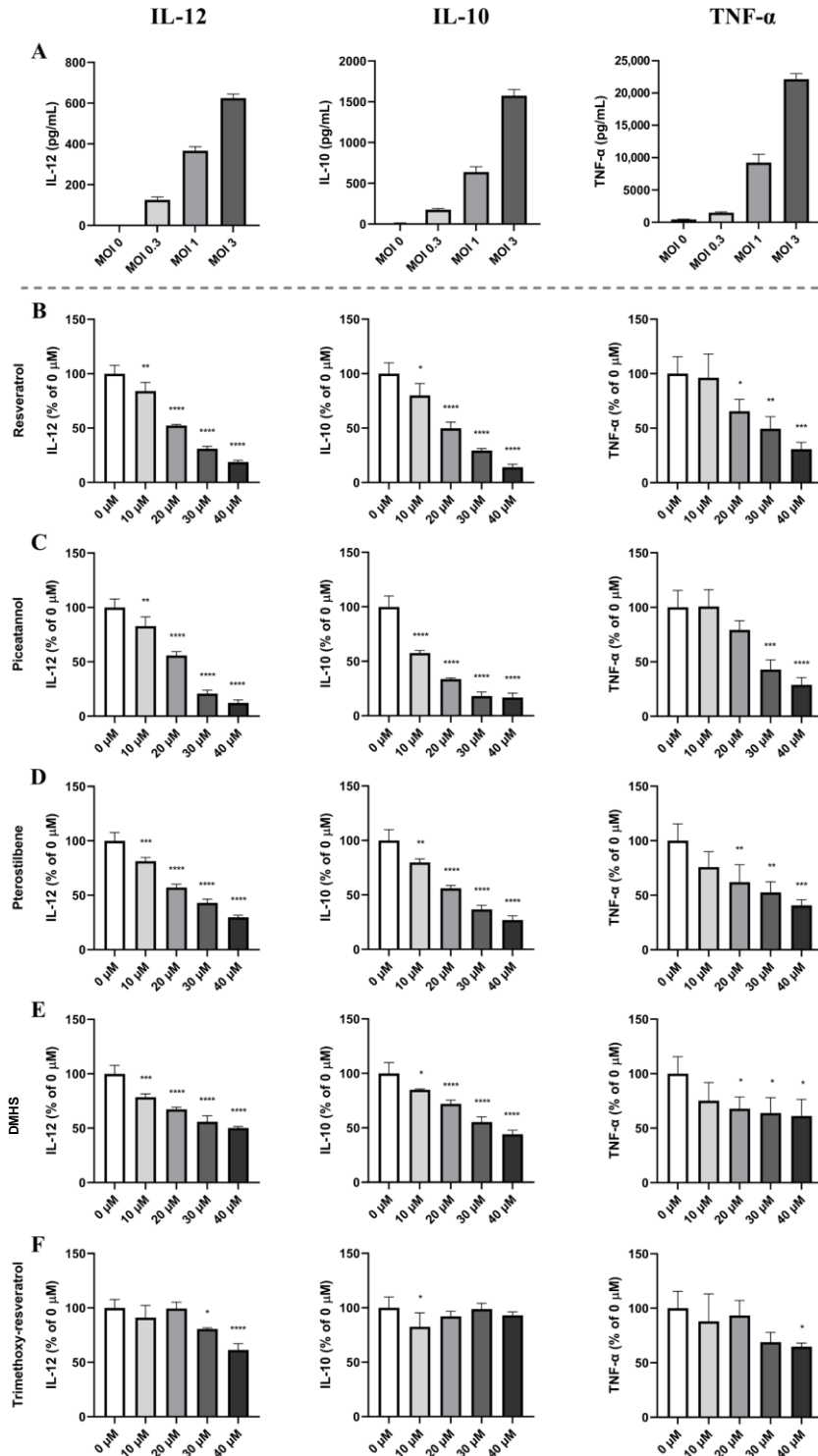


Figure 5.30. Resveratrol and piceatannol hold vigorous cytokine-inhibiting roles in *L. acidophilus* NCFM-stimulated bmDCs, and methylation of resveratrol weakens the inhibitory capabilities. Murine bmDCs were stimulated with *L. acidophilus* NCFM at multiplicity of infection (MOI) at rates of 0.3, 1, and 3 (A) and incubated for 20 h. To assess the effect of monomers on the cytokine response, bmDCs were incubated with increasing concentrations (0–40 μ M) of resveratrol (B), piceatannol (C), pterostilbene (D), DMHS (E), and trimethoxy-resveratrol (F) for 30 min before *L. acidophilus* NCFM (MOI 1) was added to the samples. Cytokine levels in the supernatant for stilbenoid-treated samples (B–F) are shown as percentages of samples with no stilbenoid treatment (0 μ M). The depicted data are representative of at least three experiments. * $p \leq 0.05$, ** $p \leq 0.01$, *** $p \leq 0.001$, **** $p \leq 0.0001$.

Number and Position of Hydroxy Groups Affect Stilbenoids Inhibition of Intracellular ROS

The antioxidant effect of the stilbenoid structures in the bmDCs was investigated by measuring their influence on the microbially induced intracellular ROS formation, as determined by oxidation of 6-carboxy-2',7'-dichlorodihydrofluorescein diacetate (carboxy-H₂DCFDA). LPS-induced ROS formation was diminished for cells treated with the stilbenoid monomers resveratrol, piceatannol, and, to a lesser extent, pterostilbene (**Figure 5.33**, panels **A**, **C**). Cells treated with DMHS, or trimethoxy-resveratrol did not show a significant decrease of ROS formation, whereas dehydro- δ -viniferin and *trans*- δ -viniferin decreased LPS-induced ROS formation (**Figure 5.33**, panels **B**, **D**) and dehydro- δ -viniferin led to slightly greater inhibition of ROS formation than *trans*- δ -viniferin.

Determination of the Total Antioxidant Capacity of Resveratrol and Resveratrol Derivatives

The antioxidant capacity of the monomeric and dimeric resveratrol derivatives was further examined by determining their total antioxidant capacity (TAC), as measured with both the 2,2'-azino-bis(3-ethylbenzothiazoline-6-sulfonic acid (ABTS) and the 2,2-diphenyl-1-picrylhydrazyl (DPPH) assay.

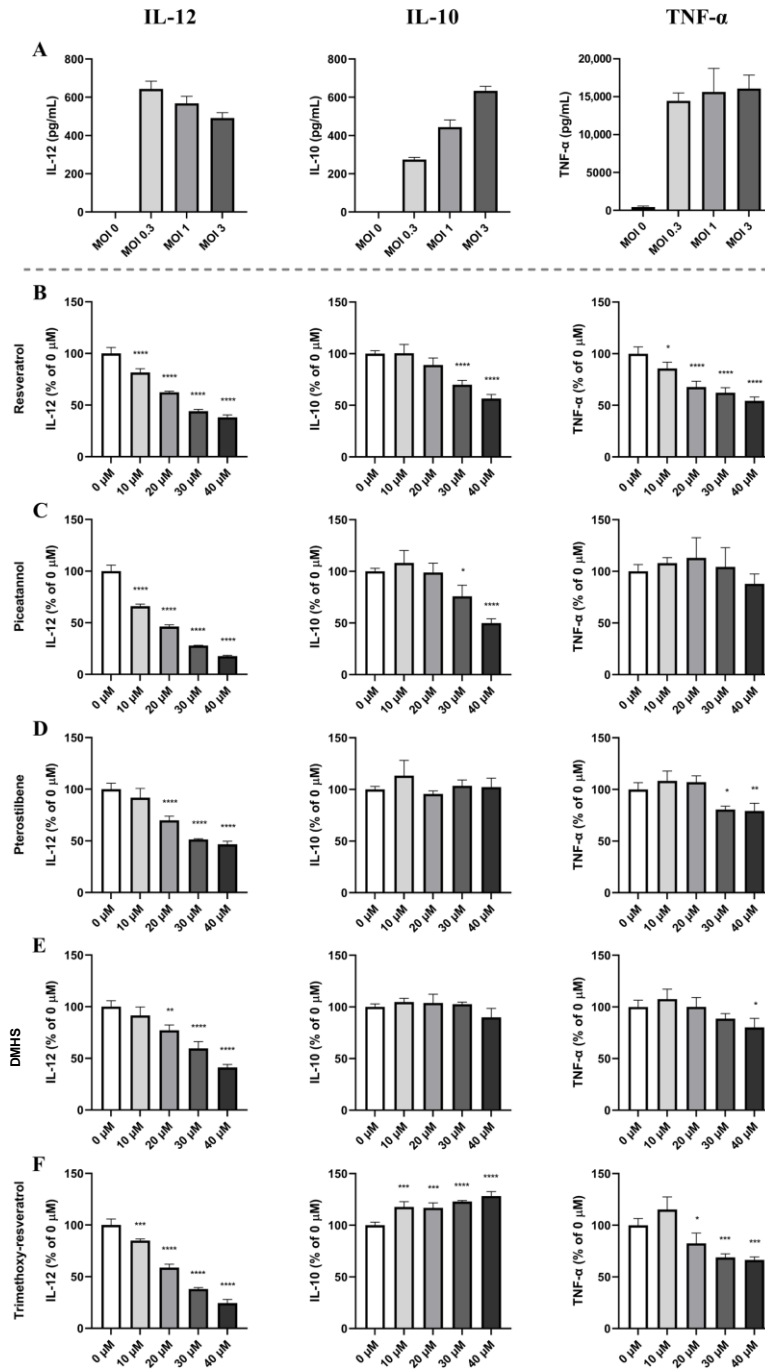


Figure 5.31. Methylation of resveratrol weakens the IL-10 inhibitor activity in *E. coli* Nissle 1917-stimulated bmDCs. Murine bmDCs were stimulated with *E. coli* Nissle 1917 at multiplicity of infection (MOI) rates of 0.3, 1, and 3 (A) and incubated for 20 h. To assess the effect of monomers on the cytokine response, bmDCs were incubated with increasing concentrations (0-40 μM) of resveratrol (B), piceatannol (C), pterostilbene (D), DMHS (E), and trimethoxy-resveratrol (F) for 30 min before *E. coli* Nissle 1917 (MOI1) was added to the samples. Cytokine levels in the supernatant for stilbenoid-treated samples (B-F) are shown as percentages of samples without stilbenoid treatment (0 μM). The depicted data are representative of at least three experiments. * $p \leq 0.05$, ** $p \leq 0.01$, *** $p \leq 0.001$, **** $p \leq 0.0001$.

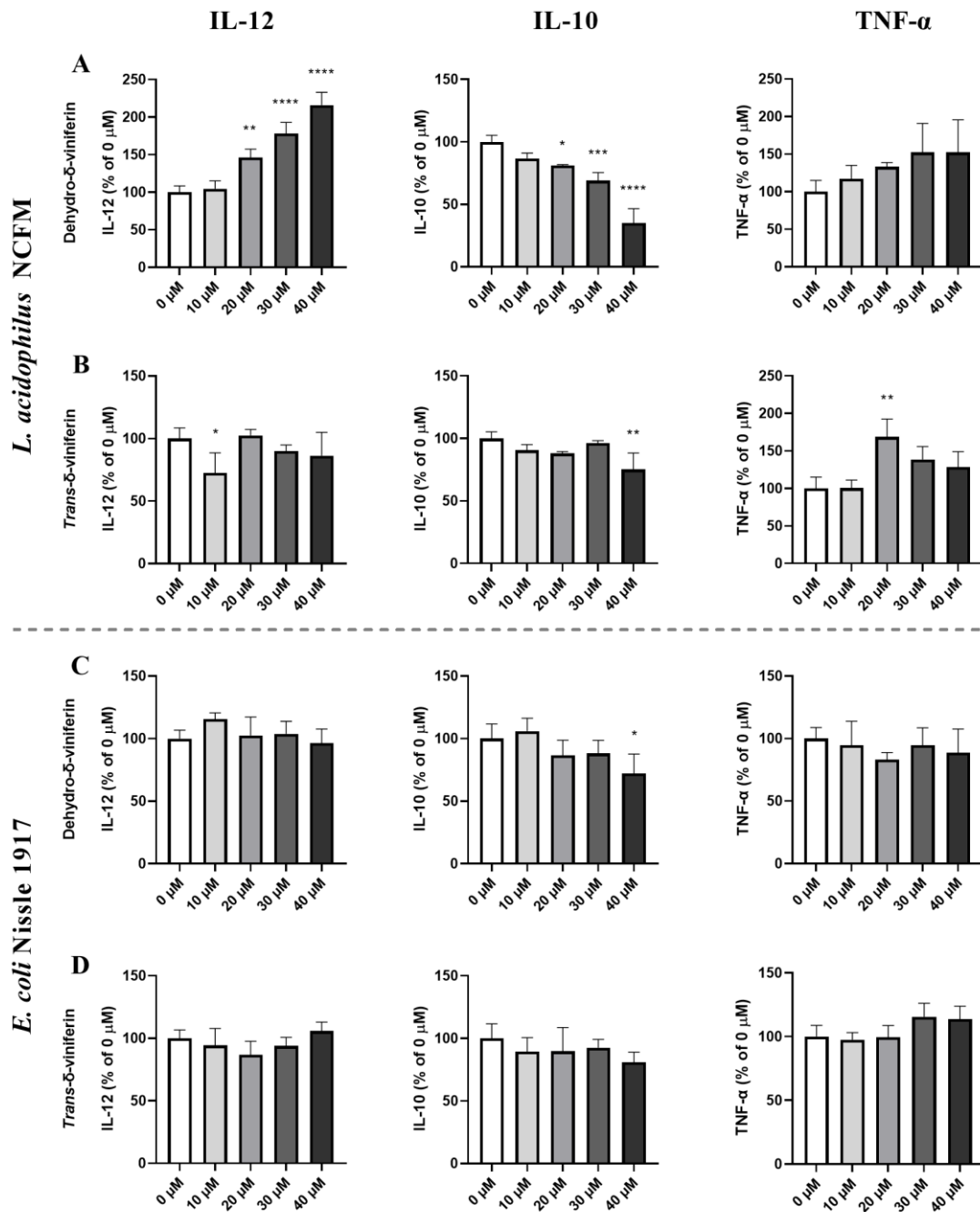


Figure 5.32. Effect of stilbenoid dimers on the bacterially induced cytokine response depends on the bacterial strain. Murine bmDCs were incubated with increasing concentrations (0–40 μ M) of dehydro- δ -viniferin (A, C) and *trans*- δ -viniferin (B, D) for 30 min before stimulation with *L. acidophilus* NCFM (multiplicity of infection (MOI) 1) (A, B) or *E. coli* Nissle 1917 (MOI 1, C, D) and incubated for 20 h. Cytokine levels in the supernatant for the stilbenoid treated samples are shown as percentages of samples without stilbenoid treatment (0 μ M). * $p \leq 0.05$, ** $p \leq 0.01$, *** $p \leq 0.001$, **** $p \leq 0.0001$.

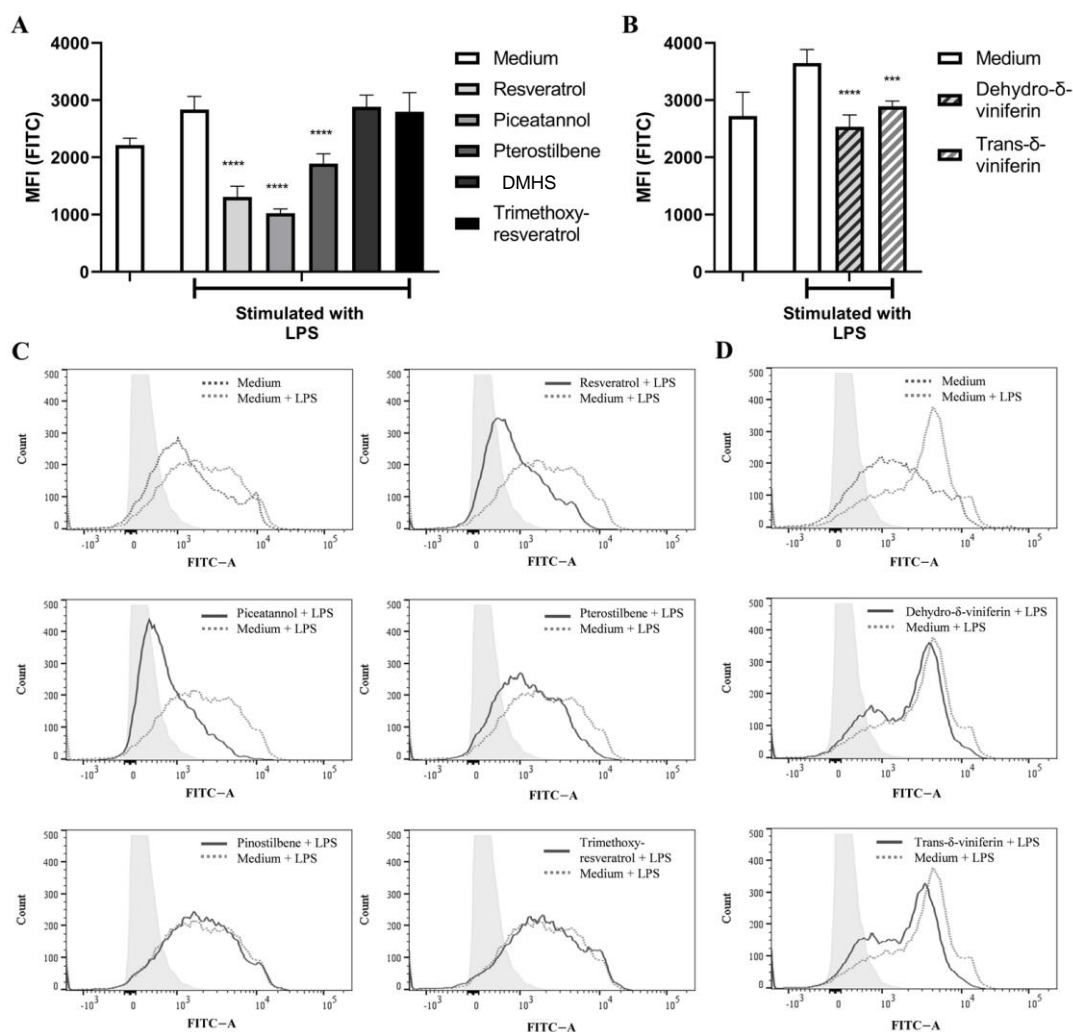


Figure 5.33. Effect of stilbenoid monomers and dimers on LPS-induced ROS formation in bmDCs. Murine bmDCs were administered carboxy-H₂DCFDA and incubated in the absence or in the presence of the given stilbenoids (30 μM) for 30 min before stimulation with LPS (100 ng/mL). After 4 h, ROS formation in bmDCs was determined by using flow cytometry to quantitate formation of oxidized carboxy-H₂DCFDA. The mean fluorescence index (MFI) is shown in panels (A) (monomers) and (B) (dimers). The original flow cytometry results for monomers and dimers are grouped in (C, D), respectively. *** $p \leq 0.001$, **** $p \leq 0.0001$.

In agreement with data on intracellular ROS formation, piceatannol and resveratrol showed the highest TAC rates in ABTS assays. Pterostilbene's TAC was lower than that of DMHS. As expected, trimethoxy resveratrol displayed no detectable TAC. Indeed, a significant correlation ($r = 0.9339$; $R_2 = 0.8722$; $p < 0.05$) was observed between the number of hydroxyl groups present in the chemical structure of each monomer and their TAC, as measured by the ABTS assay. As for stilbenoid dimers, the highest TAC was observed for *trans*-δ-viniferin, whereas the TAC of dehydro-δ-viniferin was comparable to that of DMHS (Figure 5.34A). Again, a strong positive correlation was evident between the number of hydroxy groups in all stilbenoids (monomers and dimers) and the TAC evaluated by the ABTS assay ($r = 0.7776$; $R_2 = 0.6047$; $p < 0.05$).

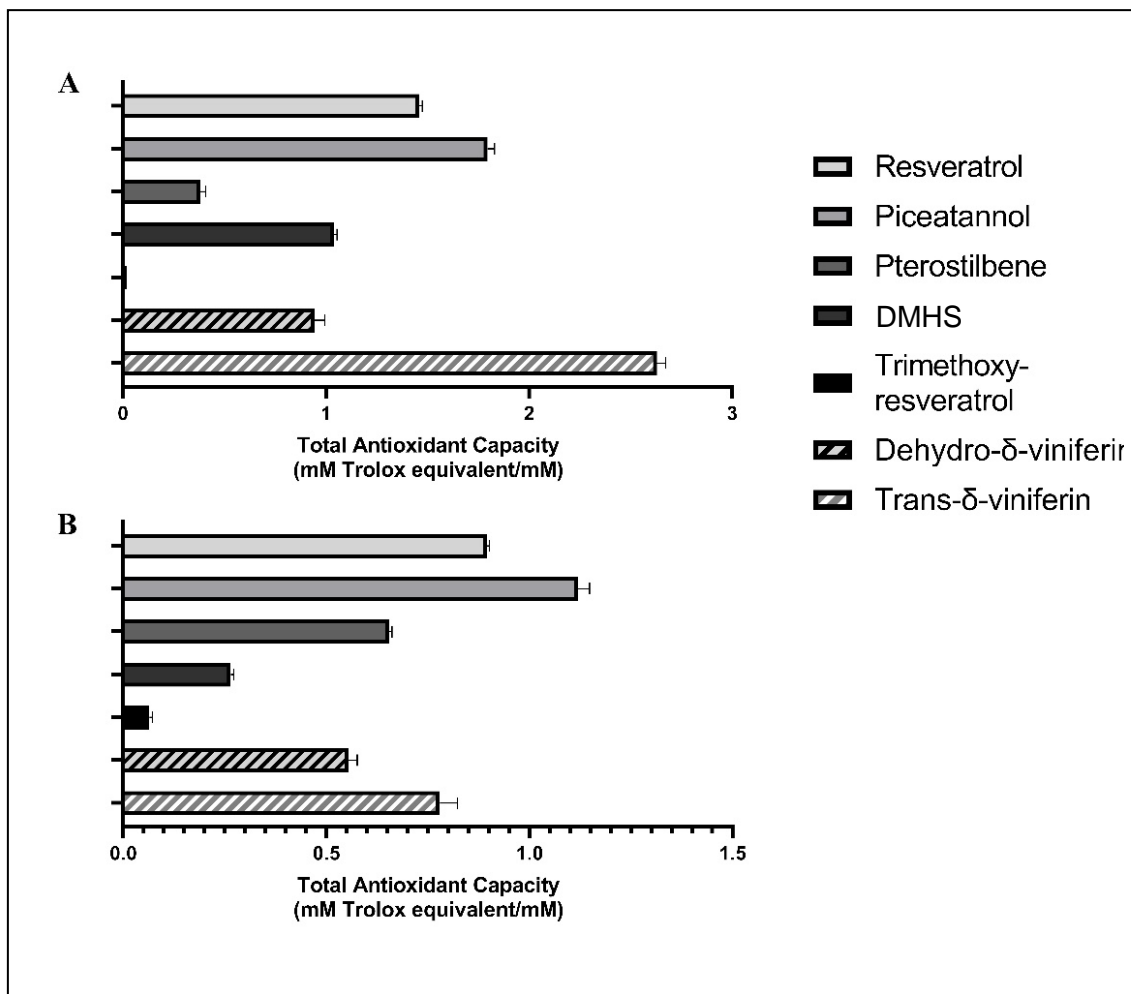


Figure 5.34. Total antioxidant capacity (TAC) in stilbenoid monomers and dimers. The TAC rates of the five monomeric stilbenoids and the two dimeric stilbenoids were determined using ABTS (A) and DPPH assay (B). TAC values were calculated for stilbenoids at an equimolar concentration (1 mM) and are expressed as mM Trolox equivalent/mM stilbenoids.

The DPPH assay confirmed that piceatannol and resveratrol had the highest TAC rates and trimethoxy-resveratrol the lowest. However, when using DPPH, pterostilbene displayed a higher TAC than DMHS, with values for pterostilbene similar to those measured for dehydro- δ -viniferin and *trans*- δ -viniferin (**Figure 5.34B**). By using the DPPH assay, a significant correlation ($r = 0.9371$; $R_2 = 0.8781$; $p < 0.05$) was observed between TAC and the number of hydroxy groups present in the chemical structure of monomers.

Resveratrol and Dehydro- δ -Viniferin Affect Map Kinases Divergently

The striking difference in *L. acidophilus* NCFM-induced IL-12 production elicited by resveratrol and dehydro- δ -viniferin prompted us to investigate the mechanisms underlying the divergent activities of the two stilbenoids. Accordingly, it has been investigated how inhibitors of the Jun N-terminal kinase (JNK) and p38 affected the IL-12 and IL-10 responses to stimulation with

L. acidophilus NCFM and how *L. acidophilus* (used alone or after a resveratrol or dehydro- δ -viniferin pretreatment) affected the expression of dual specificity phosphatase 1 (Dusp1) (**Figure 5.35**). While JNK inhibition gave a potent inhibition of IL-12 (73%) and IL-10 (96%) production, inhibition of p38 inhibition had only minor effects on IL-12 (11% inhibition), but strongly impaired IL-10 production (76% inhibition, **Figure 5.35A**). Thus, JNK activation seems indispensable for *L. acidophilus* NCFM-induced effects on IL-12 production. To investigate whether resveratrol and dehydro- δ -viniferin affect the induction of the Dusp1 expression, bmDCs were incubated for 30 min, with or without resveratrol (30 μ M) or dehydro- δ -viniferin (30 μ M), prior to stimulation with *L. acidophilus* NCFM (MOI 1). At multiple time points, cells were lysed, and RNA extracted. bmDCs stimulated with *L. acidophilus* NCFM displayed increased Dusp1 expression after 6 h, with a further increase at 8 h (**Figure 5.35B**). For cells incubated with resveratrol, the Dusp1 expression showed a threefold increase at 4 h and then dropped gradually at 6 and 8 h. Cells incubated with dehydro- δ -viniferin showed only a very weak increase in Dusp1 expression at 6 h, after which it dropped to a background level at 8 h (**Figure 5.35B**). The cytokine response in the supernatant from the stilbenoid-treated cells was also examined (**Figure 5.35C**). At 8 h after *L. acidophilus* NCFM stimulation, the IL-12 concentration in the supernatants of cells treated with dehydro- δ -viniferin increased more compared to untreated cells, and for resveratrol treated cells, the IL-12 concentration remained close to zero for 8 h, then a subtle increase appeared. The production of IL-10 was almost zero for 8 h, with a drastic increase from 8 to 20 h. Treatment with the both stilbenoids led to a decreased IL-10 production.

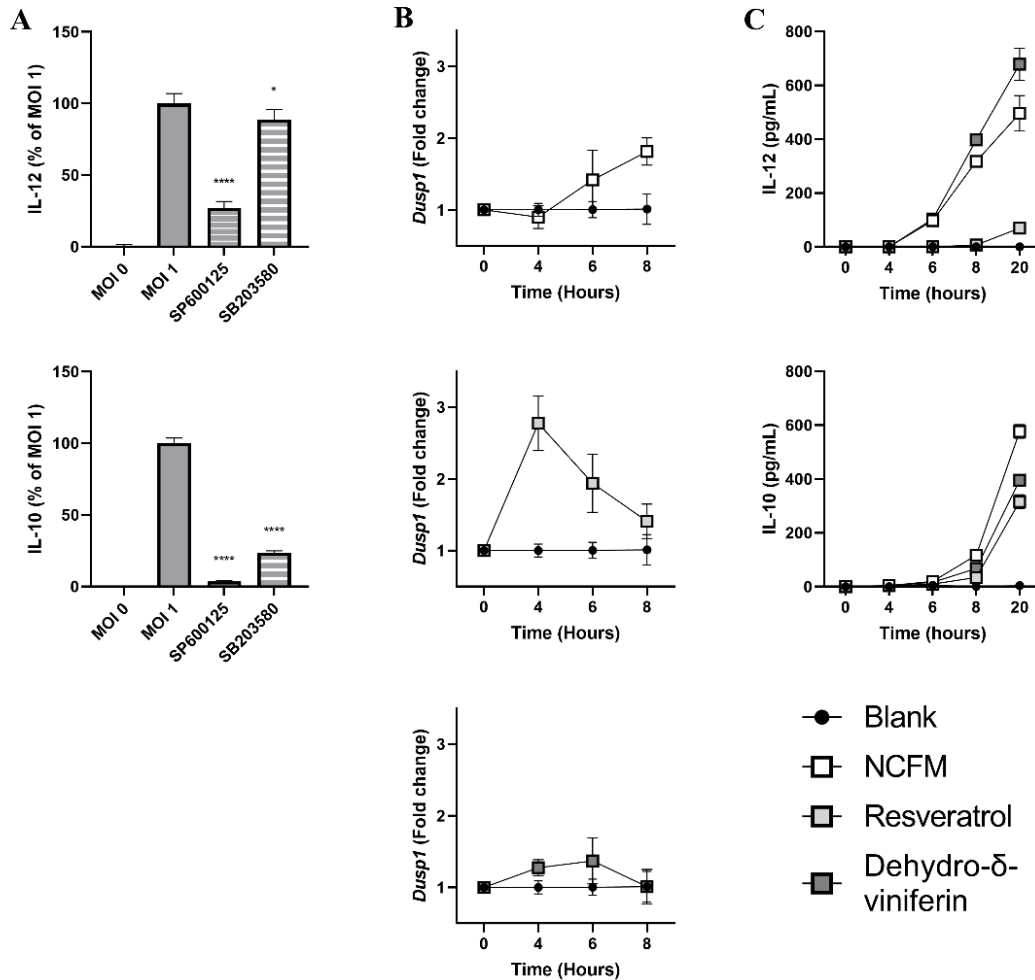


Figure 5.35. Resveratrol and dehydro- δ -viniferin interfere differently with MAP kinase pathways. Murine bmDCs were treated with or without SP600125 (JNK-inhibitor, 25 μ M) or SB203580 (p38-inhibitor, 10 μ M) for 30 min before stimulation with *L. acidophilus* NCFM (MOI 1) and incubated for 20 h (A). Cytokine levels in the supernatant for stilbenoid-treated samples are shown as percentages of samples without stilbenoid treatment (MOI 1). The expression rates of Dusp1 in bmDCs (0 to 8 h) upon stimulation with *L. acidophilus* NCFM with or without 30 min pre-incubation with resveratrol (30 μ M) or dehydro- δ -viniferin (30 μ M) are shown (B). Dusp1 expression is shown as fold change relative to unstimulated cells (black) with Actb as the reference gene. The cytokine responses in the supernatants of bmDCs stimulated with *L. acidophilus* NCFM over time (white) with or without resveratrol (30 μ M) (light grey) or dehydro- δ -viniferin (30 μ M) (dark grey) added 30 min prior to stimulation are shown (C). * $p \leq 0.05$, **** $p \leq 0.0001$.

5.2.3. Discussion

Resveratrol and its natural derivatives are regarded as anti-oxidative and anti-inflammatory compounds, but how their individual structures affect these activities is much less clear. Here, monomeric and dimeric derivatives of resveratrol have been used to scrutinize the effect of each single molecule by comparing their impact on the oxidative status of microbially stimulated dendritic cells, as well as on bacterially induced cytokine production in the same cell system. This latter approach also allowed us to take into appropriate consideration the distinct signaling pathways and cytokine production involved

in the response of bmDCs towards different bacteria [39]. The disparate effects of stilbenoids on the cytokine production induced by the two bacterial strains have not been demonstrated before, but may be expected when considering the different signaling pathways induced by the two bacteria [36]. The Gram-negative *E. coli* Nissle 1917 induces pathways involving MyD88, as well as TIR domain-containing adaptor-inducing interferon- β (TRIF)-induced TLR signaling, depending on whether stimulation takes place from the plasma or the endosomal membrane. In contrast, the Gram-positive *L. acidophilus* NCFM exclusively stimulates from the endosomal membrane and only through MyD88 [36], in a process strictly dependent on endosomal degradation [40]. These differences cause the activation of diverse signaling pathways employing various signaling molecules and acting to a different extent and with different kinetics [41,42]. Kinases at large, and in the particular mitogen-activated protein (MAP) kinases, represent a group of signaling molecules that reportedly are inhibited by stilbenoids and other polyphenols [40,43,44], but bacteria exploit different activation patterns for kinases. For example, it was previously demonstrated that IL-12 induction by the Gram-positive bacteria *L. acidophilus* and *S. aureus* is strictly dependent on JNK and less on p38 [45,46]. In contrast, for Gram-negative bacteria *E. coli*, signaling (through TRIF) is dependent on p38 signaling [47]. In addition, the rate of endosomal degradation of the bacteria may affect the relative contribution of different MAP kinases. Indeed, recent reports have indicated that the kinetics of p38 activation involved in the signaling to some Gram-positive bacteria depends on how readily bacteria are degraded in endosomes [45,48]. Hence, the effect of specific stilbenoids may depend on their ability to bind to one or more MAP-kinases, as well on which kinases are most relevant to cytokine production. This work also reports high variation of cytokine production in bmDCs depending on the stilbenoid's structure. The most striking variation was the diverging effect of resveratrol and the resveratrol dimer, dehydro- δ -viniferin, on *L. acidophilus* NCFM-induced IL-12 production. Whereas resveratrol, similarly to other stilbenoids, inhibited the *L. acidophilus* NCFM-induced production of IL-12, dehydro- δ -viniferin enhanced it. *L. acidophilus* NCFM induced IL-12 is strictly dependent on the MAP kinase JNK [46] and an early transcription of the p38-induced Dusp1 was reported to lead to a decrease in IL-12 production [45]. The results reported here indicate that dehydro- δ -viniferin almost completely suppresses *L. acidophilus* NCFM-induced Dusp1 expression, whereas resveratrol leads to an earlier and stronger Dusp1 expression. As DUSP1 inactivates both JNK and p38 [49], inhibition of Dusp1 expression by dehydro- δ -viniferin indicates that p38 activation is abrogated, resulting in persistent phosphorylation and activity of JNK. Conversely, the earlier enhanced induction of Dusp1 expression and the

almost full abrogation of IL-12 during the first 8 h in the presence of resveratrol could indicate that JNK was inhibited. Here, it is relevant that some of the kinase signaling pathways may activate both JNK and p38, and that their actions may be redundant, at contrast with other activation pathways that are highly specific and involve only one of the two MAP kinases [49,50]. The cytokine-modulating capacity of each stilbenoid may be influenced by several properties of the molecule. Firstly, the capacity of the stilbenoid to pass through the plasma membrane may affect the proportion of the stilbenoid that actually reaches intracellular targets. Methylated monomers, as well as the two dimers, more readily pass the hydrophobic membrane due to their higher lipophilicity compared to the parent compounds. In support of this, Dias et al. [51] demonstrated a 40 times higher serum concentration of trimethoxy-resveratrol than resveratrol in mice after oral administration. The documented differences in pharmacokinetics have been suggested to account for the higher biological activity of pterostilbene and other methylated compounds over the parental compound resveratrol [52]. Given the comparable effects of resveratrol and trimethoxy-resveratrol in *E. coli*-stimulated bmDCs, the differences between these stilbenoids observed in vivo seem more likely to be caused by the transformation of resveratrol into other molecules. As a matter of fact, resveratrol was demonstrated to be transformed (e.g., by oxidation by the gut commensals [53]) in the digestive tract. When investigating the capacity of each stilbenoid to affect LPS-induced ROS formation in the dendritic cells, methylated monomers were found to be much less efficient than resveratrol, as expected. Surprisingly, the stilbenoid dimers showed weak ROS-inhibiting activity in the LPS-stimulated cells and also showed a reduced antioxidant capacity when TAC was determined by DPPH assay. This suggests that the lower antioxidant capacity of the dimers is related to their lower anti-radical activity rather than to poor cellular uptake or to molecular interaction with intracellular targets involved in the activation of ROS formation, e.g., nuclear factor erythroid-derived 2-like pathway [54–56] contributing to the final effect on counteracting ROS formation [57]. Although the strength of the antioxidant effect of polyphenols has been described and depends on their structural properties, such as the Bors criteria [58], this study makes evident a linear correlation between TAC and the number of hydroxyl groups in stilbenoids, especially for their monomeric forms. This is in line with a recent paper by Platzer et al., who studied several phenolic compounds and found that the number of hydroxyl groups influenced the antioxidant activity more accurately than the Bors criteria [59]. Although the ABTS and DPPH assays are both single electron transfer-based assays and determined the anti-radical capacity of the molecules in the sample, slight differences were found between the two

methods. These discrepancies may be due to the stilbenoids' solubility in the reaction media (water and hydro-methanolic solution in ABTS and DPPH assay, respectively) and electron transfer kinetic issues [60,61], compared to the ROS formation measured in LPS-stimulated dendritic cells. Endosomal ROS formation is required for efficient degradation of some phagocytosed bacteria and is often, but not always, required to release ligands for the TLRs and, thus, for cytokine production. This makes it relevant to assess if there is a relationship between ROS formation, the requirement of bacterial degradation, and cytokine production. Efficient endosomal degradation of *L. acidophilus* NCFM is a prerequisite for cytokine production, in particular for IL-12 [36,40], as it is for many other Gram-positive bacteria [62,63]. In contrast, many Gram-negative bacteria, such as *E. coli* Nissle 1917, shed TLR-stimulating LPS from the surface and are, therefore, less dependent on endosomal degradation to induce cytokine production [64,65]. The stilbenoids affected the cytokine production induced by *L. acidophilus* and *E. coli* differently with the most pronounced effects on the *L. acidophilus*-induced cytokine production. Resveratrol and piceatannol exhibited the most potent inhibitory effects in *L. acidophilus*-induced cytokines; a part of the actions of these two stilbenoids might be due to an inhibition of the ROS formation. This is, however, purely speculative. Interestingly, in contrast to the monomeric stilbenoids, the dimeric stilbenoid dehydro- δ -viniferin enhanced the IL-12 production induced by *L. acidophilus*. Notably, IL-12 treatment of WT mice before pulmonary challenge with MRSA protected mice against bacterial growth and increased survival [66]. The IL-12-enhancing capacity reported here has not been shown, to our best knowledge, for any stilbenoids or for other polyphenols. Considering the rather potent antimicrobial activity towards Gram-positive pathogens, dehydro- δ -viniferin may represent a dual-pronged strategy for the treatment of infections by Gram-positive bacteria such as *Staphylococcus aureus*, by acting directly on the pathogen as well as indirectly, through an enhanced cellular immune response against the pathogen.

5.2.4. Materials and Methods

Generation of Murine Bone Marrow-Derived Dendritic Cells (bmDCs)

The bmDCs were generated as described previously [34,67]. In brief, the femur and tibia were removed from C57BL/6NTac mice (Taconic, Lille Skensved, Denmark). The bone marrow cells were cultivated at 3×10^5 cells/mL in RPMI medium containing 10% fetal calf serum and 15 ng/mL granulocyte-macrophage colony-stimulating factor (GM-CSF). After eight days of incubation, non-adherent bmDCs were used. All animals used as sources of bone marrow cells were housed under conditions approved by the Danish

Animal Experiments Inspectorate (Forsøgdyrstilsynet) according to The Danish Animal Experimentation Act; LBK no. 474 from 15 May 2014, and experiments were carried out in accordance with the guidelines of “The Council of Europe Convention European Treaty Series (ETS)123 on the Protection of Vertebrate Animals Used for Experimental and Other Scientific Purposes”.

Stilbenoids synthesis

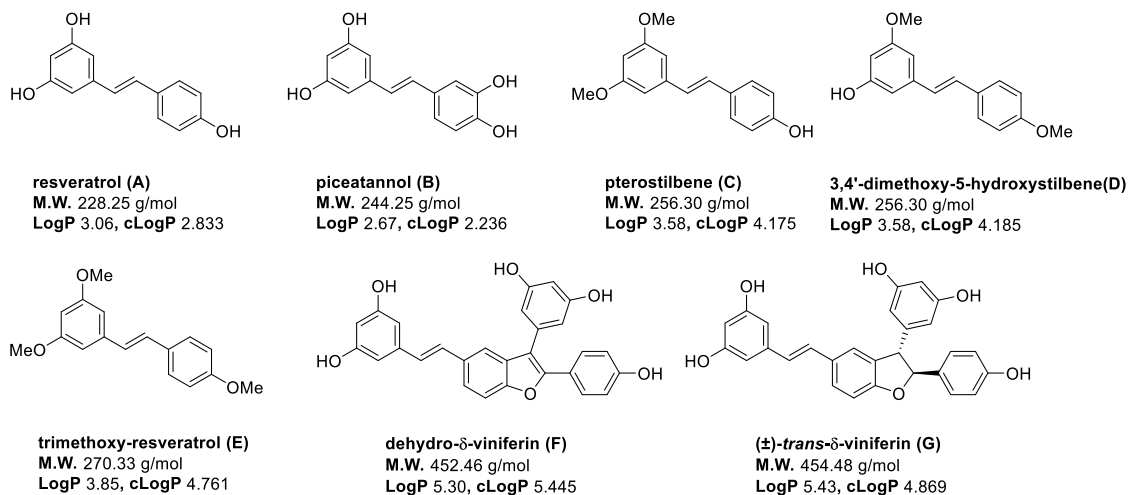
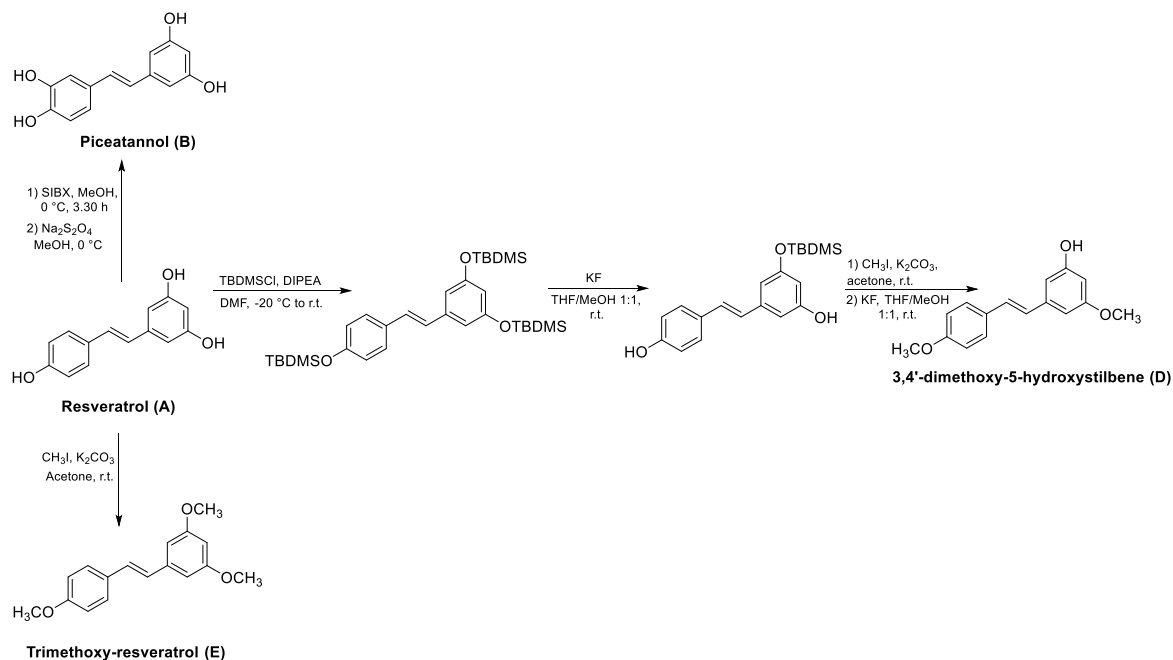


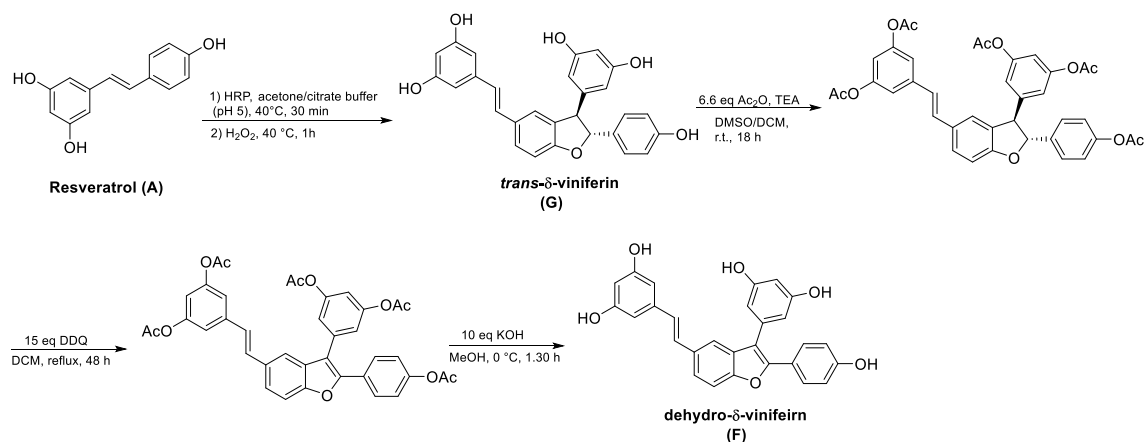
Figure 5.36. Chemical structures of the utilized stilbenoid monomers and dimers. Overview of the examined stilbenoids, listing the structure, molecular weight, LogP values and cLogP values for resveratrol (A), piceatannol (B), pterostilbene (C), pinostilbene (D), trimethoxy-resveratrol (E), dehydro- δ -viniferin (F) and *trans*- δ -viniferin(G).

Both resveratrol (A) and pterostilbene (C) were commercially available at a low price. Regioselective aromatic oxidation of resveratrol with stabilized iodoxybenzoic acid (SIBX) in MeOH at 0 °C, followed by *o*-quinone reduction by Na₂S₂O₄ afforded piceatannol (B) in modest yield (17%). Trimethoxy-resveratrol (E) was efficiently afforded by resveratrol methylation with CH₃I in presence of K₂CO₃ (9 eq), under a N₂ atmosphere, at room temperature overnight. Partial methylation of resveratrol with 2 eq of CH₃I and K₂CO₃ afforded, besides monomethylated products, an inseparable mixture of DMHS (D, 3,4'-dimethoxy-5-hydroxystilbene) and pterostilbene (C). Therefore, resveratrol was converted into tri(*t*-butyldimethylsilyl) ether (95%), which was selectively deprotected at positions 3 and 4' by KF (1 eq) at -15 °C for 6 h (56%). The obtained intermediate was subsequently methylated and deprotected to afford DMHS as a single isomer (40% over 2 steps) (Scheme 5.8) [1]. Resveratrol dimer *trans*- δ -viniferin (G) was selectively obtained in 49% yield *via* oxidative radical coupling, using horseradish peroxidase (HRP, 1 mg/ml solution) and H₂O₂ (30% solution) in a 1:1 mixture of acetone and citrate buffer (pH 5). Peracetylation of δ -viniferin using acetic anhydride (Ac₂O) and triethylamine (TEA) in DCM, followed by oxidative dehydrogenation with DDQ (20 EQ), in DCM at reflux for 48 h, and final deprotection with KOH in methanol at 0 °C

afforded the corresponding benzofuran derivative, dehydro- δ -viniferin (**F**) in 70% overall yield (**Scheme 5.9**).



Scheme 5.8. Synthesis of resveratrol methoxylated derivatives.



Scheme 5.9. Synthesis of resveratrol dimers *trans*- δ -viniferin (**G**) and dehydro- δ -viniferin (**F**)

Bacterial strains and preparation of stilbenoids samples

The Gram-negative bacterium *L. acidophilus* NCFM (Danisco, Copenhagen, Denmark) was grown anaerobically overnight at 37 °C in the Man Rogosa Sharp broth (Merk, Darmstadt, Germany). The Gram-negative bacterium *E. coli* Nissle 1917 O6:K5:H1 (Statens Serum Institute, Copenhagen, Denmark) was grown aerobically overnight at 37 °C in Luria-Bertani broth. The bacteria were subcultured twice, harvested by centrifugation at 1250 x g for 10 min, and washed twice in sterile PBS. The bacteria were seeded in Petri dishes, killed

with UV pulsation, and the bacterial viability was verified. Stilbenoids (**Figure 5.36**) were solubilized in DMSO to a concentration in excess of 10 mM (6.38 mM for *trans*- δ -viniferin), and further diluted in PBS or growth media as appropriate. Final DMSO concentrations below the 0.5% (*v/v*) thresholds did not lead to significant changes of the cytokine response in the system used in the study.

Assessment of Bacteria-Induced Cytokine Response

For determination of the appropriate MOI to be used in further tests, bmDCs (2×10^6 cells/mL) were stimulated with increasing concentration (MOI 0.3–3) of *L. acidophilus* NCFM or *E. coli* Nissle 1917 and incubated for 20 h at 37 °C, 5% CO₂ before the supernatant was harvested. For examinations of the stilbenoids' effect on the cytokine response, bmDCs (2×10^6 cells/mL) were incubated for 30 min at 37 °C, 5% CO₂ in the presence of increasing concentrations (0–40 μ M) of the individual stilbenoid, prior to stimulation with *L. acidophilus* NCFM (MOI 1) or *E. coli* Nissle 1917 (MOI 1). For assessing the effects of inhibition of MAP kinases, SP600125 (a JNK inhibitor, 25 μ M) and SB203580 (a p38 inhibitor, 10 μ M) were added to bmDCs and incubated for 30 min at 37 °C, 5% CO₂ prior to stimulation with *L. acidophilus* NCFM. After 20 h of incubation, the culture supernatants were harvested and stored at \approx 20 °C until analysis. The cytokine concentration in the culture supernatants was assessed using the DuoSet™ ELISA kits for mouse IL-12p70 (DY419), IL-10 (DY417), and TNF- α (DY410). All kits were from R&D Systems® (Minneapolis, MN, USA) and used according to the manufacturer's instructions.

Assessment of Intracellular ROS Formation

Murine bmDCs (2×10^6 cells/mL) were treated with 5 μ M carboxy-H₂DCFDA (Invitrogen™, Carlsbad, CA, USA) before the addition of resveratrol-derived stilbenoid monomers or dimers (30 μ M, final concentration) and incubated for 30 min at 37 °C and 5% CO₂. Samples were then stimulated with 100 ng/mL LPS (*E. coli* O26:B6, Sigma Aldrich, St Louis, MO, USA) and incubated for another 4 h at 37 °C and 5% CO₂. Controls included samples without stilbenoids and LPS as well as samples with stilbenoids but without LPS and samples not treated with carboxy-H₂DCFDA. Assessment of the intracellular ROS formation was carried out by measuring the intensity of the cellular fluorescence generated by oxidation of the internalized carboxy-H₂DCFDA on a BD FACS Diva flow cytometer (BD Biosciences, Franklin Lakes, NJ, USA). All events counted (20,000/sample) were included in the analysis. Comparison of the intracellular ROS formation in various samples was based on the mean fluorescent intensity

(MFI) of treated bmDCs. The flow cytometry results were analyzed using the FlowJo™ software (version 10.6.2, BD Life Sciences, Ashland, OR, USA).

In Vitro Total Antioxidant Capacity (TAC) Determination

TAC was assessed by the ABTS and DPPH assays [68] on the basis of the ability of the antioxidant molecules to reduce the radical cation of 2,2'-azino-bis-(3-ethylbenzothiazoline-6-sulfonic acid) (ABTS) and 2,2-diphenyl-1-picrylhydrazyl (DPPH). Ten microliters of a 1 mM stock solution of each species were added to 990 μ L of 80 μ M ABTS⁺ and 100 μ M-DPPH and the quenching of the absorbance at 734 nm for 1 min and at 517 nm for 30 min for ABTS^{•+} and DPPH[•], respectively, was monitored. Values obtained for each sample were compared to the concentration–response curve of the standard Trolox solution and expressed as mM of Trolox equivalent (TE).

Assessment of Fold Change in Gene Expression in bmDC

Murine bmDCs (2×10^6 cells/mL) were stimulated with *L. acidophilus* NCFM (MOI 1) and incubated at 37 °C and 5% CO₂. To determine the effect of stilbenoids on the expression of specific genes in bmDCs, cells were incubated with 30 μ M of the examined stilbenoids for 30 min at 37 °C and 5% CO₂ prior to stimulation. Supernatant from stimulated bmDCs was removed and mRNA was extracted using MagMAX-96 Total RNA Isolation Kit (AM1830, Applied Biosystems, Foster City, CA, USA). The extracted RNA (500 ng for each sample) was converted to cDNA using Applied Biosystems™ High-Capacity cDNA Reverse Transcription Kit. Applied Biosystems™ TaqMan™ qPCR with a specific Taq Man MGB probe and primer sequences were then used to estimate the expression of *Dusp1* (Mm00457274_g1). *Actb* (Mm00607939_g1) was used as the reference gene to define Δ Ct for each sample (Δ Ct_{target} = Ct_{target} - Ct_{reference}). Fold change expression was estimated using the $\Delta\Delta$ Ct method, where first the Δ Ct of the blank (unstimulated cells) from each time point is subtracted from the Δ Ct of a target sample (stimulated cells) at each time point ($\Delta\Delta$ Ct = Δ Ct_{target} - Δ Ct_{control}), with fold change in gene expression being defined by $2^{-(\Delta\Delta$ Ct)}.

Statistical Analysis

Statistical analysis was performed by using the GraphPad Prism software (version 9.3.1, GraphPad Software, San Diego, CA, USA). Unless otherwise specified, results are illustrated as means \pm SD. The results were analyzed by one-way analysis of variance (ANOVA) to determine significance. *p* values less than 0.05 were considered statistically significant and indicated by asterisks. * *p* \leq 0.05, ** *p* \leq 0.01, *** *p* \leq 0.001, **** *p* \leq 0.0001.

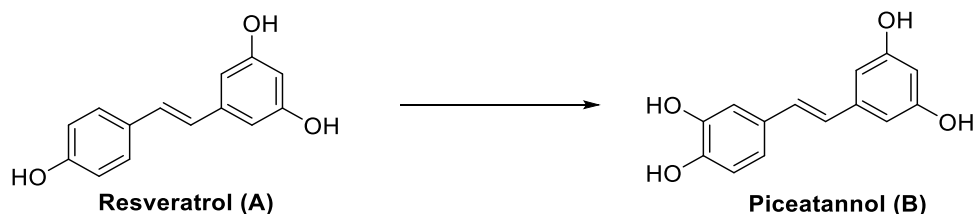
5.2.5. Conclusions

This work demonstrates that the potential of stilbenoids to affect the cytokine production induced by bacteria in murine dendritic cells depends on the specific structure of the stilbenoid, as well as on the type of microbial stimulant. Specific knowledge of stilbenoid molecular determinants modulating the cytokine response of dendritic cells, i.e., the cells orchestrating the type of immune response against pathogens, may be exploited in outlining future strategies for development of new drugs and nutraceuticals.

5.2.6. Experimental procedures for stilbenoids synthesis

All chemicals were provided by supplier and used without further purification unless otherwise stated. All reagents and solvents were of reagent grade or were purified by standard methods before use. All reactions requiring anhydrous conditions were performed under nitrogen or argon atmosphere with Schlenk-type oven-dried glassware. Melting points were determined on a model B-540 Büchi apparatus and are uncorrected. NMR data were acquired using a Varian Mercury-300 MHz spectrometer (Varian, Palo Alto, CA, USA), Bruker AV600. Chemical shifts (δ values) and coupling constants (J values) are given in ppm and Hz, respectively. Isolation and purification of the compounds were performed by flash column chromatography on silica gel 60 (230–400 mesh). The analytical thin-layer chromatography (TLC) was conducted on Supelco TLC plates (silica gel 60 F254, aluminum foil). Substances were detected with a UV-light source ($\lambda = 254$ or 365 nm) or stained with 10% phosphomolybdic acid solution (10.0 g phosphomolybdic acid in 100 mL of abs. ethanol), or with ninhydrin solution (1.5 g ninhydrin, 3.0 mL acetic acid in 100 mL of abs. ethanol), or with 2,4-dinitrophenylhydrazine solution (12 g 2,4-dinitrophenylhydrazine, 60 mL conc sulfuric acid, 80 mL water in 200 mL of 95% ethanol), or with potassium permanganate solution (1.5 g KMnO_4 , 10 g K_2CO_3 , 1.25 mL 10% NaOH in 200 mL of water).

Synthesis of (E)-4-(3,5-dihydroxystyryl)benzene-1,2-diol, piceatannol (B)



Resveratrol (228.3 mg, 1 mmol) was dissolved in 22.8 ml of methanol and the obtained solution was cooled to 0 °C in an iced bath. Then, SIBX (423.5 mg, 2.8

mmol) was added, and reaction mixture was stirred at 0 °C for 3.30 hours. After this time, 30 ml of 0.1M Na₂S₂O₄ were added to reaction mixture and the aqueous phase was extracted with EtOAc (5 x 20 ml). Combined organic layers were washed with sat. NaHCO₃, dried over Na₂SO₄, filtered, and the solvent was evaporated. Column chromatography (DCM/MeOH 95/5) afforded piceatannol (**B**) in 17% yield.

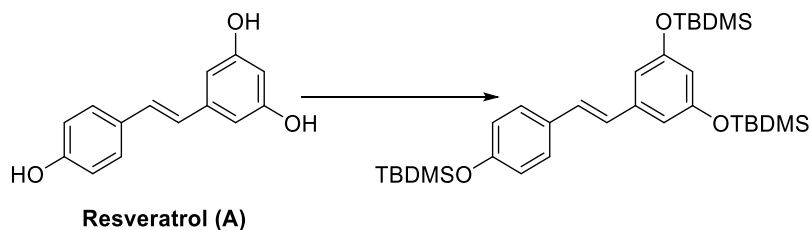
R_f: 0.31 (DCM/MeOH 9:1)

M.p.: 228-229 °C

¹H NMR (300 MHz, Methanol-*d*₄) δ 6.99 (d, *J* = 2.0 Hz, 1H), 6.91 (d, *J* = 16.2 Hz, 1H), 6.85 (dd, *J* = 8.2, 2.1 Hz, 1H), 6.80 – 6.72 (m, 2H), 6.45 (d, *J* = 2.2 Hz, 2H), 6.17 (t, *J* = 2.2 Hz, 1H).

¹³C NMR (76 MHz, Methanol-*d*₄) δ 159.66, 146.59, 146.54, 141.30, 131.03, 129.70, 126.98, 120.16, 116.41, 113.80, 105.74, 102.63.

Synthesis of (E)-((5-(4-((tert-butyldimethylsilyl)oxy)styryl)-1,3-phenylene)bis(oxy))bis(tert-butyldimethylsilane)



To a solution of resveratrol (**A**) (500 mg, 2.19 mmol) in anhydrous DMF (15 mL) at -20°C under nitrogen atmosphere, a solution of *tert*-Butyldimethylsilyl chloride (TBDMSCl, 1.32 g, 8.76 mmol, 4 eq) in anhydrous DMF (5 mL) and DIPEA (1.5 mL, 8.76 mmol, 4 eq) were added. The reaction mixture was allowed to warm to room temperature. After 16 h reaction mixture was diluted with AcOEt (70 mL) and washed with a mixture 1:1 of HCl 0,1 N/brine (5 x 30 mL). The organic layer was dried over anhydrous Na₂SO₄ and concentrated under reduced pressure. The residue was purified by flash chromatography (DCM/cyclohexane 3:7) to obtain the desired product as white sticky solid in 95% yield. Analytical data were in accordance with those reported in literature [69].

R_f: 0.7 (Cyclohexane/DCM 8:2)

¹H NMR (300 MHz, Chloroform-*d*) δ (ppm): 7.41 – 7.35 (m, 2H), 6.96 (d, *J* = 16.2 Hz, 1H), 6.87 – 6.80 (m, 4H), 6.60 (d, *J* = 2.2 Hz, 2H), 6.24 (t, *J* = 2.2 Hz, 1H), 1.00 (d, *J* = 1.1 Hz, 27H), 0.22 (d, *J* = 1.1 Hz, 18H).

^{13}C NMR (75 MHz, Chloroform-*d*) δ (ppm): 156.8 (x2C), 155.6, 139.6, 130.8, 128.6 (x2C), 127.8, 126.9, 120.5 (x2C), 111.7, 111.4 (x2C), 25.9, 25.8 (x2C), 18.4 (x9C), -4.2 (x6C) [69].

Synthesis of (E)-3-((tert-butyldimethylsilyl)oxy)-5-(4-hydroxystyryl)phenol



To a solution of protected resveratrol (600 mg, 1.05 mmol) in dry THF (12 mL) was added a solution of potassium fluoride (61 mg, 1.05 mmol, 1.0 eq) in MeOH (12 mL) at $-15\text{ }^{\circ}\text{C}$, under nitrogen atmosphere, and the mixture was vigorously stirred for 6 h. The resulting reaction mixture was concentrated under reduced pressure then diluted with AcOEt and washed with brine (2x30 mL). The organic layer was dried over anhydrous Na_2SO_4 and concentrated under reduced pressure. The resulting crude product was purified by flash chromatography (DCM/acetone 95:5) to afford the desired product as white solid in 56% yield. Analytical data were in accordance with literature report [69].

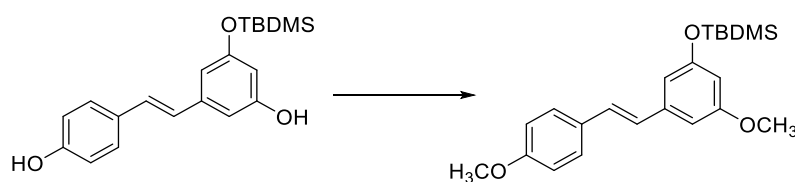
M.p.: 62-63 $^{\circ}\text{C}$

R_f: 0.39 (DCM/acetone 95:5)

^1H NMR (300 MHz, Chloroform-*d*) δ (ppm): 7.43 – 7.38 (m, 2H), 6.98 (d, $J = 16.3$ Hz, 1H), 6.89 – 6.79 (m, 3H), 6.58 (d, $J = 2.1$ Hz, 2H), 6.27 (t, $J = 2.1$ Hz, 1H), 1.00 (s, 9H), 0.23 (s, 6H).

^{13}C NMR (75 MHz, Chloroform-*d*) δ (ppm): 157.2, 156.7, 155.4, 140.0, 130.3 (x2C), 128.8, 128.2, 126.4, 115.8 (x2C), 111.3, 106.8, 106.5, 25.82, 18.35 (x3C), -4.2 (x2C) from [69].

Synthesis of (E)-tert-butyl(3-methoxy-5-(4-methoxystyryl)phenoxy)dimethylsilane



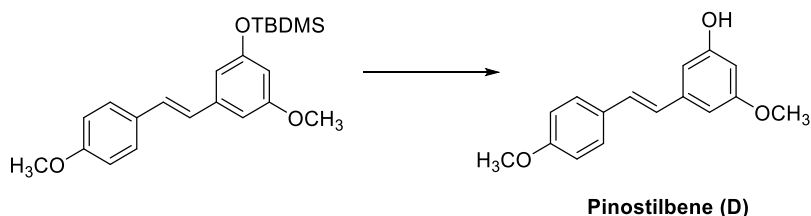
To a solution of (E)-3-((tert-butyl dimethylsilyl)oxy)-5-(4-hydroxystyryl)phenol (109 mg, 0.318 mmol) in dry acetone (1.5 mL) at room temperature, under nitrogen atmosphere, K_2CO_3 (264 mg, 1.91 mmol, 6 eq) was added. After 10 minutes stirring, CH_3I (118 μ L, 1.91 mmol, 6 eq) was added dropwise, and the obtained solution was stirred overnight. Then, the solvent was evaporated, and the residue was quenched with a NH_4Cl sat. The aqueous phase was extracted with $AcOEt$ (3 x 10 mL). The combined organic layers were washed with H_2O (20 mL), brine (20 mL), dried over anhydrous Na_2SO_4 , and concentrated under reduced pressure. The residue was purified by flash chromatography (Cyclohexane/DCM 7:3) to afford the desired product as a colorless oil in 38% yield. Analytical data were in accordance with literature report [70].

Rf: 0.31 (Cyclohexane/DCM 7:3)

1H NMR (300 MHz, Chloroform-*d*) δ (ppm): 7.49 – 7.42 (m, 2H), 7.02 (d, $J = 16.3$ Hz, 1H), 6.94 – 6.85 (m, 3H), 6.69 – 6.66 (m, 1H), 6.60 (dd, $J = 2.1, 1.4$ Hz, 1H), 6.32 (t, $J = 2.2$ Hz, 1H), 3.84 (s, 3H), 3.82 (s, 3H), 1.01 (s, 9H), 0.24 (s, 6H).

^{13}C NMR (75 MHz, Chloroform-*d*) δ (ppm): 160.8, 159.4, 156.9, 139.6, 130.0 (x2C), 128.5, 127.8, 126.6, 114.1 (x2C), 110.9, 104.8 (x2C), 55.3 (x2C), 25.7, 14.1 (x3C), -4.4 (x2C).

Synthesis of (E)-3-methoxy-5-(4-methoxystyryl)phenol, 3,4'-dimethoxy-5-hydroxystilbene (D)



To a solution of (E)-tert-butyl(3-methoxy-5-(4-methoxystyryl) phenoxy) dimethyl silane (28 mg, 0.0756 mmol) in dry MeOH (1 mL) a solution of potassium fluoride (26 mg, 0.453 mmol, 6 eq) in a 2:1 mixture of MeOH/THF (1.5 mL) was added dropwise at room temperature. The mixture was stirred under nitrogen atmosphere overnight. The resulting reaction mixture was

concentrated under reduced pressure then diluted with AcOEt and washed with brine (2×30 mL). The organic layer was dried over anhydrous Na₂SO₄ and concentrated under reduced pressure. The crude was purified by flash chromatography (cyclohexane/AcOEt 7:3) to give the product as white solid in quantitative yield. Analytical data were in accordance with literature report [71].

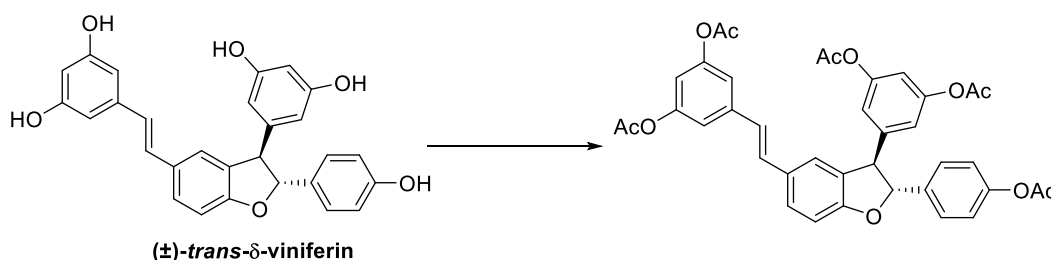
M.p.: 115-117°C

R_f: 0.29 (cyclohexane/AcOEt 7:3)

¹H NMR (300 MHz, Chloroform-*d*) δ (ppm): 7.47 – 7.41 (m, 2H), 7.02 (d, *J* = 16.3 Hz, 1H), 6.94 – 6.83 (m, 3H), 6.66 – 6.62 (m, 1H), 6.58 (dd, *J*₁ = 2.2, *J*₂ = 1.4 Hz, 1H), 6.32 (t, *J* = 2.2 Hz, 1H), 3.84 (s, 3H), 3.82 (s, 3H).

¹³C NMR (100MHz, DMSO-*d*₆) δ: 160.6, 159.0, 158.6, 139.3, 129.6 (×2C), 128.0, 127.8, 126.4, 114.1 (×2C), 106.0, 102.6, 100.6, 55.1, 55.0 from [71].

Synthesis of 5-((*E*)-2-((2*R*,3*R*)-2-(4-acetoxyphenyl)-3-(3,5-diacetoxyphenyl)-2,3-dihydrobenzofuran-5-yl)vinyl)-1,3-phenylene diacetate



Trans-δ-viniferin (**G**) (100 mg, 0.22 mmol) was dissolved in 13.5 ml of a mixture of DCM and DMSO (12.5% v/v). Acetic anhydride (140 μl, 1.45 mmol, 6.6 eq) and triethylamine (450 μl, 3.2 mmol, 14.7 eq) were added, and the obtained solution was stirred at room temperature for 16 hours. After complete consumption of the starting material, solvents were evaporated. The residue was dissolved in 10 ml of ethyl acetate and the organic phase was washed with NaHCO₃ 5%. The aqueous layer was re-extracted with EtOAc, then the combined organic layers were washed with water, dried over Na₂SO₄, filtered, and concentrated under reduced pressure. Flash chromatography (cyclohexane/ethyl acetate 6/4) afforded the desired product as a white amorphous solid in 77% yield.

R_f: (CHX/AcOEt 6/4) = 0.42

IR ν_{\max} 1768, 1606, 1508, 1488, 1369, 1276, 1261, 1196, 1125, 1023, 908.2, 764.2, 750.1 cm^{-1} .

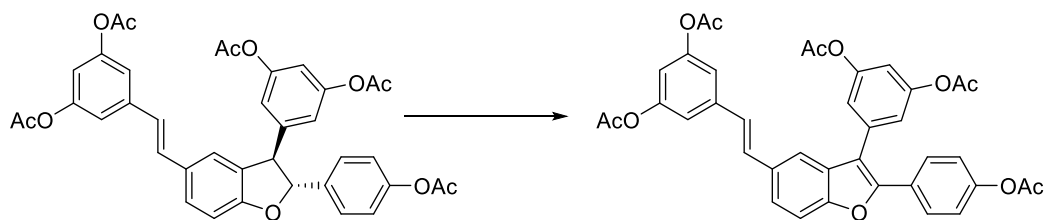
^1H NMR (300 MHz, Chloroform-*d*) δ 7.40-7.31 (m, 3H), 7.20 (s, 1H), 7.13 – 7.08 (m, 2H), 7.07 (d, $J = 2.1$ Hz, 2H), 7.01 (d, $J = 16.3$ Hz, 1H), 6.97 – 6.91 (m, 2H), 6.89 – 6.81 (m, 3H), 6.78 (t, $J = 2.1$ Hz, 1H), 5.55 (d, $J = 8.0$ Hz, 1H), 4.55 (d, $J = 8.0$ Hz, 1H), 2.30 (s, 3H), 2.29 (s, 6H), 2.27 (s, 6H).

^{13}C NMR (75 MHz, Chloroform-*d*) δ (ppm): 169.4, 169.0 (x2C), 168.9 (x2C), 159.9, 151.4 (x2C), 151.2 (x2C), 150.6, 143.7, 139.9, 137.7, 130.7, 130.2, 129.7 (x2C), 128.5, 126.9, 124.9, 123.4, 121.9 (x2C), 118.8 (x2C), 116.6 (x2C), 114.8, 113.9, 110.0, 92.4, 57.3, 21.1 (x5C).

LRMS (ESI) calcd for $\text{C}_{38}\text{H}_{32}\text{O}_{11}\text{Na}$ $[\text{M}+\text{Na}]^+$ 687.18368, found 687.18368;

LRMS (ESI) calcd for $\text{C}_{38}\text{H}_{32}\text{O}_{11}\text{K}$ $[\text{M}+\text{K}]^+$ 703.15762, found 703.15762.

Synthesis of (*E*)-5-(2-(2-(4-acetoxyphenyl)-3-(3,5-diacetoxyphenyl)benzofuran-5-yl)vinyl)-1,3-phenylene diacetate



Per-acetylated *trans*- δ -viniferin (50 mg, 0.075 mmol) was dissolved in 10 ml of freshly distilled DCM. DDQ (256 mg, 1.128 mmol, 15 eq) was added and the obtained reaction mixture was heated to reflux and stirred for 48 hours. After complete consumption of the starting material, reaction mixture was cooled to room temperature and filtered on a Celite pad. The filtrate was evaporated under reduced pressure and the crude product was purified by flash chromatography (cyclohexane/ethyl acetate 7/3) affording the desired product as a pale-pink amorphous solid in 50% yield.

R_f: (CHX/AcOEt 6/4) = 0.39

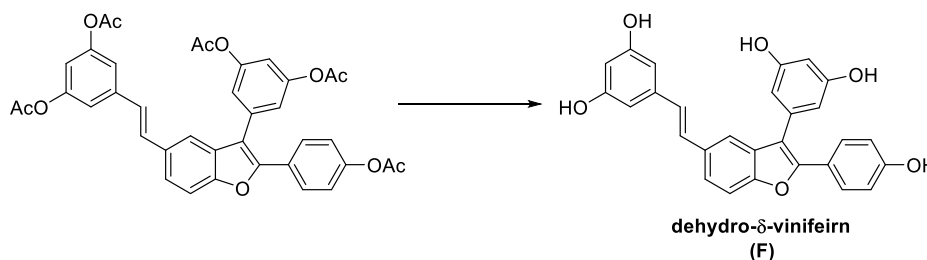
IR ν_{\max} 1767, 1611, 1584, 1506, 1440, 1369, 1276, 1261, 1196, 1123, 1022, 910.2, 764.2, 750. cm^{-1}

^1H NMR (300 MHz, Chloroform-*d*) δ (ppm): δ 7.76 – 7.71 (m, 2H), 7.62 (d, $J = 1.3$ Hz, 1H), 7.53 – 7.51 (m, 2H), 7.17 – 7.09 (m, 7H), 7.07 (d, $J = 7.7$ Hz, 1H), 7.03 (t, $J = 2.1$ Hz, 1H), 6.81 (t, $J = 2.1$ Hz, 1H), 2.31 (s, 15H).

^{13}C NMR (300 MHz, Chloroform-*d*) δ (ppm): 169.3, 169.1 (x2C), 168.9 (x2C), 153.9, 151.6, 151.3 (x2C), 150.9, 150.8, 139.8, 134.3, 132.3, 130.7, 130.1, 128.2 (x2C), 127.5 (x2C), 126.2, 123.9, 121.9 (x2C), 120.3, 118.1 (x2C), 116.8 (x2C), 115.7, 115.0, 114.1, 111.5, 21.2 (x5C).

LRMS (ESI) calcd for $\text{C}_{38}\text{H}_{30}\text{O}_{11}\text{Na}$ $[\text{M}+\text{Na}]^+$ 685.1677, found 685.16803; $\text{C}_{38}\text{H}_{30}\text{O}_{11}\text{K}$ $[\text{M}+\text{K}]^+$ 701.1415, found 701.14197.

Synthesis of (E)-5-(2-(3-(3,5-dihydroxyphenyl)-2-(4-hydroxyphenyl)benzofuran-5-yl)vinyl)benzene-1,3-diol, dehydro- δ -viniferin (F)



To the suspension of (E)-5-(2-(2-(4-acetoxyphenyl)-3-(3,5-diacetoxyphenyl) benzofuran-5-yl) vinyl)-1,3-phenylene diacetate (76 mg, 0.115 mmol, 1 eq) in MeOH at 0°C was added KOH 85% (76 mg, 1.15 mmol, 10 eq). The mixture was stirred at 0°C for 90 minutes and then acidified with aqueous HCl 0.1M to reach pH 1. MeOH was evaporated and residue was diluted with water (5 mL), extracted with AcOEt (3 x 10 mL). The combined organic phases were washed with water (10 mL), brine (10 mL), dried over anhydrous Na_2SO_4 , and concentrated under reduced pressure. The residue was purified by flash chromatography (cyclohexane/acetone 1:1) to afford the desired product as a yellow amorphous solid in 70% yield. Analytical data were in agreement with those reported in literature [72].

R_f: 0.25 (DCM/MeOH 9:1)

^1H NMR (300 MHz, Acetone-*d*₆) δ (ppm): 7.65 (d, J = 1.3, 1H), 7.63 – 7.51 (m, 4H), 7.24 (d, J = 16.3 Hz, 1H), 7.06 (d, J = 16.3 Hz, 1H), 6.91 – 6.84 (m, 2H), 6.60 (d, J = 2.2 Hz, 2H), 6.52 (d, J = 2.2 Hz, 2H), 6.45 (t, J = 2.2 Hz, 1H), 6.30 (t, J = 2.2 Hz, 1H).

^{13}C NMR (150 MHz, DMSO-*d*₆) δ (ppm): 159.5 (x2C), 158.9 (x2C), 158.6, 153.1, 151.3, 133.0, 128.8 (x2C), 128.7, 128.3, 123.6, 117.9 (x2C), 116.0, 115.8, 111.6, 107.8 (x2C), 105.1 (x2C), 102.6, 102.4.

5.3. Bibliography

1. Mattio, L.M.; Dallavalle, S.; Musso, L.; Filardi, R.; Franzetti, L.; Pellegrino, L.; D'Incecco, P.; Mora, D.; Pinto, A.; Arioli, S. Antimicrobial activity of resveratrol-derived monomers and dimers against foodborne pathogens. *Sci. Rep.* **2019**, *9*, 1–13, doi:10.1038/s41598-019-55975-1.
2. Mattio, L.; Catinella, G.; Iriti, M.; Vallone, L. Inhibitory activity of stilbenes against filamentous fungi. *Ital. J. Food Saf.* **2021**, *10*, 17–20, doi:10.4081/ijfs.2021.8461.
3. Mattio, L.M.; Catinella, G.; Dallavalle, S.; Pinto, A. Stilbenoids: A natural arsenal against bacterial pathogens. *Antibiotics* **2020**, *9*, 1–40, doi:10.3390/antibiotics9060336.
4. Mattio, L.M.; Catinella, G.; Pinto, A.; Dallavalle, S. Natural and nature-inspired stilbenoids as antiviral agents. *Eur. J. Med. Chem.* **2020**, *202*, 112541, doi:10.1016/j.ejmech.2020.112541.
5. Kempf, K.; Capello, Y.; Melhem, R.; Lescoat, C.; Kempf, O.; Cornu, A.; Génot, E.; Quideau, S. Systemic Convergent Multi-Target Actions of Plant Polyphenols Revealed by Affinity-Based Protein Profiling of Bone Cells Using C -Glucosidic Vesical (ag) in-Bearing Chemoproteomic Probes. *ACS Chem. Biol.* **2023**, *18*, 2495–2505, <https://doi.org/10.1021/acscchembio.3c00440>.
6. Liu, Y.; Patricelli, M.P.; Cravatt, B.F. Activity-based protein profiling : The serine hydrolases. *PNAS*, **1999**, *96*, 14694–14699, doi:10.1073/pnas.96.26.14694.
7. Greenbaum, D.; Medzihradszky, K.F.; Burlingame, A.; Bogoy, M. Epoxide electrophiles as activity-dependent cysteine protease profiling and discovery tools. *Chem. Biol.* **2000**, *7*, 569–581.
8. Barglow, K.T.; Cravatt, B.F. Activity-Based Protein Profiling for the Functional Annotation of Enzymes. *Nat. Methods* **2007**, *4*, 822–827.
9. Keller, L.J.; Babin, B.M.; Lakemeyer, M.; Bogoy, M. ScienceDirect Activity-based protein profiling in bacteria: Applications for identification of therapeutic targets and characterization of microbial communities. *Curr. Opin. Chem. Biol.* **2020**, *54*, 45–53, doi:10.1016/j.cbpa.2019.10.007.
10. Wright, M.H.; Sieber, S.A. Chemical proteomics approaches for identifying the cellular targets of natural products. *Nat. Prod. Rep.* **2016**, *33*, 681–708, doi:10.1039/c6np00001k.
11. Zhao, W.; Cross, A.R.; Crowe-mcauliffe, C.; Weigert-munoz, A.; Csatory, E.E.; Solinski, A.E.; Krysiak, J.; Goldberg, J.B.; Wilson, D.N.; Medina, E.; et

- al. The Natural Product Elegaphenone Potentiates Antibiotic Effects against *Pseudomonas aeruginosa*. *Angew. Chem. Int. Ed.* **2019**, *58*, 8581–8584, doi:10.1002/anie.201903472.
12. Drahl, C.; Cravatt, B.F.; Sorensen, E.J. Protein-reactive natural products. *Angew. Chemie - Int. Ed.* **2005**, *44*, 5788–5809, doi:10.1002/anie.200500900.
 13. Green, N.M. Avidin and Streptavidin. *Methods Enzym.* **1990**, *184*, 51–67, doi:https://doi.org/10.1016/0076-6879(90)84259-J.
 14. Cravatt, B.F.; Wright, A.T.; Kozarich, J.W. Activity-based protein profiling: From enzyme chemistry to proteomic chemistry. *Annu. Rev. Biochem.* **2008**, *77*, 383–414, doi:10.1146/annurev.biochem.75.101304.124125.
 15. Dückert, H.; Pries, V.; Khedkar, V.; Menninger, S.; Bruss, H.; Bird, A.W.; Maliga, Z.; Brockmeyer, A.; Janning, P.; Hyman, A.; Grimme, S.; Schürmann, M.; et al. Natural Product-Inspired Cascade Synthesis Yields Modulators of Centrosome Integrity. *Nat. Chem. Biol.* **2012**, *8*, 179–184.
 16. Speers, A.E.; Cravatt, B.F. A tandem orthogonal proteolysis strategy for high-content chemical proteomics. *J. Am. Chem. Soc.* **2005**, *127*, 10018–10019, doi:10.1021/ja0532842.
 17. Xu, C.; Soragni, E.; Chou, C.J.; Herman, D.; Plasterer, H.L.; Rusche, J.R.; Gottesfeld, J.M. Chemical Probes Identify a Role for Histone Deacetylase 3 in Friedreich's Ataxia Gene Silencing. *Chem. Biol.* **2009**, *16*, 980–989, doi:10.1016/j.chembiol.2009.07.010.
 18. Sugimoto, T.; Fujii, T.; Hatanaka, Y. Syntheses of novel photoaffinity probes for bioorganic studies on nyctinasty of leguminous plants. *Tetrahedron Lett.* **2002**, *43*, 6529–6532.
 19. Id, Y.S.; Hashidoko, Y.; Hashimoto, M. Diazirines for Photoaffinity Labeling. *Molecules* **2017**, *22*, 1389 doi:10.3390/molecules22081389.
 20. Chee, G.; Yalowich, J.C.; Bodner, A.; Wu, X.; Hasinoff, B.B. A diazirine-based photoaffinity etoposide probe for labeling topoisomerase II. *Bioorg. Med. Chem.* **2010**, *18*, 830–838, doi:10.1016/j.bmc.2009.11.048.
 21. Carrié, H.; Tran, D.T.; Rousseau, S.; Chaignepain, S.; Schmitter, J.M.; Deffieux, D.; Quideau, S. New affinity-based probes for capturing flavonoid-binding proteins. *Chem. Commun.* **2014**, *50*, 9387–9389, doi:10.1039/c4cc04557b.
 22. Cañeque, T.; Müller, S.; Rodriguez, R. Visualizing biologically active small molecules in cells using click chemistry. *Nat. Rev. Chem.* **2018**, *2*, 202–215, doi:10.1038/s41570-018-0030-x.

23. Toth, György; Koeber, K.E. Simple, Safe, Large Scale Synthesis of 5-Arylmethyl-2,2-dimethyl-1,3-dioxane-4,6-diones and 3-Arylpropanoic Acids. *Synth. Commun.* **1995**, *25*, 3067–3074.
24. Sekiya, M.; Suzuki, K. Formic Acid Reduction: VII. Reduction of Carbon-Carbon Double Bonds adjacent to Carbonyls. *Chem. Pharm. Bull.* **1970**, *18*, 1530–1534.
25. Alexander, E.R.; Wildman, R.B. Studies on the mechanism of the Leuckart Reaction. *J. Am. Chem. Soc.* **1948**, *70*, 1187–1189, doi:10.1080/03071848809416473.
26. Moore, M.L. The Leuckart reaction. In *Organic Reactions* **2004**, *7*, 301–324.
27. Clarke, H.T.; Gillespie, B.; Weisshaus, S.Z. The Action of Formaldehyde on Amines and Amino Acids. *J. Am. Chem. Soc.* **1933**, *55*, 4571–4587, doi:10.1021/ja01338a041.
28. Ozanne, A.; Pouységu, L.; Depernet, D.; Francois, B.; Quideau, S. A Stabilized Formulation of IBX (SIBX) for Safe Oxidation Reactions Including a New Oxidative Demethylation of Phenolic Methyl Aryl Ethers. *Org. Lett.* **2003**, *5*, 2903–2906.
29. Speers, A.E.; Adam, G.C.; Cravatt, B.F. Activity-Based Protein Profiling in Vivo Using a Copper (I)-Catalyzed Azide-Alkyne [3 + 2] Cycloaddition. **2003**, *4*, 4686–4687.
30. Goddard-Borger, E.D.; Stick, R. V. Erratum: An efficient, inexpensive, and shelf-stable diazotransfer reagent: Imidazole-1-sulfonyl azide hydrochloride. *Org. Lett.* **2011**, *13*, 2514, doi:10.1021/ol2007555.
31. Teuscher, K.B.; Zhang, M.; Ji, H. A Versatile Method to Determine the Cellular Bioavailability of Small-Molecule Inhibitors. *J. Med. Chem.* **2017**, *60*, 157–169, doi:10.1021/acs.jmedchem.6b00923.
32. Remsberg, C.M.; Yáñez, J.A.; Ohgami, Y.; Vega-Villa, K.R.; Rimando, A.M.; Davies, N.M. Pharmacometrics of Pterostilbene: Preclinical Pharmacokinetics and Metabolism, Anticancer, Antiinflammatory, Antioxidant and Analgesic Activity. *Phyther. Res.* **2008**, *22*, 169–179, doi:10.1002/ptr.
33. Steinman, R.M.; Nussenzweig, M.C. Avoiding horror autotoxicus: The importance of dendritic cells in peripheral T cell tolerance. *Proc. Natl. Acad. Sci. U. S. A.* **2002**, *99*, 351–358, doi:10.1073/pnas.231606698.
34. Mathiesen, R.; Eld, H.M.S.; Sørensen, J.; Fuglsang, E.; Lund, L.D.; Taverniti, V.; Frøkiær, H. Mannan Enhances IL-12 Production by Increasing Bacterial Uptake and Endosomal Degradation in L.

- acidophilus and *S. aureus* Stimulated Dendritic Cells. *Front. Immunol.* **2019**, *10*, 1–13, doi:10.3389/fimmu.2019.02646.
35. Mikkelsen, M.S.; Jespersen, B.M.; Mehlsen, A.; Engelsen, S.B.; Frøkiær, H. Cereal β -glucan immune modulating activity depends on the polymer fine structure. *Food Res. Int.* **2014**, *62*, 829–836, doi:10.1016/j.foodres.2014.04.021.
 36. Weiss, G.; Maaetoft-Udsen, K.; Stifter, S.A.; Hertzog, P.; Goriely, S.; Thomsen, A.R.; Paludan, S.R.; Frøkiær, H. MyD88 Drives the IFN- β Response to *Lactobacillus acidophilus* in Dendritic Cells through a Mechanism Involving IRF1, IRF3, and IRF7. *J. Immunol.* **2012**, *189*, 2860–2868.
 37. Arulseivan, P.; Fard, M.T.; Tan, W.S.; Gothai, S.; Fakurazi, S.; Norhaizan, M.E.; Kumar, S.S. Role of Antioxidants and Natural Products in Inflammation. *Oxid. Med. Cell. Longev.* **2016**, *2016*, doi:10.1155/2016/5276130.
 38. Dvorakova, M.; Landa, P. Anti-inflammatory activity of natural stilbenoids: A review. *Pharmacol. Res.* **2017**, *124*, 126–145, doi:10.1016/j.phrs.2017.08.002.
 39. Zeuthen, L.H.; Christensen, H.R.; Frøkiær, H. Lactic acid bacteria inducing a weak interleukin-12 and tumor necrosis factor alpha response in human dendritic cells inhibit strongly stimulating lactic acid bacteria but act synergistically with gram-negative bacteria. *Clin. Vaccine Immunol.* **2006**, *13*, 365–375, doi:10.1128/CVI.13.3.365-375.2006.
 40. Boye, L.; Welsby, I.; Lund, L.D.; Goriely, S.; Frøkiær, H. Plasma membrane Toll-like receptor activation increases bacterial uptake but abrogates endosomal *Lactobacillus acidophilus* induction of interferon- β . *Immunology* **2016**, *149*, 329–342, doi:10.1111/imm.12650.
 41. Saikh, K.U. MyD88 and beyond: a perspective on MyD88-targeted therapeutic approach for modulation of host immunity. *Immunol. Res.* **2021**, *69*, 117–128, doi:10.1007/s12026-021-09188-2.
 42. Ciesielska, A.; Matyjek, M.; Kwiatkowska, K. TLR4 and CD14 trafficking and its influence on LPS-induced pro-inflammatory signaling. *Cell. Mol. Life Sci.* **2021**, *78*, 1233–1261, doi:10.1007/s00018-020-03656-y.
 43. Cao, X.; Tian, S.; Fu, M.; Li, Y.; Sun, Y.; Liu, J.; Liu, Y. Resveratrol protects human bronchial epithelial cells against nickel-induced toxicity via suppressing p38 MAPK, NF- κ B signaling, and NLRP3 inflammasome activation. *Environ. Toxicol.* **2020**, *35*, 609–618, doi:10.1002/tox.22896.
 44. Fu, S.; Lv, R.; Wang, L.; Hou, H.; Liu, H.; Shao, S. Resveratrol, an

- antioxidant, protects spinal cord injury in rats by suppressing MAPK pathway. *Saudi J. Biol. Sci.* **2018**, *25*, 259–266, doi:10.1016/j.sjbs.2016.10.019.
45. Eld, H.M.S.; Nielsen, E.M.; Johnsen, P.R.; Marengo, M.; Kamper, I.W.; Frederiksen, L.; Bonomi, F.; Frees, D.; Iametti, S.; Frøkiær, H. Cefoxitin treatment of MRSA leads to a shift in the IL-12/IL-23 production pattern in dendritic cells by a mechanism involving changes in the MAPK signaling. *Mol. Immunol.* **2021**, *134*, 1–12, doi:10.1016/j.molimm.2021.02.025.
 46. Weiss, G.; Christensen, H.R.; Zeuthen, L.H.; Vogensen, F.K.; Jakobsen, M.; Frøkiær, H. Lactobacilli and bifidobacteria induce differential interferon- β profiles in dendritic cells. *Cytokine* **2011**, *56*, 520–530, doi:10.1016/j.cyto.2011.07.024.
 47. Teixeira-Coelho, M.; Guedes, J.; Ferreira, P.; Howes, A.; Pedrosa, J.; Rodrigues, F.; Lai, W.S.; Blackshear, P.J.; O'Garra, A.; Castro, A.G.; Saraiva, M. Differential post-transcriptional regulation of IL-10 by TLR2 and TLR4-activated macrophages. *Eur. J. Immunol.* **2014**, *44*, 856–866, doi:10.1002/eji.201343734.
 48. Eld, H.M.S.; Johnsen, P.R.; Nielsen, E.M.; Jørgensen, F.Z.; Lindstrøm-Svendsen, M.; Baldry, M.; Ingmer, H.; Frøkiær, H. Soluble C-Type Lectin-Receptor Ligands Stimulate ROS Production in Dendritic Cells and Potentiate Killing of MRSA as Well as the MRSA Induced IL-12 Production. *Front. Immunol.* **2022**, *13*, 1–12, doi:10.3389/fimmu.2022.845881.
 49. Arthur, J.S.C.; Ley, S.C. Mitogen-activated protein kinases in innate immunity. *Nat. Rev. Immunol.* **2013**, *13*, 679–692, doi:10.1038/nri3495.
 50. Huang, G.; Shi, L.Z.; Chi, H. Regulation of JNK and p38 MAPK in the immune system: Signal integration, propagation and termination. *Cytokine* **2009**, *48*, 161–169, doi:10.1016/j.cyto.2009.08.002.
 51. Dias, S.J.; Li, K.; Rimando, A.M.; Dhar, S.; Mizuno, C.S.; Penman, A.D.; Levenson, A.S. Trimethoxy-resveratrol and piceatannol administered orally suppress and inhibit tumor formation and growth in prostate cancer xenografts. *Prostate* **2013**, *73*, 1135–1146, doi:10.1002/pros.22657.
 52. Fulda, S. Resveratrol and derivatives for the prevention and treatment of cancer. *Drug Discov. Today* **2010**, *15*, 757–765, doi:10.1016/j.drudis.2010.07.005.
 53. Hu, Y.; Chen, D.; Zheng, P.; Yu, J.; He, J.; Mao, X.; Yu, B. The Bidirectional Interactions between Resveratrol and Gut Microbiota: An Insight into Oxidative Stress and Inflammatory Bowel Disease Therapy. *Biomed Res.*

Int. **2019**, 2019, 1-9, doi:10.1155/2019/5403761.

54. Li, H.; Jiang, N.; Liang, B.; Liu, Q.; Zhang, E.; Peng, L.; Deng, H.; Li, R.; Li, Z.; Zhu, H. Pterostilbene protects against UVB-induced photo-damage through a phosphatidylinositol-3-kinase-dependent Nrf2/ARE pathway in human keratinocytes. *Redox Rep.* **2017**, *22*, 501–507, doi:10.1080/13510002.2017.1329917.
55. Soeur, J.; Eilstein, J.; Léreaux, G.; Jones, C.; Marrot, L. Skin resistance to oxidative stress induced by resveratrol: From Nrf2 activation to GSH biosynthesis. *Free Radic. Biol. Med.* **2015**, *78*, 213–223, doi:10.1016/j.freeradbiomed.2014.10.510.
56. Wahdan, S.A.; Azab, S.S.; Elsherbiny, D.A.; El-demerdash, E. Piceatannol protects against cisplatin nephrotoxicity via activation of Nrf2/HO-1 pathway and hindering NF- κ B inflammatory cascade. *Naunyn-Schmiedeberg's Arch. Pharmacol.* **2019**, *392*, 1331–1345.
57. Espinosa-Diez, C.; Miguel, V.; Mennerich, D.; Kietzmann, T.; Sánchez-Pérez, P.; Cadenas, S.; Lamas, S. Antioxidant responses and cellular adjustments to oxidative stress. *Redox Biol.* **2015**, *6*, 183–197, doi:10.1016/j.redox.2015.07.008.
58. Bors, W.; Hellers, W.; Michel, C.; Saran, M. Radical chemistry of flavonoid antioxidants. In *Antioxidants in Therapy and Preventive Medicine*; Emerit et al. Ed.; Plenum Press, **1990**; pp. 165–170.
59. Platzer, M.; Kiese, S.; Tybussek, T.; Herfellner, T.; Schneider, F.; Schweiggert-Weisz, U.; Eisner, P. Radical Scavenging Mechanisms of Phenolic Compounds: A Quantitative Structure-Property Relationship (QSPR) Study. *Front. Nutr.* **2022**, *9*, 4–8, doi:10.3389/fnut.2022.882458.
60. Platzer, M.; Kiese, S.; Herfellner, T.; Schweiggert-Weisz, U.; Miesbauer, O.; Eisner, P. Common trends and differences in antioxidant activity analysis of phenolic substances using single electron transfer based assays. *Molecules* **2021**, *26*, 1244, doi:10.3390/molecules26051244.
61. Xiao, Z.; He, L.; Hou, X.; Wei, J.; Ma, X.; Gao, Z.; Yuan, Y.; Xiao, J.; Li, P.; Yue, T. Relationships between structure and antioxidant capacity and activity of glycosylated flavonols. *Foods* **2021**, *10*, 1–14, doi:10.3390/foods10040849.
62. Lisbeth, L.D.; Ingmer, H.; Frøkiær, H. D-alanylation of teichoic acids and loss of poly-N-acetyl glucosamine in *Staphylococcus aureus* during exponential growth phase enhance IL-12 production in murine dendritic cells. *PLoS One* **2016**, *11*, 1–20, doi:10.1371/journal.pone.0149092.
63. Charrel-Dennis, M.; Latz, E.; Halmen, K.A.; Trieu-Cuot, P.; Fitzgerald,

- K.A.; Kasper, D.L.; Golenbock, D.T. TLR-Independent Type I Interferon Induction in Response to an Extracellular Bacterial Pathogen via Intracellular Recognition of Its DNA. *Cell Host Microbe* **2008**, *4*, 543–554, doi:10.1016/j.chom.2008.11.002.
64. Mackowiak, P.A. Relationship between growth temperature and shedding of lipopolysaccharides by gram-negative bacilli. *Eur. J. Clin. Microbiol.* **1984**, *3*, 406–410, doi:10.1007/BF02017360.
65. Zanoni, I.; Ostuni, R.; Marek, L.R.; Barresi, S.; Barbalat, R.; Barton, G.M.; Granucci, F.; Kagan, J.C. CD14 controls the LPS-induced endocytosis of toll-like receptor 4. *Cell* **2011**, *147*, 868–880, doi:10.1016/j.cell.2011.09.051.
66. Nguyen, Q.T.; Furuya, Y.; Roberts, S.; Metzger, D.W. Role of interleukin-12 in protection against pulmonary infection with Methicillin-resistant *Staphylococcus aureus*. *Antimicrob. Agents Chemother.* **2015**, *59*, 6308–6316, doi:10.1128/AAC.00968-15.
67. Christensen, H.R.; Frøkiær, H.; Pestka, J.J. Lactobacilli Differentially Modulate Expression of Cytokines and Maturation Surface Markers in Murine Dendritic Cells. *J. Immunol.* **2002**, *168*, 171–178, doi:10.4049/jimmunol.168.1.171.
68. Valli, V.; Gómez-Caravaca, A.M.; Di Nunzio, M.; Danesi, F.; Caboni, M.F.; Bordoni, A. Sugar cane and sugar beet molasses, antioxidant-rich alternatives to refined sugar. *J. Agric. Food Chem.* **2012**, *60*, 12508–12515, doi:10.1021/jf304416d.
69. Mattarei, A.; Biasutto, L.; Romio, M.; Zoratti, M.; Paradisi, C. Synthesis of resveratrol sulfates: Turning a nightmare into a dream. *Tetrahedron* **2015**, *71*, 3100–3106, doi:10.1016/j.tet.2014.09.063.
70. Pettit, G.R.; Grealish, M.P.; Jung, M.K.; Hamel, E.; Pettit, R.K.; Chapuis, J.C.; Schmidt, J.M. Antineoplastic agents. 465. Structural modification of resveratrol: Sodium resverastatin phosphate. *J. Med. Chem.* **2002**, *45*, 2534–2542, doi:10.1021/jm010119y.
71. Li, W.; He, X.; Shi, W.; Jia, H.; Zhong, B. Pan-PPAR agonists based on the resveratrol scaffold: Biological evaluation and docking studies. *ChemMedChem* **2010**, *5*, 1977–1982, doi:10.1002/cmdc.201000360.
72. Beneventi, E.; Conte, S.; Cramarossa, M.R.; Riva, S.; Forti, L. Chemoenzymatic synthesis of new resveratrol-related dimers containing the benzo[b]furan framework and evaluation of their radical scavenger activities. *Tetrahedron* **2015**, *71*, 3052–3058, doi:10.1016/j.tet.2014.11.012.

Chapter 6: Design and Synthesis of Multi-Target Hybrid Compounds

6.1. Evaluation of stilbenoids antifungal activity against rice blast pathogen *Pyricularia oryzae* and combination of stilbenoid skeleton with quinone outside inhibitors (QoI) β -methoxyacrylic pharmacophore for the development of novel hybrid fungicides for crop protection.

6.2. Design and synthesis of multi-target hybrid compounds by merging QoI β -methoxyacrylate pharmacophore and succinate dehydrogenase inhibitors (SDHI) structural features.

General introduction

The alarming rate of resistance development has been demonstrating that pathogens adapt to pharmaceutical treatments too rapidly, especially to antibiotics and agrochemicals with a single mode of action. In this context, the development of antimicrobial agents with a single mode of action is no longer sustainable. This has motivated a change in drug development paradigms, shifting the focus towards molecules with multiple targets or, at least, multiple biological effects. Notably, natural phytoalexins comply with this definition and thus could be considered as a starting point for the design of novel antimicrobials.

In the past, high target specificity was associated with lower incidence of side effects, while compounds with multiple targets were considered unspecific and unsuitable for further developments. However, multi-target compounds also proved to have slower resistance development rates, thus becoming appealing in the search for innovative and resistance-breaking antimicrobials [1,2].

The concept of multi-target directed ligands (MTDL) was introduced for the first time by Cavalli and Bolognesi in 2008 [3]. Multi-modal bioactivity can be achieved by using intrinsically multi-effective, multitarget, or multifunctional compounds. Intrinsically multi-effective molecules have a single target, which is involved in multiple processes, all affected by its inhibition. Multi-target compounds act simultaneously on different molecular targets (e.g. one or more isoenzymes, proteins belonging to the same biological pathway, or even targets involved in different cellular processes), while multifunctional compounds have a direct target and an additional indirect activity (e.g. immunomodulatory properties) [4]. It should be noted that the simultaneous inhibition of distinct targets – especially if they are not connected to the same cellular process – represents a more challenging condition for microbial pathogens, which must react with different stress responses at the same time. In other words, multi-target antimicrobial agents potentially hamper pathogens' capability of adaptation, slowing down resistance development, and they could have relevant application in both the clinical and the agrochemical field. In this perspective, also combination approaches (i.e. the combined administration of two or more drugs, or tank-mix combinations of agrochemicals with different mode of action) are considered valuable tools. However, hybrid bifunctional compounds obtained by merging the pharmacophores of active molecules with different mechanisms of action into a single molecule should provide a synergistic interaction of the two active components, providing improved bioactivity and lower risk of resistance [5]. The rational design of multi-target

compounds requires the attentive selection the pharmacophores to combine, in order to achieve a balanced activity towards the targets. The selected bioactive scaffolds can be directly linked together or connected with a cleavable or not cleavable spacer, the former providing *in vivo* the parent drugs, that act on their respective target. Ester, amides, carbamates, and disulfide bonds are among the most common cleavable bonds used for this purpose. Hybrid compounds could be otherwise obtained by overlapping two different scaffolds into a new, smaller chemical entity which maintains the pharmacological properties of the original pharmacophores, despite having a substantially different structure [6]. In this chapter, the combination of natural and synthetic scaffolds endowed with antifungal activity will be discussed. Two classes of natural compounds, namely stilbenoids and strobilurins, were considered for this study. Due to their multiple biological activities, stilbenoids can be themselves considered multi-target molecules, while strobilurins are characterized by a well-known single mode of action, namely the inhibition of complex III (cytochrome *bc1*) of fungal mitochondrial respiratory chain. After the elucidation of stilbenoids antifungal properties, stilbenoid skeleton was combined with strobilurins pharmacophore (**Section 6.1**). Moreover, our efforts focused on the combination of quinone outside inhibitors with another class of synthetic fungicides, namely succinate dehydrogenase inhibitors (SDHI). The design and synthesis of QoI-SDHI hybrid compounds is part of an ongoing project, and it will be discussed in **Section 6.2**.

6.1. Evaluation of stilbenoids antifungal activity against rice blast pathogen *Pyricularia oryzae* and combination of stilbenoid skeleton with quinone outside inhibitors (QoI) β -methoxyacrylic pharmacophore for the development of novel hybrid fungicides for crop protection.

Published article:

“Stilbenoids as Antifungals to Counteract Rice Blast Pathogen *Pyricularia oryzae*” - *ACS Agric. Sci. Technol.*, 2024, 4, 1, 43–50. DOI:

<https://doi.org/10.1021/acsagscitech.3c00275>

Authors:

Andrea Kunova,[†] Cecilia Pinna,[†] Sharmila Ghosh, Denise Dozio, Cristina Pizzatti, Salvatore Princiotta, Paolo Cortesi, Sabrina Dallavalle, and Andrea Pinto.

Affiliations:

Department of Food, Environmental and Nutritional Sciences (DeFENS), University of Milan, Via Celoria 2, 20133 Milan, Italy.

Abstract

Fungi are among the greatest biotic threats to agricultural and food security. Intensive monoculture cropping and resistance to single-site fungicides in plant pathogens urge the discovery and development of novel compounds that possibly interfere with essential cellular processes in multiple ways. In this article, we describe our recent efforts addressed to the identification of natural compounds as multitarget biofungicides. A set of natural monomeric and dimeric compounds belonging to the class of stilbenoids were synthesized and tested against wild-type (*WT*) and strobilurin-resistant (*RES*) strains of *Pyricularia oryzae*, one of the most dangerous fungal phytopathogens. Monomers deoxyrhapontigenin, pinostilbene, and DMHS showed inhibitory activity higher than 40%, with deoxyrhapontigenin having the highest activity on mycelial growth (60 – 80% inhibition) on both *WT* and *RES* *P. oryzae* strains. Furthermore, we designed and synthesized a set of molecules having a nature-derived stilbene fragment merged with the pharmacophoric portion of strobilurins, namely, a β -methoxyacrylate moiety. We identified two molecules with activity comparable to the reference commercial fungicide azoxystrobin.

However, low mycelium growth inhibition of resistant strains indicates that these compounds most likely retain the strobilurin-like mechanism of action. Overall, the results suggest that natural stilbenoids might be used as environmentally friendly biofungicides in rice blast management.

KEYWORDS: *stilbenoids, antifungals, biopesticides, Pyricularia oryzae, rice blast pathogen, natural compounds.*

6.1.1. Introduction

Pyricularia oryzae is one of the most dangerous fungal phytopathogens. It is the cause of rice blast, a disease inflicting devastating crop losses in world rice production [7,8]. The current major strategies for containing rice blasts are the breeding of resistant varieties and the application of fungicides. Strobilurin based compounds are among the most effective fungicides in *P. oryzae* management and have played a big role in successful rice cultivation for decades [9,10]. Strobilurins are a very successful example of fungicides derived from natural compounds. They belong to the group of QoI (quinone outside inhibitors), which act on complex III (cyt *bc1* complex) in the mitochondrial respiration chain. Strobilurin A (**Figure 6.1**), isolated from *Strobilurus tenacellus* [11], was the first compound of this family, followed by strobilurin B and other natural analogues. Strobilurins share a very similar structure characterized by the β -methoxyacrylate pharmacophoric portion, an unsaturated bridge, and a side chain. Despite their high potency, natural strobilurins' use was hampered by their low stability, mainly due to a significant photolability [12].

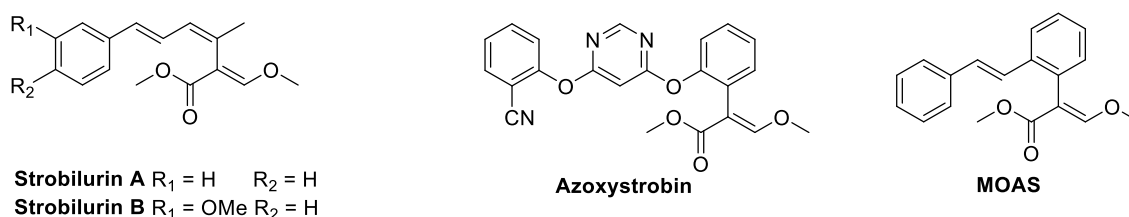


Figure 6.37. Chemical structures of the representative natural and synthetic strobilurins

Extensive chemical modifications of the strobilurin scaffold were carried out to improve the physical characteristics of the parent compounds. The first stable synthetic strobilurin, featuring a benzene ring in place of the central double bond of the original triene system, was methoxyacrylate stilbene (MOAS), which immediately became a lead synthetic strobilurin because of its stability and increased potency [13,14]. Successive studies led to the introduction into the market of various synthetic analogs, featuring broad structural variations on

the side chain as well as bioisosters of the (*E*)-methoxyacrylate group (e.g., azoxystrobin, **Figure 6.1**). Notwithstanding their enormous potential, strobilurins' single-site mode of action makes them prone to the development of resistance in fungal pathogen populations. Strobilurin resistance, most often caused by a single nucleotide mutation G143A (substitution of glycine at position 143 for alanine), is nowadays widespread and has been described in more than 50 different fungal plant pathogens, among which also *P. oryzae* [15]. This evidence poses a threat to the global rice growing sector, as widespread distribution of such resistant strains would seriously compromise rice production. Often, especially in Europe, there is a lack of valid registered alternatives to strobilurins, leaving farmers without adequate means for rice blast management. The current situation urges the discovery and development of novel, highly effective compounds to control both wild-type and QoI-resistant populations of *P. oryzae*. In the past decade, the agrochemical industry has refocused its priorities moving toward the use of biological control agents (BCAs), including naturally occurring substances, for an integrated pest management (IPM) program [16]. Recently, the use of natural products from plant extracts as biofungicides has received increasing attention because of their high diversity and versatility. Especially in the context of sustainable agricultural development, research on the transformation of agricultural byproducts into high-value-added extracts or molecules has been intensified. Several active plant byproduct extracts from *Vitaceae*, *Leguminaceae*, *Gnetaceae*, and *Dipterocarpaceae* contain natural compounds belonging to the class of stilbenoids, a family of nonflavonoid phenylpropanoids structurally characterized by the presence of a 1,2-diphenylethylene unit [17]. A comprehensive understanding of the mode of action of stilbenoids as antifungals has not yet been completely elucidated. Current evidence suggests multiple mechanisms of action spanning from disruption of the cell wall and membrane to epigenetic effects and interference with fungal mitochondrial functions [17,18]. These findings hold promise for the development of new multitarget biofungicides containing stilbenoid skeletons to protect plants from fungal phytopathogens. Remarkably, it has been demonstrated that the production of stilbenoids by plants can be activated by adverse conditions, e.g., fungal infections [19,20]. Stark-Lorenzen and co-workers indicated an enhanced resistance to *P. oryzae* of transgenic rice obtained by stable integration and expression of a gene coding for stilbene synthase from grapevine (*Vitis vinifera*) [21]. More recently, Niu et al. [22] reported that stilbenoids found in dragon's blood of *Dracaena cochinchinensis*, elicited by fungal species, showed promising activities as natural fungicides. Additionally, Cai et al. demonstrated the inhibitory effects of stilbenes on fungal mycelium growth and spore

germination [23]. In this work, we report the biological activity of a set of natural monomeric and dimeric stilbenoids (**Figure 6.2**) against rice blast, both strains sensitive and resistant to strobilurin fungicides. To the best of our knowledge, this is the first study investigating the antifungal activity of a set of plant-derived stilbenoids on *P. oryzae* strains.

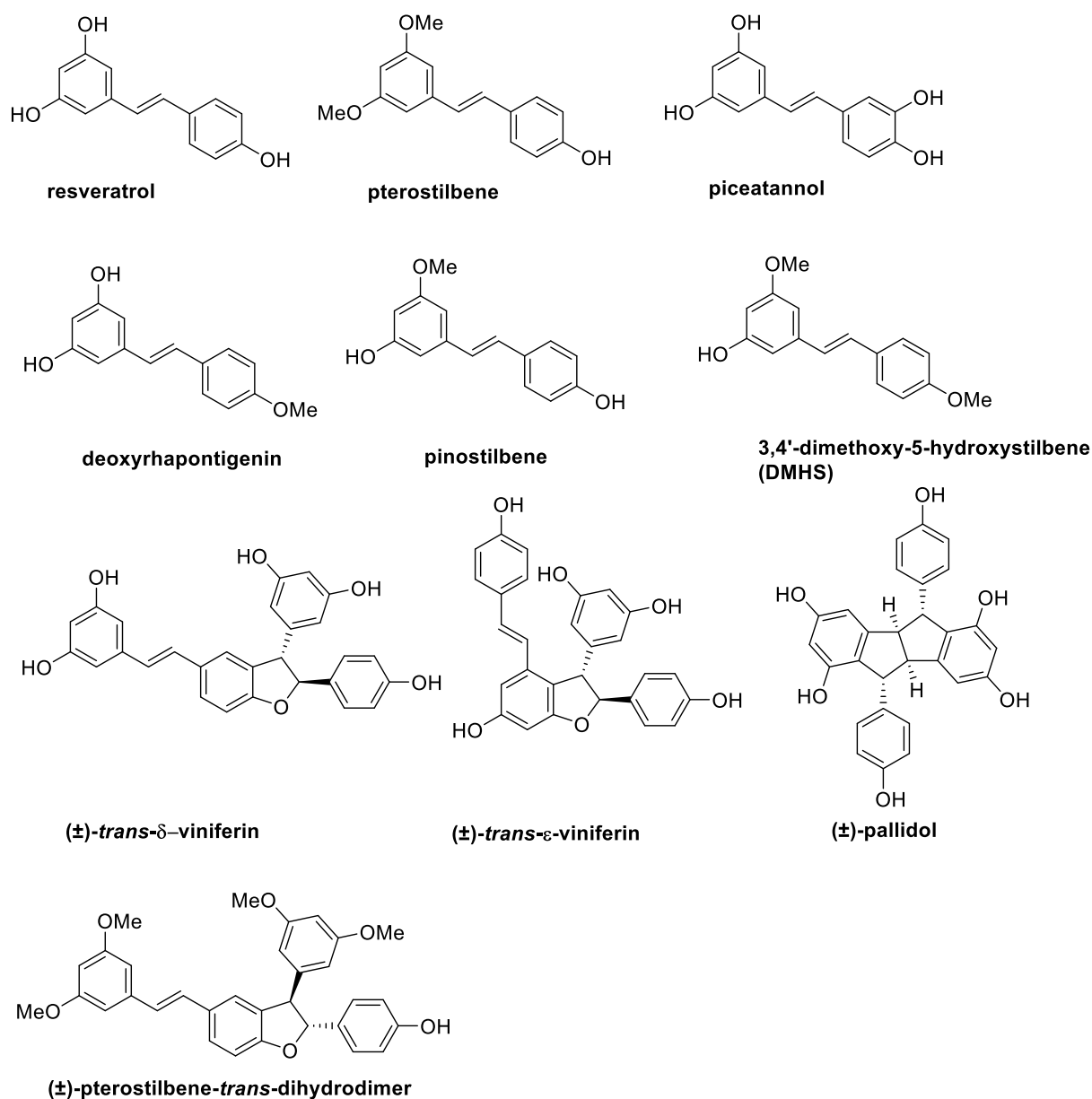


Figure 6.38. Structures of natural stilbenoids investigated in this study.

Additionally, taking inspiration from the first synthetic MOAS (**Figure 6.1**), which featured the stilbene moiety linked to the strobilurin pharmacophore, we designed and synthesized a small series of potential multitarget fungicides in which the stilbenoid skeleton was combined with the strobilurin β -methoxyacrylate moiety. The use of such multitarget fungicides could

eventually limit the onset and spread of fungicide resistance, mainly promoted by repeated treatments by agents having a single-site mechanism of action. The contribution to the biological activity of hydroxy and methoxy groups on the aromatic ring was investigated for both natural and synthetic stilbenoids to rationalize the design of novel hybrid molecules.

6.1.2. Results and Discussion

Chemistry: Synthesis of Target Compounds.

We prepared a set of natural stilbenoids including monomers (resveratrol, pterostilbene, piceatannol, deoxyrhapontigenin, pinostilbene, and 3,4'-dimethoxy-5-hydroxystilbene) and dimers (*trans*- δ -viniferin, pterostilbene-*trans*-dihydrodimer, *trans*- ϵ -viniferin, and pallidol) (**Figure 6.2**) to have an overview of the natural compounds' antifungal activity. All of these molecules were synthesized following previously reported procedures [24,25]. Synthetic procedures for the preparation of piceatannol, 3,4'-dimethoxy-5-hydroxy stilbene (DMHS) and *trans*- δ -viniferin were reported in detail in **Section 5.2.6**. Deoxyrhapontigenin and pinostilbene were prepared by partial methylation of resveratrol with CH₃I and K₂CO₃ (2 eq.), while resveratrol dimers were obtained through oxidative radical couplings with FeCl₃ (ϵ -viniferin) or horseradish peroxidase HRP (*trans*- δ -viniferin, pterostilbene-*trans*-dihydrodimer, and pallidol). Notably, monomers treatment with HRP at pH 5 afforded δ -viniferin and pterostilbene-dihydrodimer, while the same procedure in basic environment (pH 8) gave pallidol as the main product. Successively, prompted by our recent interest in the development of multitarget antifungals [26,27] and taking inspiration from the structure of MOAS, we designed and synthesized a set of molecules having the QoI pharmacophore merged with a nature-derived stilbene fragment. The series included the unsubstituted MOAS (**1**) itself and five analogues decorated with phenolic and methoxy groups (**Figure 6.3**).

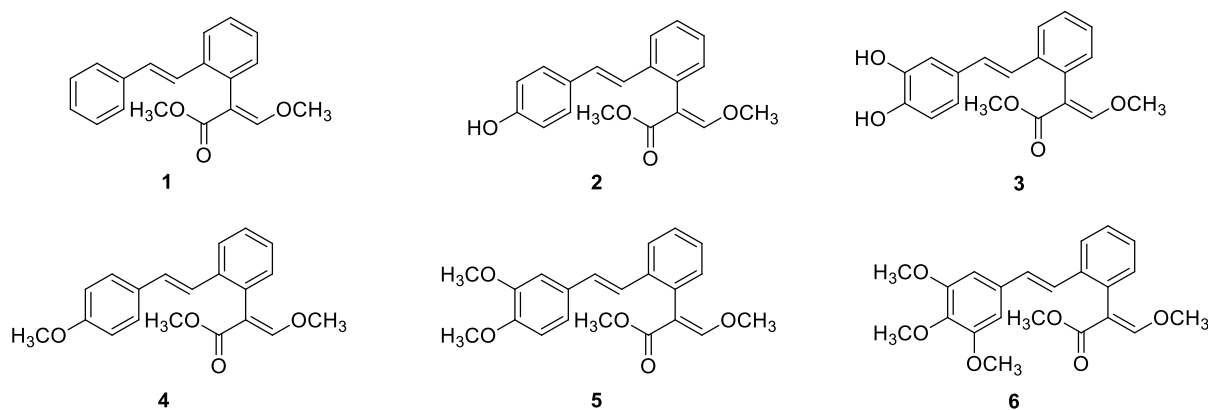
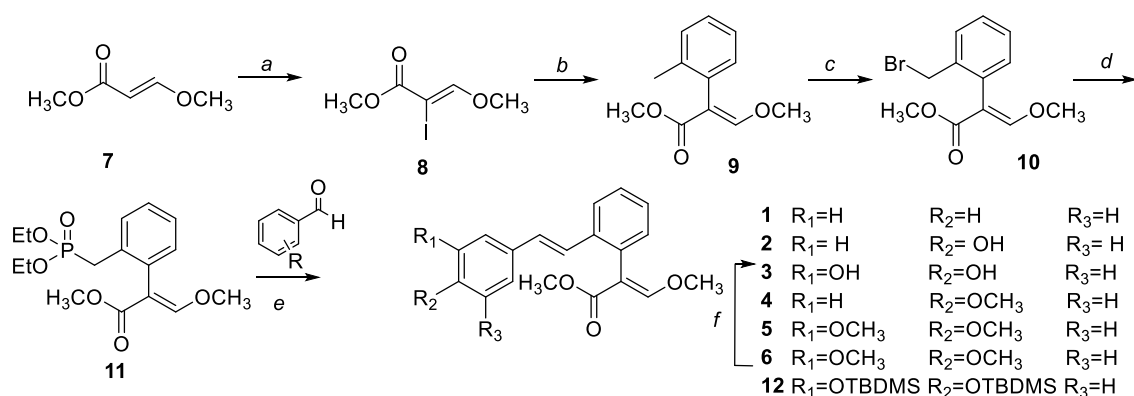


Figure 6.39. Chemical structures of the synthesized methoxyacrylate stilbene hybrids (MOAS)



Scheme 6.7. Synthesis of compounds 1-6. Reagents and conditions: (a) (1) NIS, AcOH, DCM, rt, 24 h; (2) TEA, DCM, rt, 16 h, 62%; (b) 2-tolylboronic acid, Pd(PPh₃)₄, K₃PO₄, Dioxane:H₂O 5:1, 90 ° C, 6 h, 76%; (c) NBS, AIBN, CCl₄, reflux, 6 h, 69%; (d) P(OEt)₃, 130 ° C, overnight, N₂, 54%. (e) NaH, THF, N₂, 0 ° C → rt, 20%; (f) From 12 to 3: TBAF, THF 0 ° C → rt, 1 h, 25%.

The synthetic route of compounds 1-6 involved the Suzuki coupling of α -iodo- β -methoxyacrylate 8 with 2-tolylboronic acid, to give 2-methyl aryl-BMA 9, which was converted into the corresponding benzyl bromide by radical bromination in the presence of *N*-bromosuccinimide (NBS) [26]. Benzyl bromide underwent a Michaelis-Arbuzov reaction, giving the key phosphonate intermediate 11 that was finally reacted with variously substituted aromatic aldehydes in a Horner-Wadsworth-Emmons (HWE) olefination (Scheme 1). The preparation of compound 3 involved the protection of 3,4-dihydroxy benzaldehyde with *tert*-butyldimethylsilyl chloride in the presence of imidazole and dichloroethane as a solvent to give compound 12 upon reaction with phosphonate 11. Silyl groups were eventually removed by treatment with tetrabutylammonium fluoride (TBAF) to afford compound 3.

Evaluation of the Antifungal Activity of Natural Stilbenoids and Methoxyacrylate-Stilbene Hybrids.

The biological activity of the natural stilbenoids and synthesized methoxyacrylate-stilbene hybrids was evaluated by assessing the inhibition of mycelium growth of two strobilurin-sensitive or wild-type (WT, A252 and TA102) and two strobilurin-resistant (RES, PO1312 and PO1335) strains of *P. oryzae*. The compounds were dissolved in DMSO or acetone (ACT) (see the Experimental Section for details). DMSO at a final concentration of 1% in the growth medium slightly inhibited the growth of the used *P. oryzae* strains (11% growth inhibition), while 1% ACT did not have any inhibitory effect on the growth of the strains.

Biological Evaluation of Natural Stilbenoids.

The inhibitory activity of natural stilbenoids (**Figure 6.2**) against WT and RES strains of *P. oryzae* was assessed at 200 μ M concentration (**Figure 6.4**). Specifically, resveratrol showed only minimal inhibition of mycelium growth of all tested strains. Introducing an additional -OH group on C-3 in piceatannol completely abolished its biological activity. Interestingly, replacing a phenolic -OH in resveratrol skeleton with one methoxy group (4'-OCH₃ in deoxyrhapontigenin

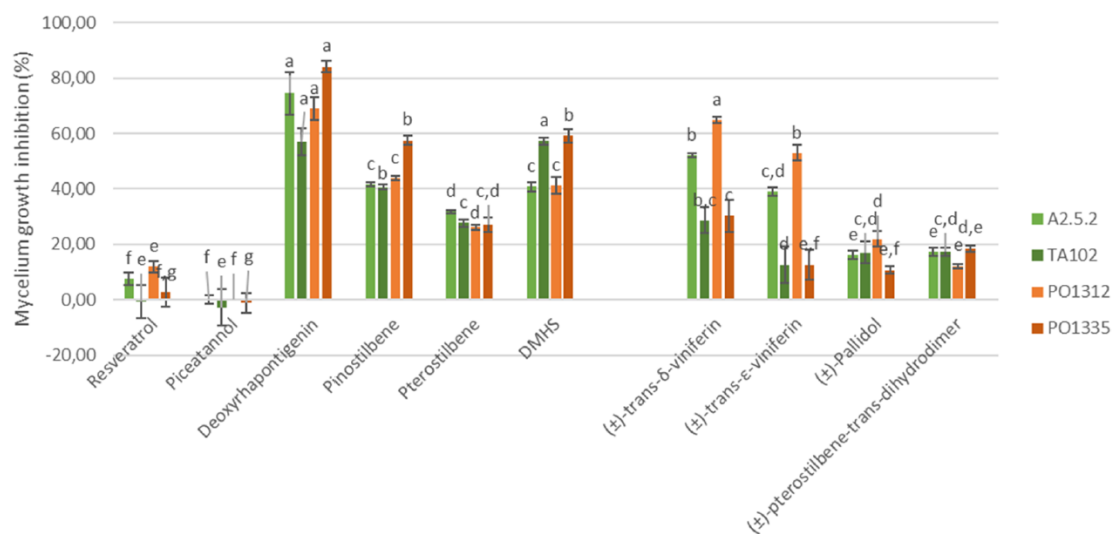


Figure 6.40. Inhibitory activity of natural stilbenes on mycelium growth of *P. oryzae* wild-type (green; A2.5.2 and TA102) and strobilurin-resistant (orange; PO1312, PO1335) strains. The error bars represent the standard deviation. Bars of the same color (the same strain) with different letters are statistically different (Tukey's HSD, $p \leq 0.05$).

and 3-OCH₃ in pinostilbene) drastically improved the activity, with 60–80% inhibition by deoxyrhapontigenin even on strobilurin-resistant strains. The position of the methoxy group seems to play a major role, as deoxyrhapontigenin shows almost double the activity of pinostilbene. The introduction of two methoxy groups was shown to be detrimental, with a reduction of activity for both DMHS (40-60%) and pterostilbene (25-30%) on WT and RES strains. Among dimers, the most active natural compound was δ -viniferin (40–60% mycelial growth inhibition), followed by the other resveratrol-derived dimer ϵ -viniferin (35-55%). Pallidol showed a modest activity (20%) as well as the tetramethoxy derivative pterostilbene dihydrodimer (15-20%). To investigate the potential correlation between the efficacy of the tested natural compounds and their physicochemical properties, Log P, and hydrophilic-lipophilic balance (HLB) were calculated using the ChemAxon calculation method on Marvin Sketch 23.7. More specifically,

methylated monomers, showing significant inhibition profiles (40-80%), are characterized by cLog P and HLB values in the range 3.55-3.69% and 7.91-8.30, respectively. Conversely, more polar compounds resveratrol and piceatannol are considerably less active in inhibiting mycelium growth (Table 6.1).

Table 6.4. Calculated Values of log *P* and HLB for Each Compound in Relation to the Antifungal Activity ^a

Compound	cLog P	HLB	Mycelium growth inhibition (%)
Deoxyrhapontigenin	3.55	8.30	60-80
DHMS	3.69	7.91	40-60
Pinostilbene	3.55	8.30	40-60
Pterostilbene	3.69	7.91	25-30
Resveratrol	3.40	8.66	10-15
Piceatannol	3.10	10.55	0
trans- δ -viniferin	5.96	9.35	40-60
trans- ϵ -viniferin	5.96	9.35	35-55
Pallidol	5.31	8.93	20
Pterostilbene-trans-dihydrodimer	6.54	7.29	15-20

^a c Log *P* and HLB values were obtained by using the ChemAxon calculation method on Marvin Sketch 23.7.

Among tested dimers, the most active δ - and ϵ -viniferin show cLog P = 5.96 and HLB > 9. Lower activities are observed for pallidol with HLB = 8.93, and pterostilbene-*trans*-dihydrodimer characterized by a higher degree of methylation, with HLB = 7.29. Importantly, other properties apart from cLog P and HLB, i.e., 3D shape, geometry, and substitution pattern (substituent and position involved), could play a crucial role in the observed biological effect. In general, the similar behavior of all natural compounds on both *WT* and *RES* strains evidence that they are not sensitive to the G143A mutation present in *RES* strains. Importantly, this result confirms that the promising activity of this class of natural compounds is not related to cyt *bc1* complex inhibition and supports the idea of creating multitarget strobilurin-stilbenoid antifungals. As deoxyrhapontigenin showed the best mycelium inhibition at a concentration of 200 μ M, we studied its activity in a more detailed, quantitative way. The mycelium growth of the four strains was assessed at diverse concentrations ranging from 5 to 200 μ M (Figure 6.5). From the data, the ED₅₀, the compound concentration that causes 50% mycelium growth inhibition, was calculated

using the 3-parameter log-logistic model (Table 6.2). The ED₅₀ value ranged from 122.3 to 237.9 μM among the four tested strains.

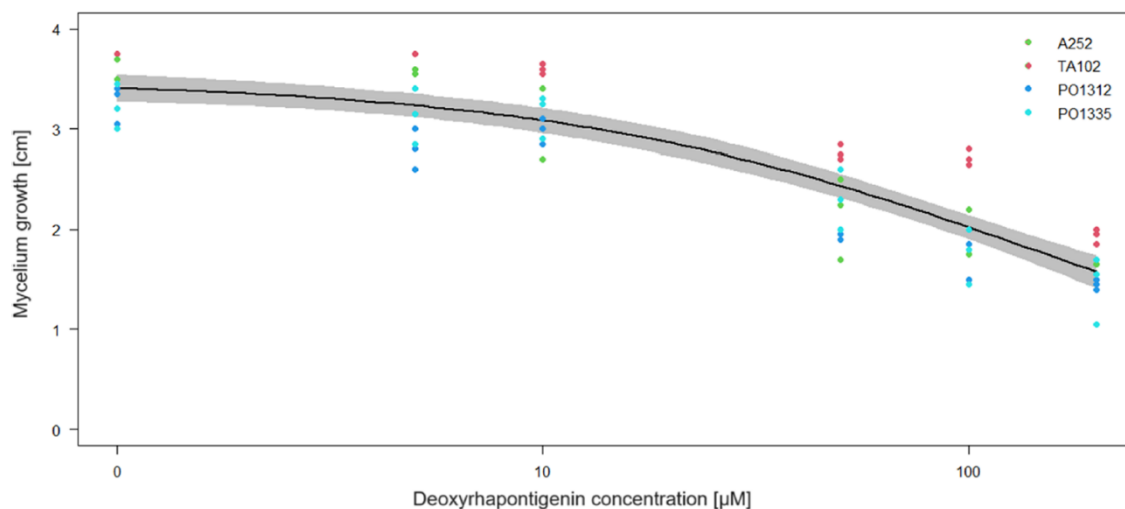


Figure 6.41. Mycelium growth dose-response curve of *P. oryzae* to increasing concentrations of deoxyrhapontigenin measured after 7 days of growth. The curve (black line) was calculated using the 3-parameter log-logistic model. The 95% confidence interval is depicted by gray shadow. The data of the four strains are indicated by colored dots.

Biological Evaluation of Synthetic Methoxyacrylate-Stilbene Hybrids.

We designed and synthesized a set of molecules having the QoI pharmacophore merged with a nature-derived stilbene fragment. The newly obtained compounds **1-6** were screened on the same wild type (WT, A252 and TA102) and strobilurin-resistant (*RES*, PO1312 and PO1335) strains of *P. oryzae* previously used to assess the activity of natural stilbenoids (Figure 6.6).

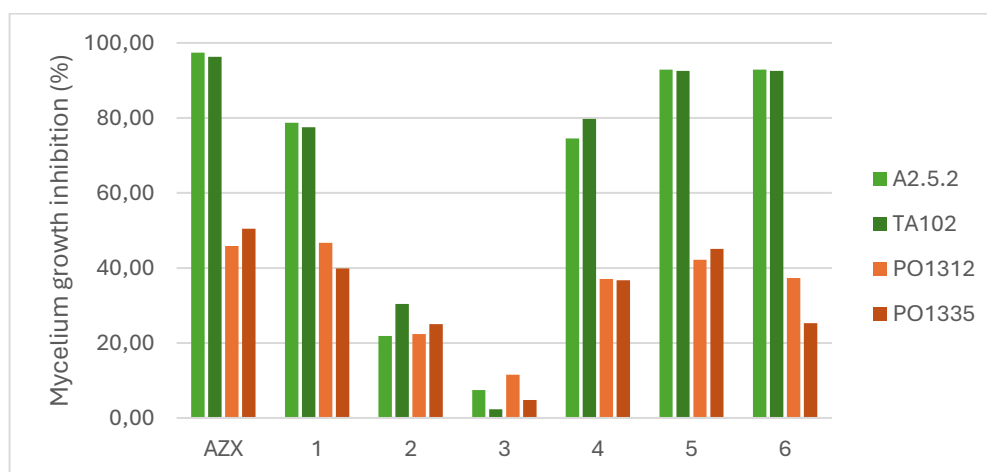


Figure 6.42. Inhibitory activity of MOAS hybrids **1-6** on mycelium growth of *P. oryzae* wild-type (green; A2.5.2, and TA102) and strobilurin-resistant (orange; PO1312, PO1335) strains. Azoxystrobin (AZX) was used as a reference compound. The error bars represent standard deviation. Bars of the same color (the same strain) with different letters are statistically different (Tukey's HSD, $p \leq 0.05$).

The synthesized hybrid molecules were tested at a final concentration of 25 mg/L, the same as that of the reference commercial fungicide azoxystrobin (AZX). AZX inhibited >90% of the growth of *WT* strains, while the *RES* strains were inhibited to <50%, confirming the influence of the G143A mutation on the activity of strobilurin fungicides. As expected, MOAS (**1**) showed a slightly lower activity on *WT* strains (<80%) compared to the commercial fungicide AZX. The introduction of polar phenolic -OH groups in compounds **2** and **3** had a deleterious effect. Increasing the number of methoxy groups from one (compound **4**) to two (compound **5**) improved the biological activity against *WT* strains from ca. 70 to >90% inhibition, respectively. An additional methoxy group in compound **6**, however, did not further boost its activity. These results highlight that the presence of methoxy groups, and their number should be considered to be a crucial parameter for the activity in *WT* strains. On the other hand, lower biological activity was observed on resistant strains (20-45%), suggesting that the most active methoxyacrylate-stilbene hybrids still act as strobilurin fungicides, being sensitive to the presence of the G143A mutation in *cyt bc1* complex. Our efforts allowed us to identify methylated stilbenoids as a promising class of natural fungicides with a low environmental impact. In particular, the monomers deoxyrhapontigenin, pinostilbene, and DMHS showed inhibitory activity higher than 40%, with deoxyrhapontigenin having the highest activity on mycelial growth (60-80% at 200 μ M concentration). Remarkably, the comparable inhibition of both *WT* and *RES* strains by the tested natural compounds outlined a mechanism of action different from strobilurins. Overall, this study suggests that natural stilbenoids might be developed into environmentally friendly biofungicides for rice blast management. Current research activities are dedicated to the evaluation of other natural chemotypes to be combined and conjugated with the most promising stilbenoids identified in this work.

6.1.3 Materials and methods

Chemistry: Synthesis of natural stilbenoids

All reagents and solvents were purchased from commercial suppliers and used without further purification. The ^1H NMR and ^{13}C NMR spectra were recorded with a Bruker AV600 (^1H , 600 MHz; ^{13}C , 150 MHz) and a Bruker AMX-300 (^1H , 300 MHz; ^{13}C 75 MHz) spectrometer. Chemical shifts (δ) are expressed in ppm and coupling constants (J) are in hertz. All reactions requiring anhydrous conditions were performed under a positive nitrogen flow, and all glassware

^{13}C NMR (75 MHz, CDCl_3) δ (ppm): 162.5, 159.7, 158.4, 141.3, 130.3, 129.9, 129.8, 128.9 (x2C), 116.5 (x2C), 106.6, 104.4, 101.4, 55.6 from [28].

Pinostilbene:

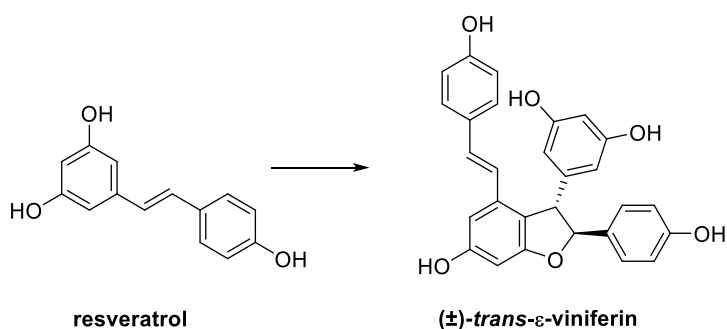
M.p.: 176-178°C

R_f: 0.29 (DCM/AcOEt 92:8)

^1H NMR (300 MHz, $\text{DMSO}-d_6$) δ (ppm): 9.19 (s, 2H), 7.54 – 7.47 (m, 2H), 7.01 – 6.82 (m, 4H), 6.39 (d, $J = 2.1$ Hz, 2H), 6.11 (t, $J = 2.1$ Hz, 1H), 3.75 (s, 3H).

^{13}C NMR (75 MHz, $\text{Acetone}-d_6$) δ (ppm): 160.1, 159.2 (x2C), 140.5, 130.7, 128.8, 128.5 (x2C), 127.4, 114.8 (x2C), 105.8 (x2C), 102.9, 55.8 from [29].

Synthesis of 5-((2S,3S)-6-hydroxy-2-(4-hydroxyphenyl)-4-((E)-4-hydroxystyryl)-2,3-dihydrobenzofuran-3-yl) benzene-1,3-diol, (**trans- ϵ -viniferin**)



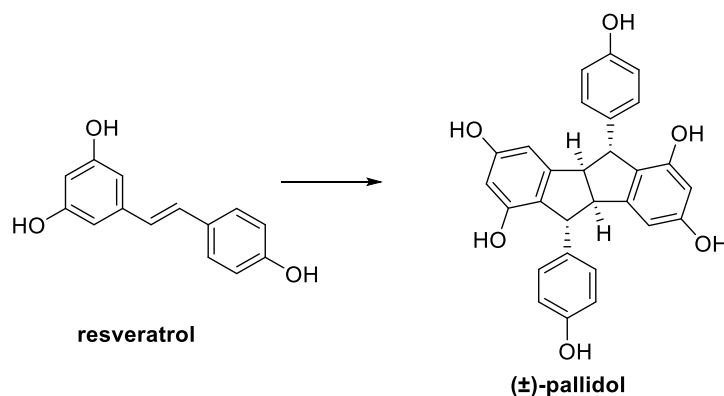
To a solution of resveratrol (2 g, 8.76 mmol, 1 eq) in MeOH (20 mL) a solution of $\text{FeCl}_3 \cdot 6\text{H}_2\text{O}$ (2.39 g, 8.85 mmol, 1.01 eq) in water (20 mL) was added dropwise. The mixture was stirred at room temperature for 48 hours. MeOH was evaporated and the residue was diluted with water (30 mL) and extracted with AcOEt (4 x 50 mL). The combined organic layers were dried over anhydrous Na_2SO_4 and concentrated under reduced pressure. The residue was purified by flash chromatography (cyclohexane/acetone 3:2) and a mixture of (\pm)-*trans*- and *cis*-analogue was obtained. A further purification by reverse phase column chromatography ($\text{H}_2\text{O}/\text{MeOH}$ 2:3) gave the desired product as a light green amorphous solid in 15% yield. Analytical data were in agreement with those reported in literature [30].

R_f: 0.30 (cyclohexane/acetone 3:2) - 0.42 ($\text{H}_2\text{O}/\text{MeOH}$ 2:3)

^1H NMR (300 MHz, CD_3OD) δ (ppm): 7.18 – 7.11 (m, 2H), 7.07 – 7.01 (m, 2H), 6.86 – 6.73 (m, 3H), 6.64 (dd, $J = 8.7, 2.1$ Hz, 3H), 6.56 (d, $J = 16.3$ Hz, 1H), 6.25 (d, $J = 2.1$ Hz, 1H), 6.20 – 6.14 (m, 3H), 5.36 (d, $J = 6.6$ Hz, 1H), 4.34 (d, $J = 6.6$ Hz, 1H).

^{13}C NMR (100 MHz, CD_3OD) δ (ppm): 162.8, 160.1, 159.8, 159.7, 158.5, 158.4, 147.4, 137.0, 136.9, 133.9, 130.5, 130.4, 128.8, 128.2, 123.8, 123.7, 120.1, 116.4 (x2C), 116.3 (x2C), 107.5 (x2C), 104.4, 102.2, 96.9, 94.9, 58.3.

Synthesis of (4*b*R,5*R*,9*b*R,10*R*)-5,10-bis(4-hydroxyphenyl)-4*b*,5,9*b*,10-tetrahydroindeno[2,1-*a*] indene-1,3,6,8-tetraol (pallidol)



To a solution of resveratrol (1 g, 4.38 mmol, 1 eq) in a mixture of acetone/phosphate buffer (pH 8) 1:1 (43.8 mL), a solution of HRP (1.75 mL, 1 mg/mL aqueous solution) was added at 40°C and the resulting mixture was stirred for 30 minutes. Then, H_2O_2 30% (0.66 mL) was added, and the mixture was stirred at the same temperature for one hour. Then, acetone was evaporated, and aqueous layer was extracted with AcOEt (3 x 50 mL). The combined organic layers were washed with brine, dried over anhydrous Na_2SO_4 , and concentrated under reduced pressure. The residue was purified by flash column chromatography (DCM/MeOH 85:15) to give the desired product as a brown solid in 21% yield. Analytical data were in agreement with those reported in literature [31].

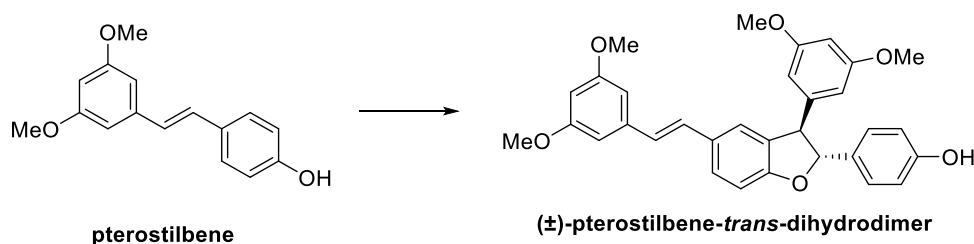
M.p.: dec. $T > 296^\circ\text{C}$

R_f: 0.15 (DCM/MeOH 9:1)

^1H NMR (300 MHz, CD_3OD) δ (ppm): 6.99 – 6.87 (m, 4H), 6.73 – 6.59 (m, 4H), 6.52 (d, $J = 2.1$ Hz, 2H), 6.10 (d, $J = 2.1$ Hz, 2H), 4.46 (s, 2H), 3.72 (s, 2H).

^{13}C NMR (75 MHz, Acetone- d_6) δ (ppm): 159.3 (x2C), 156.3 (x2C), 155.3 (x2C), 150.3 (x2C), 137.7 (x2C), 129.0 (x4C), 123.2 (x2C), 115.8 (x4C), 103.3 (x2C), 102.5 (x2C), 60.5 (x2C), 53.9 (x2C).

Synthesis of 4-((2R,3R)-3-(3,5-dimethoxyphenyl)-5-((E)-3,5-dimethoxystyryl)-2,3-dihydrobenzofuran-2-yl)phenol (pterostilbene-trans-dihydrodimer)



To a solution of pterostilbene (100 mg, 0.39 mmol, 1 eq) in a mixture of acetone/citrate buffer (pH 5) 1:1 (3.8 mL), a solution of HRP (160 μ l, 1 mg/mL aqueous solution) was added at 40°C and stirred for 30 minutes. Then H₂O₂ 30% (59 μ l, 0.573 mmol, 1.47 eq) was added and the mixture was stirred at the same temperature for 15 min. Then, acetone was evaporated, and the aqueous layer was extracted with AcOEt (3 x 50 mL). The combined organic layers were washed with brine, dried over anhydrous Na₂SO₄, and concentrated under reduced pressure. The residue was purified by flash column chromatography (cyclohexane/AcOEt 7:3) to give the desired product as a white amorphous solid in 61% yield. Analytical data were in agreement with those reported in literature [32].

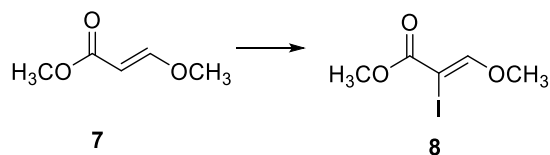
R_f: 0.2 (cyclohexane/AcOEt 3:1)

¹H NMR (300 MHz, CDCl₃) δ (ppm): 7.37 (dd, $J_1 = 8.3$, $J_2 = 0.8$ Hz, 1H), 7.24 – 7.19 (m, 3H), 7.02 (d, $J = 16.2$ Hz, 1H), 6.92 (d, $J = 8.3$ Hz, 1H), 6.88 – 6.78 (m, 3H), 6.62 (d, $J = 2.3$ Hz, 2H), 6.41 (t, $J = 2.2$ Hz, 1H), 6.36 (t, $J = 2.2$ Hz, 1H), 6.34 (d, $J = 2.2$ Hz, 2H), 5.51 (d, $J = 8.4$ Hz, 1H), 4.48 (d, $J = 8.4$ Hz, 1H), 3.81 (s, 6H), 3.75 (s, 6H).

¹³C NMR (75 MHz, CDCl₃) δ (ppm): 161.2 (x2C), 161.0 (x2C), 159.8, 156.0, 144.0, 139.8, 132.6, 132.3, 132.1, 130.9, 130.8, 129.1, 128.8, 128.0, 127.6, 126.3, 123.2, 115.6 (x2C), 109.8, 106.5 (x2C), 104.3 (x2C), 99.8, 57.9 (x2C), 55.5 (x2C).

Synthesis of methoxyacrylate-stilbene (MOAS) hybrids

Synthesis of Methyl (Z)-2-Iodo-3-methoxypropenoate (8).



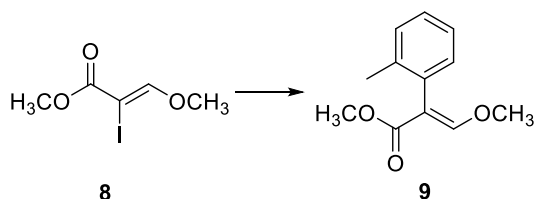
To a solution of β -methoxyacrylate (4.177 mmol) in dichloromethane (8.6 ml) 1.1 eq of *N*-iodosuccinimide and 2 eq of glacial acetic acid were added. The obtained solution was stirred at room temperature for 24 hours. Then, 3 eq of triethylamine were added and the reaction mixture was stirred for 12 hours. After completion, reaction mixture was diluted with water (15 ml) and extracted three times with Et₂O. The combined organic layers were washed with Na₂S₂O₃ (saturated solution) and NaHCO₃ (sat.), dried over Na₂SO₄ and the solvent was evaporated. The crude product was purified by column chromatography (cyclohexane/ethyl acetate 5:1 \rightarrow 85:15) giving **8** as a yellow solid in 62% yield. Spectroscopic data were in accordance with those reported in literature [26].

M.p.: 50-52 °C

¹H NMR (300 MHz, CDCl₃) δ : 7.68 (1H, s); 4.01 (3H, s); 3.81 (3H, s).

¹³C NMR (75 MHz, CDCl₃) δ 52.8, 62.0, 64.8, 164.2, 164.3.

Synthesis of methyl (E)-2-(2-methylphenyl)-3-methoxyacrylate (9).

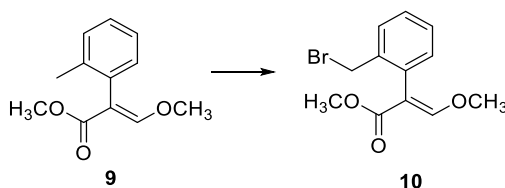


Compound **8** (300 mg, 1.240 mmol) was dissolved in a previously degassed 5:1 mixture of dioxane: H₂O (5.3 ml) under a nitrogen atmosphere. 2-methyl-1-phenylboronic acid (1.2 eq) and K₃PO₄ (3 eq) were added, and the obtained mixture was degassed again with nitrogen over 45 minutes. Then, Pd(PPh₃)₄ (0.5 mol%) was added and the reaction mixture was stirred for 8 hours at 90°C in the dark. After this time, the reaction mixture was cooled to room temperature, diluted with ethyl acetate (10 ml) and washed with water and brine. The organic layer was dried over Na₂SO₄, filtered and the solvent was evaporated. The crude product was purified by column chromatography (cyclohexane/ethyl

acetate 85:15) giving **9** as a colorless oil in 76% yield. Spectroscopic data are in agreement with those reported in literature [33].

$^1\text{H NMR}$ (600 MHz, CDCl_3) δ 7.57 (s, 1H), 7.24 – 7.21 (m, 2H), 7.21 – 7.14 (m, 1H), 7.11 (d, $J = 7.1$ Hz, 1H), 3.82 (s, 3H), 3.70 (s, 3H), 2.19 (s, 3H).

Synthesis of methyl (E)-2-(2-(bromomethyl) phenyl)-3-methoxyacrylate (**10**).

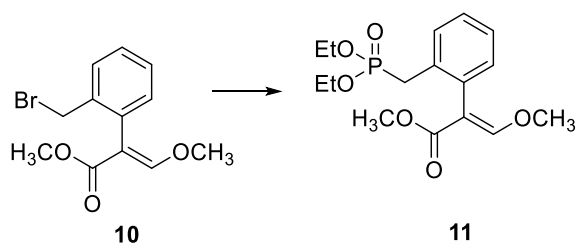


To a solution of methyl (E)-2-(2-methylphenyl)-3-methoxyacrylate **9** (0.9213 mmol) in anhydrous carbon tetrachloride (4.6 ml), 1.1 eq of *N*-bromosuccinimide (NBS) and 0.2 eq of 2,2'-azo-bisisobutyronitrile (AIBN) were added. The obtained suspension was heated to reflux and stirred for 6 hours in the dark under a nitrogen atmosphere. After completion, reaction mixture was cooled to room temperature and filtered. The filtrate was evaporated under reduced pressure. Purification by column chromatography (CyHex/EtOAc 8:2) afforded the desired product as a white solid in 64% yield. Spectroscopic data are in agreement with those reported in literature [33].

M.p.: 64-65 °C

$^1\text{H NMR}$ (600 MHz, CDCl_3) δ 7.64 (d, $J = 1.4$ Hz, 1H), 7.49 – 7.45 (m, 1H), 7.32 (m, 2H), 7.15 – 7.11 (m, 1H), 4.41 (s, 2H), 3.84 (d, $J = 1.4$ Hz, 3H), 3.71 (d, $J = 1.4$ Hz, 3H).

Synthesis of Methyl (E)-2-(2-((Diethoxyphosphoryl)methyl)phenyl)-3-methoxyacrylate (**11**).

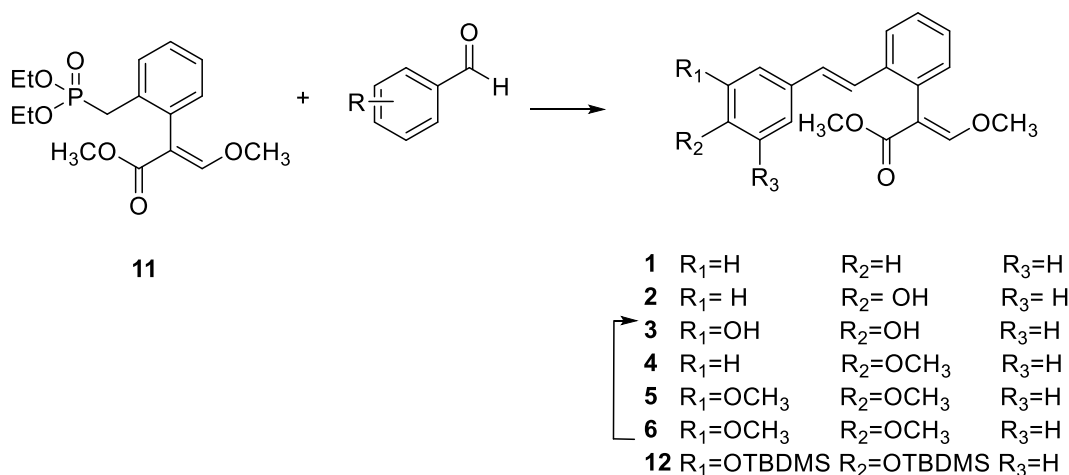


Methyl (E)-2-(2-(bromomethyl) phenyl)-3-methoxyacrylate **10** (0.64 mmol, 1 eq) was dissolved in 0.300 mL of triethyl phosphite ($\text{P}(\text{OEt})_3$, 1.72 mmol, 2.7 eq). The resulting solution was heated to 130 ° C and stirred for 6 h. After reaction completion, $\text{P}(\text{OEt})_3$ was evaporated under reduced pressure, and the crude

product was purified by column chromatography (cyclohexane/ acetone 6:4). Compound **11** was obtained as a yellow oil in a 93% yield.

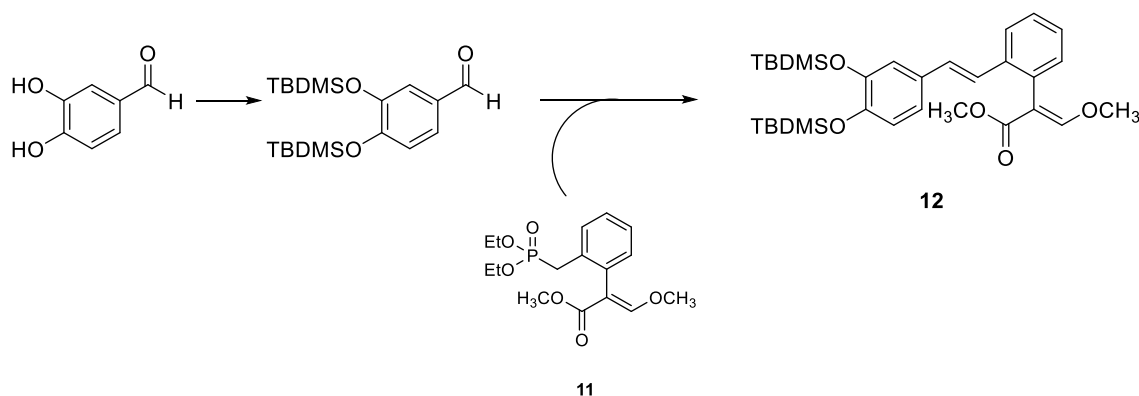
$^1\text{H NMR}$ (300 MHz, CDCl_3) δ : 7.58 (s, 1H), 7.52 (d, $J = 7.5$ Hz, 1H), 7.3 (m, 2H), 7.13 (d, $J = 7.5$, 1H), 3.96 (m, 2H), 3.83 (s, 3H); 3.70 (s, 3H); 3.10 (m, 2H).

General Procedure for the Horner–Wadsworth–Emmons (HWE) Olefination of Methyl(*E*)-2-(2-((Diethoxyphosphoryl)-methyl)phenyl)-3-methoxyacrylate (**11**) with Substituted Aldehydes (**1–6**).



A solution of 0.5M methyl (*E*)-2-(2-((diethoxyphosphoryl)methyl)phenyl)-3-methoxyacrylate **11** (0.22 mmol, 1.1 eq) and the proper aldehyde (0.20 mmol, 1 eq) in dry THF was cautiously dropped into a round-bottom flask containing 1 mmol of NaH (5 eq) in 0.50 mL of dry THF cooled at 0 ° C under nitrogen atmosphere. The obtained reaction mixture was stirred at room temperature for 2 hours and then quenched with 0.5M HCl. The aqueous layer was exhaustively extracted with ethyl acetate, and the combined organic layers were dried over Na_2SO_4 , filtered, and the solvent was evaporated under reduced pressure. The crude products were purified by column chromatography as described below.

Methyl (E)-2-(2-((E)-3,4-Bis((tert-butyldimethylsilyl)oxy)-styryl)phenyl)-3-methoxyacrylate (12).



3,4-Dihydroxy benzaldehyde (200 mg, 1.45 mmol) was suspended in dry dichloroethane (14.5 mL) under a nitrogen atmosphere. Imidazole (295 mg, 3 eq) and *tert*-butyldimethylsilyl chloride (570 mg, 2.6 eq) were added to the suspension, and the obtained reaction mixture was warmed to 60 ° C and stirred for 6 hours. After reaction completion, the suspension was cooled to room temperature and washed with brine. The aqueous layer was extracted with dichloromethane, the organic layers were dried over Na₂SO₄, filtered, and the solvent was evaporated. The crude product was purified by column chromatography (cyclohexane/ethyl acetate 95:5), giving the protected aldehyde as a yellow oil in 60% yield.

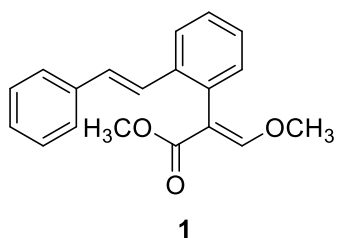
¹H NMR (600 MHz, CDCl₃) δ (ppm): 9.80 (s, 1H), 7.35 (m, 2H), 6.91 (m, 1H), 0.97 (m, 18H), 0.21 (m, 12 H).

The compound was used for the Horner-Wadsworth-Emmons (HWE) olefination of **11** following the above-reported procedure. The crude product was purified by column chromatography (cyclohexane/ acetone 9:1 → 6:4) affording the desired product as a yellow sticky solid in 20% yield.

¹H NMR (600 MHz, CDCl₃) δ (ppm): 7.69 (d, *J* = 7.7 Hz, 1H), 7.61 (s, 1H), 7.31 (dt, *J* = 1.2, 7.5 Hz, 1H), 7.24 (dt, *J* = 1.2, 7.3 Hz, 1H), 7.15 (dd, *J* = 1.3, 7.6 Hz, 1H), 6.95 (d, *J* = 2 Hz, 1H), 6.92 (d, *J* = 16.3 Hz, 1H), 6.92 (d, *J* = 2.2 Hz, 1H), 6.80 (d, *J* = 8.4 Hz, 1H), 3.80 (s, 3H), 3.69 (s, 3H), 1.04 (s, 9H), 1.03 (s, 9H), 0.26 (s, 6H), 0.24 (s, 6H).

¹³C NMR (300 MHz, CDCl₃) δ (ppm): 168.2, 159.9, 146.9, 146.7, 136.7, 131.6, 131.5, 131.1, 129.0, 128.0, 126.9, 125.1, 124.7, 121.1, 120.0, 119.0, 110.6, 61.9, 51.6, 29.6, 26.0 (3C), 25.9 (3C), 18.5, 18.4, -4.0 (4C).

Methyl (*E*)-3-Methoxy-2-(2-((*E*)-styryl)phenyl)acrylate (1).

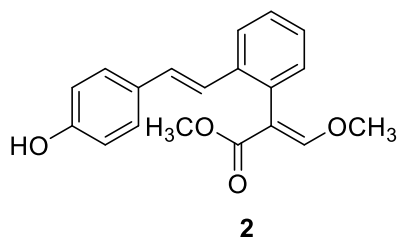


The crude product was purified by flash chromatography (cyclohexane/ ethyl acetate 9:1 → 7:3) affording the desired product as a white solid in 15% yield.

¹H NMR (600 MHz, CDCl₃) δ (ppm): 7.73 (d, *J* = 7.8 Hz, 1H), 7.64 (s, 1H), 7.46 (d, *J* = 7.8 Hz, 2H), 7.34 (t, *J* = 7.5 Hz, 3H), 7.27 (m, 2H), 7.18 (d, *J* = 7.8 Hz, 1H), 7.08 (d, *J* = 16.3 Hz, 1H), 7.04 (d, *J* = 16.3 Hz, 1H), 3.81 (s, 3H), 3.69 (s, 3H).

¹³C NMR (300 MHz, CDCl₃) δ (ppm): 168.5, 160.2, 137.8, 136.6, 131.9, 131.4, 129.6, 128.8 (2C), 128.2, 127.6, 127.4, 127.1, 126.7 (2C), 125.2, 110.6, 62.1, 51.9

Methyl (*E*)-2-(2-((*E*)-4-hydroxystyryl)phenyl)-3-methoxyacrylate (2).



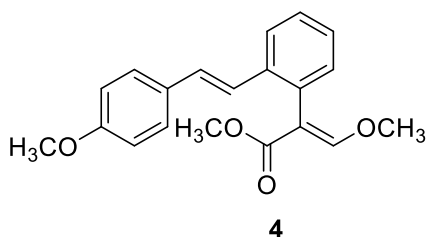
A solution 0.5 M methyl (*E*)-2-(2-((diethoxyphosphoryl)-methyl)phenyl)-3-methoxyacrylate 11 (0.30 mmol, 1.1 equiv) and 4-((*tert*-butyldimethylsilyl)oxy)benzaldehyde (0.27 mmol, 1 eq) in dry THF was cautiously dropped

into a round-bottom flask containing 1.33 mmol of NaH (5 eq) suspended in 0.63 mL of dry THF cooled at 0 °C under nitrogen atmosphere. The obtained reaction mixture was stirred at room temperature for 3 h and then quenched with NaHCO₃ 5%. The aqueous layer was exhaustively extracted with ethyl acetate and the organic phase was dried over Na₂SO₄, filtered, and the solvent was evaporated under reduced pressure. The crude product was purified by column chromatography (cyclohexane/acetone 9:1) affording the desired deprotected product as a yellow sticky solid in 16% yield.

¹H NMR (400 MHz, CDCl₃) δ 7.71 (d, *J* = 7.7 Hz, 1H), 7.66 (s, 1H), 7.38–7.32 (m, 3H), 7.28 (td, *J* = 7.4, 1.2 Hz, 1H), 7.19 (dd, *J* = 7.7, 1.2 Hz, 1H), 7.00 (d, *J* = 16.2 Hz, 1H), 6.93 (d, *J* = 16.2 Hz, 1H), 6.83 (d, *J* = 8.6 Hz, 2H), 3.82 (s, 3H), 3.71 (s, 3H).

¹³C NMR (400 MHz, CDCl₃) δ: 168.8, 160.2, 155.5, 136.8, 131.4, 131.2, 130.5, 129.1, 128.1, 127.9, 126.9, 124.9, 124.7, 115.6, 110.6, 62.0, 51.9.

Methyl (*E*)-3-Methoxy-2-(2-((*E*)-4-methoxystyryl) phenyl)-acrylate (4).

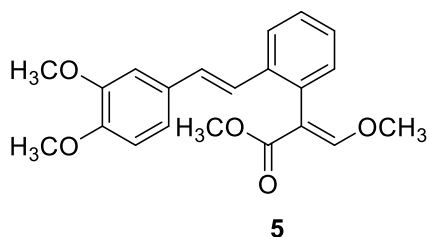


The crude product was purified by preparative TLC (cyclohexane/ethyl acetate 8:2) affording the desired product as a yellow sticky solid in 10% yield.

¹H NMR (600 MHz, CDCl₃) δ (ppm): 7.70 (d, *J* = 7.8 Hz, 1H), 7.63 (s, 1H), 7.39 (d, *J* = 8.6 Hz, 2H), 7.32 (t, *J* = 7.1 Hz, 1H), 7.25 (t, *J* = 7.3 Hz, 1H), 7.16 (d, *J* = 7.8 Hz, 1H), 6.99 (d, *J* = 16.3 Hz, 1H), 6.93 (d, *J* = 16.3 Hz, 1H), 6.88 (d, *J* = 8.6 Hz, 2H), 3.83 (s, 3H), 3.80 (s, 3H), 3.68 (s, 3H).

¹³C NMR (600 MHz, CDCl₃) δ (ppm): 168.4, 160, 159.2, 136.8, 131.5, 131.2, 130.5, 129.3, 128.9, 128, 127.7, 126.8, 124.9, 124.8, 114.1, 110.6, 61.9, 55.3, 51.7.

Methyl (*E*)-2-(2-((*E*)-3,4-dimethoxystyryl) phenyl)-3-methoxyacrylate (5).

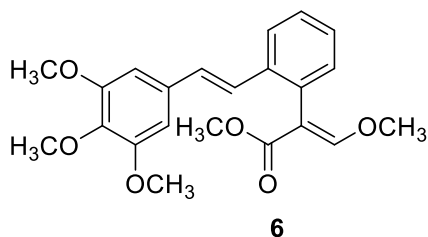


The crude product was purified by flash chromatography (cyclohexane/ethyl acetate 9:1 → 7:3) followed by preparative HPLC affording the desired product as a colorless oil in 10% yield.

¹H NMR (600 MHz, CDCl₃) δ (ppm): 7.69 (d, *J* = 7.9 Hz, 1H), 7.62 (s, 1H), 7.33 (t, *J* = 7.4 Hz, 1H), 7.26 (t, *J* = 7.9 Hz, 1H), 7.17 (d, *J* = 7.4 Hz, 1H), 7.09 (d, *J* = 8.3 Hz, 1H), 6.98 (d, *J* = 16 Hz, 1H), 6.97 (d, *J* = 3.6 Hz, 1H), 6.92 (d, *J* = 16.3 Hz, 1H), 6.85 (d, *J* = 8.3 Hz, 1H), 3.93 (s, 3H), 3.90 (s, 3H), 3.81 (s, 3H), 3.68 (s, 3H).

¹³C NMR (600 MHz, CDCl₃) δ (ppm): 168.4, 160.0, 149.0, 148.8, 136.7, 131.5, 131.2, 130.9, 129.2, 128.0, 126.9, 125.3, 124.9, 119.5, 111.3, 110.6, 109.4, 61.9, 55.9, 51.7.

Methyl (E)-3-Methoxy-2-(2-((E)-3,4,5-trimethoxystyryl)-phenyl)acrylate (6).

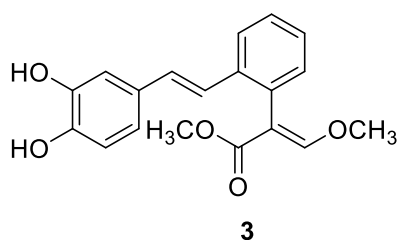


The crude product was purified by flash chromatography (cyclohexane/ethyl acetate 9:1 → 7:3) followed by preparative HPLC affording the desired product as a yellow oil in 10% yield.

¹H NMR (600 MHz, CDCl₃) δ (ppm): 7.69 (d, *J* = 7.8 Hz, 1H), 7.63 (s, 1H), 7.33 (dt, *J* = 7.4, 1.2 Hz, 1H), 7.28 (dt, *J* = 7.4, 1.1 Hz, 1H), 7.18 (dd, *J* = 7.5, 1.1 Hz, 1H), 6.95 (s, 2H), 6.67 (s, 2H), 3.90 (s, 6H), 3.86 (s, 3H), 3.82 (s, 3H), 3.69 (s, 3H).

¹³C NMR (600 MHz, CDCl₃) δ (ppm): 168.3, 160.0, 153.3, 137.9, 136.4, 133.5, 131.6, 131.3, 129.5, 128.0, 127.2, 126.7, 125.1, 110.6, 103.8, 62.0, 60.9, 56.2, 53.4, 51.7.

Methyl (E)-2-(2-((E)-3,4-Dihydroxystyryl) phenyl)-3-methoxyacrylate (3).



A 0.05 M solution of **12** in dry THF was prepared under a nitrogen atmosphere and cooled to 0 °C in an iced bath. 2.6 eq of tetrabutylammonium fluoride (TBAF) were added to the solution, which was warmed up to room temperature and stirred for 1 hour. After completion, the reaction

was neutralized with water and the aqueous layer was extracted 3 times with ethyl acetate. The organic phase was washed with 0.1 N HCl, dried over Na₂SO₄, and filtered. The solvent was evaporated under reduced pressure. The crude product was purified by column chromatography (dichloromethane/methanol 98:2), affording the desired product as a colorless oil with a 25% yield.

¹H NMR (600 MHz, CDCl₃) δ (ppm): 7.68 (s, 1H), 7.64 (d, *J* = 7.9 Hz, 1H), 7.25 (td, *J* = 1.2, 7.4 Hz, 1H), 7.16 (td, *J* = 1.2, 7.6 Hz, 1H), 7.05 (dd, *J* = 1.2, 7.6 Hz, 1H), 6.91 (d, *J* = 2.2 Hz, 1H), 6.84 (d, *J* = 16.3 Hz, 1H), 6.80 (d, *J* = 16.3 Hz, 1H), 6.76 (dd, *J* = 2.2, 8.2 Hz, 1H), 6.70 (d, *J* = 8.2 Hz, 1H), 3.80 (s, 3H), 3.66 (s, 3H).

¹³C NMR (600 MHz, CDCl₃) δ (ppm): 169.1, 160.5, 143.9, 143.7, 136.8, 131.5 (2C), 131.3, 129.2, 128.2, 127.1, 125.0 (2C), 120.2, 115.6, 113.1, 110.7, 62.3, 51.9.

Biology: In Vitro Biological Activity of Natural and Synthetic Methoxyacrylate-Stilbene Compounds.

Fungal Strains. In this study, four strains of *P. oryzae* were used: two strains sensitive to quinone outside inhibitor (QoI) fungicides (WT): A252 and TA102, and two strains resistant to QoI (RES): PO1312 and PO1336. The strains belong to a vast collection of *P. oryzae* monoconidial isolates maintained at the Laboratory of plant pathology, University of Milan. The strains were maintained as single-spore isolates on malt-agar medium (MA: 20 g/L malt extract, Oxoid, U.K.; 15 g/L agar, Oxoid, U.K.) at 4 ° C.

Inhibition of Mycelium Growth of *P. oryzae*. The *P. oryzae* mycelium inhibition by the tested compounds was evaluated as previously described [26,27]. Briefly, a 0.5 cm mycelium plug obtained from actively growing fungal colonies of *P. oryzae* strains was transferred to MA medium plates supplemented or not with tested compounds in three biological replicates. The natural stilbenoids were tested at the concentration of 200 µM, while the synthesized methoxyacrylate-stilbene hybrids were tested at the concentration of 25 mg/L. Due to the low solubility of the tested molecules in water, they were dissolved in DMSO or acetone. Therefore, multiple controls were included: MA medium without any supplement (MA), MA medium supplemented with DMSO or acetone (ACT) at a final concentration of 1% *v/v*. To assess the activity of the synthesized methoxyacrylate-stilbene hybrids, the commercial fungicide azoxystrobin (AZX) was used as a reference. The plates were incubated at 24 °C in the dark. The mycelium growth was measured at 7 days after inoculation (DAI), and the inhibition of mycelium growth (%) was calculated by comparing the mycelium growth on control (corresponding solvent) and compound-supplemented plates. The inhibition percentage was calculated as $I\% = (C - T)/C \times 100$, where C = mycelium growth in the control medium and T = mycelium growth in the medium added to the tested compound. For AZX, the control was MA medium, while for tested compounds, it was DMSO or ACT. For the quantitative analysis of deoxyrhapontigenin activity, the compound was tested at the following concentrations: 5–10–50–100–200 µM as previously described.

Statistical Analysis of the Mycelium Inhibition Growth Data. The statistical analyses were performed using R software, version 4.2.2. The percentage data of mycelium growth inhibition were square root arcsine transformed and submitted to ANOVA, followed by Tukey's post hoc test for multiple comparison ($P = 0.05$), using the TukeyC package [34]. For the quantitative study of deoxyrhapontigenin activity, the dose-response curve for mycelium growth was plotted by nonlinear regression analysis using a three-parameter log – logistic model, employing the drc package. The ED₅₀ value (the compound

concentration causing 50% inhibition of mycelium growth) was estimated by interpolation from the fitted regression curve.

6.2. Design and synthesis of multi-target hybrid compounds: combination of QoI β -methoxyacrylate pharmacophore and succinate dehydrogenase inhibitors (SDHI) structural features.

6.2.1. Introduction

Despite the increasing spread of fungal resistant strains, whose impact on agricultural production was previously outlined, quinone outside inhibitors still play a central role in the fungicides market. Therefore, to date a considerable research interest in QoIs implementation remains, with the main aim of bypassing resistance mechanisms through the introduction of structural modifications or the design of strobilurin-based hybrid compounds. Among the 55 classes of fungicides listed by the Fungicide Resistance Action Committee (FRAC), another important class of antifungal agents that have been extensively used in crop protection (e.g. against *Sclerotinia sclerotiorum*, *Rhizoctonia solani*, and *Botrytis cinerea*) is represented by succinate dehydrogenase inhibitors (SDHIs, **Figure 6.43**) [35–37]. As QoIs, SDHIs activity is due to interference with the mitochondrial respiration chain. Succinate dehydrogenase, also known as succinate ubiquinone oxidoreductase or complex II, is responsible for the direct

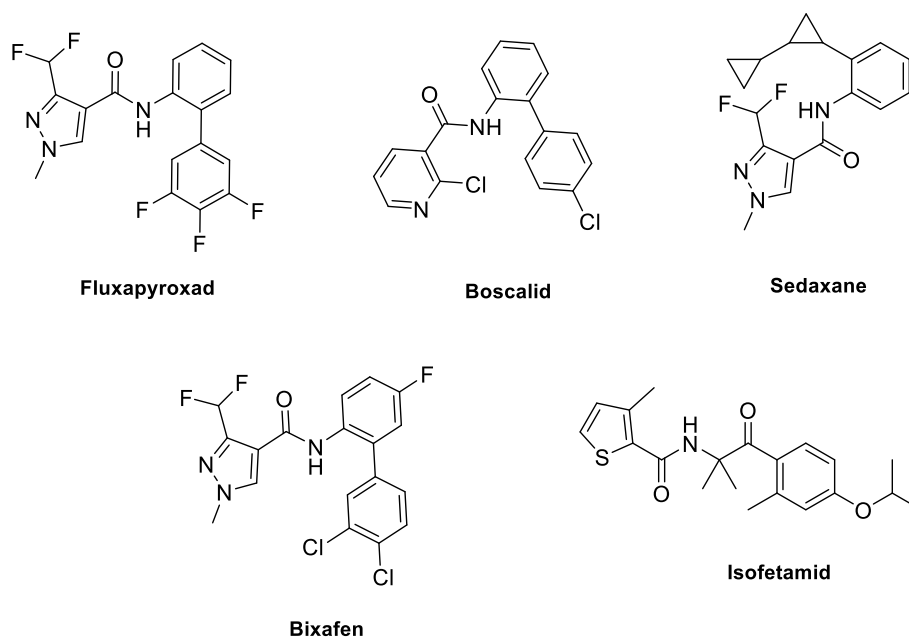


Figure 6.43. Chemical structures of commercially available SDH inhibitors

transfer of succinate-derived electrons to the ubiquinone pool, thus playing a pivotal role in cell respiration [38,39]. Commercial SDHIs target the ubiquinone binding pocket, physically blocking substrate access to the enzyme, and preventing succinate oxidation cycle. Thanks to this unique mode of action,

SDHIs have not shown cross-resistance with other commercial fungicides so far, remaining a valuable tool in crop protection [40–42]. However, as for quinone outside inhibitors, the prolonged use of SDHIs over the past decades led to the development of resistance in fungal pathogens, arousing the demand for novel succinate dehydrogenase inhibitors [43–46].

Due to their high potential as fungicides and their broad-spectrum activity, QoIs and SDHIs are still largely used in crop diseases management. However, resistance development by fungal phytopathogens is posing a serious challenge to these classes of agrochemicals, frustrating their usage, and preventing efficient crop management. In this context, the development of bifunctional fungicides resulting from the combination of QoIs and SDHIs pharmacophores might represent a promising strategy to overcome the limitations caused by fungal resistance. In this work, we developed a small collection of dual-compounds obtained by merging the strobilurin β -methoxyacrylate pharmacophore with the structural features involved in SDHIs bioactivity. The obtained products **13b-c** were tested against two wildtype (WT) and two strobilurin-resistant (*RES*) strains of rice blast pathogen *Pyricularia Oryzae*. We also evaluated the antifungal potency of synthetic intermediates **19a-c** that, in spite of lacking the QoI pharmacophore, could represent novel SDHIs with improved biological activity.

6.2.2. Results and Discussion

Design and synthesis of QoI-SDHI hybrid compounds

SAR studies on both classes of fungicides are reported in literature [39,47] and allowed the identification of the key structural features that should be maintained in the design of hybrid compounds. As already highlighted in the previous sections, the characteristic feature of all the QoIs is represented by the methyl-(*E*)- β -methoxyacrylate pharmacophore, or a bioisosteric equivalent, attached to a phenyl ring with a side chain – usually a (hetero)aryloxy moiety – in an adjacent *ortho*-position (aryl- β -methoxyacrylate, aryl-BMA) [48]. On the other hand, despite their structural diversity, all SDHIs share a common essential feature, which is the amide bond. The amidic carbonyl is directly connected to a “core” moiety, usually an aromatic or heterocyclic ring, which is essential for binding and *in vivo* potency, as it enters deeply into the active site of succinate dehydrogenase. On the other side of the amide bond, a “linker” is attached. The linker is usually an alkyl chain, or a substituted or unsubstituted (hetero) aromatic group bearing, on the *ortho* position, a large hydrophobic group which is a further component of the molecule [39]. Notably, pyrazole-4-carboxamide emerged as a valuable scaffold leading to improved antifungal

activity [49,50]. The combination of these key structural features with the aryl-BMA pharmacophore from QoIs is depicted in **Figure 6.44**. Briefly, the 3-(difluoromethyl)-1H-pyrazole-4-carboxamide core was connected, *via* amidic bond, to a biphenyl moiety whose distal ring was decorated with β -methoxyacrylate.

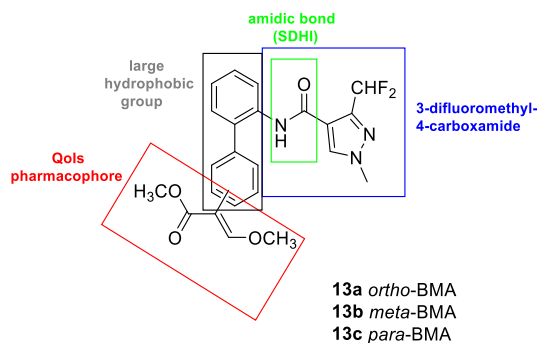
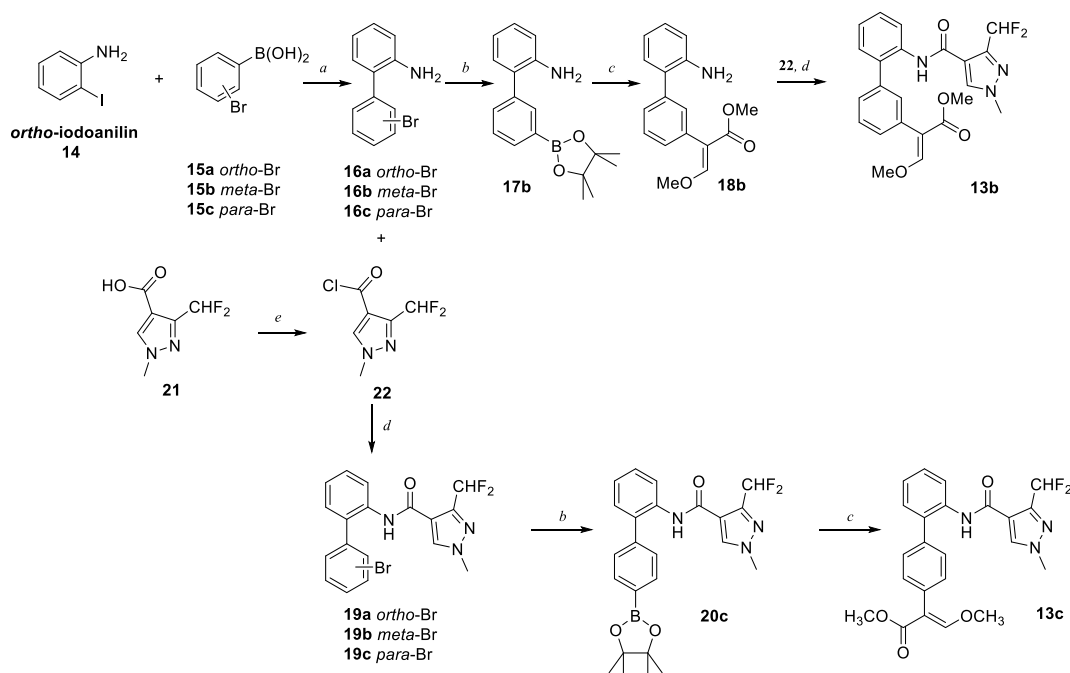


Figure 6.44. Combination of QoIs and SDHIs structural features.

The preparation of QoI-SDHI hybrids required the construction of the biphenyl core *via* Suzuki coupling between *ortho*-iodoaniline and *ortho*-, *meta*- or *para*-(bromophenyl) boronic acid in presence of Pd(PPh₃)₄ and K₃PO₄, followed by the decoration of the distal ring with β -methoxyacrylate and the formation of the amidic bond with 3-(difluoromethyl)-1H-pyrazole-4-carbonyl chloride. The synthetic process for the QoI-SDHI hybrids **13b-c** and of intermediates **19a-c** is depicted in **Scheme 6.8**. For yield optimization purposes, synthetic steps followed a different sequence depending on the substituent positioning on the distal aromatic ring. Indeed, different substitution patterns led to significant differences in isolated yields of synthetic intermediates. For instance, the *meta*-substituted product **13b** was obtained by first converting 3'-bromo-[1,1'-biphenyl]-2-amine (**16b**) into the corresponding boronic ester (**17b**) using bis(pinacolato)diboron in presence of Pd(dppf)Cl₂·CH₂Cl₂ and KOAc. In these conditions, the product was easily isolated by column chromatography in 80% yield. Then, Suzuki coupling with α -iodo- β -methoxyacrylate afforded methyl-(*E*)-2-(2'-amino-[1,1'-biphenyl]-3-yl)-3-methoxyacrylate (**18b**). Final coupling with 3-(difluoromethyl)-1H-pyrazole-4-carbonyl chloride **22** in the presence of TEA in dichloromethane yielded **13b** in 80% yield. Attempts to perform the amidic coupling on **16b** first, and then convert it into the corresponding boronic ester **17b**, as it was done for compound **13c**, led to poor yields (< 30%) and difficulties during purification procedures, due to the formation of a large number of byproducts. On the other hand, the preparation of compounds **13c**, bearing β -methoxyacrylate in *para*- position, required amidic coupling within 4'-bromo-[1,1'-biphenyl]-2-amine **16c** and **22** first, and then the formation of the

corresponding boronic ester (**20c**) and the final insertion of β -methoxyacrylate. However, none of the two synthetic routes afforded the *ortho*-substituted analogue **13a**, although N-(2'-bromo-[1,1'-biphenyl]-2-yl)-3-(difluoromethyl)-1-methyl-1H-pyrazole-5-carboxamide **19a** was successfully isolated by coupling 2'-bromo-[1,1'-biphenyl]-2-amine **16a** with 3-(difluoromethyl)-1H-pyrazole-4-carbonyl chloride **22**.



Scheme 6.8. Synthesis of QoI-SDHI hybrids. Reagents and conditions: (a) Pd(PPh₃)₄, K₃PO₄, EtOH, reflux, 16h (55-60%); (b) bis(pinacolato)diboron, Pd(dppf)Cl₂·CH₂Cl₂, KOAc, dioxane, N₂, 100°C, dark, 5h (80%); (c) Pd(dppf)Cl₂·CH₂Cl₂, K₂CO₃, H₂O/dioxane 1:4, N₂, 80°C, 16h (55%); (d) TEA, CH₂Cl₂, rt, 2h (75-80%); (e) SOCl₂, toluene, N₂, rt, 3h (quant. yield)

Biological evaluation of hybrid compounds **13b-c** and brominated intermediates **19a-c**.

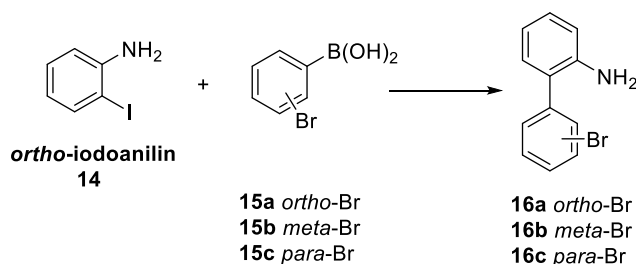
The antifungal activity of hybrid compounds **13b-c** and brominated intermediates **19a-c** was evaluated on two wildtype (*WT*, A252 and TA102) and two strobilurin-resistant (*RES*, PO21-01 and PO21-07) strains of blast fungus *P. oryzae*. Hybrid compounds **13b-c** and *ortho*- and *meta*-intermediates **19a-b** showed modest biological activity, with mycelium growth inhibition values ranging from 10% to 35% on both *WT* and *RES* strains. More encouraging results were provided by *para*-substituted intermediate **19c**, with 70% mycelium growth inhibition on *WT* and 40% inhibition of *RES*. These values are comparable to that of the reference compound azoxystrobin, possibly suggesting that also **19c** is susceptible to the G143A mutation.

6.2.3. Materials and methods

Chemistry: Synthesis of QoI-SDHI hybrid compounds

All reagents and solvents were purchased from commercial suppliers and used without further purification. The ^1H NMR and ^{13}C NMR spectra were recorded with a Bruker AV600 (^1H , 600 MHz; ^{13}C , 150 MHz) and a Bruker AMX-300 (^1H , 300 MHz; ^{13}C 75 MHz) spectrometer. Chemical shifts (δ) are expressed in ppm and coupling constants (J) are in hertz. All reactions requiring anhydrous conditions were performed under a positive nitrogen flow, and all glassware was oven dried. Isolation and purification of the compounds were performed by flash column chromatography on silica gel 60 (230 – 400 mesh). Thin layer chromatography (TLC) analyses were performed by using commercial silica gel 60 F₂₅₄ aluminum sheets. Preparative HPLC purification was performed using a Waters 1525 Binary Pump equipped with a Waters 2489 UV-detector and a column Luna 5 Silica (100 Å), 250 × 21.2 mm₂. HPLC purifications were performed with an isocratic elution (hexane/isopropanol 95:5), flow rate = 15 mL/min, λ = 220 nm. Hydrophilic lipophilic balance (HLB) and log P were calculated using the ChemAxon calculation method on Marvin Sketch 23.7.

General procedure for the synthesis of 2', 3' or 4'-bromo-[1,1'-biphenyl]-2-amine (16a-c).



In a round-bottom flask, a solution of 2-iodoaniline **14** (447 mg, 2 mmol) in ethanol (4.4 ml) was prepared under a nitrogen atmosphere. Bromophenylboronic acid (1.2 eq) and K₃PO₄ (2.5 eq) were added, and the obtained solution was degassed by bubbling nitrogen for 30 minutes. Pd(PPh₃)₄ (5% mol) was added and the reaction mixture was heated to 78°C and stirred for 16 hours. After this time, the solution was cooled to room temperature and the solvent was evaporated. The residue was diluted with ethyl acetate and the organic layer was washed with water and brine, dried over Na₂SO₄, filtered and evaporated under reduced pressure. The crude products were purified as described below.



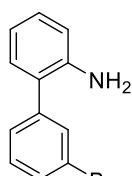
16a

2'-bromo-[1,1'-biphenyl]-2-amine (16a).

The crude product was purified by flash chromatography (hexane/ethyl acetate 95:5) giving **16a** as brown oil in 55% yield. Spectroscopic data are in accordance with those reported in literature [51].

$^1\text{H NMR}$ (600 MHz, CDCl_3) δ 7.71 (d, $J = 8.0$ Hz, 1H), 7.40 (td, $J = 7.4, 1.3$ Hz, 1H), 7.34 (dd, $J = 7.5, 1.8$ Hz, 1H), 7.27 – 7.19 (m, 2H), 7.04 (dd, $J = 7.5, 1.8$ Hz, 1H), 6.85 (td, $J = 7.4, 1.3$ Hz, 1H), 6.80 (d, $J = 8.0$ Hz, 1H), 3.46 (bs, 2H).

$^{13}\text{C NMR}$ (75 MHz, CDCl_3) δ 143.7, 140.2, 133.3, 132.0, 130.4, 129.4, 129.3, 128.0, 127.3, 124.4, 118.4, 115.7. From [51].



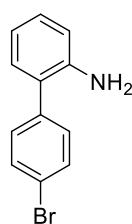
16b

3'-bromo-[1,1'-biphenyl]-2-amine (16b).

The crude product was purified by flash chromatography (hexane/ethyl acetate 100:0 \rightarrow 90:10) giving **16b** as yellowish oil in 55% yield. Spectroscopic data are in accordance with those reported in literature [52].

$^1\text{H NMR}$ (600 MHz, CDCl_3) δ 7.62 (t, $J = 1.5$ Hz, 1H), 7.48 (dt, $J = 7.9, 1.5$ Hz, 1H), 7.40 (dt, $J = 7.7, 1.5$ Hz, 1H), 7.31 (t, $J = 7.8$ Hz, 1H), 7.18 (td, $J = 7.7, 1.6$ Hz, 1H), 7.10 (dd, $J = 7.6, 1.6$ Hz, 1H), 6.84 (td, $J = 7.6, 1.5$ Hz, 1H), 6.79 (dd, $J = 7.7, 1.4$ Hz, 1H).

$^{13}\text{C NMR}$ (100 MHz, CDCl_3) δ 168.4, 140.3, 134.4, 132.3, 131.2, 131.0, 130.5, 129.9, 128.9, 127.8, 124.7, 123.1, 122.5, 24.6. From [52].



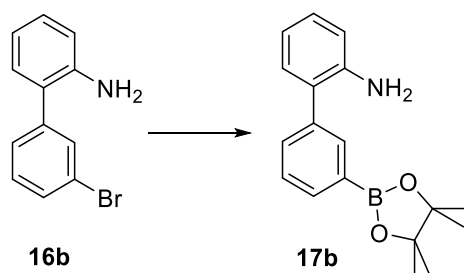
16c

4'-bromo-[1,1'-biphenyl]-2-amine (16c).

The crude product was purified by flash chromatography (hexane/ethyl acetate 100:0 \rightarrow 90:10) giving **16c** as yellowish oil in 30% yield.

$^1\text{H NMR}$ (600 MHz, CDCl_3) δ 7.55 (d, $J = 8.4$ Hz, 2H), 7.35 (d, $J = 8.4$ Hz, 2H), 7.23 (td, $J = 7.7, 1.5$ Hz, 1H), 7.13 (dd, $J = 7.6, 1.5$ Hz, 1H), 6.97 – 6.87 (m, 2H).

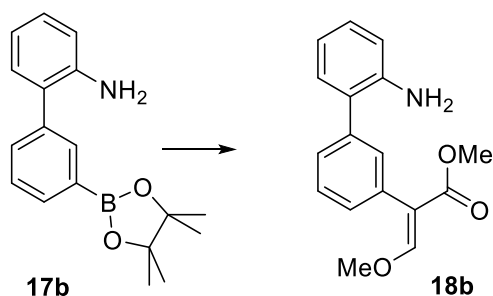
Synthesis of 3'-(4,4,5,5-tetramethyl-1,3,2-dioxaborolan-2-yl)-[1,1'-biphenyl]-2-amine (17b).



In a round-bottom flask a solution of 3'-bromo-[1,1'-biphenyl]-2-amine **16b** (80 mg, 0.3224 mmol) in dry dioxane (3 ml) was prepared. Potassium acetate (3 eq), bis(pinacolato)diboron (1.2eq) and [1,1'-Bis(diphenylphosphino) ferrocene] palladium(II) dichloride (3% mol) were added, and the reaction mixture was heated to 100°C and stirred for 2 hours. After this time, dioxane was evaporated under reduced pressure. The residue was diluted with ethyl acetate and washed with water. The organic layer was dried over Na₂SO₄, filtered and the solvent was evaporated. Compound **17b** was obtained after purification by flash chromatography (hexane/ethyl acetate 95:5 → 90:10) as a white solid in 85% yield.

¹H NMR (300 MHz, CDCl₃) δ 7.88 (t, *J* = 1.8 Hz, 1H), 7.79 (dt, *J* = 7.3, 1.3 Hz, 1H), 7.59 – 7.54 (m, 1H), 7.44 (t, *J* = 7.6 Hz, 1H), 7.20 – 7.12 (m, 2H), 6.89 – 6.77 (m, 2H), 1.34 (s, 12H).

Synthesis of methyl (E)-2-(2'-amino-[1,1'-biphenyl]-3-yl)-3-methoxyacrylate (18b).

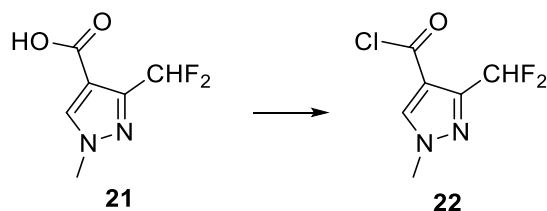


In a round-bottom flask 3'-(4,4,5,5-tetramethyl-1,3,2-dioxaborolan-2-yl)-[1,1'-biphenyl]-2-amine **17b** (95 mg, 0.3218 mmol) was solubilized in a 4:1 dioxane/water mixture (10 ml) under a nitrogen atmosphere. K₂CO₃ (2 eq) and methyl (Z)-2-iodo-3-methoxyacrylate **8** (1 eq) were added, followed by [1,1'-Bis(diphenylphosphino)ferrocene] palladium (II) dichloride (2% mol). The reaction mixture was heated to 80°C and stirred for 16 hours. After completion, the reaction mixture was cooled to room temperature. Aqueous NaHCO₃ (5%) was added and the aqueous phase was extracted 5 times with ethyl acetate. The combined organic layers were dried over Na₂SO₄ and filtered, and the solvent

was evaporated. The crude product was purified by flash chromatography (hexane/ethyl acetate 7:3) to afford compound **18b** as a yellow oil in 60% yield.

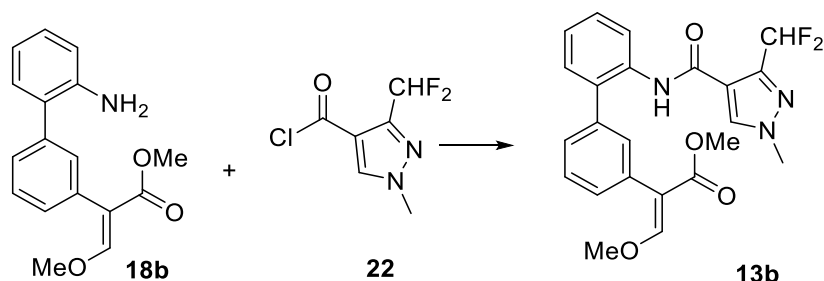
$^1\text{H NMR}$ (600 MHz, CDCl_3) δ 7.58 (s, 1H), 7.46 (t, $J = 1.5$ Hz, 1H), 7.43 (t, $J = 7.7$ Hz, 1H), 7.36 (dt, $J = 7.7, 1.5$ Hz, 1H), 7.33 (dt, $J = 7.7, 1.5$ Hz, 1H), 7.20 – 7.12 (m, 2H), 6.84 (td, $J = 7.4, 1.2$ Hz, 1H), 6.80 (dd, $J = 8.0, 1.2$ Hz, 1H), 3.87 (s, 3H), 3.75 (s, 3H).

Synthesis of 3-(difluoromethyl)-1-methyl-1H-pyrazole-4-carbonyl chloride (**22**).



Commercial 3-(difluoromethyl)-1-methyl-1H-pyrazole-4-carboxylic acid **21** (176.1 mg, 1 mmol) was dissolved in dry toluene (2 ml) under a nitrogen atmosphere and thionyl chloride (20 eq) was added to the solution. The obtained reaction mixture was heated to 90°C and stirred for 2 hours. After reaction completion the clear solution was cooled to room temperature and toluene and thionyl chloride were evaporated. The crude product was diluted with a 1:1 heptane/toluene mixture and evaporated under reduce pressure. This procedure was repeated until all the excess of thionyl chloride had been removed. 3-(Difluoromethyl)-1-methyl-1H-pyrazole-4-carbonyl chloride **22** was obtained as a yellow solid in 96% yield and used for the following synthetic step without further purification. Spectroscopic data match with those found in literature [53].

Synthesis of methyl (E)-2-(2'-(3-(difluoromethyl)-1-methyl-1H-pyrazole-4-carboxamido)-[1,1'-biphenyl]-3-yl)-3-methoxyacrylate (**13b**).



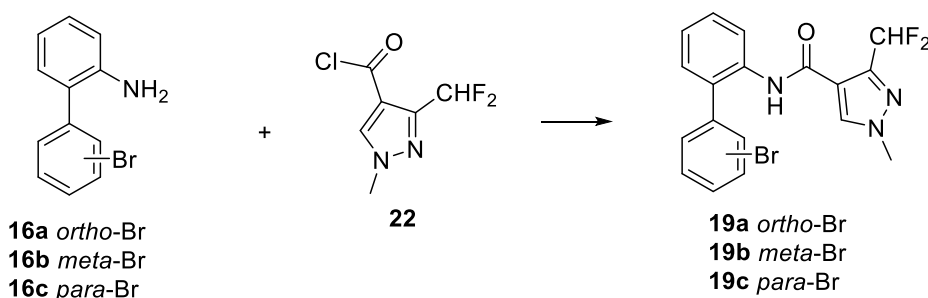
In a round-bottom flask a solution of **18b** (35 mg, 0.1235 mmol) in dry dichloromethane (1 ml) was prepared under a nitrogen atmosphere. Triethylamine (4 eq) was added, followed by a solution of **22** (1 eq) in dry dichloromethane (1 ml). The obtained reaction mixture was stirred at room

temperature for 2 hours. After reaction completion the solvent was evaporated and the crude product was purified by flash chromatography (hexane/ethyl acetate 7:3 → 1:1), affording **13b** as a yellow sticky solid in 80% yield.

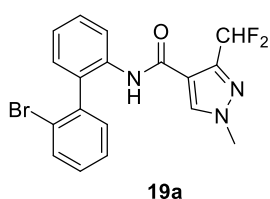
¹H NMR (600 MHz, CDCl₃) δ 8.41 (d, *J* = 8.3 Hz, 1H), 7.80 (bs, 1H), 7.78 (s, 1H), 7.57 (s, 1H), 7.49 (t, *J* = 7.6 Hz, 1H), 7.42 – 7.35 (m, 3H), 7.31-7.27 (m, 2H), 7.19 (td, *J* = 7.5, 1.2 Hz, 1H), 7.08 (t, *J* = 54.2 Hz, 1H), 3.91 (s, 3H), 3.82 (s, 3H), 3.74 (s, 3H).

¹³C NMR (150 MHz, CDCl₃) δ 168.04, 160.11, 159.56, 145.42, 137.53, 134.70, 133.23, 132.47, 132.29, 130.64, 130.07, 129.91, 129.03, 128.58, 128.40, 124.24, 121.32, 116.81, 110.97, 109.79, 62.10, 51.56, 39.44.

General procedure for the preparation of *N*-(2', 3' or 4'-bromo-[1,1'-biphenyl]-2-yl)-3-(difluoromethyl)-1-methyl-1H-pyrazole-4-carboxamide (**19a-c**).



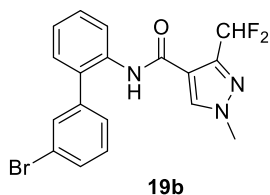
In a round-bottom flask the proper bromo-[1,1'-biphenyl]-2-amine (**16a**, **b** or **c**, 100 mg, 0.4030 mmol) was dissolved in dry dichloromethane (4 ml) under a nitrogen atmosphere and 4 eq of triethylamine were added to the solution followed by a solution of **22** (0.4030 mmol, 78.4 mg, 1 eq) in dry dichloromethane (2 ml). The reaction mixture was stirred at room temperature until the reagents were consumed (3-16h). After completion, the reaction mixture was diluted with dichloromethane and the organic layer was washed with aqueous NH₄Cl (sat.) and brine, dried over Na₂SO₄ and filtered, and the solvent was evaporated. Compound **19a-c** were obtained after column chromatography as described below.



***N*-(2'-bromo-[1,1'-biphenyl]-2-yl)-3-(difluoromethyl)-1-methyl-1H-pyrazole-4-carboxamide (**19a**)** was obtained after chromatographic purification (hexane/ethyl acetate 3:7) as a yellow solid in 60% yield.

$^1\text{H NMR}$ (600 MHz, CDCl_3) δ 8.34 (d, $J = 8.3$ Hz, 1H), 7.81 (s, 1H), 7.69 (d, $J = 7.9$ Hz, 1H), 7.58 (bs, 1H), 7.45 (td, $J = 7.5, 1.5$ Hz, 1H), 7.40 (td, $J = 7.4, 1.4$ Hz, 1H), 7.33 – 7.26 (m, 2H), 7.23 (td, $J = 7.4, 1.4$ Hz, 1H), 7.18 (dt, $J = 7.6, 1.6$ Hz, 1H), 6.61 (t, $J = 54.2$, 1H), 3.89 (s, 3H).

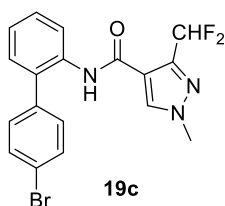
$^{13}\text{C NMR}$ (100 MHz, CDCl_3) δ 159.4, 138.8, 135.2, 135.0, 133.2, 132.5, 131.9, 130.2, 130.0, 129.9, 129.0, 128.0, 127.9, 124.6, 124.4, 122.3, 117.2, 111.0 (t, $J = 234$ Hz, 1C), 39.7.



N-(3'-bromo-[1,1'-biphenyl]-2-yl)-3-(difluoromethyl)-1-methyl-1H-pyrazole-4-carboxamide (19b) was obtained after column chromatography (hexane/ethyl acetate 4:6) as a white oil in 65% yield.

$^1\text{H NMR}$ (600 MHz, CDCl_3) δ 8.27 (d, $J = 8.3$ Hz, 1H), 7.81 (s, 1H), 7.77 (bs, 1H), 7.57 – 7.51 (m, 2H), 7.45 – 7.39 (m, 1H), 7.35 – 7.29 (m, 2H), 7.25 – 7.17 (m, 2H), 6.72 (t, $J = 54.1$ Hz, 1H), 3.91 (s, 3H).

$^{13}\text{C NMR}$ (100 MHz, CDCl_3) δ 159.4, 143.2, 140.1, 134.9, 134.5, 132.3, 132.0, 131.0, 130.4, 130.1, 128.8, 128.1, 124.9, 122.9, 122.7, 110.9 (t, $J = 234$ Hz, 1C), 39.6.

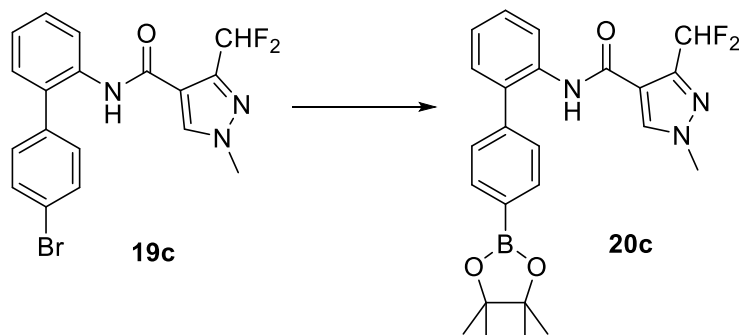


N-(4'-bromo-[1,1'-biphenyl]-2-yl)-3-(difluoromethyl)-1-methyl-1H-pyrazole-4-carboxamide (19c) was obtained after chromatographic purification (hexane/ethyl acetate 8:2 \rightarrow 6:4) as a white solid in 50% yield.

$^1\text{H NMR}$ (600 MHz, CDCl_3) δ 8.21 (d, $J = 8.2$ Hz, 1H), 7.82 (s, 1H), 7.76 (bs, 1H), 7.59 – 7.54 (m, 2H), 7.41 (m, 1H), 7.27 – 7.22 (m, 4H), 6.70 (t, $J = 54.2$ Hz, 1H), 3.91 (s, 3H).

$^{13}\text{C NMR}$ (100 MHz, CDCl_3) δ 159.6, 137.1, 135.1, 134.6, 132.7, 132.1 (x2C), 131.1 (x2C), 130.3, 128.8, 128.7, 125.2, 123.2, 122.3, 117.0, 111.2 (t, $J = 234$ Hz, 1C), 39.7.

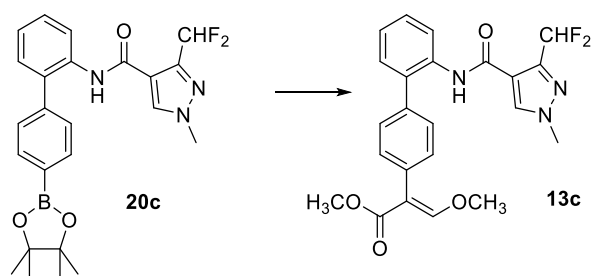
Synthesis of 3-(difluoromethyl)-1-methyl-N-(4'-(4,4,5,5-tetramethyl-1,3,2-dioxaborolan-2-yl)-[1,1'-biphenyl]-2-yl)-1H-pyrazole-4-carboxamide (20c).



In a round-bottom flask a solution of N-(4'-bromo-[1,1'-biphenyl]-2-yl)-3-(difluoromethyl)-1-methyl-1H-pyrazole-4-carboxamide **19c** (260 mg, 0.64 mmol) in dry dioxane (7 ml) was prepared. Potassium acetate (2.5 eq), bis(pinacolato)diboron (1.2 eq) and [1,1'-Bis(diphenylphosphino)ferrocene] palladium(II) dichloride (5% mol) were added, and the reaction mixture was heated to reflux and stirred for 6 hours. After this time, dioxane was evaporated under reduced pressure. The residue was diluted with ethyl acetate and washed with water and brine. The organic layer was dried over Na₂SO₄, filtered and the solvent was evaporated. Flash column chromatography (dichloromethane/methanol 95:5 → 90:10) afforded **20c** as a white solid in 80% yield.

¹H NMR (600 MHz, CDCl₃) δ 8.26 (d, *J* = 8.1 Hz, 1H), 7.88 (d, *J* = 7.9 Hz, 2H), 7.75 (bs, 1H), 7.66 (s, 1H), 7.43 – 7.38 (m, 3H), 7.29 – 7.26 (m, 1H), 7.21 (t, *J* = 7.4 Hz, 1H), 6.80 (t, *J* = 54.6 Hz, 1H), 3.91 (s, 3H), 1.36 (s, 12H).

Synthesis of ethyl (E)-2-(2'-(3-(difluoromethyl)-1-methyl-1H-pyrazole-4-carboxamido)-[1,1'-biphenyl]-4-yl)-3-methoxyacrylate (13c).



In a round-bottom flask compound **20c** (100 mg, 0.22 mmol) was solubilized in a 4:1 dioxane/water mixture (6.8 ml) under a nitrogen atmosphere. Potassium carbonate (2 eq) and methyl (Z)-2-iodo-3-methoxyacrylate **8** (1.1 eq) were added, followed by [1,1'-Bis(diphenylphosphino)ferrocene] palladium(II) dichloride (5% mol). Reaction mixture was heated to 80°C and stirred for 16 hours. After completion, reaction mixture was cooled to room temperature and dioxane was evaporated under reduced pressure. Aqueous NaHCO₃ (5%) was

added and the aqueous phase was extracted five times with ethyl acetate. The combined organic layers were washed with NH₄Cl and brine, dried over Na₂SO₄ and filtered, and the solvent was evaporated. The crude product was purified by flash chromatography (toluene/ethyl acetate 7:3) to afford compound **13c** as a yellowish oil in 60% yield.

¹H NMR (600 MHz, CDCl₃) δ 8.33 (d, *J* = 8.2 Hz, 1H), 7.68 (bs, 1H), 7.61 (s, 1H), 7.56 (s, 1H), 7.47 (d, *J* = 8.0 Hz, 2H), 7.40 (ddd, *J* = 8.6, 7.6, 1.6 Hz, 1H), 7.38 – 7.35 (m, 2H), 7.32 (dd, *J* = 7.6, 1.6 Hz, 1H), 7.21 (m, 1H), 6.93 (t, *J* = 54.2 Hz, 1H), 3.92 (s, 3H), 3.91 (s, 3H), 3.77 (s, 3H).

¹³C NMR (150 MHz, CDCl₃) δ 167.96, 159.89, 159.41, 144.62 (t, *J* = 26.6 Hz, 1xC), 136.51, 134.71, 132.92, 132.72, 132.51, 130.86 (2xC), 129.83, 128.80 (2xC), 128.36, 124.53, 121.82, 116.96, 110.97, 110.12 (t, *J* = 236.3 Hz, 1xC), 62.15, 51.60, 39.51.

Biology: In Vitro Biological evaluation of hybrid compounds 13b-c and intermediates 19a-c.

For fungal strains preparation, inhibition of mycelium growth of *P. oryzae*, and statistical analysis of biological data, see **Section 6.1.3**.

6.2.4. Bibliography

1. Brötz-Oesterhelt, H.; Brunner, N.A. How many modes of action should an antibiotic have? *Curr. Opin. Pharmacol.* **2008**, *8*, 564–573, doi:10.1016/j.coph.2008.06.008.
2. Gajdács, M. The concept of an ideal antibiotic: Implications for drug design. *Molecules* **2019**, *24*, 892, doi:10.3390/molecules24050892.
3. Cavalli, A.; Bolognesi, M.L.; Minarini, A.; Rosini, M.; Tumiatti, V.; Recanatini, M. Melchiorre, C. Multi-target-directed ligands to combat neurodegenerative diseases. *J. Med. Chem* **2008**, *51*, 347–372.
4. Gray, D.A.; Wenzel, M. Multitarget Approaches against Multiresistant Superbugs. *ACS Infect. Dis.* **2020**, *6*, 1346–1365, doi:10.1021/acsinfecdis.0c00001.
5. Muller-Schiffmann, A.; Sticht, H.; Korth, C. Hybrid Compounds: From Simple Combinations to Nanomachines. *Biodrugs* **2012**, *26*, 21–31.
6. De Oliveira Pedrosa, M.; Marques Duarte da Cruza, R.; de Oliveira Viana, J.; de Mouraa, R.O.; Ishikib, H.M.; Barbosa Filhoc, J.M.; Dinizc, M.F.F.M.; Scottic, M.T.; Scottic, L.; Bezerra Mendonça, F.J.J. Hybrid Compounds as Direct Multitarget Ligands: A Review. *Current Topics in Medicinal Chemistry* **2017**, *17*, 1044–1079, doi:10.2174/1568026616666160927.
7. Asibi, A.E.; Chai, Q.; Coulter, J.A. Rice blast: A disease with implications for global food security. *Agronomy* **2019**, *9*, 1–14, doi:10.3390/agronomy9080451.
8. Dean, R.; Van Kan, J.A.L.; Pretorius, Z.A.; Hammond-Kosack, K.E.; Di Pietro, A.; Spanu, P.D.; Rudd, J.J.; Dickman, M.; Kahmann, R.; Ellis, J.; Foster, G. D. The Top 10 fungal pathogens in molecular plant pathology. *Mol. Plant Pathol.* **2012**, *13*, 414–430, doi:10.1111/j.1364-3703.2011.00783.x.
9. Allen, H.K.; Donato, J.; Wang, H.H.; Cloud-Hansen, K.A.; Davies, J.; Handelsman, J. Call of the wild: Antibiotic resistance genes in natural environments. *Nat. Rev. Microbiol.* **2010**, *8*, 251–259, doi:10.1038/nrmicro2312.
10. Hammerum, A.M.; Heuer, O.E. Human health hazards from antimicrobial-resistant escherichia coli of animal origin. *Clin. Infect. Dis.* **2009**, *48*, 916–921, doi:10.1086/597292.
11. Anke, T.; Oberwinkler, F.; Steglich, W.; Schramm, G. The strobilurins - new antifungal antibiotics from the basidiomycete *Strobilurus tenacellus*. *J. Antibiot.* **1977**, *30*, 806–810, doi:10.7164/antibiotics.30.806.
12. Musso, L.; Fabbrini, A.; Dallavalle, S. Natural Compound-Derived

- Cytochrome bc1 Complex Inhibitors as Antifungal Agents. *Molecules* **2020**, *25*, 4582; doi:10.3390/molecules25194582.
13. Sauter, H. Strobilurins and other complex III inhibitors. In *Modern Crop Protection Compounds*; Kramer, W., Schimer, U., Eds.; **2012**; pp. 584–627.
 14. Earley, F.; Sauter, H.; Rheinheimer, J.; Rieck, H.; Coqueron, P.-Y.; Whittingham, W.G.; Walter, H. Fungicides Acting on Oxidative Phosphorylation. In *Modern Crop Protection Compounds*; Wiley, **2011**; pp. 559–691.
 15. Fernández-ortuño, D.; Torés, J.A.; De Vicente, A.; Pérez-garcía, A. The QoI Fungicides, the Rise and Fall of a Successful Class of Agricultural Fungicides. In *Fungicides*; Odile Carisse Ed.; **2010**, pp. 203–220, doi:10.5772/13205.
 16. Leahy, J.; Mendelsohn, M.; Kough, J.; Jones, R. Biopesticide Oversight and Registration at the U.S. Environmental Protection Agency. In *Biopesticides: State of the Art and Future Opportunities*; ACS Publications, 2014; 1172, 3–18.
 17. Tran, T.M.; Atanasova, V.; Tardif, C.; Richard-Forget, F. Stilbenoids as Promising Natural Product-Based Solutions in a Race against Mycotoxigenic Fungi: A Comprehensive Review. *J. Agric. Food Chem.* **2023**, *71*, 5075–5092, doi:10.1021/acs.jafc.3c00407.
 18. Jeandet, P.; Vannozzi, A.; Sobarzo-Sanchez, E.; Uddin, M.S.; Bru, R.; Martinez-Marquez, A.; Clement, C.; Cordelier, S.; Manayi, A.; Nabavi, S.F.; et al. Phytostilbenes as agrochemicals: biosynthesis, bioactivity, metabolic engineering and biotechnology. *Nat. Prod. Rep.* **2021**, *38*, 1282–1329, doi:10.1039/d0np00030b.
 19. Song, P.; Yu, X.; Yang, W.; Wang, Q. Natural phytoalexin stilbene compound resveratrol and its derivatives as anti - tobacco mosaic virus and anti - phytopathogenic fungus agents. *Sci. Rep.* **2021**, *11*, 16509–16519, doi:10.1038/s41598-021-96069-1.
 20. Adrian, M.; Jeandet, P.; Weston, L.A.; Bessis, R. Biological Activity of Resveratrol, a Stilbenic Compound from Grapevines, Against *Botrytis cinerea*, the Causal Agent for Gray Mold. *J. Chem. Ecol.* **1997**, *23*, 1689–1702, doi:10.1023/B.
 21. Stark-Lorentz, P.; Nelke, B.; Hanbler, G.; Mühlbach, H.P.; Thomzik, J.E. Transfer of a grapevine stilbene synthase gene to rice (*Oryza sativa* L.). *Plant Cell Rep.* **1997**, *16*, 668–673.
 22. Niu, S.; Liu, T.; Deng, Y.; Wang, W.; Zhang, Y.; Hong, W.; Zhang, D.; Hua, J.; Luo, S. Industrial Crops & Products Production and evaluation of

- antifungal stilbenoids in *Dracaena cochinchinensis* elicited by fungal inoculation. *Ind. Crop. Prod.* **2020**, *145*, 112148, doi:10.1016/j.indcrop.2020.112148.
23. Cai, X.; Qi, J.; Xu, Z.; Huang, L.; Li, Y.; Ren, X. Three stilbenes make difference to the antifungal effects on ochratoxin A and its precursor production of *Aspergillus carbonarius*. *Food Microbiol.* **2022**, *103*, 103967, doi:10.1016/j.fm.2021.103967.
 24. Mattio, L.M.; Pinna, C.; Catinella, G.; Musso, L.; Pedersen, K.J.; Krogfelt, K.A.; Dallavalle, S.; Pinto, A. Synthesis and antimicrobial activity of δ -viniferin analogues and isosteres. *Molecules* **2021**, *26*, 7594, doi:10.3390/molecules26247594.
 25. Mattio, L.M.; Dallavalle, S.; Musso, L.; Filardi, R.; Franzetti, L.; Pellegrino, L.; D'Incecco, P.; Mora, D.; Pinto, A.; Arioli, S. Antimicrobial activity of resveratrol-derived monomers and dimers against foodborne pathogens. *Sci. Rep.* **2019**, *9*, 1–13, doi:10.1038/s41598-019-55975-1.
 26. Zuccolo, M.; Kunova, A.; Musso, L.; Forlani, F.; Pinto, A.; Vistoli, G.; Gervasoni, S.; Cortesi, P.; Dallavalle, S. Dual-active antifungal agents containing strobilurin and SDHI-based pharmacophores. *Sci. Rep.* **2019**, *9*, 1–12, doi:10.1038/s41598-019-47752-x.
 27. Kunova, A.; Palazzolo, L.; Forlani, F.; Catinella, G.; Musso, L.; Cortesi, P.; Eberini, I.; Pinto, A.; Dallavalle, S. Structural Investigation and Molecular Modeling Studies of Strobilurin-Based Fungicides Active against the Rice Blast Pathogen *Pyricularia oryzae*. *Int. J. Mol. Sci.* **2021**, *22*, 3731. <https://doi.org/10.3390/ijms22073731>.
 28. Polunin, K.E.; Schmalz, H. Application of Chromium-Arene Complexes in the Organic Synthesis . Efficient Synthesis of Stilbene Phytoalexins 1. *Russ. J. Coord. Chem.* **2004**, *30*, 271–280.
 29. Lee, H.S.; Lee, B.W.; Kim, M.R.; Jun, J. Syntheses of Resveratrol and its Hydroxylated Derivatives as Radical Scavenger and Tyrosinase Inhibitor. **2010**, *31*, 4–8, doi:10.5012/bkcs.2010.31.04.971.
 30. Vo, D.D.; Elofsson, M. Total Synthesis of Viniferifuran, Resveratrol-Piceatannol Hybrid, Anigopreissin A and Analogues – Investigation of Demethylation Strategies. *Adv. Synth. Catal.* **2016**, *358*, 4085–4092, doi:10.1002/adsc.201601089.
 31. Snyder, S.A.; Breazzano, S.P.; Ross, A.G.; Lin, Y.; Zografos, A.L. Total Synthesis of Diverse Carbogenic Complexity within the Resveratrol Class from a Common Building Block. *J. Am. Chem. Soc.* **2009**, *131*, 1753–1765.
 32. Velu, S. S.; Buniyamin, I.; Ching, L. K.; Feroz, F.; Noorbacha, I.; Gee, L.

- C.; Awang, K. Regio- and Stereo-selective Biomimetic Synthesis of Oligostilbenoid Dimers from Resveratrol Analogues: Influence of the Solvent, Oxidant and Substitution. *Chem. Eur. J.* **2008**, *14*, 11376-11384, doi:10.1002/chem.200801575.
33. Li, J.; Qian, B.; Huang, H. Silver-Catalyzed Olefination of Acetals and Ketals with Diazoesters to β - Alkoxyacrylates. *Organi Lett.* **2018**, *20*, 7090–7094, doi:10.1021/acs.orglett.8b03040.
 34. Faria, J. C.; Jelihovschi, E. G.; Allaman, I. B. Conventional Tukey Test; UESC: Ilheus, Bahia, Brasil, 2022.
 35. Veloukas, T.; Karaoglanidis, G.S. Biological activity of the succinate dehydrogenase inhibitor fluopyram against *Botrytis cinerea* and fungal baseline sensitivity. *Pest Manag Sci* **2012**, *68*, 858–864, doi:10.1002/ps.3241.
 36. Chen, Y.; Zhang, A.; Wang, W.; Zhang, Y.; Gao, T. Baseline sensitivity and efficacy of thifluzamide in *Rhizoctonia solani*. *Ann Appl Biol.* **2012**, *161*, 247-254, doi:10.1111/j.1744-7348.2012.00569.x.
 37. Yanase, Y.; Kishi, J.; Inami, S.; Katsuta, H. Biological activity and disease controlling efficacy of penthiopyrad. *J. Pestic. Sci.* **2013**, *38*, 188–193, doi:10.1584/jpestics.D12-063.
 38. Kifong, L.; Shen, Y.-Q.; Jiang, L.-N.; Zhu, X.-L.; Yang, W.-C.; Huang, W.; Yang, G.-F. Succinate Dehydrogenase: An Ideal Target for Drug Discovery. In *Discovery and Synthesis of Crop Protection Products*; **2015**; pp. 175–194.
 39. Sierotzki, H.; Scalliet, G. A review of current knowledge of resistance aspects for the next-generation succinate dehydrogenase inhibitor fungicides. *Phytopathology* **2013**, *103*, 880–887, doi:10.1094/PHYTO-01-13-0009-RVW.
 40. Li, S.; Li, D.; Xiao, T.; Zhang, S.; Song, Z. Design, Synthesis, Fungicidal Activity, and Unexpected Docking Model of the First Chiral Boscalid Analogues Containing Oxazolines. *J. Agric. Food Chem.* **2016**, *64*, 8927–8934, doi:10.1021/acs.jafc.6b03464.
 41. Xiong, L.; Zhu, X.; Gao, H.; Fu, Y.; Hu, S.; Jiang, L.; Yang, W.; Yang, G. Discovery of Potent Succinate-Ubiquinone Oxidoreductase Inhibitors via Pharmacophore-linked Fragment Virtual Screening Approach. *J. Agric. Food Chem.* **2016**, *64*, 4830–4837, doi:10.1021/acs.jafc.6b00325.
 42. Xiong, L.; Li, H.; Jiang, L.; Ge, J.; Yang, W.; Zhu, X.L.; Yang, G. Structure-Based Discovery of Potential Fungicides as Succinate Ubiquinone Oxidoreductase Inhibitors. *J. Agric. Food Chem.* **2017**, *65*, 1021–1029, doi:10.1021/acs.jafc.6b05134.

43. Miles, T.D.; Miles, L.A.; Fairchild, K.L.; Wharton, P.S. Screening and characterization of resistance to succinate dehydrogenase inhibitors in *Alternaria solani*. *Plant Pathology* **2014**, *63*, 155–164, doi:10.1111/ppa.12077.
44. Lalève, A.; Gamet, S.; Walker, A.; Debieu, D.; Toquin, V.; Fillinger, S. Site-directed mutagenesis of the P225, N230 and H272 residues of succinate dehydrogenase subunit B from *Botrytis cinerea* highlights different roles in enzyme activity and inhibitor binding. *Environmental Microbiology* **2014**, *16*(7), 2253–2266 doi:10.1111/1462-2920.12282.
45. Angelini, R.M.D.M.; Masiello, M.; Rotolo, C.; Faretra, F. Molecular characterisation and detection of resistance to succinate dehydrogenase inhibitor fungicides in *Botryotinia fuckeliana* (*Botrytis cinerea*). *Pest Manag Sci.* **2014**, *70*, 1884–1893, doi:10.1002/ps.3748.
46. Ortuño, D.F.; Chen, F.; Schnabel, G.; Sciences, L. Resistance to Pyraclostrobin and Boscalid in *Botrytis cinerea* Isolates from Strawberry Fields in the Carolinas. *Plant disease* **2012**, *96*(8), 1198.
47. Sauter, H.; Steglich, W.; Anke, T. Strobilurins — new fungicides for crop protection Strobilurins: Evolution of a New Class of Active Substances. *Angew. Chem. Int. Ed.* **1999**, *38*, 1328-1349.
48. Papadopoulos, J.S.; Agarwala, R. COBALT: constraint-based alignment tool for multiple protein sequences. *Bioinformatics* **2007**, *23*, 1073–1079, doi:10.1093/bioinformatics/btm076.
49. Wang, X.; Wang, A.; Qiu, L.; Chen, M.; Lu, A.; Li, G.; Yang, C.; Xue, W. Expedient Discovery for Novel Antifungal Leads Targeting Succinate Dehydrogenase: Pyrazole-4-formylhydrazide Derivatives Bearing a Diphenyl Ether Fragment. *J. Agric. Food Chem.* **2020**, *68*, 14426–14437, doi:10.1021/acs.jafc.0c03736.
50. Zhang, A.; Zhou, J.; Tao, K.; Hou, T.; Jin, H. Design, synthesis and antifungal evaluation of novel pyrazole carboxamides with diarylamines scaffold as potent succinate dehydrogenase inhibitors. *Bioorganic Med. Chem. Lett.* **2018**, *28*, 3042–3045, doi:10.1016/j.bmcl.2018.08.001.
51. Pan, X.; Wilcox, C.S. Synthesis of Dibenzazepinones by Palladium-Catalyzed Intramolecular Arylation of *o*-(2'-Bromophenyl) anilide Enolates. *J. Org. Chem.* **2010**, *75*, 6445–6451, doi:10.1021/jo101137r.
52. Horng, J.; Liu, Y.; Chuang, S. Synthesis, Isolation, and Characterization of Mono- and Bis- norbornene-Annulated Biarylaminines through Pseudo-Catellani Intermediates. *Org. Lett.* **2019**, *21*, 1182–1186, doi:10.1021/acs.orglett.9b00119.
53. Tyagi, S.; Cook, C.D.; Didonato, D.A.; Key, J.A.; McKillican, B.P.; Eberle,

W.J.; Carlin, T.J.; Hunt, D.A.; Marshall, S.J.; Bow, N.L. Bioinspired Synthesis of a Sedaxane Metabolite Using Catalytic Vanadyl Acetylacetonate and Molecular Oxygen. *J. Org. Chem.* **2015**, *80*, 11941–11947, doi:10.1021/acs.joc.5b01700.

Chapter 7: Target-based virtual screening for the identification of novel scaffolds for the treatment of *Pyricularia oryzae* infections.

Published article:

“Exploration of Novel Scaffolds Targeting Cytochrome *b* of *Pyricularia oryzae*.” - *Int. J. Mol. Sci.* **2023**, *24*, 2705. <https://doi.org/10.3390/ijms24032705>

Authors:

Cecilia Pinna^{1 †}, Tommaso Laurenzi^{1 †}, Fabio Forlani¹, Luca Palazzolo², Claire Beatrice Nolan¹, Michael S. Christodoulou¹, Paolo Cortesi¹, Andrea Pinto¹, Ivano Eberini^{2,3*}, Andrea Kunova^{1*}, and Sabrina Dallavalle.

Affiliations:

¹Department of Food Environmental and Nutritional Science (DeFENS), University of Milan, 20133 Milano, Italy.

²Department of Pharmacological and Biomolecular Sciences (DiSFeB), University of Milan, 20133 Milano, Italy.

³Data Science Research Center (DSRC), University of Milan, 20133 Milano, Italy.

Abstract

The fulfilment of the European “Farm to Fork” strategy requires a drastic reduction in the use of “at risk” synthetic pesticides; this exposes vulnerable agricultural sectors—among which is the European rice culture—to the lack of efficient means for the management of devastating diseases, thus endangering food security. Therefore, novel scaffolds need to be identified for the synthesis of new and more environmentally friendly fungicides. In the present work, we employed our previously developed 3D model of *P. oryzae* cytochrome *bc1* (cyt *bc1*) complex to perform a high-throughput virtual screening of two commercially available compound libraries. Three chemotypes were selected, from which a small collection of differently substituted analogues was designed and synthesized. The compounds were tested as inhibitors of the cyt *bc1* enzyme function and the mycelium growth of both strobilurin-sensitive (*WT*) and -resistant (*RES*) *P. oryzae* strains. This pipeline has permitted the identification of thirteen compounds active against the *RES* cyt *bc1* and five compounds that inhibited the *WT* cyt *bc1* function while inhibiting the fungal mycelia only minimally. Serendipitously, among the studied compounds we identified a new chemotype that is able to efficiently inhibit the mycelium growth of *WT* and *RES* strains by ca. 60%, without inhibiting the cyt *bc1* enzymatic function, suggesting a different mechanism of action.

KEYWORDS: *high-throughput virtual screening; rice blast; antifungals; cytochrome bc1 enzymatic inhibition; design and synthesis.*

7.1. Introduction

Pyricularia oryzae Cavara is one of the most devastating pathogens worldwide [1]. Apart from being the major fungal pathogen of rice, causing rice blast, its host-specialized pathotypes also infect other cereal crops, such as wheat, causing a devastating wheat blast mainly in South America and South Asia [2–4], and turf grasses, causing gray leaf spot disease [5–7]. Agricultural production faces more and more restricted use of synthetic pesticides, which have already been drastically reduced in number over the past 20 years. However, to ensure a stable yield and to limit losses due to pests and pathogens, only a few efficient means with a low impact on the environment and human health are available. This is particularly true for the European rice sector, where after the withdrawal of tricyclazole from use in 2016 [8], only four fungicide classes are being used for the management of rice diseases and rice blast in particular. Strobilurins (quinone outside inhibitors, QoI, and FRAC 11) and demethylation inhibitors (DMI, FRAC 3) are synthetic fungicides that can be used in integrated disease management approaches, while sulphur (FRAC M02) and *Bacillus subtilis* QST 713 (FRAC BM02) can also be applied in biological agriculture [9]. However, such a limited portfolio of available products prompts the growers to repeatedly use the same compounds, especially on susceptible varieties largely grown in Europe, which in turn greatly increases the risk of resistance development in the pathogen populations. Fungicides with a single-site mode of action are especially at high risk of resistance development. This is also the case with QoI fungicides, which inhibit the electron transfer between cytochrome *b* and cytochrome *c* in the mitochondrial respiratory chain [10,11]. Strobilurins were introduced to the market in 1996 and still represent one of the most used fungicide classes [12–14]. Their mechanism of action has been studied in great detail; they act within the inner mitochondrial membrane, in particular on complex III by binding to the quinol oxidation site (Qo) of cytochrome *b*. This binding blocks the electron transfer between cytochrome *b* and cytochrome *c1*, which, in turn, leads to an energy deficiency in the fungal cells that halts oxidation of the reduced nicotinamide adenine dinucleotide (NADH) and synthesis of adenosine triphosphate (ATP), ultimately leading to cell death [15]. The resistance to strobilurins is most often determined by a single amino acid substitution from glycine to alanine (G143A), and until now, it has been detected in approximately 50 different pathogens [16,17]. Among these,

strobilurin resistance in *P. oryzae* was first observed in strains isolated from perennial ryegrass, *Lolium perenne* [18], followed by its diffused presence in wheat isolates (*Triticum aestivum*) [2,19]. In rice isolates, QoI-resistance was first described in 2013 in Japan [20] and was absent from Europe until 2021, when it was detected in Italy [21]. This poses a threat to the European risiculture sector, as widespread distribution of such resistant strains would seriously compromise rice blast management with the available means. The current situation urges the discovery and development of novel, highly effective compounds that would be able to control both wild-type (*WT*) and QoI-resistant (*RES*) populations of *P. oryzae*. In our previous work, we developed and validated the first three-dimensional model of the *P. oryzae* cytochrome *bc1* (cyt *bc1*) complex containing azoxystrobin as a ligand [14]. Here, we exploit the model for the identification of compounds with novel scaffolds that would be able to inhibit mitochondrial respiration and consequently the mycelium growth in both *WT* and *RES* isolates of *P. oryzae*.

7.2. Results

Virtual Screening and Identification of Potential Inhibitors of the Qo-Site of Cytochrome *b*

We employed the 3D model of the *P. oryzae* cyt *bc1* complex previously developed by our group [14] to perform a high-throughput virtual screening (HTVS) on two libraries of commercially available compounds, Agrochem and Biodesign, provided by Asinex (<https://www.asinex.com> accessed on 25 January 2023). The extra-precision glide score (XPG score) and its molecular weight-normalized value, as well as the binding mode and the number and type of molecular interactions, were used as selection criteria for the identification of the most promising structures. In particular, we narrowed our scope by focusing on molecules with the most favorable XPG score/mw and whose binding mode was characterized by the presence of relevant interactions resembling those of metyltetraprole [14]. This compound, a novel QoI fungicide with a unique tetrazolinone pharmacophore, was selected as a reference molecule as it is also active against QoI-resistant (*RES*) fungal pathogens [22,23]. From this procedure, eleven compounds emerged as potential hits for the development of antifungal agents (Supplementary Table S1). During this selection phase, the synthetic feasibility of the top-scoring structures was taken into consideration as well. Eventually, based on the above considerations, we selected compounds **1a**, **2a**, and **3** (Figure 7.1) for their further implementation. Compound **3** is the result of a modification of the original library compound, where a fluorine atom was removed from the chlorobenzene ring.

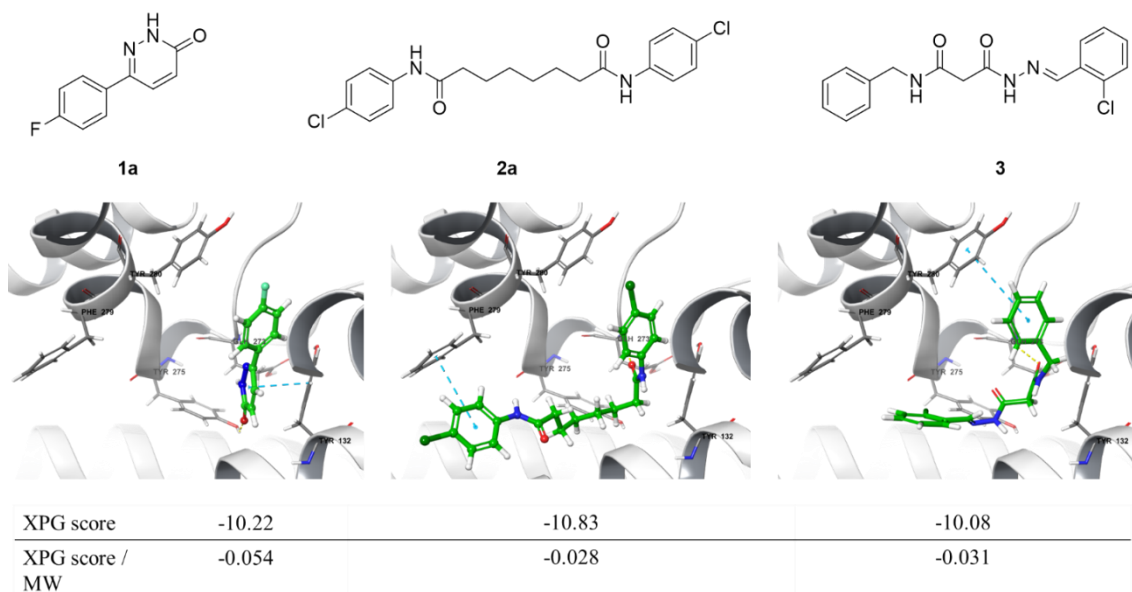
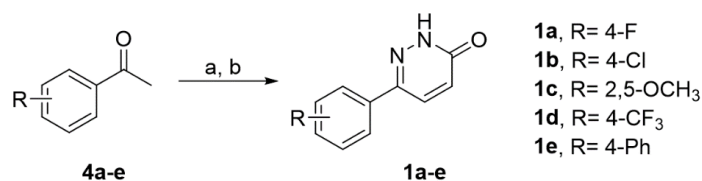


Figure 7.45. Structures, top-scoring docking poses and glide scores of compounds **1a**, **2a** and **3**; protein (gray cartoons), interacting residues (gray sticks), hydrogen-bonds (yellow dashes), and π - π interactions (blue dashes).

Synthesis of selected compounds and their analogues

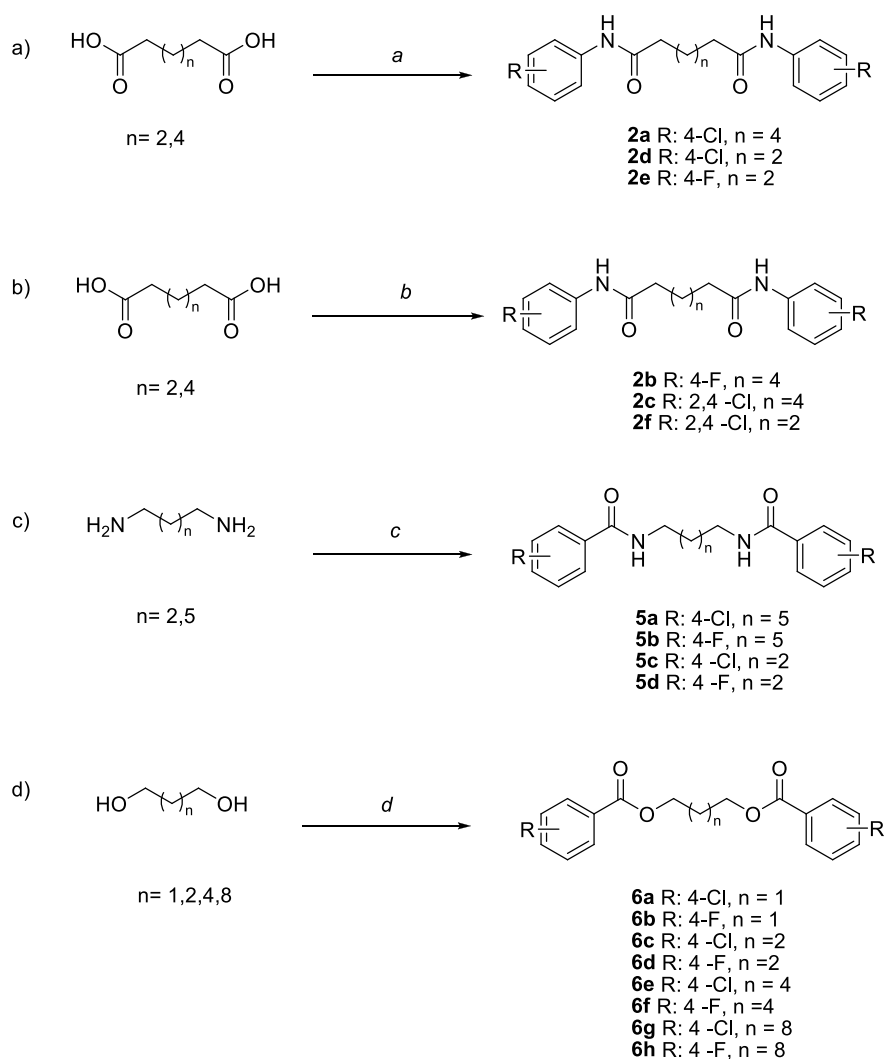
Compound **1a** displayed a strobilurin-like binding mode since its 4-fluorophenyl ring was placed near the Gly143 residue. Although its XPG score value was not among the most favorable, this molecule was associated with a relevant linearized XPG score/mw value, due to its low molecular weight. Interestingly, the compound showed a π - π interaction with Tyr132, similar to that formed by metyltetraprole [14], and an H-bond with the Tyr275 residue (Figure 1). Aiming at exploring the effect of different substitution patterns on the 6-phenylpyridazin3(2H)-one scaffold, compounds **1a-e** were synthesized simply by reacting variously substituted acetophenones with glyoxylic acid and hydrazine in a two-step procedure (**Scheme 9**) [24].



Scheme 9. Synthesis of compounds **1a-e**. Reagents and conditions: (a) glyoxylic acid, AcOH, reflux, 16 h; (b) NH₄OH; N₂H₄·H₂O, reflux, 2 h (10–70%).

Compound **2a** was characterized by a strobilurin-like binding mode with an XPG score of -10.828 (**Figure 7.45**). Three series of homologues (**2a-f**, **5a-d**, and **6a-h**, **Scheme 7.10**) were designed and synthesized in order to investigate the role of the amide group and its substitution with an ester group, as well as the effects of the aliphatic chain length. Compounds **2a**, **2d**, and **2e** were obtained

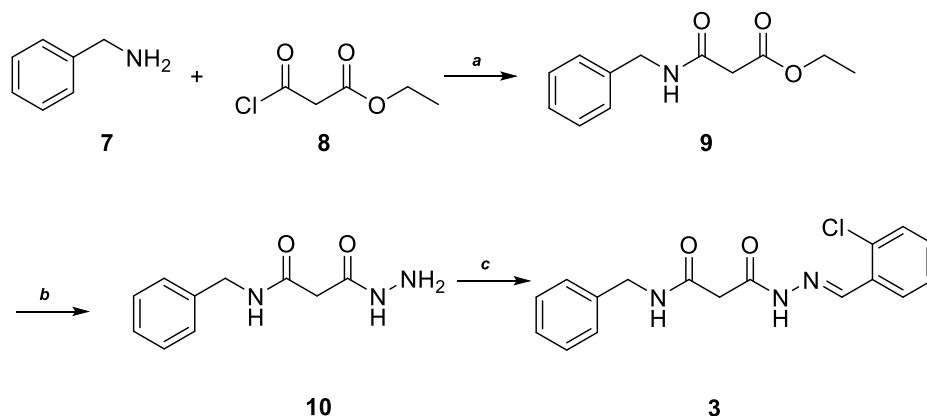
via amide coupling by reacting the appropriate aniline with adipic or suberic acid, in the presence of HATU and DIPEA. The efforts to obtain **2b**, **2c**, and **2f** by similar synthetic procedures involving the use of coupling reagents (HATU and EDCI) were not successful. These compounds were obtained by producing in situ adipoyl or suberoyl chloride, which was then reacted with 4-fluoroaniline or 2,4-dichloroaniline in the presence of triethylamine. 4-Halobenzoyl chlorides and aliphatic diamines (butanediamine and heptanediamine) afforded compounds **5a–d**, while esters **6a–h** were obtained by reacting the proper benzoyl chloride with propane-, butane-, hexane- and decanediol.



Scheme 7.10. Synthesis of compounds **2a–f**, **5a–d**, and **6a–h**. Reagents and conditions: (a) 4-haloaniline, HATU, DIPEA, rt, N₂, 16 h (40–51%); (b) (i) SOCl₂, DMF (cat.), reflux, 90 min; (ii) 4-haloaniline, TEA, DCM, rt, N₂, 16 h (69–70%); (c) 4-halobenzoyl chloride, TEA, DCM, rt, N₂, 2 h (30–90%); (d) 4-halobenzoyl chloride, TEA, toluene, rt, N₂, 3 h (40–97%).

Hydrazone **3** displayed π -stacking interaction between the benzyl ring and Tyr280, while the carbonyl group interacted via H-bond with Glu273 (**Figure**

7.45). This promising pattern of interactions prompted us to synthesize **3** through the synthetic pathway shown in **Scheme 7.11**. Benzylamine **7** was reacted with ethyl malonyl chloride **8** in the presence of TEA. Then, intermediate **9** was treated with hydrazine to afford the corresponding hydrazide (**10**), which was finally reacted with 2-chlorobenzaldehyde, giving a mixture of cis- and trans-isomers of compound **3**.



Scheme 7.11. Synthesis of compound **3**. Reagents and conditions: (a) TEA, dry DCM, N₂, rt, 3 h (55%); (b) NH₂-NH₂·H₂O, EtOH, reflux, 16 h (89%); (c) 2-chlorobenzaldehyde, EtOH, reflux, 6 h (72%).

Enzymatic Inhibition of Cytochrome *bc*1 Complex by the Compounds

A total of 24 compounds were screened for the inhibitory action on the QoI-targeted cyt *bc*1 mitochondrial complex (complex III). The cyt *bc*1 function was evaluated in vitro by measuring the NADH-dependent cyt *c* reduction activity (NADH:cyt *c* oxidoreductase activity) of the mitochondrial fractions isolated from the strobilurin-sensitive A252 (WT), and -resistant PO21_01 (RES) *P. oryzae* strains. In this assay, the electron-donor quinol is the mitochondria-native ubiquinol, which is electron-recharged through the NADH-oxidation mediated by complex I. As reported in **Table 7.5** and **Figure 7.46**, the cyt *bc*1 function of the WT strain mitochondrial fraction was clearly inhibited by five compounds ($p < 0.01$) and azoxystrobin. Interestingly, the cyt *bc*1 activity of the RES mitochondrial fraction was inhibited by 13 compounds. As expected, azoxystrobin did not show ($p > 0.01$) inhibitory action on the cyt *bc*1 function from the RES strain. The obtained results of the azoxystrobin activities on the mitochondrial fractions from the WT and RES strains validated the measured NADH:cyt *c* oxidoreductase activity as an indicator of the QoI-targeted cyt *bc*1 function.

These results indicate compounds **3**, **5a**, **6b**, and **6c** as a group of molecules of interest for their evident action on the cyt *bc*1 function in both the WT and the RES strains (**Figure 7.46**). This subset of compounds was further tested for the inhibition of the cyt *bc*1 function assayed specifically by measuring the

decylubiquinol:cyt c oxidoreductase activity. This assay uses decylubiquinol (DBH₂), a synthetic quinol, as the electron-donor substrate for the reduction of cyt c mediated by the mitochondrial cyt *bc1* (Table 7.6). Here, azoxystrobin (25 μM) also inhibited the DBH₂:cyt c oxidoreductase activity of the mitochondrial fraction from the *WT* strain ($p < 0.01$), whereas no inhibition was evident in the *RES* strain. All the tested compounds (**3**, **5a**, **6b**, and **6c**) showed inhibitory action ($p < 0.01$) on the DBH₂:cyt c oxidoreductase activity of the mitochondrial fraction from the *RES* strain. Compounds **3** and **6c** inhibited the activity of the mitochondrial fraction from the *WT* strain ($p < 0.05$).

Mycelium Growth Inhibition by the Compounds

The compounds **1a**, **2a**, and **3** and their analogues were tested in parallel for their inhibitory activity against both QoI-sensitive (*WT*) and -resistant (*RES*) strains of *P. oryzae*. As the compounds were dissolved in DMSO, the effect of 1% DMSO on fungal growth was also assessed. It had minimal inhibitory activity on both the *WT* and the *RES* strains (<10% inhibition of mycelial growth). Thus, the inhibitory activity of DMSO 1% was subtracted from the inhibition calculation of the tested compounds (see Materials and Methods for details). The overview of the inhibitory activity of all the tested compounds on the mycelial growth of the *WT* (A2.5.2.) and *RES* (PO21_01) strains of *P. oryzae* is summarized in Figure 7.47. Azoxystrobin (AZX) showed >95% inhibition of the *WT* strain, while it showed only ca. 25% inhibition of the *RES* strain. Out of all tested compounds, only **1b** showed ca. 60% inhibition of both the *WT* and the *RES* strains of *P. oryzae*, and an additional six compounds (**1d**, **1e**, **2c**, **3**, **5a**, **b**) showed a weak activity (>10% inhibition) against both the *WT* and the *RES* strains. In parallel, the compounds were screened on a panel of an additional six phytopathogenic fungi: *Penicillium expansum*, *Aspergillus niger*, *Mucor pyriformis*, *Botrytis cinerea*, *Fusarium culmorum*, and *F. graminearum* (Figure 4). In this case, the addition of 1% DMSO strongly inhibited the growth of *M. pyriformis* (ca. 40%), *B. cinerea* (ca. 20%), and *F. graminearum* (<15%), while it had only a minimum inhibitory effect on other fungi (<10%). Surprisingly, DMSO seemed to have a positive effect on the growth of *F. culmorum* (Supplementary Figure S1). Only compounds belonging to group **1** (Figure 7.48a), the analogues of **1a**, showed some activity against the tested fungi. None of the tested compounds inhibited *A. niger* and *B. cinerea*. Compound **1e** showed weak inhibitory activity (ca. 20% inhibition) against *P. expansum* and *M. pyriformis*. *Fusarium culmorum* was weakly inhibited by the compounds **1b** and **1d** (ca. 20% inhibition), while *F. graminearum* was the most inhibited pathogen. Its mycelium growth was reduced by compound **1a** by almost 40% and by its analogue **1b** by

ca. 60%. Weak activity of **1d** and **1e** (almost 20% inhibition) against *F. graminearum* was also observed.

Table 7.5. Inhibitory action of the tested compounds on the cyt bc1 function by measurements of the mitochondrial NADH:cyt c oxidoreductase activity.

Compound (200 μ M)	inhibitory action ^a (%; <i>p</i> -value)	
	WT	RES
azoxystrobin ^b	+ (81.4 \pm 5.3; 0.0014)	– (17.2 \pm 6.4; 0.0425)
1a	– (7.0 \pm 4.3; 0.1073)	– (–0.3 \pm 2.2; 0.8192)
1b	– (7.3 \pm 5.5; 0.1495)	+ (14.7 \pm 2.5; 0.0097)
1c	– (0.5 \pm 2.9; 0.7980)	– (10.2 \pm 4.3; 0.0536)
1d	+ (29.9 \pm 17.8; 0.0093)	+ (38.8 \pm 9.5; < 0.0010)
1e	– (3.9 \pm 16.5; 0.5891)	+ (28.9 \pm 9.4; < 0.0010)
2a	– (–2.1 \pm 25.2; 0.8978)	– (3.8 \pm 7.2; 0.4536)
2b	– (7.3 \pm 22.9; 0.6339)	– (18.9 \pm 5.4; 0.0256)
2c	– (11.3 \pm 21.9; 0.4666)	+ (30.7 \pm 6.9; < 0.0010)
2d	– (–10.6 \pm 13.7; 0.3136)	– (11.2 \pm 5.4; 0.0694)
2e	– (15.6 \pm 7.4; 0.0673)	+ (26.1 \pm 4.3; 0.0090)
2f	– (17.4 \pm 14.5; 0.0319)	– (17.6 \pm 3.5; 0.0127)
3	+ (48.8 \pm 7.9; < 0.0010)	+ (64.0 \pm 6.5; < 0.0010)
5a	+ (63.0 \pm 21.4; 0.0027)	+ (56.9 \pm 23.1; 0.0018)
5b	– (10.1 \pm 14.8; 0.3591)	+ (32.3 \pm 9.6; < 0.0010)
5c	– (9.2 \pm 7.1; 0.1512)	– (20.2 \pm 5.5; 0.0239)
5d	– (21.2 \pm 17.8; 0.0332)	– (15.4 \pm 7.8; 0.0789)
6a	– (46.0 \pm 27.7; 0.0250)	+ (66.8 \pm 9.5; < 0.0010)
6b	+ (56.3 \pm 16.8; 0.0017)	+ (64.7 \pm 12.5; < 0.0010)
6c	+ (48.5 \pm 3.2; < 0.0010)	+ (70.6 \pm 5.2; < 0.0010)
6d	– (23.6 \pm 11.3; 0.0248)	+ (77.3 \pm 11.0; < 0.0010)
6e	– (–35.0 \pm 29.5; 0.1763)	– (21.1 \pm 25.9; 0.1019)
6f	– (–10.0 \pm 24.1; 0.5459)	+ (74.5 \pm 6.6; < 0.0010)
6g	– (–49.8 \pm 44.1; 0.1898)	– (14.1 \pm 6.3; 0.0599)
6h	– (–2.9 \pm 6.8; 0.5294)	– (2.9 \pm 7.1; 0.5540)

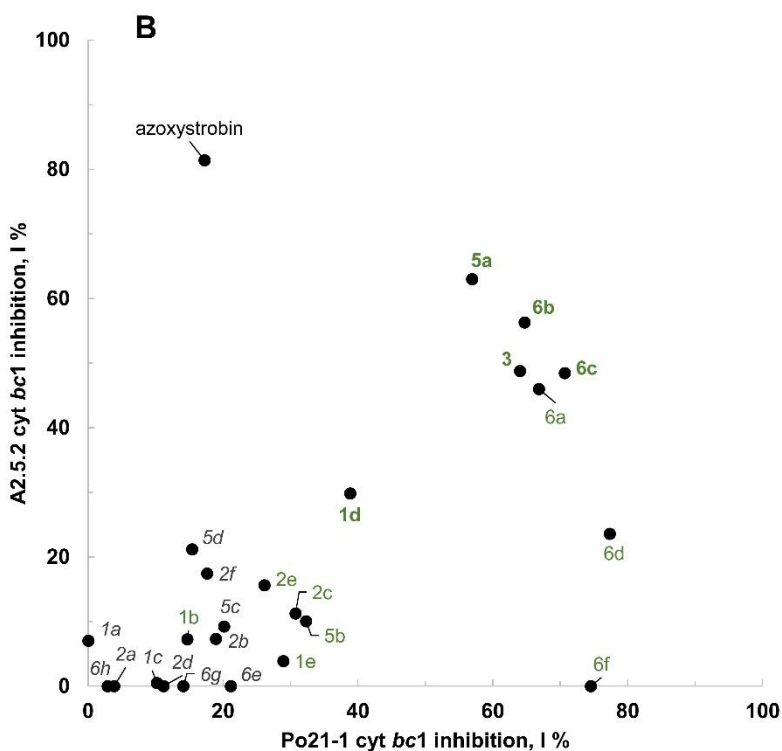
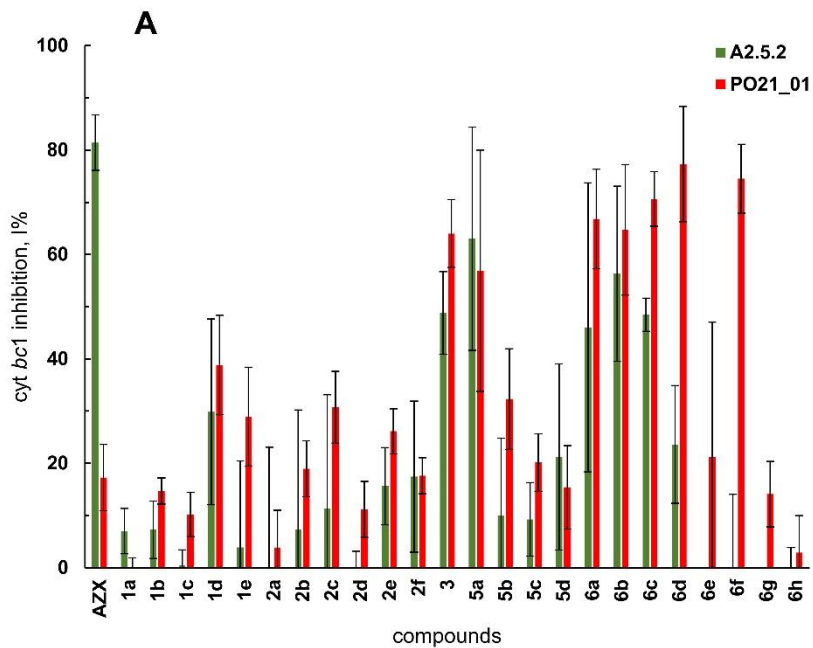


Figure 7.46. Enzymatic inhibition of cytochrome *bc1* by the compounds. (A) NADH:cyt c oxidoreductase activity of the mitochondrial fractions from strobilurin-sensitive A2.5.2 (green bars) and -resistant PO21_01 (red bars) strains was assayed in the presence of compounds. Enzyme inhibition is reported as a percentage (I%) of the control activity where the tested compound is replaced by DMSO, the diluent used for compound stocks. AZX, azoxystrobin. Error bars represent standard deviation of the mean. (B) Graphical representation of the inhibitory action of compounds on the mitochondrial *cyt bc1* enzyme function of the strobilurin-sensitive A2.5.2 and -resistant PO21_01 strains. In italics, no statistically relevant inhibition for both strains ($p > 0.01$); in green, statistically relevant inhibition for the strobilurin-resistant strain ($p < 0.01$); in boldfaced green, statistically relevant inhibition for both strains ($p < 0.01$); in regular typing, statistically relevant inhibition for strobilurin-sensitive strain ($p < 0.01$).

Table 7.6. Inhibitory action of a subset of compounds on the cyt *bc1* function by measurements of the mitochondrial decylubiquinol:cyt c oxidoreductase activity.

Compound (200 μ M)	Inhibitory action ^a (%; <i>p</i> -value)	
	WT	RES
Azoxystrobin^b	+ (82.1 \pm 9.1; < 0.0010)	– (22.5 \pm 17.3; 0.0440)
3	– (37.6 \pm 22.6; 0.0204)	+ (29.2 \pm 13.3; < 0.0080)
5a	– (4.9 \pm 23.3; 0.6601)	+ (37.4 \pm 11.5; 0.0019)
6b	– (–4.4 \pm 38.2; 0.8106)	+ (44.4 \pm 6.3; < 0.0010)
6c	– (45.9 \pm 20.5; 0.0208)	+ (54.1 \pm 17.4; 0.0084)

^a Inhibitory action on the cyt *bc1* function of mitochondrial fractions prepared from the strobilurin-sensitive (*WT*) A2.5.2 and -resistant (*RES*) PO21_01 strains is reported as positive (+) and marked bold only if the percent inhibition value is significantly above zero ($p < 0.01$; null t-test). ^b Azoxystrobin was tested at 25 μ M.

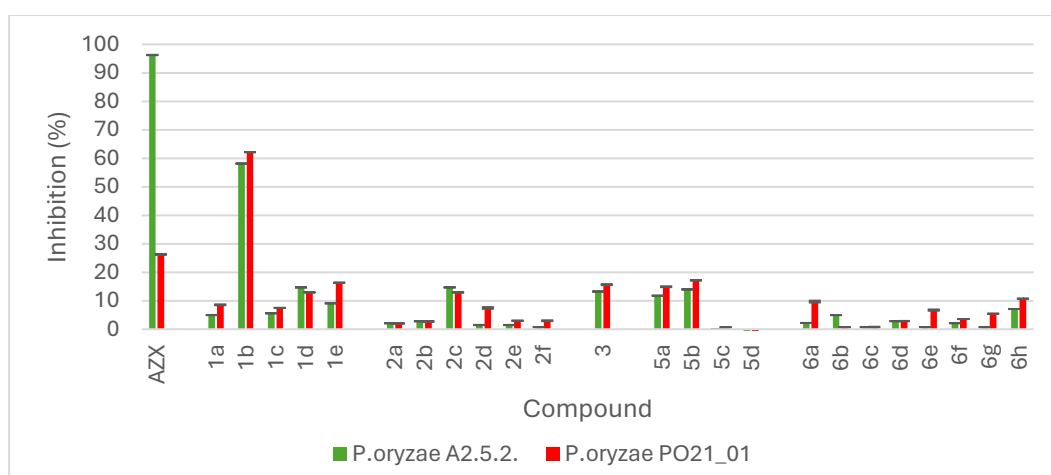


Figure 7.47. Inhibition of mycelium growth of *Pyricularia oryzae* QoI-sensitive A2.5.2. (green) and -resistant PO21_01 (red) strains on malt extract agar by the tested compounds of the series 1–6 and azoxystrobin (AZX) at a concentration 25 mg/L a.i. Error bars represent the standard deviation of the mean.

In Silico ADME/TOX Predictions

We performed a toxicokinetics (ADME/TOX) characterization of the compounds of interest, **1b**, **3**, **5a**, **6b**, and **6c**, which showed activity on the cyt *bc1* function. Descriptors were calculated using the ACD/Percepta program suite. The ADME/TOX characterization is reported in **Table 7.7**: most of the tested compounds, except for **1b** and **6b**, showed poor oral bioavailability (%F), especially when taking into consideration the liver and gut firstpass effect. The apparent volume of distribution (*V*_d) values were determined together with the predicted tendency of each evaluated molecule to bind specific plasma proteins. The *V*_d values are well below the determined limit associated with a total body fat distribution (*V*_d > 200), suggesting a reduced level of lipophilicity and bioaccumulation. Considering the analyses involving the CYP450 superfamily, none of the selected molecules was predicted to undergo significant biotransformations due to the CYP450 isoforms considered by the software.

However, the **6b** and **6c** diesters showed a potential inhibitory activity affecting the CYP450 isoform CYP1A2.

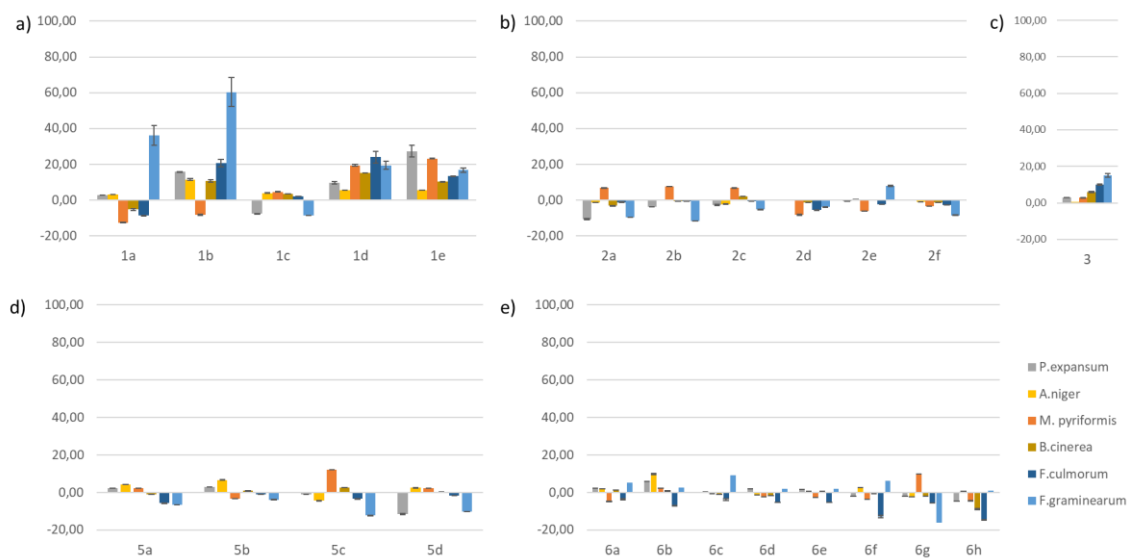


Figure 7.48. Inhibition of mycelium growth of six pathogenic fungal species on malt extract agar by the tested compounds (25 mg/L). a) – e) groups 1 - 6 of the tested compounds. Error bars represent the standard deviation of the mean.

Table 7.7. Toxicokinetics (ADME) characterization of hit compounds performed with the ACD/Percepta suite. The parameters reported are: %F of oral bioavailability (determined ignoring and considering the first-pass effect), volume of distribution (Vd), and probabilities of being Cyt P450 substrates and/or inhibitors.

Compound	Oral Bioavailability (%F)		Vd (L/Kg)	Protein Binding	P450 substrate	P450 inhibition
	No first-pass	first-pass				
1b	98.9*	65.3*	0.51	Human serum albumin	N.A.	N.A.
3	37.3	33.2	2.1	Human serum albumin	N.A.	N.A.
5a	33.1	17.9	5.6	Majority of plasma proteins	N.A.	N.A.
6b	91.6*	80.6*	10	Lipoproteins -Albumin (less extent)	N.A.	Probable CYP1A2 efficient inhibitor (IC ₅₀ < 10µM)
6c	42.3	36.4	5.5	Lipoproteins -Albumin (less extent)	N.A.	Probable CYP1A2 efficient inhibitor (IC ₅₀ < 10µM)

*: Oral bioavailability (%F) above 50% are to be considered significant; N.A.: not significant/reliable prediction.

The toxicological endpoints considered of relevance for in silico hazard identification are reported in **Table 7.8**. All the molecules were shown to have the physicochemical properties suitable for blood–brain barrier penetration and potential CNS activity. An endocrine disruption risk assessment was evaluated based on the predicted binding affinity to estrogen receptor- α (ER α), and compounds **5a**, **6b**, and **6c** were predicted as weak ER α binders. None of the tested molecules was predicted to be an eye/skin irritant. Finally, aquatic life toxicity was assessed, an extremely relevant parameter for compounds intended to be released into the environment, such as pesticides and agrochemical active ingredients.

Table 7.8. Toxicological endpoints selected for the hazard identification procedure. For each compound, BBB penetration, endocrine system disruption, eye/skin irritation, and aquatic toxicity were predicted using the ACD/Percepta suite.

Compound	BBB Penetration	Endocrine System Disruption	Eye/Skin Irritation	Aquatic Toxicity
3	Yes	No binding to ER α (LogRBA < -3)	N.A.	N.A.
5a	Yes	Weak ER α binder (-3 < LogRBA < 0)	N.A.	Ciliate Protozoa IGC50 = 0.72 mg/L
6b	Yes	Weak binding to ER α (-3 < LogRBA < 0)	N.A.	Ciliate Protozoa IGC50 = 1.1mg/L
6c	Yes	Weak ER α binder (-3 < LogRBA < 0)	N.A.	Water flea LC50 = 2.6 mg/L

N.A.: not significant/reliable prediction; IGC50: inhibition growth concentration; LC50: lethal concentration.

7.3. Discussion

In this study, we employed a three-dimensional model of *P. oryzae* cytochrome *bc1* complex to screen two libraries of commercially available compounds (Agrochem and Biodesign). Virtual Screening procedures implement rapid conformational search and empirical scoring functions to predict ligand-receptor interactions and metrics proportional to the binding free energy. Usually, predicted ligand affinities are within one order of magnitude of experimental values [25]. Molecular interactions from docking calculations may also be useful to predict the mode of action and activity of docked molecules [14,26]. Compounds with the best glide score and whose binding mode was characterized by the presence of relevant interactions were selected as promising novel scaffolds for the synthesis of a small collection of molecules, including 6-phenylpyridazin3(2H)-ones, aryl-amides, aryl-esters and hydrazones. The obtained compounds were tested both by enzymatic assays with the isolated mitochondrial fractions containing the target of strobilurin

fungicides (cyt *bc1*; complex III) and by biological assays on a panel of seven phytopathogenic fungi including wild-type and a QoI-resistant strains of *P. oryzae*.

The enzymatic assay based on measurements of NADH:cyt *c* oxidoreductase activity was used to screen compounds for the inhibition of the cyt *bc1* function. Strong inhibition of the *WT* mitochondrial fraction was observed already at 25 μ M of azoxystrobin, while only a limited inhibition was detected on *RES* mitochondrial fraction even at 200 μ M (25% inhibition, $p = 0.06$), thus validating the NADH:cyt *c* oxidoreductase activity assay as an indicator of the strobilurin-targeted cyt *bc1* function.

The cyt *bc1* function of mitochondrial fraction from both *P. oryzae* *WT* and *RES* strains was inhibited by five compounds. On the other hand, *RES* mitochondrial fraction was inhibited by additional eight compounds. In particular, both mitochondrial fractions (*WT* and *RES*) were inhibited by ca. 50% by the compounds **3**, **5a**, **6b** and **6c** in the NADH:cyt *c* oxidoreductase activity assay (Table 7.5, Figure 7.46). Considering altogether the enzyme inhibition results, the structural criteria that have driven the selection of compounds helped the discovery of new chemotypes with different size and shape, preferentially active on the cyt *bc1* in the *P. oryzae* *RES* strain. In particular, compounds of the series **1** are characterized by rigid structure, whereas compounds of the series **5** and **6** have higher flexibility and the chains with different lengths are tolerated.

The compounds **5a** and **6b** did not show the inhibition of the DBH₂:cyt *c* oxidoreductase activity whereas their inhibition of the NADH:cyt *c* oxidoreductase activity was evident. These different results could be explained by the use of two diverse quinols involved in the enzyme reaction, the synthetic DBH₂ or the mitochondrial ubiquinol. We hypothesize that the tested compounds could compete with the two quinols differently for the Qo site.

Surprisingly, compounds **3**, **5a**, **6b** and **6c** showed only a minimal inhibition of the fungal mycelia, both in the *WT* and *RES* strain of *P. oryzae*. This could indicate a poor bioavailability, most likely due to various mechanisms such as detoxification by the fungal cell, low absorption, or inability to penetrate the cell wall, which impedes the molecule to bind to the cyt *bc1* target.

On the other hand, compound **1b** displayed the best mycelium inhibition activity in vitro (ca. 60% inhibition) both in *WT* and *RES* *P. oryzae*. **1b** differs from **1a** only by a chloro- substituent at the para position in place of the fluorine, suggesting that the presence of a chlorine atom strongly enhances the biological activity of the 6-phenylpyridazin3(2*H*)-one core. Interestingly, **1b**

showed only a low inhibition of the putative molecular target in enzymatic assays, and a similar mycelium inhibition of both strobilurin-sensitive and -resistant strains of *P. oryzae*. These results together suggest that **1b** biological activity is due to a different mechanism of action which will be investigated further.

A preliminary *in silico* ADME/TOX analysis was carried out, showing that the most promising compounds have a very reduced propensity to bioaccumulation in adipose tissue (low predicted Vd), a relevant hazard factor for potential pesticides; however, compounds **6(b,c)** were predicted as potential strong CYP1A2 inhibitors and weak ER α binders (along with **5a**), suggesting that further and thorough *in vitro/in vivo* toxicological characterization is advisable. Summing up, the HTVS campaign using the 3D model of *P. oryzae* cytochrome *bc1* complex led to the identification of novel chemotypes potentially active on the *cyt bc1* enzyme in the strobilurin-sensitive and resistant *P. oryzae*. Future efforts will focus on improving the physicochemical properties of the most active compounds, along with conducting formulation studies aimed at increasing their bioavailability.

7.4. Materials and Methods

Molecular modelling, virtual screening and ADME/TOX analysis

The 3D model of *P. oryzae* cytochrome *bc1* complex was built upon the crystallographic structure of bovine *cyt bc1* co-crystallized with azoxystrobin (PDB ID: 1SQB), as described in [14]. High-throughput virtual screening (HTVS) was performed using Glide [27,28] on the chemoteques Agrochem (13,524 molecules) and Biodesign (170,269 molecules), provided by Asinex (<https://www.asinex.com>). Screening molecules were prepared using LigPrep (LigPrep, Schrödinger, LLC, New York, NY, 2021), to generate relevant tautomeric states and enantiomers for each chiral center. HTVS protocol consisted of three subsequent stages applying flexible-ligand docking algorithms with increasing complexity (namely: HTVS, Standard Precision and Extra Precision) to the top-scoring compounds from each run. The virtual screening resulted in 308 molecules, with a docking score (XPG score) ranging between -10.060 and -12.907 kcal/mol. Compounds were then clustered according to their interaction fingerprints (SIFT) and compared to the binding mode of methyltetraprole and known active strobilurins [14]. Compounds were ranked after normalizing the docking XPG score by their molecular weight (MW). Because large molecules usually have the highest affinity, this metric, also known as “ligand efficiency”, provides an approximation of the

compounds affinity by atomic mass units, which may be helpful to score compounds of varying sizes and identify potential active molecules also within small MW ranges[27,28].

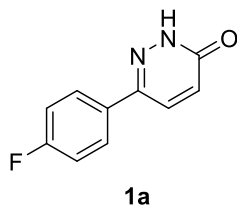
ADME/TOX descriptors for the most promising compounds were predicted *in silico* using ACD/Percepta (Advanced Chemistry Development, Inc., Pharma Algorithms, Inc.) software suite. All the predictors computed by this software have been developed with the use of large, validated databases, QSAR models, and the integration of expert knowledge of organic chemistry and toxicology.

Chemistry

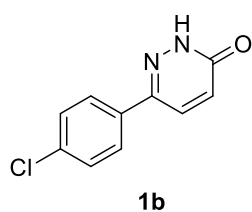
All the reagents and solvents were purchased from commercial suppliers and used without any further purification. The ¹H NMR and ¹³C NMR spectra were recorded with a Bruker AV600 (¹H, 600 MHz; ¹³C, 150 MHz) spectrometer. The chemical shifts (δ) are expressed in ppm, and the coupling constants (J) are in Hz. All the reactions requiring anhydrous conditions were performed under a positive nitrogen flow, and all glassware was oven dried. Isolation and purification of the compounds were performed by flash column chromatography on silica gel 60 (230–400 mesh). TLC analyses were performed using commercial silica gel 60 F254 aluminium sheets. All the final products showed a purity > 95% by NMR spectroscopy.

General Procedure for the Synthesis of 6-Phenylpyridazin-3(2H)-ones (1a–e)

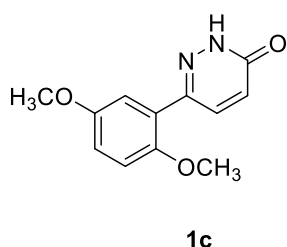
In a round-bottom flask, the appropriate acetophenone (1 eq) was dissolved in glacial acetic acid. To the obtained solution (0.5 M), glyoxylic acid (1.2 eq) was added, and the reaction mixture was refluxed overnight. Then, the reaction was cooled to room temperature and a solution of NH₄OH (32%) was added until pH 8 was reached. The aqueous phase was extracted three times with dichloromethane. Then, hydrazine hydrate (10 eq) was added to the aqueous layer and the reaction mixture was heated to reflux for two hours. The resulting precipitate was filtered and washed with water.



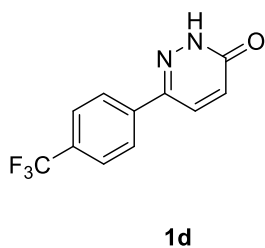
6-(4-Fluorophenyl)pyridazin-3(2H)-one (1a): white powder, 50% yield. $^1\text{H NMR}$ (600MHz, CD_3OD): δ 8.04 (d, $J = 9.8$ Hz, 1H), 7.93 (m, 2H), 7.23 (m, 2H), 7.08 (d, $J = 9.8$ Hz, 1H) $^{13}\text{C NMR}$ (150MHz, CD_3OD): δ 165.1 (d, $J = 249.0$ Hz), 163.2, 146.4, 133.4, 132.4, 130.9, 129.3 (d, $J = 8.9$ Hz, 2C), 116.7 (d, $J = 22.0$ Hz, 2C).



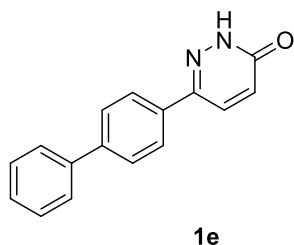
6-(4-Chlorophenyl)pyridazin-3(2H)-one (1b): white powder, 70% yield. $^1\text{H NMR}$ (600MHz, CD_3OD): δ 8.05 (d, $J = 9.9$ Hz, 1H), 7.90 (d, $J = 8.8$ Hz, 2H), 7.56 (d, $J = 8.8$ Hz, 2H), 7.01 (d, $J = 9.9$ Hz, 1H). $^{13}\text{C NMR}$ (150MHz, $\text{DMSO}-d_6$): δ 160.1, 124.7, 133.9, 133.5, 131.3, 130.2, 128.9 (2C), 127.4 (2C).



6-(2,5-Dimethoxyphenyl)pyridazin-3(2H)-one (1c): white powder, 60% yield. $^1\text{H NMR}$ (600 MHz, CD_3OD): δ 7.90 (d, $J = 9.8$ Hz, 1H), 7.14 (d, $J = 3$ Hz, 1H), 7.07 (d, $J = 8.9$ Hz, 1H), 7.01 (dd, $J = 3.0, 8.9$ Hz, 1H), 6.97 (d, $J = 9.8$, 1H), 3.84 (s, 3H), 3.80 (s, 3H). $^{13}\text{C NMR}$ (150 MHz, CD_3OD): δ 163.3, 155.3, 152.7, 147.2, 137.6, 128.8, 126.1, 117.2, 116.2, 114.0, 56.7, 56.2.



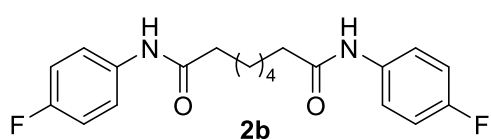
6-(4-(Trifluoromethyl)phenyl)pyridazin-3(2H)-one (1d): light brown powder, 60% yield. $^1\text{H NMR}$ (600 MHz, CD_3OD): δ 8.08 (m, 3H), 7.78 (d, $J = 8.2$ Hz, 2H), 7.10 (d, $J = 9.9$ Hz, 1H). $^{13}\text{C NMR}$ (150 MHz, CD_3OD): δ 163.2, 145.7, 139.6, 133.2, 132.2 (q, $J = 22.0$ Hz), 131.0, 127.6 (2C), 126.8 (2C), 125.5 (q, $J = 272.0$ Hz).



6-([1,1'-Biphenyl]-4-yl)pyridazin-3(2H)-one (1e): light brown powder, 10% yield. $^1\text{H NMR}$ (600 MHz, $\text{DMSO}-d_6$): δ 8.10 (d, $J = 9.8$ Hz, 1H), 7.96 (d, $J = 8.5$ Hz, 2H), 7.79 (d, $J = 8.5$, 2H), 7.73 (d, $J = 7.8$ Hz, 2H), 7.49 (t, $J = 7.8$ Hz, 2H), 7.40 (t, $J = 7.8$ Hz, 1H), 7.01 (d, $J = 9.8$ Hz, 1H). $^{13}\text{C NMR}$ (150 MHz, $\text{DMSO}-d_6$): δ 160.2, 143.4, 140.7, 139.3, 133.6, 131.4, 130.1, 129.0 (2C), 127.8, 127.1 (2C), 126.6 (2C), 126.2 (2C).

General Procedure for the Synthesis of Compounds **2b**, **2c**, and **2f**

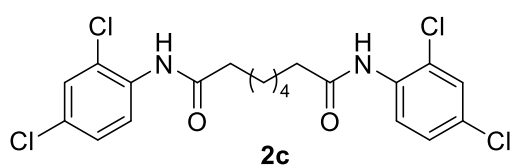
Suberic or adipic acid (2 mmol) was dissolved in thionyl chloride (1.45 mL, 10 eq) under a nitrogen atmosphere in a round-bottom flask. Three drops of dimethylformamide were added, and the reaction mixture was heated to reflux for 90 min. After complete consumption of the starting material, the reaction mixture was cooled to room temperature, diluted with a 1:1 toluene/heptane mixture, and evaporated under reduced pressure. This procedure was repeated two more times until the excess of thionyl chloride was completely removed. The corresponding acyl chloride was obtained in quantitative yield, and it was used for the next step without further purification. The obtained adipoyl/suberoyl chloride was dissolved in anhydrous dichloromethane (15 mL) under a nitrogen atmosphere, and the solution was cooled to 0 °C in an ice bath. The appropriate anilines (2.2 eq) (4-fluoroaniline for **2b** and 2,4-dichloroaniline for **2c** and **2f**) and triethylamine (4 eq) were added; then, the reaction mixture was warmed to room temperature and stirred for 24 h. The resulting precipitate was filtered and washed with water, giving the desired products.



***N*¹,*N*⁸-bis(4-fluorophenyl)octanediamide**

(**2b**): white solid, 70% yield.

¹H NMR (600 MHz, DMSO-*d*₆): δ 9.95 (s, 2H), 7.61 (m, 4H), 7.11 (m, 4H), 2.28 (t, *J* = 7.4 Hz, 4H), 1.59 (m, 4H), 1.32 (m, 4H). ¹³C NMR (150 MHz, DMSO-*d*₆): δ 171.1 (2C), 157.8 (d, *J* = 249.0 Hz, 2C), 135.7 (2C), 120.7 (d, *J* = 9.0 Hz, 4C), 115.2 (d, *J* = 22.0 Hz, 4C), 36.3 (2C), 28.5 (2C), 25.0 (2C).



***N*¹,*N*⁸-bis(2,4-dichlorophenyl)**

octanediamide (2c**):** white solid,

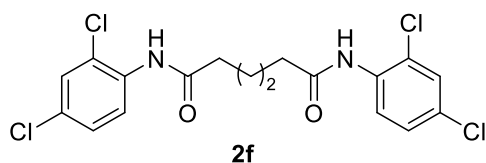
60% yield. ¹H NMR (600 MHz, DMSO-*d*₆):

δ 9.52 (s, 2H), 7.70 (d, *J* = 8.8 Hz, 2H), 7.64

(d, *J* = 2.10 Hz, 2H), 7.39 (dd, *J* = 8.8 Hz, *J* =

2.10 Hz, 2H), 2.34 (t, *J* = 6.9 Hz, 4H), 1.60 (m, 4H), 1.36 (m, 4H). ¹³C NMR (150

MHz, DMSO-*d*₆): δ 171.7 (2C), 134.2 (4C), 129.2 (2C), 128.8 (2C), 127.4 (4C), 35.6 (2C), 28.3 (2C), 25.0 (2C).



***N*¹,*N*⁸-bis(2,4-dichlorophenyl)adipamide**

(**2f**): white solid, 50% yield. ¹H NMR (600

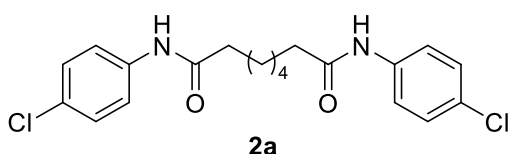
MHz, DMSO-*d*₆): δ 9.54 (s, 2H), 7.72 (d, *J* =

8.2 Hz, 2H), 7.65 (d, *J* = 2.1 Hz, 2H), 7.40

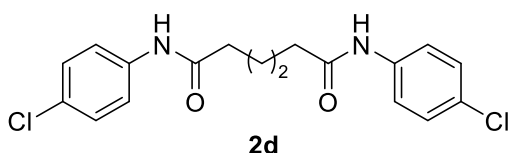
(dd, $J = 8.2, 2.1$ Hz, 2H), 2.42 (m, 4H), 1.65 (m, 4H). ^{13}C NMR (150 MHz, DMSO- d_6): δ 171.5 (2C), 134.2 (4C), 129.3 (2C), 128.8 (2C), 127.5 (4C), 35.5 (2C), 24.8 (2C).

General Procedures for the Synthesis of Compounds 2a, 2d, and 2e

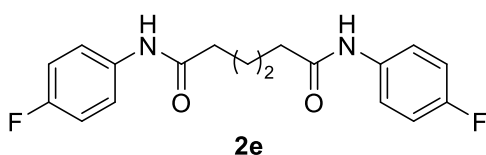
In a round-bottom flask, suberic or adipic acid (1 mmol) was dissolved in 8 mL of anhydrous THF under a nitrogen atmosphere. 1-[Bis(dimethylamino)methylene]-1H-1,2,3-triazolo [4,5-b] pyridinium 3-oxide hexafluorophosphate (HATU, 2.2 eq) and diisopropylamine (2.2 eq) were added and the reaction mixture was stirred at room temperature for 30 min. Then, 2 equivalents of the selected aniline (4-chloro or 4-fluoroaniline) were added, and the obtained solution was stirred at room temperature for 16 h. After reaction completion, the obtained solid was filtered and washed with water. No further purification was needed.



N^1, N^8 -bis(4-chlorophenyl)octanediamide (2a): white solid, 60% yield. ^1H NMR (600 MHz, DMSO- d_6): δ 9.98 (s, 2H), 7.62 (d, $J = 8.7$ Hz, 4H), 7.32 (d, $J = 8.7$ Hz, 4H), 2.29 (t, $J = 7.4$ Hz, 4H), 1.59 (m, 4H), 1.32 (m, 4H). ^{13}C NMR (150 MHz, DMSO- d_6): δ 171.4 (2C), 138.3 (2C), 128.5 (4C), 126.4 (2C), 120.5 (4C), 36.3 (2C), 28.4 (2C), 24.9 (2C).



N^1, N^8 -bis(4-chlorophenyl)adipamide (2d): white solid, 50% yield. ^1H NMR (600 MHz, DMSO- d_6): δ 10.04 (s, 2H), 7.62 (d, $J = 8.7$ Hz, 4H), 7.33 (d, $J = 8.7$ Hz, 4H), 2.33 (m, 4H), 1.62 (m, 4H). ^{13}C NMR (150 MHz, DMSO- d_6): δ 171.3 (2C), 138.3 (2C), 128.5 (4C), 126.4 (2C), 120.5 (4C), 36.2 (2C), 24.7 (2C).

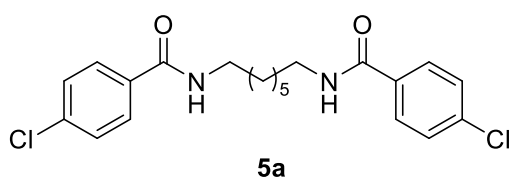


N^1, N^6 -bis(4-fluorophenyl)adipamide (2e): white solid, 55% yield. ^1H NMR (600 MHz, DMSO- d_6): δ 9.88 (s, 2H), 7.55 (m, 4H), 7.06 (m, 4H), 2.27 (m, 4H), 1.58 (m, 4H). ^{13}C NMR (150 MHz, DMSO- d_6): δ 170.9 (2C), 157.8 (d, $J = 237.0$ Hz), 135.7 (2C), 120.8 (d, $J = 8.9$ Hz, 4C), 115.1 (d, $J = 22.0$ Hz, 4C), 36.1 (2C), 24.9 (2C).

General Procedure for the Synthesis of Compounds 5a–d

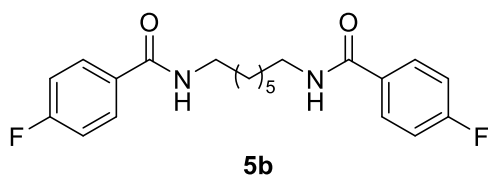
A solution of butanediamine or heptanediamine (1 mmol) in dry dichloromethane (2.5 mL) was prepared in a round-bottom flask under a

nitrogen atmosphere, and then, triethylamine (4 eq) was added. In the meantime, a solution of 4-halobenzoyl chloride (2 mmol) in anhydrous dichloromethane (2.5 mL) was prepared and then added dropwise to the former solution. The reaction mixture was stirred at room temperature until the starting materials were completely consumed (2–3 h). The obtained white precipitate was filtered and washed with NaHCO₃ (soln. 5%), HCl 0.5 M, and water.



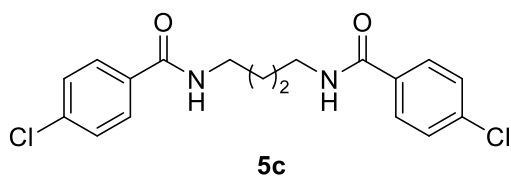
***N,N'*-(heptane-1,7-diyl)bis(4-chlorobenzamide) (5a)**: white solid, 30% yield. ¹H NMR (600 MHz, DMSO-*d*₆): δ 8.50 (t, *J* = 5.5 Hz, 2H), 7.84 (d, *J* = 8.3 Hz, 4H), 7.52 (d, *J* = 8.3 Hz, 4H), 3.23 (m, 4H),

1.51 (m, 4H), 1.31 (m, 6H). ¹³C NMR (150 MHz, DMSO-*d*₆): δ 165.0 (2C), 135.8 (2C), 133.4 (2C), 129.1 (4C), 128.3 (4C), 39.5 (2C overlapped to the solvent signal), 29.0 (2C), 28.5, 26.4 (2C).



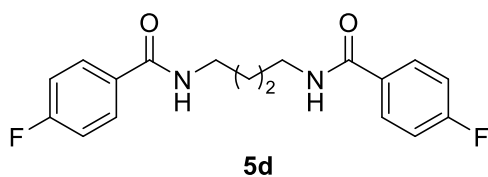
***N,N'*-(heptane-1,7-diyl)bis(4-fluorobenzamide) (5b)**: white solid, 80% yield. ¹H NMR (600 MHz, DMSO-*d*₆): δ 8.45 (t, *J* = 5.2 Hz, 2H), 7.98 (m, 4H), 7.27 (m, 4H), 3.25 (m, 4H), 1.51 (m, 4H), 1.31 (m,

6H). ¹³C NMR (150 MHz, DMSO-*d*₆): δ 165.0 (2C), 163.7 (d, *J* = 248.0 Hz, 2C), 131.2 (2C), 129.7 (d, *J* = 9.0 Hz, 4C), 115.1 (d, *J* = 22.0 Hz, 4C), 39.5 (2C overlapped to the solvent signal), 29.0 (2C), 28.5, 26.5 (2C).



***N,N'*-(butane-1,4-diyl)bis(4-chlorobenzamide) (5c)**: white solid, 90% yield. ¹H NMR (600 MHz, DMSO-*d*₆): δ 8.54 (t, *J* = 5.6 Hz, 2H), 7.85 (d, *J* = 8.4 Hz, 4H), 7.52 (d, *J* = 8.4 Hz, 4H), 3.28 (m, 4H),

1.56 (m, 4H). ¹³C NMR (150 MHz, DMSO-*d*₆): δ 165.0, 135.8, 133.4, 129.1, 128.3, 39.0, 26.6.



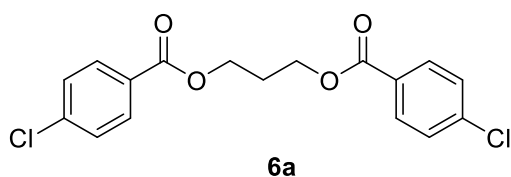
***N,N'*-(butane-1,4-diyl)bis(4-fluorobenzamide) (5d)**: white solid, 65% yield. ¹H NMR (600 MHz, DMSO-*d*₆): δ 8.48 (t, *J* = 5.3 Hz, 2H), 7.90 (m, 4H), 7.28 (m, 4H), 3.28 (m, 4H), 1.56 (m, 4H). ¹³C NMR

(150 MHz, DMSO-*d*₆) δ: 165.0 (2C), 163.7 (d, *J* = 248.1 Hz, 2C), 131.1 (2C), 129.7

(d, $J = 8.8$ Hz, 4C), 115.1 (d, $J = 21.5$ Hz, 4C), 39.5 (2C overlapped to the solvent signal), 26.7 (2C).

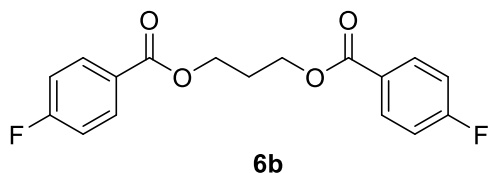
General Procedure for the Synthesis of Compounds 6a–h

In a round-bottom flask, the selected diol (1 mmol) was dissolved in anhydrous toluene (10 mL) under a nitrogen atmosphere. Triethylamine (4 eq) was added, followed by the proper 4-halobenzoyl chloride (2 eq). The reaction mixture was stirred under reflux for 2–16 h. After reaction completion, the solvent was evaporated under reduced pressure. The crude product was purified by flash chromatography (see below).



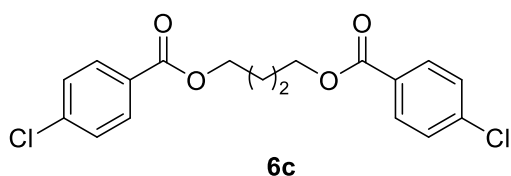
Propane-1,3-diyl bis(4-chlorobenzoate) (6a). The crude product was purified by flash chromatography (cyclohexane/ethyl acetate 9:1), giving the desired product as a white solid in 96% yield.

$^1\text{H NMR}$ (600 MHz, CDCl_3): δ 7.94 (d, $J = 8.5$ Hz, 4H), 7.38 (d, $J = 8.5$ Hz, 4H), 4.49 (t, $J = 6.2$ Hz, 4H), 2.25 (m, 2H). $^{13}\text{C NMR}$ (150 MHz, CDCl_3): δ 165.7 (2C), 139.6 (2C), 131.1 (4C), 128.8 (4C), 128.6(2C), 62.1 (2C), 28.3.



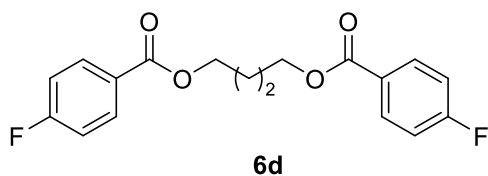
Propane-1,3-diyl bis(4-fluorobenzoate) (6b). The crude product was purified by flash chromatography (cyclohexane/ethyl acetate 9:1), giving the desired product as a white solid in 97% yield.

$^1\text{H NMR}$ (600 MHz, CDCl_3): δ 8.04 (m, 4H), 7.09 (m, 4H), 4.49 (t, $J = 6.2$ Hz, 4H), 2.25 (m, 2H). $^{13}\text{C NMR}$ (150 MHz, CDCl_3): δ 165.8 (d, $J = 254.0$ Hz, 2C), 165.5 (2C), 132.1 (d, $J = 9.7$ Hz, 4C), 126.3 (2C), 115.5 (d, $J = 22.4$ Hz, 4C), 61.8 (2C), 28.2.



Butane-1,4-diyl bis(4-chlorobenzoate) (6c). The crude product was purified by flash chromatography (cyclohexane/ethyl acetate 85:15 \rightarrow 50:50), giving the desired product as a white solid in 55% yield.

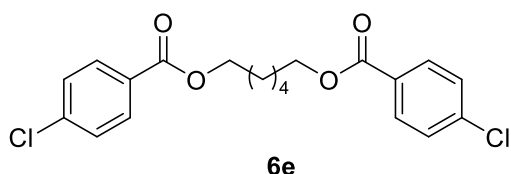
$^1\text{H NMR}$ (600 MHz, CDCl_3): δ 7.96 (d, $J = 8.5$ Hz, 4H), 7.41 (d, $J = 8.5$ Hz, 4H), 4.39 (m, 4H), 1.94 (m, 4H). $^{13}\text{C NMR}$ (150 MHz, CDCl_3): δ 165.8 (2C), 139.6 (2C), 131.1 (4C), 128.9 (4C), 64.8 (2C), 25.6 (2C).



Butane-1,4-diyl bis(4-fluorobenzoate) (6d). The crude product was purified by flash chromatography (cyclohexane/ethyl acetate

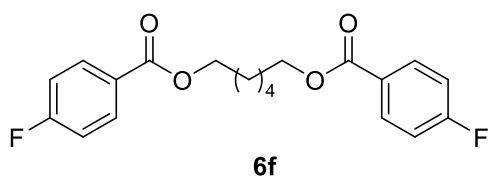
85:15 → 50:50), giving the desired product as a white solid in 55% yield.

$^1\text{H NMR}$ (600 MHz, CDCl_3): δ 8.05 (m, 4H), 7.10 (m, 4H), 4.39 (m, 4H), 1.94 (m, 4H). $^{13}\text{C NMR}$ (150 MHz, CDCl_3): δ 165.74 (d, $J = 253.0$ Hz, 2C), 165.72 (2C), 132.2 (d, $J = 9.3$ Hz, 4C), 126.6 (2C), 115.6 (d, $J = 22.0$ Hz, 4C), 64.7 (2C), 25.7 (2C).



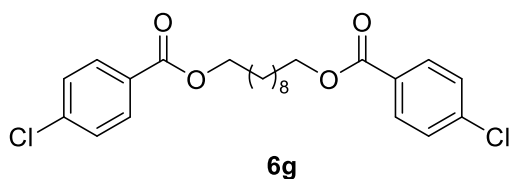
Hexane-1,6-diyl bis(4-chlorobenzoate) (6e). The crude product was purified by flash chromatography (cyclohexane/ethyl acetate 95:5), giving the desired product as a white solid in 55% yield.

$^1\text{H NMR}$ (600 MHz, CDCl_3): δ 7.96 (d, $J = 8.6$ Hz, 4H), 7.40 (d, $J = 8.6$ Hz, 4H), 4.32 (t, $J = 6.7$ Hz, 4H), 1.80 (m, 4H), 1.46 (m, 4H). $^{13}\text{C NMR}$ (150 MHz, CDCl_3): δ 165.7 (2C), 139.2 (2C), 130.8 (4C), 128.8 (2C), 128.6 (4C), 65.0 (2C), 28.5 (2C), 25.7 (2C).



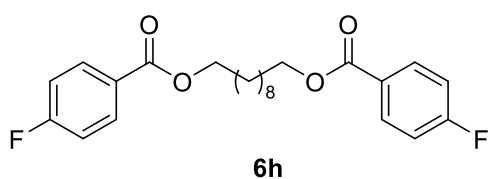
Hexane-1,6-diyl bis(4-fluorobenzoate) (6f). The crude product was purified by flash chromatography (cyclohexane/ethyl acetate 95:5), giving the desired product as a white solid in 65% yield.

$^1\text{H NMR}$ (600 MHz, CDCl_3): δ 8.04 (m, 4H), 7.10 (m, 4H), 4.32 (t, $J = 6.3$ Hz, 4H), 1.80 (m, 4H), 1.53 (m, 4H). $^{13}\text{C NMR}$ (150 MHz, CDCl_3): 165.66 (d, $J = 254.0$ Hz, 2C), 165.62 (2C), 132.0 (d, $J = 9.3$ Hz, 4C), 126.6 (2C), 115.4 (d, $J = 22.0$ Hz, 4C), 65.0 (2C), 28.6 (2C), 25.7 (2C).



Decane-1,10-diyl bis(4-chlorobenzoate) (6g). The crude product was purified by flash chromatography (cyclohexane/ethyl acetate 95:5), giving the desired product as a white solid in 40% yield.

$^1\text{H NMR}$ (600 MHz, CDCl_3): δ 7.97 (d, $J = 8.5$ Hz, 4H), 7.40 (d, $J = 8.5$ Hz, 4H), 4.30 (t, $J = 6.8$ Hz, 4H), 1.75 (m, 4H), 1.42 (m, 4H), 1.34 (m, 8H). $^{13}\text{C NMR}$ (150 MHz, CDCl_3): δ 165.7 (2C), 139.1 (2C), 130.8 (4C), 128.9 (2C), 128.6 (4C), 65.3 (2C), 29.3 (2C), 29.1 (2C), 28.6 (2C), 25.9 (2C).

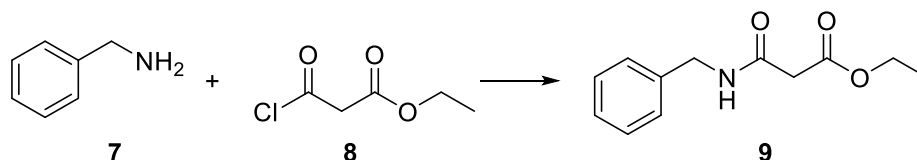


Decane-1,10-diyl bis(4-fluorobenzoate) (6h). The crude product was purified by flash chromatography (cyclohexane/ethyl acetate 9:1) and then recrystallized from hexane. **4f** was obtained as a white solid in

70% yield. $^1\text{H NMR}$ (600 MHz, CDCl_3): δ 8.05 (m, 4H), 7.10 (m, 4H), 4.30 (t, $J = 6.8$ Hz, 4H), 1.76 (m, 4H), 1.43 (m, 4H), 1.34 (m, 8H). $^{13}\text{C NMR}$ (150 MHz,

CDCl₃): δ 165.9 (2C), 165.8 (d, $J = 252.0$ Hz, 2C), 132.2 (d, $J = 9.3$ Hz, 4C), 126.9 (2C), 115.6 (d, $J = 23.0$ Hz, 4C), 65.4 (2C), 29.6 (2C), 29.4 (2C), 28.9 (2C), 26.2 (2C).

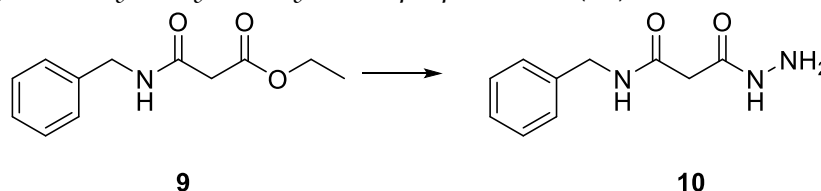
Synthesis of Ethyl 3-(Benzylamino)-3-oxopropanoate (9)



Ethyl malonyl chloride (2 mmol) was dissolved in dry dichloromethane (5 mL) in around-bottom flask under a nitrogen atmosphere. Benzylamine (1 eq) and triethylamine (1.5 eq) were added to the solution, and the reaction mixture was stirred at room temperature for 3 h. After completion, the reaction mixture was washed with HCl 1M and water. The organic layer was dried over anhydrous Na₂SO₄, and the solvent was evaporated. The crude product was purified by flash chromatography (cyclohexane/ethyl acetate 8:2 \rightarrow 7:3), giving **9** as a colorless oil in 55% yield.

¹H NMR (600 MHz, CDCl₃): δ 7.45 (bs, 1H), 7.34 (m, 2H), 7.29 (m, 3H), 4.47 (d, $J = 5.6$ Hz, 2H), 4.19 (q, $J = 7.1$ Hz, 2H), 3.36 (s, 2H), 1.28 (t, $J = 7.1$ Hz, 3H).

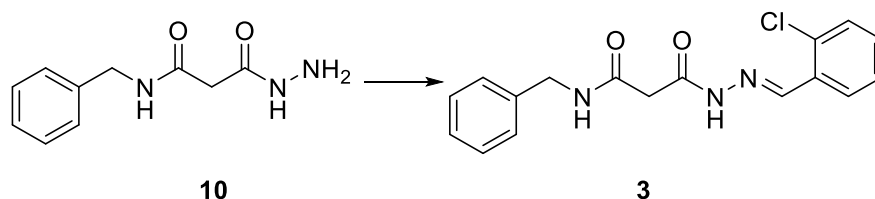
Synthesis of N-Benzyl-3-hydrazinyl-3-oxopropanamide (10)



Compound **7** (0.904 mmol) was dissolved in ethanol (2 mL) and treated with hydrazine hydrate (2 eq). The reaction mixture was heated to reflux and stirred until the starting material was consumed (16 h). Then, the reaction mixture was cooled to room temperature, and the obtained white precipitate was filtered (167 mg, 89% yield) and used for the next step without further purification.

¹H NMR (600 MHz, DMSO-*d*₆): δ 9.12 (s, 1H), 8.46 (m, 1H), 7.29 (m, 5H), 4.29 (d, $J = 6.0$ Hz, 2H), 4.26 (bs, 2H), 3.03 (s, 2H).

Synthesis of N-Benzyl-3-(2-(2-chlorobenzylidene) Hydrazinyl)-3 oxopropanamide (3).



2-chloro benzaldehyde (1 eq) was added to a suspension of N-benzyl-3-hydrazinyl-3-oxopropanamide **9** (0.240 mmol) in ethanol (5 mL), and the reaction mixture was heated to reflux for 6 h. Then, the solvent was evaporated. The crude product was purified by flash chromatography (dichloromethane/methanol 98:2). (E)-N-benzyl-3-(2-(2-chlorobenzylidene)hydrazinyl)-3-oxopropanamide and (Z)-N-benzyl-3-(2-(2-chlorobenzylidene)hydrazinyl)-3-oxopropanamide were obtained, as a mixture, in 51% and 25% yields, respectively. The following ¹H NMR and ¹³C NMR are referred to the 1:2 mixture of (E)-N-benzyl-3-(2-(2-chlorobenzylidene)hydrazinyl)-3-oxopropanamide and (Z)-N-benzyl-3-(2-(2-chlorobenzylidene)hydrazinyl)-3-oxopropanamide:

¹H NMR (600 MHz, DMSO-*d*₆): δ 11.8 (bs, 1H, minor isomer), 11.6 (bs, 1H, major isomer), 8.59 (t, J = 5.6 Hz, 1H, minor isomer), 8.58 (s, 1H, minor isomer), 8.57 (t, J = 5.9 Hz, 1H, major isomer), 8.36 (s, 1H, major isomer), 7.97–7.93 (m, 1H minor isomer + 1H major isomer), 7.55–7.50 (m, 1H minor isomer + 1H major isomer), 7.45 (td, J = 1.8, 7.5, Hz, 1H, minor isomer), 7.44–7.40 (m, 2H, major isomer), 7.35–7.28 (m, 2H major isomer + 2H minor isomer), 7.27–7.24 (m, 2H minor isomer + 1H major isomer), 7.23–7.18 (m, 2H minor isomer + 2H major isomer), 4.31 (d, J = 6.2 Hz, 2H, minor isomer), 4.29 (d, 6.1 Hz, 2H, major isomer), 3.60 (s, 2H, major isomer), 3.32 (s, 2H, minor isomer).

¹³C NMR (150 MHz, DMSO-*d*₆): *d* 169.4, 166.4, 166.1, 163.4, 142.5, 139.2 (2C), 138.8, 133.1, 132.9, 131.4 (3C), 131.1, 129.8 (2C), 128.3 (2C), 128.1 (2C), 127.6 (2C), 127.5 (4C), 127.2 (4C), 42.9, 42.2 (2C), 41.6.

Biological evaluation

Fungal Strains

In this study, strains belonging to seven different species were used. *Pyricularia oryzae* A2.5.2 (sensitive to strobilurins; WT) [29] and PO21_01 (resistant to strobilurins, RES), *Penicillium expansum* EM22, *Mucor pyriformis* EM14, *Botrytis cinerea* EM1, *Fusarium culmorum* FcUK [30], and *F. graminearum* ITA1601 [31] made a part of a fungal collection and were maintained in the laboratory of

plant pathology of the University of Milan; *Aspergillus niger* ITEM9076 and ITEM9077 were obtained from the Agro-Food Microbial Culture Collection ITEM (Institute of Sciences of Food Production—ISPA, CNR, Bari, Italy). The strains were maintained as single-spore isolates on a malt-agar medium (MA: 20 g/L malt extract, Oxoid, UK; 15 g/L agar, Oxoid, UK) at 4 °C.

Enzyme Inhibition Assays for the Measurement of QoI Action

P. oryzae mitochondrial fractions from the A2.5.2 and PO21_01 strains were prepared as described previously [11], with the following modification. The final collected mitochondrial pellet was suspended in mitochondrial buffer (3 mL; 0.5 M sucrose, 10 mM KH₂PO₄, 10 mM KCl, 10 mM MgCl₂, 0.2 mM EDTA, pH 7.2), divided into 3 Eppendorf tubes, and centrifuged for 20 min at 4 °C, at 10000 rpm (rotor F45–24-11, Eppendorf). Each pellet was resuspended in 0.2 mL of the same buffer and stored at -80 °C until use. The strobilurin-like (QoI) action was evaluated by measuring the cyt *bc1*-mediated cyt *c* reduction in the presence of the tested compounds (200 μM) and the isolated mitochondrial fractions. The cyt *c* reduction activity was measured through a spectrophotometrical assay ($\lambda = 550$ nm) based on the synthetic quinol, decylubiquinol (DBH₂), for the determination of the DBH₂:cyt *c* oxidoreductase activity described in [11]. The cyt *bc1*-mediated cyt *c* reduction was also detected by measuring the NADH:cyt *c* oxidoreductase activity. The measured activity is based on the native mitochondrial ubiquinol as the quinol substrate whose electron recharging is ensured by the coupled NADH-oxidation reaction of the mitochondrial complex I. The assay was carried out as described for the DBH₂:cyt *c* oxidoreductase activity assay, replacing DBH₂ with NADH (25 μL of 4 mM stock, freshly prepared in 0.05 M Tris-HCl, 1 mM EDTA, pH 7.7). Azoxystrobin (31697, Sigma Aldrich, Milano, Italy) was used as the reference QoI. In both assays, one enzyme unit (U) is the amount that yields one micromole of reduced cyt *c* under the assay conditions ($\epsilon^{550} = 16.3$ mM⁻¹ cm⁻¹), and for the inhibition studies, the enzyme rate in the presence of the tested molecule (rate_{molecule}) was compared to that achieved in the presence of the compound-diluent DMSO (rate_{DMSO}), in order to calculate the percent inhibition (I%) as follows:

$$I (\%) = (\text{rate}_{\text{DMSO}} - \text{rate}_{\text{molecule}} / \text{rate}_{\text{DMSO}}) \times 100 \quad (1)$$

In Vitro Fungal Mycelium Growth Inhibition by the Compounds

The inhibitory activity of the novel compound fungicides on the mycelium growth of the different fungi was evaluated as described previously [11,32], with slight modifications. The fungi were divided into two groups: fast- and

medium/slow-growing. The fast-growing fungi were *B. cinerea* EM1, *M. pyriformis* EM14, *F. culmorum* FcUK, and *F. graminearum* ITA1601. The medium/slow-growing fungi included *P. oryzae* A2.5.5 and PO21_01, *P. expansum* EM22, and *A. niger* ITEM9076 and ITEM9077. A mycelium plug (0.5 cm in diameter) obtained from an actively growing fungal colony was transferred to MA medium plates supplemented or not with tested compounds at the concentration of 25 mg/L in two biological replicates. Due to the low solubility of the tested dual molecules in water, they were dissolved in dimethyl sulfoxide (DMSO). Therefore, two controls were included: the MA medium (C, control for azoxystrobin) and the MA medium supplemented with DMSO at the final concentration of 1% v/v (C, control for tested compounds). The plates were incubated at 24 °C in the dark. The mycelium growth was measured for fast-growing fungi at 2–4 days after inoculation (dai), and for the medium/slow-growing fungi at 6 and 7 dai. The inhibition of mycelium growth (%) was calculated by comparing the mycelium growth on the control and the compound-supplemented plates. The inhibition percentage was calculated as $I\% = (C - T)/C \times 100$, where C = mycelium growth in the control medium and T = mycelium growth in the medium added with the tested compound.

7.5. Bibliography

1. Dean, R.; Van Kan, J.A.L.; Pretorius, Z.A.; Hammond-Kosack, K.E.; Di Pietro, A.; Spanu, P.D.; Rudd, J.J.; Dickman, M.; Kahmann, R.; Ellis, J.; Foster, G. D. The Top 10 fungal pathogens in molecular plant pathology. *Mol. Plant Pathol.* **2012**, *13*, 414–430, doi:10.1111/j.1364-3703.2011.00783.x.
2. Ceresini, P.C.; Castroagudin, V.L.; Rodrigues, F.A.; Rios, J.A.; Acique-Perez, C.E.; Intra Moreira, S.; Croll, D.; Alves, E.; De Carvahlo, G.; Nunes Maciel, J.L.; et al. Wheat blast : from its origins in South America to its emergence as a global threat. *Mol. Plant Pathol.* **2019**, *20*, 155–172, doi:10.1111/mpp.12747.
3. Valent, B. The Impact of Blast Disease: Past, Present, and Future. *Methods Mol. Biol.* **2021**, 2356, 1–18.
4. Cruz, C. D.; Valent, B. Wheat blast disease : danger on the move. *Trop. Plant Pathol.* **2017**, *42*, 210–222, doi:10.1007/s40858-017-0159-z.
5. Gladieux, P.; Condon, B.; Ravel, S.; Soanes, D.; Nunes Maciel, J.L.; Nhani Jr, A.; Chen, L.; Terauchi, R.; Lebrun, M.H.; Tharreau, D.; et al. Gene Flow between Divergent Cereal- and Grass-Specific Lineages of the Rice Blast Fungus *Magnaporthe oryzae*. *Am. Soc. Microbiol.* **2018**, *9*, e01219-17.
6. Milazzo, J.; Pordel, A.; Ravel, S.; Tharreau, D. First Scientific Report of *Pyricularia oryzae* Causing Gray Leaf Spot Disease on Perennial Ryegrass (*Lolium perenne*) in France. *Plant Dis.* **2019**, *103*, 1024.
7. June, U.; Valent, B.; Cruppe, G.; Stack, J.P.; Cruz, C.D. Recovery Plan for Wheat Blast Caused by *Magnaporthe oryzae* Pathotype Triticum. **2021**, *22*, 182–212.
8. European Commission, *Final Review Report for the Active Substance Tricyclazole*; Bruxelles, Belgium, 2016;
9. Fitogest Available online: <https://fitogest.imagelinenetwork.com/it/> (accessed on Dec 6, 2022).
10. Bartlett, D.W.; Clough, J.M.; Godwin, J.R.; Hall, A.A.; Hamer, M.; Parr-dobrzanski, B. The strobilurin fungicides. *Pest Manag. Sci.* **2002**, *58*, 649–662, doi:10.1002/ps.520.
11. Zuccolo, M.; Kunova, A.; Musso, L.; Forlani, F.; Pinto, A.; Vistoli, G.; Gervasoni, S.; Cortesi, P.; Dallavalle, S. Dual-active antifungal agents containing strobilurin and SDHI-based pharmacophores. *Sci. Rep.* **2019**, *9*, 1–12, doi:10.1038/s41598-019-47752-x.
12. Balba, H. Review of strobilurin fungicide chemicals Review of strobilurin fungicide chemicals. *J. Environ. Sci. Health Part B*, **2007**, *42*, 441–451.

doi:10.1080/03601230701316465.

13. Lamberth, C. Complex III inhibiting strobilurin esters, amides, and carbamates as broad-spectrum fungicides. In *Bioactive Carboxylic Compound Classes: Pharmaceuticals and Agrochemicals*; Wiley-VCH Verlag GmbH & Co. KGaA:Weinheim, Germany, 2016; pp. 371–384.
14. Kunova, A.; Palazzolo, L.; Forlani, F.; Catinella, G.; Musso, L.; Cortesi, P.; Eberini, I.; Pinto, A.; Dallavalle, S. Structural Investigation and Molecular Modeling Studies of Strobilurin-Based Fungicides Active against the Rice Blast Pathogen *Pyricularia oryzae*. *Int. J. Mol. Sci.* **2021**, *22*, 3731.
15. Leadbeater, A.J. Plant Health Management: Fungicides and Antibiotics. In *Encyclopedia of Agriculture and Food Systems*; Elsevier: Amsterdam, The Netherlands, 2014; pp. 408–424 ISBN 9780080931395.
16. FRAC List of Plant Pathogenic Organisms Resistant to Disease Control Agents. Available online: www.frac.info (accessed on Nov 16, 2022).
17. Fernández-ortuño, D.; Torés, J.A.; De Vicente, A.; Pérez-garcía, A. The QoI Fungicides, the Rise and Fall of a Successful Class of Agricultural Fungicides. In *Fungicides* Carisse, O., Ed.; InTech: Rijeka, Croatia, **2010**; pp. 203–220. ISBN 978-953-307-266-1.
18. Kim, Y.; Dixon, E.W.; Vincelli, P.; Farman, M.L. Field Resistance to Strobilurin (QoI) Fungicides in *Pyricularia grisea* Caused by Mutations in the Mitochondrial Cytochrome b Gene. *Am. Phytopathol. Soc.* **2003**, *93*, 891–900.
19. Castroagudín, V.L.; Ceresini, P.C.; Oliveira, S.C. De; Reges, J.T.A.; Maciel, J.L.N.; Bonato, A.L. V; Dorigan, A.F.; Mcdonald, B.A. Resistance to QoI Fungicides Is Widespread in Brazilian Populations of the Wheat Blast Pathogen *Magnaporthe oryzae*. *Phytopathology* **2015**, *105*, 284–294.
20. Miyagawa, N.; Fuji, M. Occurrence of QoI-fungicide-resistant strains of *Magnaporthe oryzae* on rice and fungicidal effective. In Proceedings of the 23rd Symposium of PSJ Research Committee on Fungicide Resistance, Gifu, Japan, 2013; pp. 25-35.
21. Tenni, D.; Sinetti, A.; Waldner, M.; Torriani, S.F.F.; Romani, M. First report of QoI resistance in Italian population of *Pyricularia oryzae*. *J. Plant Dis. Prot.* **2021**, *128*, 1705–1709, doi:10.1007/s41348-021-00494-3.
22. Matsuzaki, Y.; Yoshimoto, Y.; Arimori, S.; Kiguchi, S.; Harada, T.; Iwahashi, F. Discovery of metyltetraprole: Identification of tetrazolinone pharmacophore to overcome QoI resistance. *Bioorganic Med. Chem.* **2020**, *28*, 115211, doi:10.1016/j.bmc.2019.115211.

23. Matsuzaki, Y.; Kiguchi, S.; Suemoto, H.; Iwahashi, F. Antifungal activity of metyltetraprole against the existing QoI-resistant isolates of various plant pathogenic fungi. *Pest Manag. Sci.* **2019**, *76*, 1743–1750. doi:10.1002/ps.5697.
24. Xu, Q.; Wang, Y.; Xu, J.; Sun, M.; Tian, H.; Zuo, D.; Guan, Q.; Bao, K.; Wu, Y.; Zhang, W. Synthesis and bioevaluation of 3,6-diaryl-[1,2,4]triazolo[4,3-*b*]pyridazines as antitubulin agents. *ACS Med. Chem. Lett.* **2016**, *7*, 1202–1206.
25. Eberini, I.; Guerini, A.; Mantegazza, M.; Gianazza, E.; Baroni, A.; Caterina, M.; Donghi, D.; Galliano, M.; Beringhelli, T. Computational and experimental approaches assess the interactions between bovine b - lactoglobulin and synthetic compounds of pharmacological interest. **2008**, *26*, 1004–1013, doi:10.1016/j.jmgm.2007.08.006.
26. Cotterill, J. V; Palazzolo, L.; Ridgway, C.; Price, N.; Rorije, E.; Moretto, A.; Peijnenburg, A.; Limited, F.S.; Hutton, S.; Yo, Y. Predicting estrogen receptor binding of chemicals using a suite of in silico methods – Complementary approaches of (Q)SAR, molecular docking and molecular dynamics. *Toxicol. Appl. Pharmacol.* **2019**, *378*, 114630, doi:10.1016/j.taap.2019.114630.
27. Schultes, S.; De Graaf, C.; Haaksma, E.E.J.; De Esch, I.J.P.; Leurs, R.; Krämer, O. Ligand efficiency as a guide in fragment hit selection and optimization. *Drug Discov. Today Technol.* **2010**, *7*.
28. Hopkins, A.L.; Groom, C.R.; Alex, A. Ligand efficiency: A useful metric for lead selection. *Drug Discov. Today Technol.* **2010**, *7*, e157–e162.
29. Kunova, A.; Pizzatti, C.; Bonaldi, M.; Cortesi, P. Sensitivity of Nonexposed and Exposed Populations of *Magnaporthe oryzae* from Rice to Tricyclazole and Azoxystrobin. *Plant Dis.* **2014**, *98*, 512–518.
30. Pasquali, M.; Spanu, F.; Scherm, B.; Balmas, V.; Hoffmann, L.; Hammond-kosack, K.E.; Beyer, M.; Migheli, Q. FcStuA from *Fusarium culmorum* Controls Wheat Foot and Root Rot in a Toxin Dispensable Manner. *PLoS ONE* **2013**, *8*, e57429, doi:10.1371/journal.pone.0057429.
31. Pasquali, M.; Beyer, M.; Bohn, T.; Hoffmann, L. Comparative Analysis of Genetic Chemotyping Methods for *Fusarium*: Tri13 Polymorphism Does not Discriminate between 3- and 15-acetylated Deoxynivalenol Chemotypes in *Fusarium graminearum*. *J. Phytopathol.* **2011**, *159*, 700–704. doi:10.1111/j.1439-0434.2011.01824.x.
32. Kunova, A.; Bonaldi, M.; Saracchi, M.; Pizzatti, C.; Chen, X.; Cortesi, P. Selection of *Streptomyces* against soil borne fungal pathogens by a

standardized dual culture assay and evaluation of their effects on seed germination and plant growth. *BMC Microbiol.* **2016**, *16*, 272, doi:10.1186/s12866-016-0886-1.

